Investigation of mTOR-independent regulation of macroautophagy

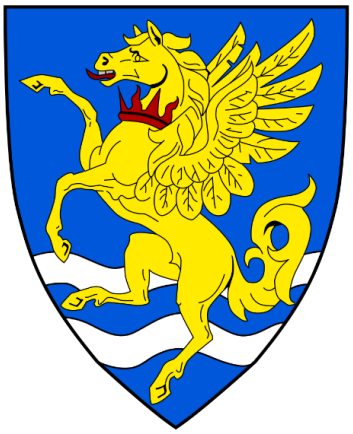

Richard Ian Odle

Robinson College

Babraham Institute

This dissertation is submitted for the degree of Doctor of Philosophy

September 2019

Declaration

This dissertation is the result of my own work and includes nothing which is the outcome of work done in collaboration except as declared in the Preface and specified in the text. It is not substantially the same as any that I have submitted, or, is being concurrently submitted for a degree or diploma or other qualification at the University of Cambridge or any other University or similar institution except as declared in the Preface and specified in the text. I further state that no substantial part of my dissertation has already been submitted, or, is being concurrently submitted for any such degree, diploma or other qualification at the University of Cambridge or any other University or similar institution except as declared in the Preface and specified in the text. The length does not exceed 60,000 words.

Richard Odle

Investigation of mTOR-independent regulation of macroautophagy

Richard Ian Odle

Macroautophagy is a critical catabolic response to cellular stress, enabling lysosomal-mediated breakdown of cytosolic cargo. The nutrient-responsive mTORC1 kinase complex has been described as a master regulator of cellular metabolism. Indeed, mTORC1 inhibits autophagy via repressive phosphorylation of the key autophagy regulators ATG13, ULK1, ATG14 and TFEB. Consequently, mTORC1 has become a candidate therapeutic target in neurodegeneration and cancer; however, its essential role in other cellular programs has prompted the investigation of mTORC1-independent regulation of autophagy. This thesis explores the role of CMGC kinase family members ERK1/2 and CCNB1-CDK1 in the regulation of autophagy.

The ERK1/2 signalling cascade is activated in a high proportion of cancers. ERK2 has been proposed as a regulatory kinase of TFEB; however, we found little evidence to suggest that ERK1/2 was a direct kinase responsible for TFEB phosphorylation, including at the putative site S142. Furthermore, whilst we observed that hyperactivation of the ERK1/2 pathway did lead to increases in total TFEB protein levels in HEK293, this appeared to be a cell line specific finding. We therefore concluded ERK1/2 was not likely to be a critical regulator of TFEB.

It has been proposed that autophagy must be repressed during mitosis, otherwise nuclear envelope breakdown will expose the genome to the cytosolic autophagy machinery. Here we show that autophagy initiation, as measured by markers of the omegasome, is indeed repressed throughout mitosis. Furthermore, autophagy regulators undergo mitotic hyperphosphorylation, including at known repressive sites, in a manner dependent on CDK1 but not mTORC1. Indeed, we find mTORC1 is likely inactive as a result of CDK1-dependent hyperphosphorylation of RAPTOR. Thus, we conclude that mTORC1 is substituted by CDK1, as the master repressor of autophagy during mitosis. These results suggest that autophagy regulation is uncoupled from nutrient status during nuclear envelope breakdown as a mechanism to prevent genomic instability, a hallmark of cancer.

Acknowledgements

First and foremost, my many thanks to the boss (Simon) for taking a leap of faith with his first medic. He has allowed me the room to develop my own independent thinking, whilst guiding me and shaping the project along the way. His support for both my scientific and personal development has been fantastic. Hopefully I'm the start of many medical Cookies! Pam, you've been a wonderful mentor, teacher and a great laugh to share a bay with. To Bob and Bex for their advice, encouragement and contributions to my project (as well as a good old natter!). AK and Matt, it's been emotional guys. I'm going to miss the random and never-ending science chats, as well as the healthy doses of sarcasm on a daily basis. Emma DW, who am I going to go to with my crazy autophagy theories now!? Your expertise, calm nature and kindness were always valued in what can be rather stressful circumstances! Anne for keeping me company in pessimism row and listening to my panics! Prassana, for being so cheerful and optimistic every time I spoke to her. To my fellow students in crime, cheers for all the laughs and encouragement along the way! Jack and Kate for looking after me when I first appeared, looking and feeling completely lost. Emma and Megan for being awesome office buddies. Rachael for the random chats and her valiant attempts to rescue my pot-plant Spike, who tragically passed away after being knocked on the floor one too many times.

My many thanks to the wider team at the Babraham Institute, who's passion for core science and research is refreshing in a cynical target-led world. I owe a lot of my newfound appreciation of microscopy to Simon (Walker) and Hanneke for showing me the ropes. I'm pretty sure Simon must have dreaded seeing me at the door of his office by the end of my PhD given the number of questions I had, but it was worth it! David and Judith for being so friendly and kind in the face of rather unreasonable requests! Couldn't have asked for a better assessor in Nick, who was always willing to talk through autophagy ideas and point me in the right direction. Maria for finding countless reagents and being so supportive along the way! Oli and his lab have also been very supportive during the years! Mike, Giulia, Chiara, Izzy and Piotr, thanks for letting me tag along on all the fun public engagement activities whilst contributing very little and collecting the prestigious title of "delegator-in-chief".

I have to take this opportunity to pay special thanks to two individuals, without which I would simply not be where I am today. I could not have asked for better mentorship over the years than what I have got from Andrew Sharkey and Gary Doherty. If I look back to the imposter-syndrome ridden person who started university, I struggle to see myself. They have both played huge roles in shaping my development and helping me through the low spots. I will always be forever grateful to have applied to Robinson.

To Cinzia, Shiv and the rest of the Coleman lab that were responsible for making me catch the academia bug. I was incredibly lucky to have Cinzia as my supervisor in my undergraduate project and thank you for making me believe I could do it! You guys built the foundations and I'm forever grateful for that. Hopefully I'll bump into some of you over the coming years in the clinical world!

I have been incredibly lucky to have had such supportive friends over the years. Of note, Lee, you've always been there mate through thick and thin. Emma and Giorgio, thanks for all of your help, a place of respite in sunny Taunton, and for being such kind and decent friends. Ed for showing me the delights of Japan, a much-needed holiday during the hard slog!

To my parents. I know it has sometimes been challenging with me working and not being able to see me as much as you hope you would. So, thank you for your continued support of what I'm trying to do.

我的女朋友，谢谢。我爱你! You've had the hardest job over the last year watching me stress out and keeping me calm. I'm pretty content with life right now and a large part of that is down to you.

Should you have been bored enough to read all of this, I hope what you have acquired is the overwhelming sense of gratitude I have for the many people featured above, and the many more who if I had included would have made this acknowledgements longer than the thesis. I've had a fantastic time and wouldn't change any of it. Final thanks go to my brother Stephen. Whilst he may no longer be with us, his aspirations to pursue what he loved are ideals I've carried with me that have driven me to academic medicine. Whilst no academic or personal achievement will ever bring him back, I will settle for the hope that he would be proud that I am pursing what I love.

Acknowledgement of assistance received during thesis

Initial training and subsequent mentoring

General lab practice – Kathy Balmanno and Pamela Lochhead

Tissue culture – Kathy Balmanno

Western blot – Kathy Balmanno (chemiluminescence) and Andrew Kidger (fluorescent/ Li-COR)

qRT-PCR – Anne Ashford and Matthew Sale

Immunofluorescence/ Confocal imaging – Hanneke Okkenhaug, Simon Walker, Andrew Kidger, Pamela Lochhead and Becky Gilley

Live-cell imaging – Simon Walker, Oliver Florey

Nuclear/ Cytosolic Fractionation – Pamela Lochhead

Molecular biology – Pamela Lochhead and Becky Gilley

Immunoprecipitation – Matthew Sale, Kate Stuart

Flow cytometry – Attila Bebes and Rebecca Roberts

Data obtained from a technical service provider (e.g. DNA sequencing, illustrations, simple bioinformatics information etc)
Sequencing of DNA constructs performed by Genewiz

Data produced jointly (e.g. where it was necessary or desirable to have two pairs of hands)
HEK293 GFP-ATG13 H2B-mCherry live cell imaging (Figure 4.8.B) – Oliver Florey, Simon Walker

High content microscopy (Figure 5.17 and 5.18) – Andrew Kidger

Data/materials provided by someone else (e.g. one-off analysis, bioinformatics analysis, where parallel data or technical provision in a very different area is needed to provide a connected account in the thesis)

Mass spectrometry (Table 5.1 and Table 5.2) - David Oxley

EdU staining (Figure 3.14), HeLa (paclitaxel treatment) (Figure 5.15.B) – Andrew Kidger

Cell lines and plasmids (outlined in materials and methods):

HAP1 parental, HAP1 GFP-RAPTOR, HEK293 GFP-ATG13, HEK293 mRFP-EGFP-LC3 - Nick Ktistakis (Babraham Institute)

pOPH-ATG13, GST-HA-RagB WT (Addgene #19301), GST-HA RagD WT (Addgene #19307), GST-HA $RagB^{GTP}$ (Q99L; Addgene #19303), GST-HA $RagD^{GDP}$ (S77L; #19308), GFP-ATG14 (Addgene #24295)- Nick Ktistakis group (Babraham Institute).

HA-hULK1 - Do-Hyung Kim (Addgene plasmid # 31963)

TFEB-GFP (WT (Addgene #38119) and Δ30 (Addgene #44445)) – Shawn Ferguson

H2B-mCherry- Robert Benezra (Addgene #20972)

HA-RAPTOR (WT, A7, D7) – Robert Schneider

pPOM121-mCherry (Euroscarf #P30554) – Jan Ellenberg

Publication associated with this thesis

Odle, R. I. *et al.* (2019) 'An mTORC1-to-CDK1 Switch Maintains Autophagy Suppression during Mitosis', *Molecular Cell*. Cell Press. doi: 10.1016/J.MOLCEL.2019.10.016.

Odle, R. I. and Cook, S. J. (2020) 'Macroautophagy is repressed during mitosis – seeing is believing', *Autophagy*, pp. 1–2. doi: 10.1080/15548627.2020.1725405.

Contents

Abbreviations

Abbreviation	Full term and aliases
3MA	3-Methyladenine
4E-BP1	Eukaryotic translation initiation factor 4E-binding protein 1
4-HT	4-Hydroxytamoxifen
5-FU	5-Flurouracil
ADP	Adenosine diphosphate
AID	Auxin-inducible degrons
AKAP149	A-kinase anchor protein 1
AKT	RAC-alpha serine/threonine-protein kinase
AMP	Adenosine monophosphate
AMPK	5' adenosine monophosphate-activated protein kinase
APC/C	Anaphase-promoting complex
ARs	A*utophagy Regulators (ATG13, ULK1, ATG14, TFEB)*
ATG(number)	Autophagy-related protein (number)
ATP	Adenosine triphosphate
BAF	Barrier-to-autointegration factor
BCA	bicinchoninic acid
BCL2	Apoptosis regulator Bcl-2
bHLH	Basic Helix Loop Helix
CAK	CDK-activating kinase
CCLE	Cancer Cell Line Encyclopedia
CCNB1	Cyclin B1
CDC4	Cell division control protein 4
CDK	Cyclin-Dependent Kinase
ChIP	Chromatin Immunoprecipitation
CK	Casein kinase
CLEAR	Coordinated Lysosomal Expression and Regulation
CMGC	Abbreviation based on CDKs, MAPKs, GSKs and CDK-like kinases
CREB	cAMP response element binding protein
CRM1/ XPO1	Exportin-1/ Chromosome region maintenance 1 protein homolog
cvt	cytoplasm to vacuole targeting
DDR	DNA Damage Response
DEPDC5	DEP domain-containing protein 5
DEPTOR	DEP domain-containing mTOR-interacting protein
DFCP1	Double FYVE domain-containing protein 1
DNA	Deoxyribonucleic acid
DRAM1	DNA damage-regulated autophagy modulator protein 1
E2F3	Transcription factor E2F3
EBV	Epstein Barr Virus
eEF2K	Eukaryotic elongation factor 2 kinase
EGF	Epidermal growth factor
eIF(4E or other eIF proteins)	Eukaryotic translation initiation factor (4E or other eIF proteins)
EPG-8	Ectopic P Granules – 8
ER	Endoplasmic reticulum
ERK1	Mitogen-Activated Protein Kinase 3 / Extracellular Signal-Regulated Kinase 1
ERK2	Mitogen-Activated Protein Kinase 1 / Extracellular Signal-Regulated Kinase 2
FBXW7	F-box/WD repeat-containing protein 7

FC	Flow cytometry
FIP200	focal adhesion kinase family-interacting protein of 200 kDa
FKBP12	FK506 binding protein 12
FLCN	Folliculin
FNIP	Folliculin-interacting protein
FYVE	FYVE zinc finger domain (name associated with Fab1, YOTB, Vac1, EEA1)
GAP	GTPase-activating protein
GATOR	GAP activity towards Rags
GDP	guanosine diphosphate
GEF	Guanine nucleotide exchange factor
GFP	Green Fluorescent Protein
Gly	Glycine
GSK3	Glycogen Synthase Kinase 3
GTP	guanosine triphosphate
HBSS	Hanks' Balanced Salt Solution
HBXIP	Hepatitis B virus X-interacting protein/ LAMTOR5
HCM	High content microscopy
HEK293	Human Embryonic Kidney 293
IB	Immunoblot
IF	Immunofluorescence
IGF	Insulin Growth Factor
IGFR	Insulin Growth Factor Receptor
IKK	Inhibitor of nuclear factor kappa-B kinase
IP	Immunoprecipitation
IPO8	Importin 8
JNK	Mitogen-Activated Protein Kinase 8/ c-Jun N-terminal kinase
LAMP	Lysosome-associated membrane glycoprotein
LAMTOR	Late endosomal/lysosomal adaptor and MAPK and MTOR activator
LC3	Microtubule-associated proteins 1A/1B light chain 3B
LKB1	Serine/threonine-protein kinase STK11
LRS	Leucyl-tRNA synthetase
MALAT1	Metastasis associated lung adenocarcinoma transcript 1
MAP4K3	Mitogen-activated protein kinase kinase kinase kinase 3
MAPKAPK2	MAP kinase-activated protein kinase 2
MAPK	Mitogen-activated protein kinase
MAPKK	Mitogen-activated protein kinase kinase
MAPKKK	Mitogen-activated protein kinase kinase kinase
MAT1	CDK-activating kinase assembly factor MAT1
MDM2	E3 ubiquitin-protein ligase Mdm2
MEF	Mouse Embryonic Fibroblast
MEK1	Dual specificity mitogen-activated protein kinase kinase 1
MEKK3	Mitogen-activated protein kinase kinase kinase 3
MITF	Microphthalmia-Associated Transcription Factor
mLST8	Target of rapamycin complex subunit LST8
MNK	MAP kinase-interacting serine/threonine-protein kinase
mRNA	Messenger RNA
mTOR	Mechanistic/ mammalian Target of Rapamycin
mTORC	Mechanistic/ mammalian Target of Rapamycin Complex
NDP52	Calcium-binding and coiled-coil domain-containing protein 2
NEDD8	Neural precursor cell expressed developmentally down-regulated protein 8

NF-κB	Nuclear factor NF-kappa-B p105 subunit
NPRL	Nitrogen permease regulator 2-like protein
Nup107	Nuclear pore complex protein Nup107
OIS	Oncogene Induced Senescence
P38	Mitogen-activated protein kinase 14
P62/ SQSTM1	Sequestosome-1
PAGE	polyacrylamide gel electrophoresis
PBS	Phosphate-buffered saline
PDK1	Pyruvate dehydrogenase kinase isoform 1
PERK	PKR-like endoplasmic reticulum kinase
PH	Pleckstrin homology
PI	phosphatidylinositol
PI(3)P	Phosphatidylinositol 3-phosphate
PIP_2	Phosphatidylinositol (4,5)-bisphosphate
PIP_3	Phosphatidylinositol (3,4,5)-trisphosphate
PK(A/B/C)	Protein Kinase (A/B/C)
PLK	Polo-like kinase
PP2A	Serine/threonine-protein phosphatase 2A
PPP3CB	Calcineurin catalytic isoform beta
PUMA	p53 up-regulated modulator of apoptosis
qRT-PCR	Real-Time Quantitative Reverse Transcription polymerase chain reaction
Rab	Ras-related protein Rab
Raf	RAF proto-oncogene serine/threonine-protein kinase
RAPTOR	Regulatory-associated protein of mTOR
Ras	Ras protein
RCC	Renal Cell Carcinoma
RFP	Red fluorescent protein
Rheb	Ras homolog enriched in brain/ GTP-binding protein Rheb
RIPA	Radioimmunoprecipitation assay
RIPK1	Receptor-interacting serine/threonine-protein kinase 1
RNA	Ribonucleic acid
RSK	90 kDa ribosomal protein S6 kinase
RUBICON	Run domain Beclin-1-interacting and cysteine-rich domain-containing protein
S(site)	Serine(site)
S6	40S ribosomal protein S6
S6K	70 kDa ribosomal protein S6 kinase 1
SAC	Spindle Assembly Checkpoint
SDS	Sodium Dodecyl Sulfate
Sec13	Protein SEC13 homolog
Seh1L	Nucleoporin SEH1
SH2	Src Homology 2
shRNA	Short hairpin RNA
siRNA	Small interfering RNA
SMA	Superior mesenteric artery
SNARE	Soluble NSF attachment protein Receptor
SOS	Son of sevenless
STUB1	E3 ubiquitin-protein ligase CHIP/ STIP1 homology and U box-containing protein 1
T(site)	Threonine(site)
TASCC	TOR-autophagy spatial coupling compartment
TBK1	Serine/threonine-protein kinase TBK1/ TANK-binding kinase 1

TCGA	The Cancer Genome Atlas
TFE3	Transcription Factor Binding to IGHM Enhancer 3
TFEB	Transcription factor EB
TFEC	Transcription Factor EC
TMEM192	Transmembrane 192
Tor	Target of Rapamycin
TOS motif	TOR signalling motif
TSC	Tuberous sclerosis complex
TSC1	Hamartin
TSC2	Tuberin
ULK	Unc-51 like kinase
UVRAG	UV radiation resistance-associated gene protein
VEGF	Vascular Endothelial Growth Factor
VMP1	vacuole membrane protein 1
VPS34	Phosphatidylinositol 3-kinase VPS34
Wdr(24/59)	WD repeat-containing protein
WEE1	Wee1-like protein kinase
WIPI	WD repeat domain phosphoinositide-interacting protein 1
Wnt	Mnemonic based on wingless-type MMTV integration site
Y(site)	Tyrosine(site)
ZKSCAN3	Zinc finger protein with KRAB and SCAN domains 3

List of Figures

List of Tables

1 Introduction

1.1 Overview of autophagy

Autophagy, a word derived from the Greek for 'self-eating', is a cellular catabolic program involving the sequestration of cytoplasmic cargo into double membraned structures termed autophagosomes. These then fuse with lysosomes (autolysosomes) enabling subsequent lysosome-mediated degradation of the enclosed cargo. Several distinct types of macroautophagy exist, which can be categorised by the selectivity of sequestered substrates (Feng *et al.*, 2013). This project will focus on starvation-induced non-selective (bulk) macroautophagy. Autophagy serves as a response to multiple stressors and has been linked with healthy ageing. For example, the promotion of autophagy in several cellular and animal models has been linked with beneficial outcomes such as improved proficiency of DNA damage repair (Liu *et al.*, 2015) and increased longevity (reviewed: Nakamura and Yoshimori, 2018). In addition, promotion of autophagy in several neurodegenerative disease models such as Huntington's and Alzheimer's disease has led to beneficial outcomes (reviewed: Menzies *et al.*, 2017). However, autophagy has also been implicated as a survival mechanism in several cancers (reviewed: Levy, Towers and Thorburn, 2017), though this is somewhat countered by its tumour suppressive effects (reviewed: Yun and Lee, 2018). For example, forced expression of Beclin1, which stimulated autophagy, lead to decreased cell proliferation in MCF7 (Liang *et al.*, 1999); whilst silencing Beclin1, which decreased autophagy, increased cell migration in glioblastoma models (Catalano *et al.*, 2015). In addition, autophagy deficient mice (mosaic ATG5 -/- mice or hepatocyte specific ATG7 -/-) develop multiple liver tumours, albeit benign, likely as a result of p62 accumulation sequestering Keap1 leading to a failure in the oxidative stress response (Takamura *et al.*, 2011). Due to the contribution autophagy has in many disease processes, much research has focused on the potential therapeutic modulation of autophagy. The majority of this work has focused on mTORC1 (mammalian/ mechanistic target of rapamycin complex 1), a critical signalling network hub that integrates a number of stress-induced signals and thus represses autophagy in basal conditions. However, mTORC1 is an essential gene and its inhibition results in high-levels of toxicity in animal models and establishing a therapeutic window is challenging (reviewed: Xie, Wang and Proud, 2016). There is therefore keen interest in the investigation of mTORC1-independent regulation of autophagy, and specifically how autophagy can be initiated with minimal effects on other effector pathways.

1.2 Autophagy initiation

The molecular basis for autophagosome formation is still not entirely understood, despite intensive research. The membrane origin for autophagosomes has been a subject of intense debate, with various organelles being proposed including: the late endosome, endoplasmic reticulum (ER), Golgi apparatus and plasma membrane. Evidence supporting the endoplasmic reticulum primarily revolves around the omegasome intermediate structure, which enables recruitment of various autophagy proteins required for the expansion of the isolation membrane (reviewed: Mari, Tooze and Reggiori, 2011; Lamb, Yoshimori and Tooze, 2013). Direct evidence was established through visualisation of the phagophore by 3-dimensional electron tomography, with several direct connections between rough ER membrane and phagophore/ autophagosome membrane (Ylä-Anttila *et al.*, 2009). Since then it has been identified in both yeast (Kotani *et al.*, 2018) and mammalian (Valverde *et al.*, 2019) cells that ATG2 acts as a tether between the ER and Pre-autophagosomal structure/ omegasome. Indirect evidence comes from the localisation of relevant FYVE-containing proteins. VPS34 (Phosphatidylinositol 3-kinase catalytic subunit type 3) is the only known class III PI3 kinase in the mammalian cell, and promotes the synthesis of PI(3)P (reviewed: Vanhaesebroeck *et al.*, 2010) at the omegasome intermediate structure. FYVE domains act as phosphatidylinositol-3-phosphate (PI(3)P) sensors (Gaullier *et al.*, 1998). Ridley and colleagues identified Double FYVE domain-containing protein 1 (DFCP1) as being unique at the time among FYVE-containing proteins for its localisation to the ER and Golgi as opposed to endosomes (Ridley *et al.*, 2001). During starvation, DFCP1 strongly co-localises with LC3, whereas much weaker co-localisation is observed for other PI(3)P sensors such as an isolated FYVE domain from FENS-1 (an endosomal linked PI(3)P sensor (Ridley *et al.*, 2001)) (Axe *et al.*, 2008). WIPI2 (WD repeat domain phosphoinositide-interacting protein 2), a mammalian orthologue for yeast Atg18 and another FYVE-containing protein, also recruits to the omegasome at the ER (Polson *et al.*, 2010; Dooley *et al.*, 2014). Whilst linked, It has been proposed that WIPI2 acts downstream of DFCP1, due to WIPI2 depletion leading to accumulation of DFCP1 positive puncta (Polson *et al.*, 2010). WIPI2 has been shown to be critical for LC3 (microtubule-associated proteins 1A/1B light chain 3B) lipidation at the site of the omegasome via recruitment of the ATG16L1 complex (Dooley *et al.*, 2014). Finally, the ER protein VMP1 (vacuole membrane protein 1), is known to be required for autophagy in higher eukaryotes (Ropolo *et al.*, 2007), and autophagy proteins are localised to pre-existing VMP1 puncta during autophagosome synthesis (Koyama-Honda *et al.*, 2013).

Two complexes are involved in the initiation of the autophagosome: ULK1-ATG13-FIP200 and VPS34-Beclin1-ATG14L. The ULK1 complex consists of: ULK1 (Unc-51 like

kinase 1) (Ganley *et al.*, 2009), ATG13 (Autophagy related protein 13) (Ganley *et al.*, 2009), FIP200 (Fak family kinase-interacting protein of 200kDa) (Hara *et al.*, 2008), and Atg101 (Autophagy related protein 101) (Hosokawa et al. 2009); all of which are required for autophagosome synthesis. ULK1 is the human homolog of the yeast Atg1 protein kinase (reviewed: Lin and Hurley, 2016). It is only in the last few years that the functions and substrates of ULK1 have begun to emerge. The ULK1 and VPS34 complexes appear to be responsible for the omegasome intermediate structure originating from the ER. ULK1 complex members closely associate with the omegasome marker DFCP1 in starvation conditions and ULK1 puncta are dramatically reduced in response to wortmannin, which inhibits the formation of omegasomes (Karanasios *et al.*, 2013). Since VPS34 is thought to act downstream of ULK1, it is proposed that the reduction in ULK1 puncta in response to wortmannin is due to the collapse of a positive feedback mechanism (Karanasios *et al.*, 2013). Supporting this, live-cell imaging experiments reveal that preformed ULK1 puncta are relatively stable compared to preformed ATG5 puncta upon treatment with wortmannin, which abolished the formation of new ULK1 puncta (Koyama-Honda *et al.*, 2013). During autophagy, ULK1 autophosphorylates its kinase domain activation loop at T180, and mutation of this site prevents ULK1 activation and localisation to phagophores (Bach *et al.*, 2011). ULK1 is also suggested to autophosphorylate two sites at the c-terminus, 1042 and 1046, which promotes KLHL20-association and ULK1 degradation (Liu *et al.*, 2016). ULK1 phosphorylates Beclin1 at S14 which is required for autophagic VPS34 complex activity (Russell *et al.*, 2013). ULK1 also phosphorylates ATG14 (Autophagy related protein 14) at S29, which increases VPS34 activity (Park *et al.*, 2016; Wold *et al.*, 2016). Indeed, the formation of ATG14 puncta is dependent upon an intact ULK1 complex (Itakura and Mizushima, 2010; Park *et al.*, 2016). In addition, ULK1 also phosphorylates VPS34 at S249, though the functional significance of this is unclear (Egan *et al.*, 2015). The ULK1 complex is partially responsible for the recruitment of the ATG16L1 complex, with FIP200 directly binding to ATG16L1 between the coiled-coil and WD40 repeat domains (Gammoh *et al.*, 2013). Mutation of this FIP200 binding domain on ATG16L1 completely impairs amino starvation-induced autophagy (Gammoh *et al.*, 2013; Fletcher *et al.*, 2018).

DFCP1 accumulates near pre-existing VPS34-containing vesicles upon amino acid starvation (Axe *et al.*, 2008). The ULK1 complex, as assessed by FIP200 puncta, forms a punctate distribution at ER sub-domains enriched for phosphatidylinositol synthase which catalyses the formation of phosphatidylinositol (PI), the precursor for PI(3)P (Nishimura *et al.*, 2017). The importance of VPS34 in autophagosome formation is established through both genetic silencing (Jaber *et al.*, 2012) and selective small-molecule inhibition (Dowdle *et al.*, 2014; Ronan *et al.*, 2014) of VPS34 preventing mature autophagosome formation.

VPS34 forms multiple complexes with two distinct complexes involved in the regulation of autophagy and endocytic pathways, both of which contain Beclin1 and Vps15 (reviewed: Ohashi, Tremel and Williams, 2019). Complex I also contains ATG14, whilst complex II contains UVRAG (UV radiation resistance-associated gene protein). Whilst complex II is primarily implicated in endocytic pathways, it is also proposed to have a role in autophagosome maturation/ fusion with lysosomes (Liang *et al.*, 2008). UVRAG is suggested to be phosphorylated at S498 by mTORC1 which suppresses autophagosome maturation due to an enhanced interaction of UVRAG with the negative-regulator RUBICON (Kim *et al.*, 2015), where RUBICON binds to VPS34 and inhibits its lipid-kinase activity (Sun *et al.*, 2011). In contrast, mTORC1 has also been suggested to phosphorylate UVRAG at S550 and S571, enhancing VPS34 lipid kinase activity (Munson *et al.*, 2015). Thus there is disagreement over whether complex II is important for autophagic flux and some groups have suggested it has no involvement in autophagosome maturation (Jiang *et al.*, 2014; Munson *et al.*, 2015). This may explain the findings that whilst PI(3)P generated from complex I catalysed reactions increases during nutrient starvation, total cellular PI(3)P actually decreases (Munson *et al.*, 2015).

It is widely believed that the majority of autophagy regulation is at the initial stages of autophagosome synthesis (Bento *et al.*, 2016). The latter stages of autophagy include the ATG5-ATG12-ATG16L1 complex which mediates maturation and localisation of the developing autophagosome (Fujita *et al.*, 2008); loss of this complex prevents autophagy (Kuma, 2002; Itakura and Mizushima, 2010), with ATG5 knockout a common tool used to inactivate autophagy both in cellular and animal models. ATG16L1 binds to FIP200 which recruits it to the developing autophagosome membrane (Nishimura *et al.*, 2013). In addition, residues within the coiled coil domain of ATG16 enable direct lipid-binding to PI3P within the pre-autophagosomal structure (PAS) (Dudley *et al.*, 2019). WIPI2 is a PI(3)P effector protein which is also required for the recruitment of the ATG16 complex to the omegasome, with subsequent autophagosome membrane formation and LC3 lipidation (Polson *et al.*, 2010; Dooley *et al.*, 2014). ATG16L1 is directly phosphorylated by ULK1 at S278 in response to amino acid deprivation or *Salmonella enterica* infection, promoting ATG16L1 caspase-dependent cleavage though the functional significance of this is unclear (Alsaadi *et al.*, 2019). It has recently been shown that WIPI2 is a direct substrate for mTORC1, with phosphorylation at S395 promoting its interaction with the E3 ubiquitin ligase HUWE1, which targets WIPI2 for degradation (Wan *et al.*, 2018). After ATG16L1 complex recruitment, ATG3 conjugated to LC3 (mammalian homologue of ATG8; Microtubule-associated proteins 1A/1B light chain 3) can then bind to ATG12, which stimulates the E2-like activity of ATG3, thus enabling lipidation of LC3 (Metlagel *et al.*, 2013; Sakoh-

Nakatogawa *et al.*, 2013). The LC3 family in humans consists of three separate genes (LC3A, LC3B and LC3C) which have high levels of homology with rat Map1LC3 (He *et al.*, 2003). In addition, there are other Atg8 homologs in human cells such as the GABARAPs. These have functional differences. For example, whilst all of the Atg8 homologs interact with ULK1, GABARAPs positively regulate ULK1 activity whilst LC3 negatively regulate ULK1 activity (Grunwald *et al.*, 2019). Immediately after translation of LC3, ATG4 cleaves the c-terminus of LC3 to enable exposure of a glycine residue. This residue is then conjugated to phosphatidylethanolamine via a process catalysed by ATG3, and this lipidated form of LC3 is denoted as LC3-II (Maruyama and Noda, 2018). LC3 lipidation is inhibited by knockout of any of the preceding complexes (Itakura and Mizushima, 2010). It is worth noting the temporal dynamics of these events. Whilst ATG5 is viewed as a late-event, its recruitment to and dispersal from the omegasome is synchronous with ULK1 (Koyama-Honda *et al.*, 2013). By contrast, LC3 and p62 are recruited synchronously, reaching a maximal intensity approximately 2 minutes after the DFCP1 peak, but plateauing due to their retention on the completed autophagosome (Koyama-Honda *et al.*, 2013). These dynamics fit with a model whereby autophagosomes bud from an omegasome structure as proposed by Axe and colleagues (Axe *et al.*, 2008) (diagrammatically represented in Figure 1.1).

Upon completion and closure of the autophagosome, it then fuses with lysosomes to mediate degradation of the sequestered cargo. The SNARE protein Syntaxin 17 has been identified as critical to autophagosome-lysosome fusion, being recruited to completed autophagosomes and mediating its fusion with the endosome/ lysosome (Itakura, Kishi-Itakura and Mizushima, 2012). Debate surrounds whether autophagosome degradation is mediated by direct fusion with lysosomes or indirect via the endocytic system (reviewed: Ganley, 2013). The processes of fusion and degradation of sequestered contents are frequently perturbed by various treatments and conditions, resulting in an accumulation of autophagosomes. This has experimental implications, discussed in Section 1.6.

1.3 Signalling pathways relevant to autophagy

1.3.1 mTOR signalling

The serine/threonine kinase mechanistic target of rapamycin (mTOR) represents a major effector arm of the PI3 Kinase signalling axis. It is constitutively arranged in two protein complexes. mTORC1 is the best characterised complex, with important roles in translational control, autophagy and growth regulation (reviewed: Saxton and Sabatini, 2017). The complex consists of mTOR, RAPTOR (Kim *et al.*, 2002) and mLST8 (Kim *et al.*, 2003). PRAS40 is a direct inhibitor of the mTORC1 complex, disassociating in response to

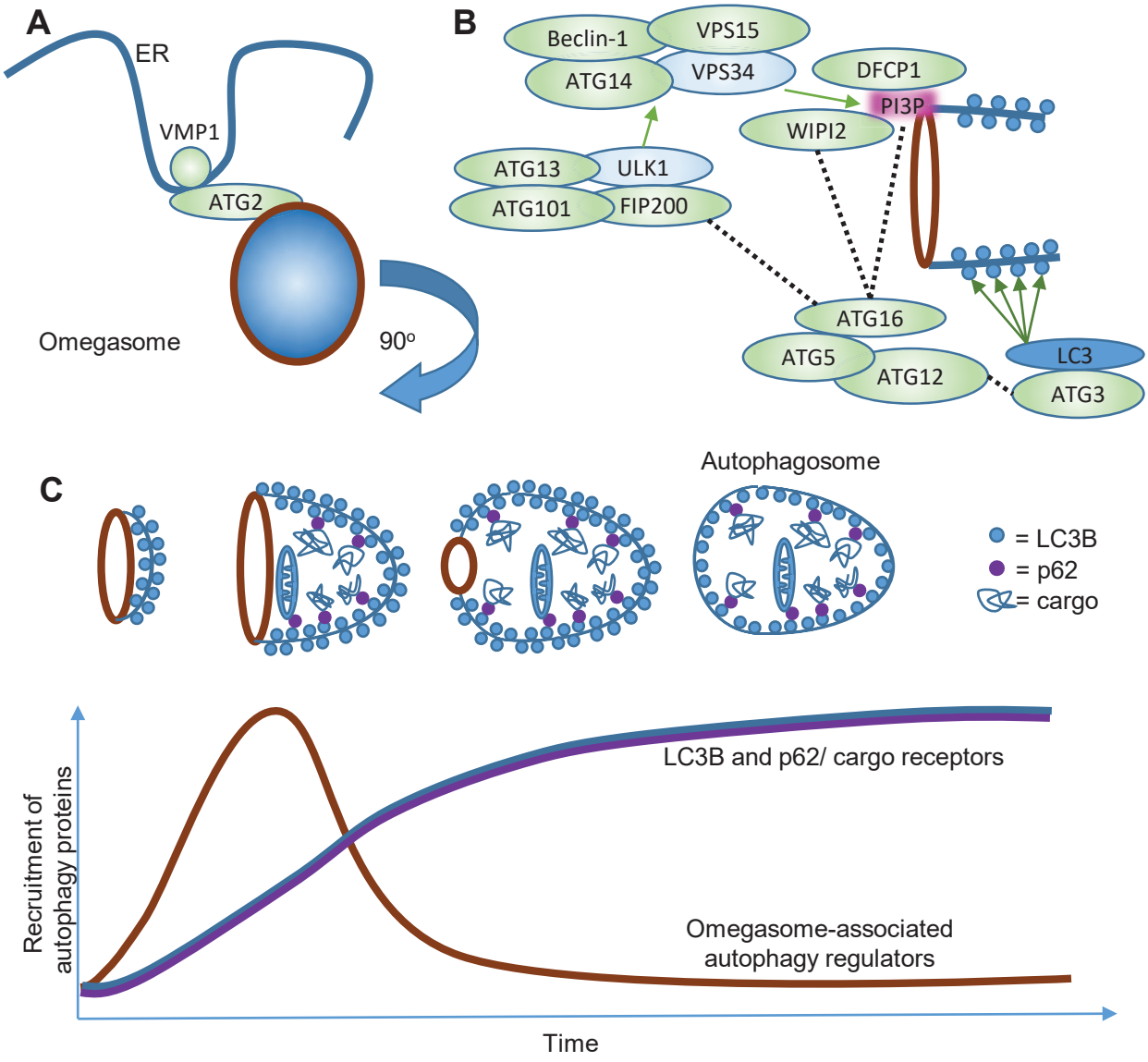

Figure 1.1: Overview of autophagosome synthesis.
(A) The omegasome intermediate, which is an extension of the phagophore, is localised to the ER by pre-existing VMP1 puncta. **(B)** Cross-sectional view rotated 90° on A. The omegasome then acts as a platform upon which various autophagy regulators can be recruited. The ULK1 complex is essential for autophagosome initiation and known substrates include ATG14, Beclin1 and VPS34. VPS34 is responsible for the synthesis of PI(3)P, which enables the recruitment of FYVE-containing proteins DFCP1 and WIPI2. WIPI2, in conjunction with FIP200, then recruits the ATG16-ATG5-ATG12 complex. ATG12 binds to ATG3, which is conjugated to LC3-I. This interaction then enables lipidation of LC3 on the developing autophagosome. **(C)** View is a cross-sectional view in same orientation as B. LC3B and cargo receptors, such as p62, are incorporated into the developing autophagosome; whilst autophagy regulators are associated with the omegasome. As a result, when the autophagosome 'buds-off' omegasome-associated proteins disperse, whilst LC3 and p62 remain. This has implications in puncta dynamics during imaging experiments, discussed in Chapter 4. The graph is an over-simplification since there is slight variation in omegasome-associated proteins, such as ATG14 and DFCP1 being recruited slightly after ATG5 and ULK1 (Koyama-Honda et al., 2013). Figure based on schematics and results from Karanasios et al., 2013 and Koyama-Honda et al., 2013

insulin (Wang *et al.*, 2007). mTORC2 consists of mTOR, RICTOR, mSin1 and protor; it is mainly involved in regulation of the cytoskeleton and PI3K signalling to AKT (reviewed: Saxton and Sabatini, 2017). DEPTOR is a direct inhibitor of both complexes, though feedback activation of the PI3K/mTORC2/AKT signalling axis can result in mTORC2 activation when DEPTOR is overexpressed (Peterson *et al.*, 2009). mTORC1 forms a dimeric structure though there is disagreement whether this is a direct dimerization of mTOR (Aylett *et al.*, 2016), or whether RAPTOR binds between the two mTOR subunits (Yip *et al.*, 2010).

1.3.1.1 Growth factors regulate mTORC1 activity via the PI3K signalling axis

Growth factors mediate their effects on mTORC1 through signalling cascades, such as the well characterised PI3K pathway, to signal to the GTPase 'Ras homolog enriched in brain' (Rheb). A majority of growth factors signal via AKT (reviewed: Huang and Manning, 2008). The archetypal growth factor, Insulin Growth Factor-1 (IGF), binds to IGFR which activates class I PI3Ks, catalysing the phosphorylation of $PI(4,5)P_2$ to $PI(3,4,5)P_3$ (reviewed: Jean and Kiger, 2014). Class I PI3K consist of four different p110 catalytic domains (α, β, γ and δ). p110 α, β and δ associate with the p85 regulatory subunit, while p110γ associates with p101 or p84/p87 regulatory subunits (reviewed: Bilanges, Posor and Vanhaesebroeck, 2019). The SH2 (Src homology 2) domain of p85 interacts with tyrosine-phosphorylated receptor tyrosine kinase, leading to the de-repression of the p110-p85 dimer (reviewed: Bilanges, Posor and Vanhaesebroeck, 2019). AKT and PDK1 bind to PIP_3 via their pleckstrin homology (PH) domains, and small-molecule inhibition of this interaction (such as PIT-1) inactivates the PI3K/PDK1/AKT signalling axis (Miao *et al.*, 2010). Conversely, PTEN dephosphorylates PIP_3 to PIP_2 (Maehama and Dixon, 1998), inactivating AKT. Activating *PIK3CA* (encodes the class IA PI3K catalytic subunit p110α) and inactivating PTEN mutations are prevalent in cancer, resulting in PI3K signalling hyperactivation (reviewed: Chalhoub and Baker, 2009). PI3K signalling promotes phosphorylation of both T308 and S473 of AKT, resulting in its synergistic activation (Alessi *et al.*, 1996). PIP_3 activates PDK1, and PDK1 phosphorylates AKT at T308 (Alessi *et al.*, 1997). Curiously PDK1-/- embryonic stem cells have no alterations in 4E-BP1 phosphorylation yet striking reductions in P-S6K (T389) (Wang *et al.*, 2001), despite both phosphorylation events being catalysed by mTORC1. Likewise, selective small-molecule inhibition of PDK1 (GSK2334470) which caused robust dephosphorylation of S6K at T389 (Najafov *et al.*, 2011; Sathe *et al.*, 2018) appeared to have no effect on 4E-BP1 phosphorylation (Castel *et al.*, 2016; Sathe *et al.*, 2018). This suggests that PDK1 inhibition affects different mTORC1 substrates differentially, though how this occurs is unclear. In parallel to PDK1, PI3K signalling also activates mTORC2 (though the mechanism appears poorly understood)

which phosphorylates AKT at S473 (Sarbassov *et al.*, 2005). mTORC2 is likely not the only enzyme that phosphorylates AKT at S473 since in certain tissues, such as skeletal muscle, P-AKT (S473) is maintained despite PP242 (An ATP-competitive mTOR inhibitor) treatment (Feldman *et al.*, 2009).

Rheb is a GTPase which is absolutely required for mTORC1 activity (Saucedo *et al.*, 2003). Given Rheb's intrinsically low activity, it is negatively regulated by the TSC1-TSC2 complex, whereby TSC2 is a GTPase activating protein (GAP) for Rheb (Garami *et al.*, 2003; Inoki *et al.*, 2003; Tee *et al.*, 2003; Zhang *et al.*, 2003). The TSC complex, consisting of TSC1 and TSC2 interacting via coiled-coil domains (van Slegtenhorst *et al.*, 1998), acts to integrate signals from a wide range of inputs. PKB/AKT directly phosphorylates TSC2 (Inoki *et al.*, 2002) to inhibit its ability to inactivate Rheb (Inoki *et al.*, 2003), by promoting its disassociation from the lysosome (Menon *et al.*, 2014). In addition, other inputs filter into the TSC complex, such as IKKβ-catalysed phosphorylation of S487 and S511 on TSC1 leading to suppression of TSC1 and activation of mTORC1 (Lee *et al.*, 2007). Inactivation of the TSC complex leads to hyperactivation of mTORC1 in a manner independent of amino acids (Gao *et al.*, 2002). Rheb directly binds to mTORC1 via the catalytic domain of mTOR and LST8 (Long *et al.*, 2005). Like inactivation of TSC1/2, overexpression of Rheb can also activate mTORC1 in the absence of amino acids (Long *et al.*, 2005). The mechanism by which mTORC1 continues signalling, despite the absence of amino acids, when the Rheb pathway is hyperactivated is unclear. One notion that has been explored is that Rheb-mediated activation of mTORC1 leads to increased binding affinity to its substrates (4E-BP1 was investigated) whilst its catalytic activity, as assessed by mTOR autophosphorylation, remains at similar levels (Sato *et al.*, 2009). In contrast, previous studies have established that interaction between $Rheb^{GTP}$ and mTORC1 in cells, increases mTORC1's *in vitro* kinase activity (Long *et al.*, 2005). Indeed, it has recently been demonstrated that Rheb binding causes an allosteric conformational change in mTOR which promotes accelerated catalysis (Yang *et al.*, 2017).

Curiously, Rheb knockout murine models can develop an inner cell mass and persist to E11.5 (Goorden *et al.*, 2011), unlike mTORC1 components which are essential, with no homozygous knockouts identified at E8.5 (Murakami *et al.*, 2004). Rheb-/- lysates from E11.5 show drastically reduced, but not absent, phosphorylation of 4E-BP1 and S6 (Goorden *et al.*, 2011). Why mTORC1 signalling appears to persist in early development of Rheb -/- mouse models is unclear. Regardless, there is consensus that PI3K class I signalling mediates the growth factor-dependent activation of mTORC1 and this is diagrammatically represented in Figure 1.2.

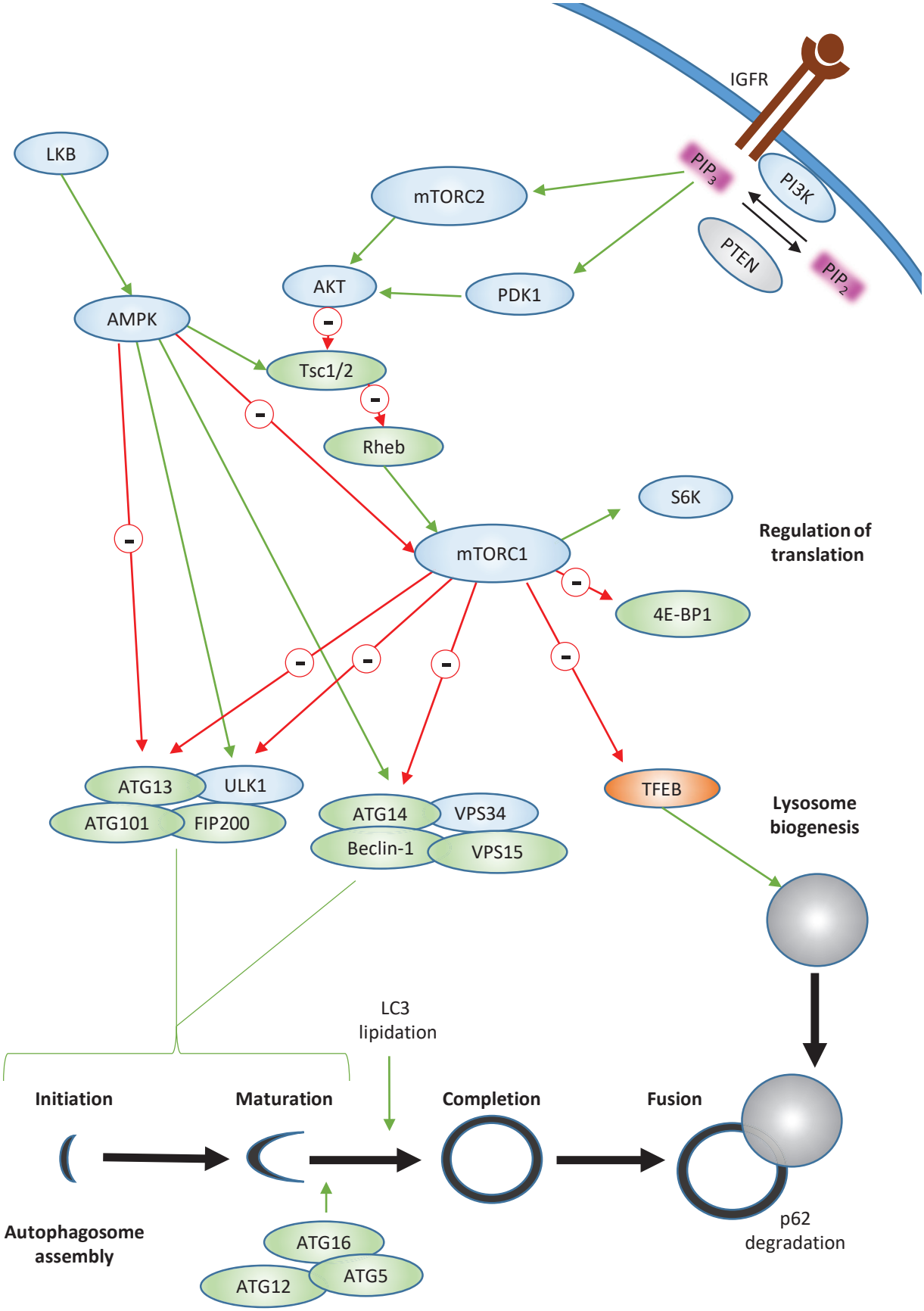

Figure 1.2: Overview mTOR and AMPK signalling in autophagy regulation.
The PI3K/AKT/mTORC1 signalling axis represents a major effector arm of growth factor signalling, linking growth factor availability with anabolic processes. Whilst represented as a linear cascade, it has a number of points of cross-talk with other pathways, with the AMPK pathway represented in this example.

1.3.1.2 Lysosomes co-ordinate mTORC1 activity in response to amino acid availability

mTORC1 is responsive to a range of stimuli including growth factors and nutrients, which utilise different mechanisms of activation. In contrast to growth factors, sensing of amino acids appears to depend upon a separate class of GTPases to Rheb known as Rags (Kim *et al.*, 2008), which are proposed to promote co-localisation of mTOR with Rheb at the lysosomal surface and thus act independently of TSC1/2 (Sancak *et al.*, 2008, 2010). Notably, Rheb is still required for amino acid-induced activation of mTORC1 (Smith *et al.*, 2005), suggesting the two systems are co-operative and not redundant. This model is not without controversy, with suggestions that Rheb is actually localised at the Golgi apparatus, co-localising with Giantin (Manifava *et al.*, 2016). Furthermore, overexpression of Rheb can promote mTORC1 activation, even in the absence of amino acids (Long *et al.*, 2005). Rheb has been suggested to also contribute to the amino acid response, with amino acids promoting localisation of Rheb to lysosomes in response to amino acids in a manner dependent upon MCRS1 (Fawal, Brandt and Djouder, 2015). Another possibility is that Golgi-localised Rheb promotes activation of lysosome-associated mTORC1 at the Golgi-lysosome contact site (Hao *et al.*, 2017). Curiously, forced localisation of overexpressed Rheb to either lysosomes or Golgi, achieved by fusion with Rab7 or Rab9a (lysosome) and Rab1A or Rab33B (Golgi), promoted mTORC1 activation even during amino acid starvation (Hao *et al.*, 2017). Regardless, it is generally agreed that mTORC1 recruitment to lysosomes is absolutely required for its activation and there is a range of evidence to support this. It has been suggested that forced localisation of mTORC1 to the lysosome promotes its activation regardless of amino acid status (Sancak *et al.*, 2010). This mechanism of regulation appears to not be universal. For example, osteoclasts show lysosomal localisation of mTOR in both fed and starvation conditions, despite an inactivation of mTOR in the latter (Wang *et al.*, 2017). Likewise, some groups observe minimal or no loss of co-localisation between mTOR and lysosomal markers upon amino acid starvation, even in cell lines used within the original studies (i.e. HeLa) (Korolchuk *et al.*, 2011; Manifava *et al.*, 2016). Overall, there is consensus that mTORC1 must localise to lysosomes to become active, but whether this is solely regulated by amino acid availability and how this promotes interaction with Rheb is controversial.

It has been observed that mTORC1 immunoprecipitated from cells starved of amino acids has reduced kinase activity against S6K and 4E-BP1 (Kim *et al.*, 2002). Whilst it was originally argued that mTORC1 kinase activity is not decreased during amino acid withdrawal, since S2481 autophosphorylation was not decreased in cells (Peterson *et al.*, 2000); immunoprecipitated mTORC1 from starved cells does show reduced S2481 phosphorylation suggesting mTORC1 activity is specifically decreased (Soliman *et al.*,

2010). It has been suggested that total phosphorylation of S2481 within the cell is predominantly associated with mTORC2 (Copp, Manning and Hunter, 2009), providing an explanation for the discrepancy in findings.

1.3.1.3 Regulation of Rag-GTPases

Whilst Rag-GTPases are required for mTORC1 localisation to lysosomes, they do not themselves directly interact with the lysosome surface. Instead they interact with the Ragulator complex, where the p18 domain of the Ragulator complex tethers Rag-GTPases to the lysosome surface (Sancak *et al.*, 2010) (Figure 1.3). Depletion of Ragulator components (p18, C7orf59, HBXIP, p14) prevents Rag-GTPase localisation to lysosomes (Sancak *et al.*, 2010; Bar-Peled *et al.*, 2012).

Whilst universally agreed to be critical, there is debate as to how Rag-GTPases communicate amino acid status to mTORC1 activation. The original hypothesis was that Rag-GTPase heterodimers exist in one of two states, either as an active complex ($RagA/B^{GTP}$, $RagC/D^{GDP}$) or an inactive complex ($RagA/B^{GDP}$, $RagC/D^{GTP}$). This hypothesis was stimulated by mutations in Rag-GTPases, such that they were constitutively GTP or GDP-loaded, resulting in the corresponding mTORC1 activity (Sancak *et al.*, 2010). *in vitro* Rag heterodimer binding to mTORC1 is independent of whether RagA/B are bound to GDP or GTP, with Rag proteins displaying minimal GTPase activity such that RagA/B are constitutively in a GTP-bound state (Oshiro, Rapley and Avruch, 2014). However, a number of guanine nucleotide exchange factors (GEFs) and GTPase-activating proteins (GAPs) have now been proposed for the Rag-GTPases (reviewed: Powis and De Virgilio, 2016). The Ragulator complex acts as a GEF for RagA/B, with its interaction being strengthened upon amino acid deprivation and it is proposed this tight association prevents mTORC1 binding to Rags (Bar-Peled *et al.*, 2012).

mTORC1 is not responsive to all amino acids but is instead regulated by availability of select amino acids. It has been known for several years that leucine is a critical amino acid in the activation of mTORC1. Several mechanisms have been proposed for how this occurs. LRS (leucyl-tRNA synthetase) was found to interact with mTORC1 and RagD in a leucine-dependent manner, where it is a GAP for RagD thereby stimulating the formation of an active Rag heterodimer and mTORC1 activation (Han *et al.*, 2012), though it has subsequently been challenged that FNIP1/2-Folliculin is more likely to function as the RagC/D GAP (Tsun *et al.*, 2013) after its recruitment to the lysosomes by association with $RagA/B^{GDP}$ during starvation (Petit, Roczniak-Ferguson and Ferguson, 2013). Thus, it is proposed FLCN (Folliculin) recruits to RagA/B during starvation and is primed to convert Rag C/D-associated GTP to GDP upon reintroduction of amino acids, resulting in mTORC1

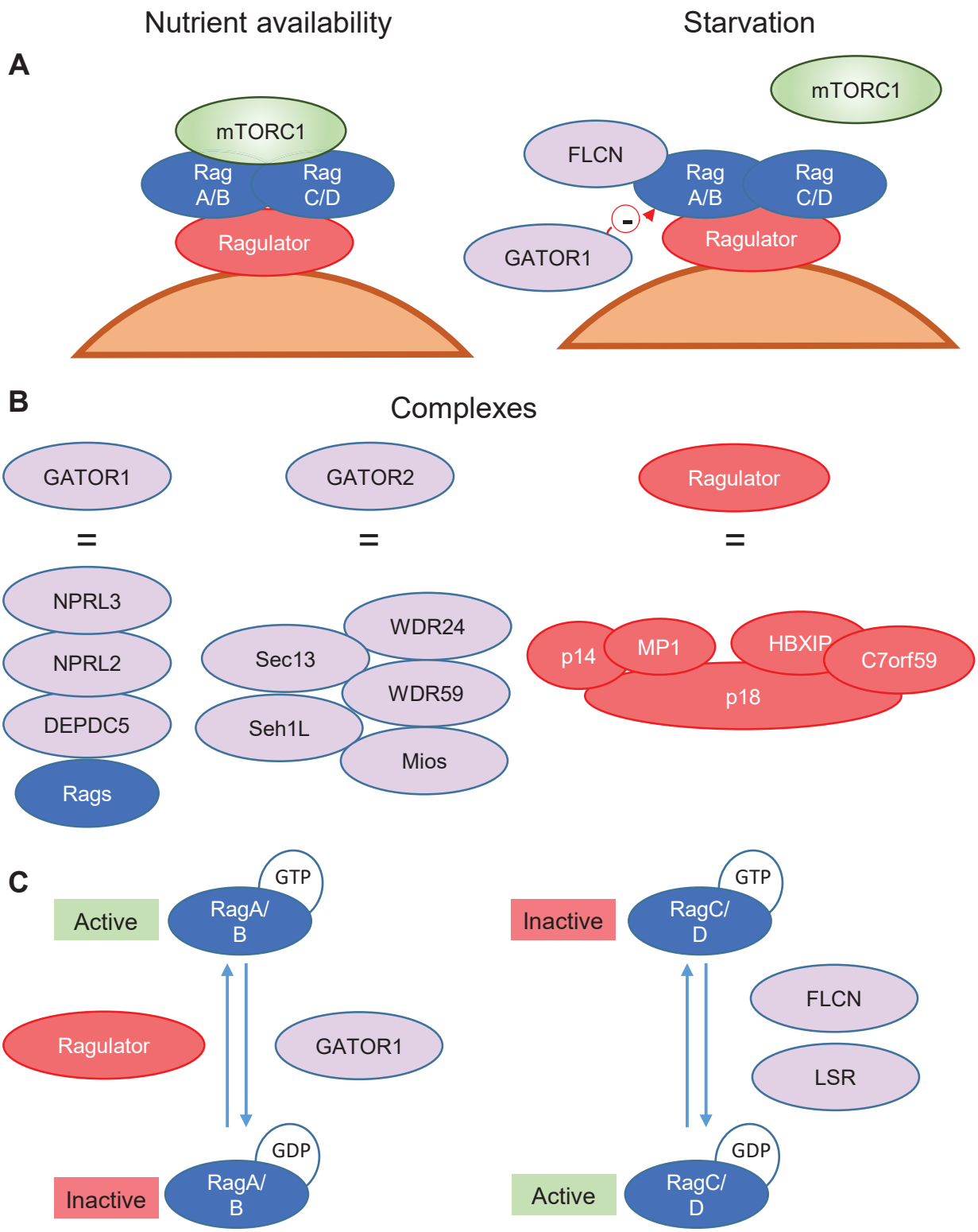

Figure 1.3: Schematic of GATOR1, GATOR2 and Ragulator.
(A) Schematic representation of how GEFs interact with Rag-GTPases dependent upon nutrient status. FLCN binds to RagA/B during starvation, enabling it rapidly to act as a GAP for RagC/D upon nutrient replenishment. **(B)** Note aliases for Ragulator components frequently used in the literature are as follows: LAMTOR1 (p18), LAMTOR2 (p14), LAMTOR3 (MP1), LAMTOR4 (C7orf59), LAMTOR5 (HBXIP). **(C)** Identified GEF (Ragulator) and GAPs (LSR, FLCN, GATOR1) for Rag-GTPases. The active Rag heteroduplex consists of RagA/B^{GTP},RagC/D^{GDP}, whilst the inactive Rag heteroduplex consists of RagA/B^{GDP},RagC/D^{GTP}.

activation (Figure 1.3). Curiously different substrates of mTORC1 appear to be differentially regulated by Folliculin, since 4E-BP1 is not dephosphorylated by FLCN siRNA, whilst S6K and TFEB are (Petit, Roczniak-Ferguson and Ferguson, 2013).

There are two GATOR (GAP activity towards Rags) complexes. GATOR1 consists of: DEPDC5, NPRL2 and NPRL3. DEPDC5 directly interacts with RagA/B and is responsible for GAP activity of the GATOR1 complex towards RagA/B (Bar-Peled *et al.*, 2013). In cells expressing DEPDC5 shRNA, mTOR was localised to the lysosomes regardless of nutrient availability (Bar-Peled *et al.*, 2013). GATOR2, which inhibits GATOR1, consists of: Seh1L, Sec13, Wdr24, Wdr59 and Mios. These interact with the sestrins, which inhibit mTORC1 in response to amino acid deprivation (Chantranupong *et al.*, 2014). It has been proposed that sestrin2 acts as a direct leucine sensor, whereby the presence of leucine disrupts the sestrin2-GATOR2 interaction (Wolfson *et al.*, 2016). This has been suggested to be a cell line-dependent mechanism, where in other cell lines, like HeLa, leucine deprivation is proposed to signal through the metabolite intermediate Acetyl-CoA, whereby reduced Acetyl-CoA results in less acetylation of RAPTOR and lower mTORC1 activity (Son *et al.*, 2019). Overall, GATOR complexes are responsible for signalling amino acid availability to mTORC1 activation. In addition, GATOR components have also been implicated in mTORC1-independent roles; for example, Wdr24-/- cells exhibit reduced lysosomal proteolytic activity (Cai *et al.*, 2016). Curiously, as far as I am aware, no post-translational modifications of GATOR1 or GATOR2 components have been reported. Phosphorylation of DEPDC5 (and GATOR2 components) has been detected in multiple mass spectrometry screens (i.e S1530, source: phosphositeplus), suggesting this may be an interesting line of enquiry. Overall, GEFs and GAPs are critical to regulating the activity state of Rag-GTPases in response to amino acid availability (diagrammatically represented in Figure 1.3)

In contrast to leucine sensing by Sestrins, which likely occurs in the cytosol, arginine sensing is proposed to occur via the amino acid transporter SLC38A9 in the lysosomal lumen (Wang *et al.*, 2015). This appears to be both via a direct mechanism, whereby SLC38A9 binds to Rag-GTPases, and an indirect mechanism, with arginine required for SLC38A9 mediated efflux of amino acids (including leucine) from the lysosome to the cytosol (Wyant *et al.*, 2017). Furthermore, SLC38A9 interacts with the vacuolar H+ ATPase (Wang *et al.*, 2015), and mTORC1 activity is promoted by the vacuolar H+ ATPase through its interaction with Ragulator in an amino acid-dependent manner (Zoncu *et al.*, 2011). Furthermore, cytosolic sensing of arginine by the CASTOR1 protein, which interacts with GATOR2, also activates mTORC1 in a parallel pathway to SLC38A9 (Chantranupong *et al.*, 2016). Challenging the hypothesis that arginine regulates mTORC1 activity through

Rag-GTPases, Carroll and colleagues found that arginine deprivation had no effect on mTORC1 localisation (Carroll *et al.*, 2016). Instead, they proposed that arginine prevented TSC2 localisation to the lysosomes thereby enabling maximal growth factor signalling to mTORC1 via Rheb (Carroll *et al.*, 2016). Overall, it is likely that leucine and arginine sensing to mTORC1 occurs via multiple redundant mechanisms. The reason for this is unclear. It may be that these sensing pathways mediate distinct additional mTORC1-independent effector mechanisms, or it may be an intended redundancy to enable continued signalling in case of a pathway becoming disabled.

1.3.1.4 mTORC1 activity is also modulated by RAPTOR post-translational modifications

RAPTOR is a specific component of the mTORC1 complex, and as a result, offers a selective way of modulating mTORC1 activity. RAPTOR is regulated by a multitude of phosphorylation events in response to various stimuli such as amino acids and epidermal growth factor (EGF) (Foster *et al.*, 2010). Several kinases have been implicated including AMPK (Gwinn *et al.*, 2008), CDK1 (Gwinn, Asara and Shaw, 2010), PLK1 (Ruf *et al.*, 2017), RSK1/2 (Carrière *et al.*, 2008), ERK1/2 (Carriere *et al.*, 2011), JNK1/2 (Kwak *et al.*, 2012), p38β (Wu *et al.*, 2011), GSK3 (Stretton *et al.*, 2015), ICK (Wu *et al.*, 2012) and ULK1 (Dunlop *et al.*, 2011). In addition to the text below, a table with all known RAPTOR phosphorylation sites is outlined (Table 1.1) and diagrammatically represented in Figure 1.4. AMPK phosphorylates RAPTOR at S722 and S792 to inactivate mTORC1 by promoting the RAPTOR:14-3-3 interaction. The phosphorylation of RAPTOR by CDK1 is discussed extensively in Section 1.7.2. ULK1 phosphorylates RAPTOR at S792, S855, S859, S863 and S877 preventing substrate binding to mTORC1 and thereby inhibiting mTORC1 signalling, effectively acting as a positive feedback loop (Dunlop *et al.*, 2011), though a separate group suggested that ULK1 inhibited mTORC1 kinase activity (Jung *et al.*, 2011). Intestinal Cell Kinase (ICK) phosphorylates Raptor at T906. Whilst mutation of T906 impaired mTORC1 activation in response to insulin, the phosphorylation itself was not modified by insulin, suggesting basal T906 phosphorylation was important for mTORC1 activity though the mechanism is not understood (Wu *et al.*, 2012). GSK3 phosphorylates RAPTOR at S859; unlike other kinases which regulate RAPTOR, this promotes RAPTOR binding to mTOR and thereby stimulates mTORC1 activity (Stretton *et al.*, 2015). PLK1 hyperphosphorylation of RAPTOR has been proposed to mediate mTORC1 dissociation from the lysosomes during interphase, resulting in its inactivation (Ruf *et al.*, 2017); however, it has also been shown that overexpression of constitutively active PLK1 in HCT116 cells results in increased mTORC1 activity, though via an unknown mechanism (Renner *et al.*, 2010). The PLK1-targeted sites on RAPTOR are currently unidentified.

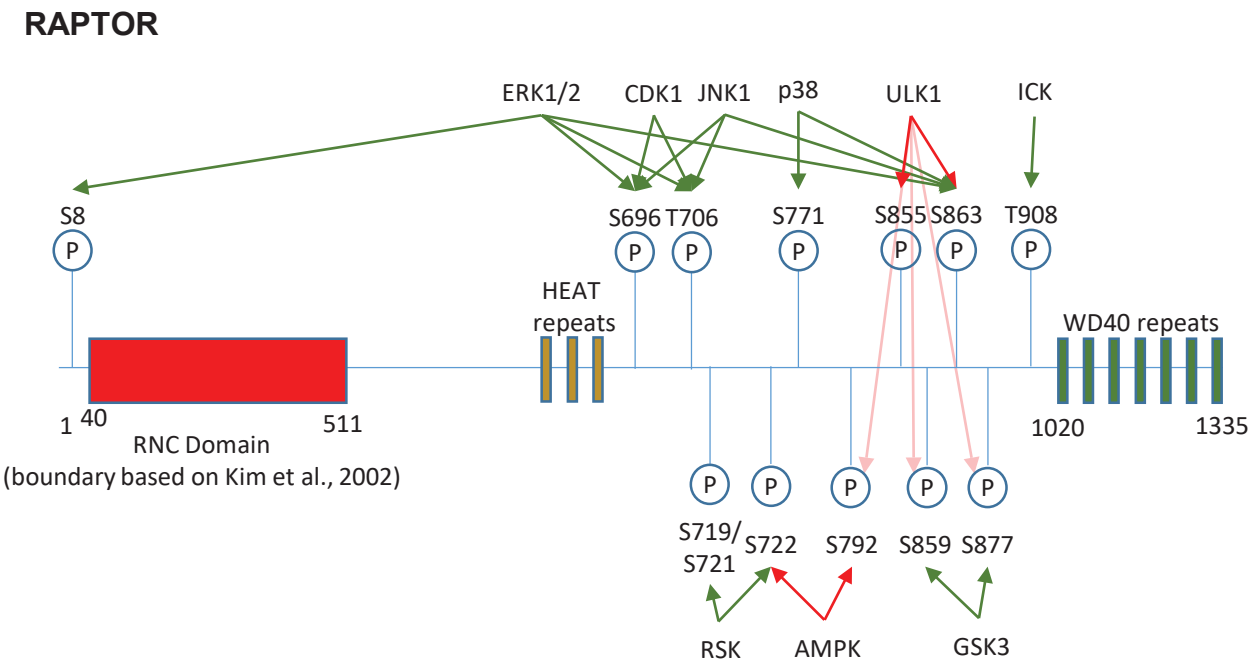

Figure 1.4: Schematic representation of key domains and regulatory sites on RAPTOR. RAPTOR (Uniprot identifier: Q8N122-1) consists of three core domains: RNC (Raptor N-terminal conserved), HEAT repeats (also referred to as the armadillo domain) and WD40 repeats (which forms a β-propeller structure). Between the HEAT repeats and WD40 repeats lies a region where the vast majority of regulatory phosphorylation events occur.

It has been argued that S863 functions as a master site of mTORC1 activity, by enabling subsequent hierarchical phosphorylation (i.e. S855 and S859). For example, GSK3-catalysed phosphorylation of S859 is dependent upon S863 phosphorylation (Stretton *et al.*, 2015). However, it is notable that both phosphorylation of 4E-BP1 and S6 are robust, albeit slightly reduced, after a mutation to alanine of this site (Foster *et al.*, 2010). Furthermore, upstream regulators of RAPTOR that inactivate mTORC1 activity, such as ULK1, also phosphorylate RAPTOR at S863 (Dunlop *et al.*, 2011), suggesting it is not a clear predictive marker of mTORC1 activity.

The MAPK kinase pathways are also heavily implicated in the phosphorylation of RAPTOR. Curiously, these do not impact mTORC1 activity in response to amino acids or insulin, but rather are induced by select stimuli, such as phorbol 13-myristate 12-acetate (PMA). ERK1/2 phosphorylates RAPTOR at S8, S696 and S863 to stimulate mTORC1 activity in response to PMA (Carriere *et al.*, 2011), whilst the ERK1/2 substrate RSK1/2 phosphorylates RAPTOR at S719, S721 and S722, also stimulating mTORC1 activity in cells. JNK, like ERK1/2, also phosphorylates RAPTOR at S696 and S863, in addition to T706, to stimulate mTORC1 activity in cells in response to osmotic stress (sorbitol treatment) (Kwak *et al.*, 2012). p38β, selectively in response to arsenite, phosphorylates RAPTOR at S771 and S863, which in common with the other MAPK pathways stimulates mTORC1 activity (Wu *et al.*, 2011). Overall, some phosphorylation sites, such as S722 and S863 are implicated in both mTORC1 activation and inhibition, suggesting that their effect is mediated in combination with other sites (Table 1.1). Thus, multisite phosphorylation of RAPTOR acts as a critical point, integrating a plethora of upstream signals to mTORC1. This complexity in multi-site phosphorylation must be considered when evaluating the effects of site-directed mutants.

All of the currently identified RAPTOR phosphorylation sites, with the exception of S8, occur in the linker region between the armadillo domain (HEAT repeats) and WD repeats (Aylett *et al.*, 2016) (Figure 1.4). The formation of the mTORC1 complex requires the interaction between the armadillo domains of both RAPTOR and mTOR (Aylett *et al.*, 2016). Apart from GSK3, no regulatory phosphorylation has been directly implicated in altering the RAPTOR:mTOR interaction. It is unclear how a majority of phosphorylation events regulate mTORC1 activity; though, it is clear that the region between the armadillo domain and WD repeats plays a critical role.

Phosphosite	Kinase	Effect
S8	ERK1/2	Activating
S696	CDK1	Activating (proposed)
	ERK1/2	Activating
	JNK1/2	Activating
T706	CDK1	Activating (proposed)
	JNK1/2	Activating
S719	RSK1/2	Activating
S721	RSK1/2	Activating
S722	AMPK	Inactivation
	RSK1/2	Activating
	Mitotic (not proline directed)	Activating (proposed)
S771	p38β	Activating
S792	AMPK	Inactivation
	ULK1	Inactivation
S855	Mitotic (not proline directed)	Activating (proposed)
	ULK1	Inactivation
S859	Mitotic (not proline directed)	Activating (proposed)
	ULK1	Inactivation
	GSK3	Activating
S863	Mitotic (proline directed)	Activating (proposed)
	ERK1/2	Activating
	JNK	Activating
	p38β	Activating
	ULK1	Inactivation
S877	Mitotic (proline directed)	Activating (proposed)
	ULK1	Inactivation
	GSK3	Activating
T908	ICK	Activating

Table 1.1: RAPTOR is phosphorylated at multiple sites.

Known RAPTOR phosphorylation sites are listed with the respective kinase known to catalyse it. Where the direct kinase is not known for mitotic phosphorylation events, this is annotated with mitotic and whether the site is proline-directed or not.

1.3.1.5 mTOR phosphorylation

mTOR is known to be phosphorylated at multiple sites, but this depends upon which complex mTOR is in. mTOR autophosphorylation at S2481 is mainly attributed to mTORC2 but is also present in mTORC1 (Copp, Manning and Hunter, 2009). S6K phosphorylates mTOR at S2448 (Chiang and Abraham, 2005; Holz and Blenis, 2005), and this appears to be specific to mTORC1 (Copp, Manning and Hunter, 2009). The functional effect of S2448 phosphorylation on mTORC1 is unclear and site-directed mutagenesis has no effect on mTORC1 activity (as assessed by p70 S6K phosphorylation) (Sekulić *et al.*, 2000). Phosphorylation of mTOR at S1261 has been shown to increase mTORC1 activity, though the kinase responsible remains unidentified (Acosta-Jaquez *et al.*, 2009). It has been suggested that DYRK2 phosphorylates mTOR at T631 to promote its degradation via the proteasome (Mimoto *et al.*, 2017). IKKα has been shown to phosphorylate mTOR at S1415, increasing mTORC1 kinase activity yet promoting the dissociation of RAPTOR (Dan *et al.*, 2014). Overall, whilst it is known that mTOR is phosphorylated, and some mechanisms have been elucidated, it is poorly understood relative to RAPTOR.

1.3.1.6 mTORC2 regulation

Both the regulation and function of mTORC2 is poorly understood relative to mTORC1. mTORC2 is independently regulated to mTORC1, for example, Ragulator is not required for mTORC2 activity but is required for mTORC1 (Sancak *et al.*, 2010). mTORC2 is activated in a PI3K class I-dependent manner but the mechanism is not understood. Whilst the mTORC2 specific component mSin1 contains a PH domain, this appears not to be required for mTORC2 activity and mediates recruitment to the plasma membrane in a PIP_3-independent manner (Ebner *et al.*, 2017). mTORC2 is regulated by negative-feedback with AKT-dependent phosphorylation of the mTOR kinase domain at T2173 impairing mTORC2 kinase activity (Hálová *et al.*, 2013). Likewise, S6K phosphorylates RICTOR at T1135, which impairs mTORC2 phosphorylation of AKT at S473 (Dibble, Asara and Manning, 2009).

A few substrates have been identified for mTORC2. The most well characterised is that mTORC2 phosphorylates AKT at S473 increasing its activity (Sarbassov *et al.*, 2005). Another example of an mTORC2 substrate is SGK1, where mTORC2 catalyses phosphorylation at S422 (García-Martínez and Alessi, 2008). Importantly, Garcia-Martinez and Alessi's study verified that mTORC1 did not phosphorylate SGK1 as had been originally proposed (Hong *et al.*, 2008).

1.3.1.7 mTORC1 regulates translation through phosphorylation of S6K and 4E-BP1

mTORC1 regulation of translation is primarily regulated through its phosphorylation of S6K and 4E-BP1. Both of these substrates have a Tor signalling motif (TOS) which consists of 5 amino acids absolutely required for their mTORC1-dependent phosphorylation (Schalm and Blenis, 2002). Curiously, neither ATG13 or ULK1 appear to have conserved TOS motifs (Hosokawa, Hara, *et al.*, 2009) and there is no identified TOS motif for TFEB either. TOS motifs are loosely conserved throughout evolution, though some variability is observed. For example, the human S6K TOS motif is FDIDL whilst in Drosophila S6K it is FDLEL (Schalm and Blenis, 2002). It appears that TOS motifs may be required for RAPTOR binding, since mutation of TOS motifs impairs the mTORC1:4E-BP1 and mTORC1:S6K interactions (Nojima *et al.*, 2003), though curiously this does not prevent phosphorylation of 4E-BP1 at T37/46 (Beugnet, Wang and Proud, 2003). PRAS40 also contains a TOS motif, and it is argued that it directly inhibits mTORC1 phosphorylation of S6K and 4E-BP1 by competing with these substrates for RAPTOR binding via the TOS motif (Wang *et al.*, 2007). Phosphorylation of PRAS40 at S183 by mTORC1 promotes the dissociation of PRAS40 from RAPTOR, enabling mTORC1 to then interact with and phosphorylate S6K and 4E-BP1 (Oshiro *et al.*, 2007). Curiously, the structural assessment of Raptor's RNC (RAPTOR N-terminal conserved) domain found marked similarities with Caspases, and it is speculated this may enable recognition of TOS domains since caspases recognise four-residue sequences with an aspartic acid at position four (Aylett *et al.*, 2016). As far as I am aware, how mTORC1 interacts with other substrates which do not have a TOS motif is not understood, and it has not been evaluated if PRAS40 inhibits phosphorylation of ATG13, ULK1 and TFEB. Wang and Proud speculated in a review that since T37/46 phosphorylation was dependent upon an N-terminal RAIP motif in 4E-BP1, but was not dependent on the C-terminal TOS motif (Beugnet, Wang and Proud, 2003), that the TOS motif was only important in rapamycin-sensitive phosphorylation events (Wang and Proud, 2011). Indeed, the phosphorylation of ULK1 and TFEB are both insensitive to rapamycin, supporting this hypothesis.

4E-BP1 binds to and inhibits the action of eIF4E, thereby preventing its involvement in cap-dependent translation (Gingras *et al.*, 1996). eIF4E, in complex with eIF4G, eIF4A and eIF4F, binds to the 5'-caps of mRNAs, which enables the 40S subunit of the ribosome to correctly identify the AUG start codon (reviewed: Sonenberg and Hinnebusch, 2009). Therefore, eIF4E regulates a number of cap-dependent genes required for cell proliferation such as cyclin D1 (Rosenwald *et al.*, 1993). mTORC1 phosphorylation of 4E-BP1 occurs at T37, T46, S65 and T70 (Brunn *et al.*, 1997; Mothe-Satney *et al.*, 2000). The current model

suggests that S65 and T70 are primed by T37 and T46 phosphorylation (Gingras *et al.*, 1999). These phosphorylation events cause dissociation of 4E-BP1 from eIF4E, enabling cap-dependent translation to proceed. 4E-BP1 is also phosphorylated at S101 by an unknown kinase which does not respond to insulin stimulation or mTOR inhibition, and this acts as a priming site for S65 phosphorylation (Wang *et al.*, 2003).

S6K phosphorylation impacts translation through several pathways. Like 4E-BP1, it too is implicated in cap-dependent translation and the overexpression of S6K stimulates cap-dependent translation, whilst a T389A mutant impairs it (Holz *et al.*, 2005). S6K phosphorylates eIF4B at S422, enabling its recruitment into the 7-methylguanosine cap complex (Holz *et al.*, 2005). In addition, S6K is implicated in ribosomal biogenesis. S6K catalyses phosphorylation of the 40S ribosomal protein S6 at several residues (S235, S236, S240, S244 and S247) (Krieg, Hofsteenge and Thomas, 1988). Furthermore, S6K phosphorylates eukaryotic elongation factor 2 kinase (eEF2k), resulting in eEF2k inactivation and eEF2 dephosphorylation (Wang *et al.*, 2001), where eEF2 phosphorylation usually represses general translation (Redpath *et al.*, 1993).

1.3.2 The PI3K/AKT/mTORC1 signalling axis is the master regulator of autophagy initiation

mTORC1 is widely viewed as the master repressor of autophagy, with only its phosphorylation of DAP1 shown to upregulate autophagy as part of a negative feedback loop (Koren, Reem and Kimchi, 2010). mTOR has been shown to phosphorylate and repress ULK1 (Kim *et al.*, 2011), ATG13 (Jung *et al.*, 2009; Puente, Hendrickson and Jiang, 2016), ATG14 (Yuan, Russell and Guan, 2013), AMBRA1 (Nazio *et al.*, 2013) and TFEB (Martina *et al.*, 2012; Settembre *et al.*, 2012) in nutrient-rich conditions. mTOR phosphorylates ULK1 on S758 (S757 in the mouse) (Kim *et al.*, 2011), preventing ULK1's association with AMPK, and delaying the autophagic response to nutrient starvation (Shang *et al.*, 2011). Loss of this phosphorylation promotes a rapid rise in ULK1 activity upon starvation due to AMPK phosphorylation (Kim *et al.*, 2011). Furthermore, it has been suggested that mTOR phosphorylation of ULK prevents its targeting to membrane organelles, with sequestration in the cytosol (Jung *et al.*, 2009). The extent to which ULK1 and ULK2 individually contributes to starvation-induced autophagy is debated, though it is generally accepted there is redundancy between them in activating starvation-induced autophagy (Alers *et al.*, 2011; McAlpine *et al.*, 2013). Combined loss of ULK1/2 completely impairs starvation-induced autophagy (McAlpine *et al.*, 2013). Upstream of mTORC1, AKT also phosphorylates ULK1 at S774 (Bach *et al.*, 2011), though any direct functional consequence of this phosphorylation is unclear. Finally, AMBRA1 interacts with the

ubiquitin ligase TRAF6, where the AMBRA1-TRAF6 interaction promotes ULK1 ubiquitylation, leading to ULK1 self-association and increased kinase activity (Nazio et al., 2013). mTORC1 phosphorylation of AMBRA1 at S52 prevents AMBRA1's ability to promote ULK1 Lys-63-linked ubiquitylation (Nazio *et al.*, 2013).

The effect of ATG13 phosphorylation by mTOR is suggested to be species dependent. In *Saccharomyces cerevisiae*, it was observed that Tor-mediated hyperphosphorylation of ATG13 prevented its association with ATG1 (Kamada *et al.*, 2000); however, more recent evidence suggests that the ATG1-ATG13 complex is constitutively formed regardless of Tor activity (Kraft *et al.*, 2012). In mammals, a stable ULK1-ATG13 complex is present even in nutrient sufficient and mTOR active conditions (Hosokawa et al. 2009). There is only a 16% sequence homology between mammalian and yeast ATG13 (Hosokawa et al. 2009). ATG13 is critical for starvation-induced autophagy (Alers *et al.*, 2011; McAlpine *et al.*, 2013). The presence of ATG13 stabilises ULK1, and knockdown of ATG13 leads to a significant decrease in ULK1 protein levels in HeLa cells (Jung *et al.*, 2009). mTOR phosphorylation of ATG13 at S258, in combination with an AMPK-mediated phosphorylation at S224, leads to a decrease in ULK1 activity (Puente, Hendrickson and Jiang, 2016). It has been shown that inhibition of mTOR leads to an increase in ATG13 puncta and this correlates with other members of the ULK1 complex (Karanasios *et al.*, 2013).

mTORC1's direct phosphorylation of ATG14 is poorly characterised relative to other substrates. Five sites were identified that mTORC1 could phosphorylate *in vitro*: S3, S223, T233, S383 and S440. Whether all these sites were phosphorylated in cells was not established (Yuan, Russell and Guan, 2013). Regardless, mutation of these sites led to an increase in VPS34 activity in cells, suggesting that mTORC1 directly represses VPS34 complex I (Yuan, Russell and Guan, 2013). mTORC1 has also been implicated in the repression of the VPS34 complex II via direct phosphorylation of UVRAG at S498, promoting VPS34 complex II interaction with the negative interactor RUBICON (Kim *et al.*, 2015).

Lysosomal biogenesis is stimulated through TFEB nuclear localisation upon loss of mTOR signalling (Martina *et al.*, 2012; Settembre *et al.*, 2012; Zhou *et al.*, 2013) (Section 1.4.2.1). mTOR inactivation appears necessary but not sufficient for lysosomal biogenesis, as ATG5$^{-/-}$ MEFs display no cathepsin B or L activation upon treatment with mTOR inhibitors (Zhou *et al.*, 2013). Whilst TFEB nuclear localisation is required for cathepsin B and L activation, TFEB activity is not affected in ATG5$^{-/-}$ MEFs suggesting these are two separate phenomena and that autophagic machinery is required for lysosomal activation (Zhou *et*

al., 2013). A summary of how mTORC1 mediates an overarching control of all stages of the autophagy process is provided in Figure 1.2. An overview of known phosphorylation events regulating ATG13, ULK1 and TFEB is provided in Figure 1.5.

mTORC1 primarily stimulates anabolic processes, but when amino acids are depleted and mTORC1 inactivated, it mediates the initiation of catabolic processes to achieve a homeostatic replenishment of amino acids. This replenishment of amino acids via macroautophagy after prolonged starvation appears to be sufficient to reactivate mTORC1, though this process is dependent upon provision of glutamine (Tan, Sim and Long, 2017).

Despite mTORC1 phosphorylating all of its known substrates in an amino acid-dependent manner, there is evidence of differential regulation between substrates. The clearest example of this is the sensitivity of mTORC1 substrate phosphorylation to rapamycin (Kang *et al.*, 2013). There may also be differences in where mTORC1 phosphorylates its substrates. Phosphorylated 4E-BP1 does not reside at the lysosomes *in vivo*, suggesting it is phosphorylated after mTORC1 activation at the lysosome (Manifava *et al.*, 2016). By contrast, TFEB must localise to the lysosome to be phosphorylated by mTORC1 (Roczniak-Ferguson *et al.*, 2012). Clearer evidence is required to definitively come to any conclusion.

1.3.3 AMPK signalling

AMPK (5' adenosine monophosphate-activated protein kinase) is a heterotrimer consisting of two regulatory subunits (β and γ) and one catalytic subunit (α). LKB1 activates AMPKα by catalysing its phosphorylation at T172 (Hawley *et al.*, 2003; Hong *et al.*, 2003). AMP binds to the γ regulatory subunit which stimulates the T172 phosphorylation, whilst ADP inhibits the T172 phosphatase PP2c (Oakhill *et al.*, 2010, 2011). As such, AMPK is a nutrient-dependent kinase, being activated directly by alterations in cellular AMP/ATP and ADP/ATP ratios.

AMPK also has considerable crosstalk with mTORC1. AKT directly phosphorylates AMPKα at S485, leading to decreased T172 phosphorylation (Horman *et al.*, 2006). AMPK phosphorylates TSC2, stimulating its activity and repressing mTORC1 activity (Inoki, Zhu and Guan, 2003). AMPK also directly represses mTORC1 via its multisite phosphorylation of RAPTOR (Gwinn *et al.*, 2008). An overview of how mTOR and AMPK crosstalk regulates autophagy is provided in Figure 1.2.

AMPK both directly and indirectly interacts with autophagic machinery. AMPK upregulates ULK1 activity via multisite phosphorylation (Bach *et al.*, 2011; Kim *et al.*, 2011);

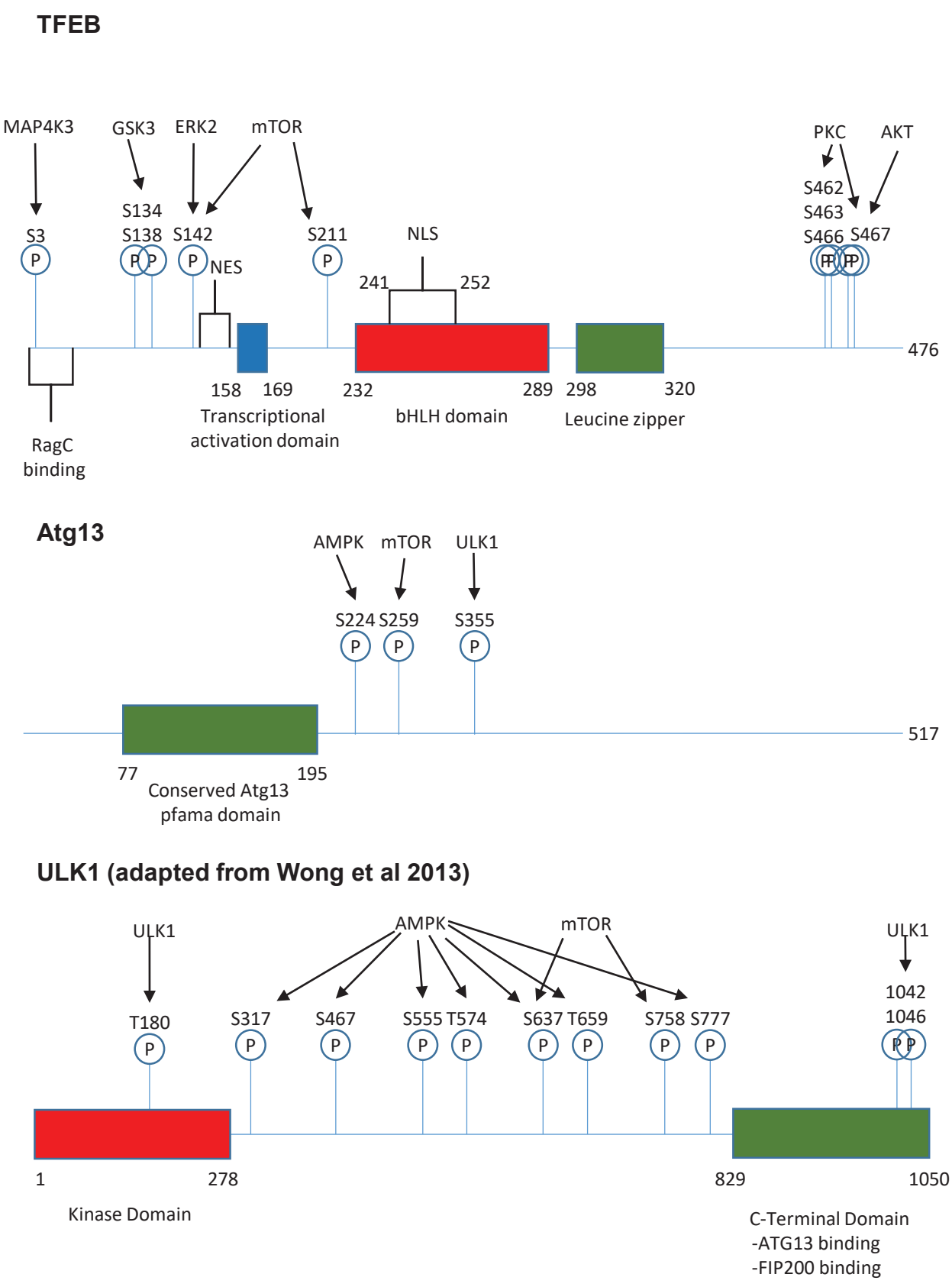

Figure 1.5: Schematic representation of key domains and regulatory sites on ATG13, ULK1 and TFEB.
Schematics for TFEB (Uniprot identifier: P19484), ATG13 (Uniprot identifier: O75143-1) and ULK1 (Uniprot identifier: O75385-1) are provided. For TFEB, NLS = Nuclear localisation signal. NES = Nuclear export signal and is between amino acids 140-149.

with S555 mediating its interaction with 14-3-3 chaperone protein (Bach *et al.*, 2011). AMPK also directly phosphorylates Beclin1 at S91/94 to mediate activation of the ATG14-containing VPS34 complex. It also catalyses phosphorylation of T163/165 on VPS34 to mediate the inhibition of non-autophagic VPS34 complexes (Kim *et al.*, 2013). AMPK has been shown to be important for autophagy signalling in select circumstances, such as bacterial invasion by *Salmonella enterica* (Losier *et al.*, 2019). Curiously, AMPK-mediated signalling has been suggested to promote repressive phosphorylation of ATG13 at S224 (Puente, Hendrickson and Jiang, 2016). The authors speculate that whilst AMPK has generally been shown to stimulate autophagy, repressive phosphorylation of ATG13 may enable 'fine-tuning' of this response (Puente, Hendrickson and Jiang, 2016).

1.3.4 GSK3 signalling

GSK3 exists as two isoforms (α and β) and is ubiquitously expressed (reviewed: Cormier and Woodgett, 2017). The most well characterised pathway involving GSK3 is the Wnt signalling pathway. Wnt ligand binding to its receptor leads to inactivation of GSK3, preventing its multisite phosphorylation of β-catenin (Aberle *et al.*, 1997). This phosphorylation event also demonstrates another property of GSK3, its need for a priming phosphorylation at the +4 position, since CK1 phosphorylation of β-catenin at S45 is required of GSK3 phosphorylation at S41,37,33 (Amit *et al.*, 2002; Liu *et al.*, 2002).

1.3.4.1 Links between GSK3 and mTORC1

GSK3 phosphorylates RICTOR at two sites. S1235 phosphorylation during ER-stress impairs mTORC2 kinase activity (Chen *et al.*, 2011); whilst T1695 phosphorylation, located within a CDC4 Phospho-degron, enables FBXW7-mediated ubiquitination and subsequent RICTOR degradation (Koo *et al.*, 2015). GSK3 phosphorylates TSC2 at multiple sites, promoting its activation and subsequent inhibition of mTORC1 signalling (Inoki *et al.*, 2006). Conversely, GSK3 is phosphorylated by AKT at GSK3α (S21) and GSK3β (S9) to mediate its inactivation (Cross *et al.*, 1995), and GSK3 is inactive in response to insulin (Ding, Chen and McCormick, 2000). GSK3 has also been suggested to enhance mTORC1 activity via RAPTOR phosphorylation (Stretton *et al.*, 2015) and GSK3 overexpression has been shown to stimulate mTORC1 (Azoulay-Alfaguter *et al.*, 2015). mTORC1 has also been implicated in the localisation of GSK3β, with inhibition of mTOR leading to GSK3 nuclear localisation (Bautista *et al.*, 2018).

1.3.5 MAPK signalling

The MAPK (Mitogen-activated protein kinase) family is a highly conserved group of proline-directed serine/ threonine kinases. MAPK signalling cascades classically consist of three tiers: MAPK, MAPKK and MAPKKK. Three main groupings of MAPK exist (reviewed:

Johnson and Lapadat, 2002): ERK (Extracellular Signal-Regulated Kinase), which consists of ERK1/2 and ERK5, and is primarily involved in cell responses to growth factor stimulation; JNK (Mitogen-activated protein kinase 8) and p38 (p38 MAPK). JNK and p38 are involved in stress responses (reviewed: Roskoski, 2012), and they also regulate a plethora of other responses such as integrin signalling and interleukin response (reviewed: Johnson and Lapadat, 2002). ERK1/2 represents the best characterised of the ERK group and are activated downstream of the RAS-RAF-MEK pathway. This pathway has a prominent role in cell proliferative signalling, and components are frequently mutated in cancer (Dhillon *et al.*, 2007). Classically depicted as a linear pathway it also consists of a number of negative feedback mechanisms, such as the family of DUSPs (Dual-specificity phosphatases), that enable intrinsic re-activation of the pathway upon loss of ERK1/2 signalling (reviewed: Caunt *et al.*, 2015). These mechanisms are diagrammatically summarised in Figure 1.6.

The RAS GTPase family, of which there are four proteins (*HRAS, NRAS, KRAS4A* and *KRAS4B*), are well characterised activators of the ERK1/2 signalling cascade (reviewed: Pylayeva-Gupta, Grabocka and Bar-Sagi, 2011). Receptor tyrosine kinase (RTK) activation, as a result of ligand binding, promotes dimerization and trans-autophosphorylation. SH2 containing-proteins, of which GRB2 is a classic example, recognise phosphorylated tyrosine. GRB2 is in a preformed complex with the GEF SOS, mediating its recruitment to the membrane, which in turn activates RAS by maintaining it in a GTP bound state (reviewed: Kolch, 2000). Constitutive activation of RAS is frequently a result of mutation at Gly^{12}, which impairs binding of GAPs and prevents GTP hydrolysis (Scheffzek *et al.*, 1997). The RAF family (*ARAF, BRAF, CRAF*) of protein are activated by RAS^{GTP} binding to the inhibitory N-terminus of RAF, enabling recruitment of RAF to the plasma membrane. This stimulates multisite phosphorylation (reviewed: Wellbrock, Karasarides and Marais, 2004) and hetero/homodimerization (Weber *et al.*, 2001; Rushworth *et al.*, 2006). *BRAF* V600E is a highly prevalent mutation in cancer and enables RAS-independent activation of the ERK1/2 signalling cascade (H. Davies *et al.*, 2002). Activated RAF proteins then phosphorylate MEK1/2 at S218 and S222 (S222/S226 for MEK2), thereby activating them (Alessi *et al.*, 1994). MEK1/2 in turn phosphorylates and activates ERK1/2 at T202/Y204 (T185/Y187 for ERK2) in a hierarchical manner, whereby the tyrosine then threonine is phosphorylated (Haystead *et al.*, 1992). ERK1/2 can then phosphorylate a plethora of substrates, almost exclusively at serine/threonine proline-directed sites, a well-established example being RSK at T359 and T363 which mediates its activation (Dalby *et al.*, 1998). In addition, activated ERK1/2 translocates from the cytosol to the nucleus (Chen, Sarnecki and Blenis, 1992). Overall, ligand binding to growth factor

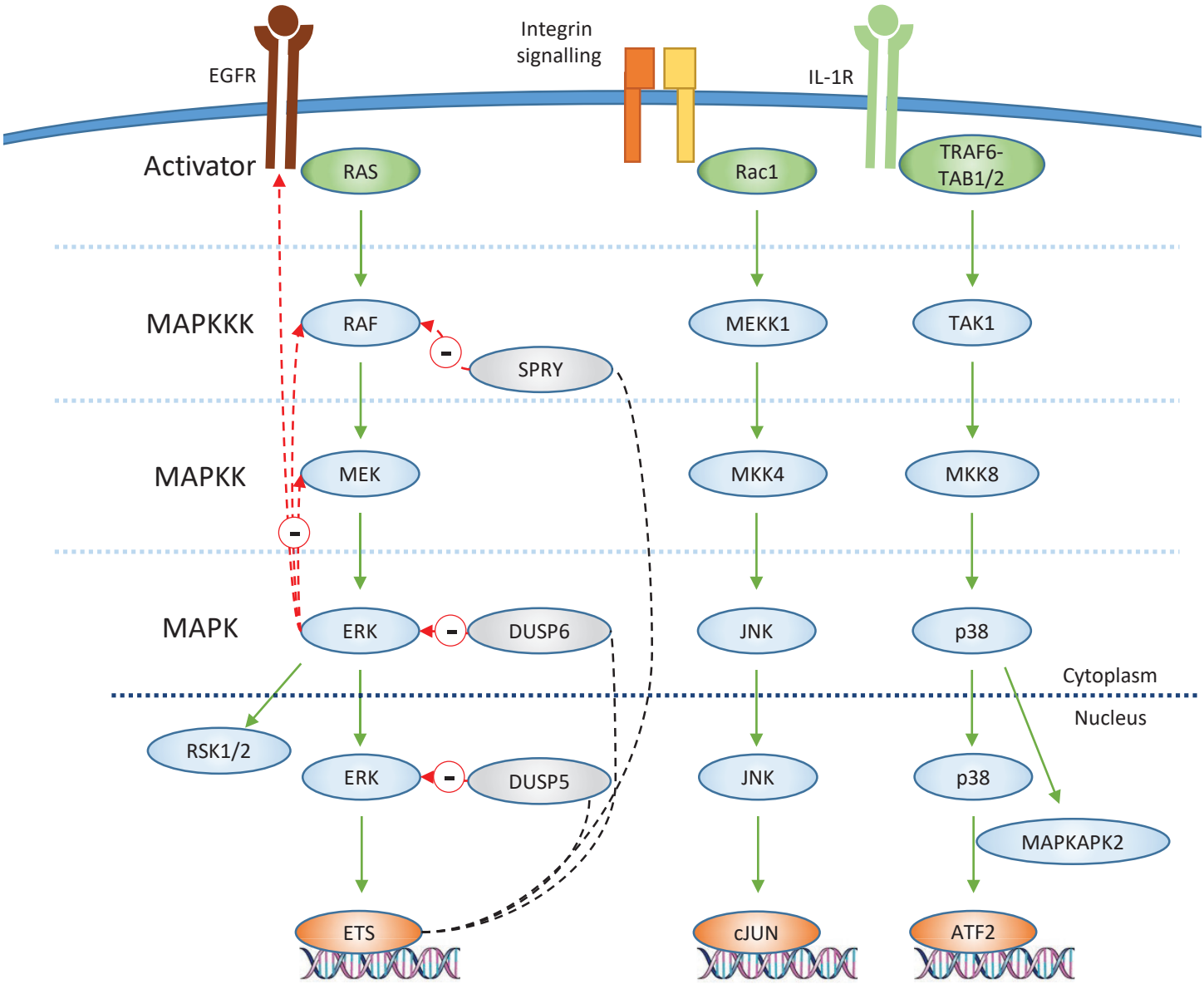

Figure 1.6: Schematic of MAPK signalling.
Schematic is modified from (Caunt et al., 2015) and (Johnson and Lapadat, 2002). For each of the three pathways, an example linear pathway is provided; however, there is a large diversity of pathways that feed into the MAPKs, with differing degrees of cross-talk. EGFR= Epidermal Growth Factor Receptor; IL-1R = Interleukin-1 receptor.

receptors mediates receptor tyrosine kinase activation which triggers the activation of the ERK1/2 signalling cascade.

The role of the ERK1/2 kinases in autophagy is relatively ambiguous. There is limited evidence to suggest that the ERK1/2 pathway promotes autophagy. ERK1/2 pathway activation in HR1 cells (HEK293 with an inducible *ΔCRAF:ER*) significantly increased LC3B and SQSTM1/p62 levels at the mRNA and protein levels over 48 hours of 4-HT treatment (Kim *et al.*, 2014). The transcription factor cAMP response element-binding protein (CREB), which can be activated by ERK1/2 signalling (Impey *et al.*, 1998), upregulates a number of autophagic genes, including TFEB, in ChIP-seq (Chromatin Immunoprecipitation-sequencing) experiments (Seok *et al.*, 2014). Ultimately, dissecting the involvement of ERK1/2 regulation of autophagy from other pathways is complicated, as evidenced by BRAF inhibition in *BRAF* V600E colorectal cancer lines promoting autophagy through an AMPK dependent mechanism as a result of p90RSK phosphorylation of LKB1 (Sueda *et al.*, 2016).

The p38 and JNK pathways, classically seen as stress responders, have also been implicated in autophagy regulation in a context-dependent manner. p38 inhibition or knockdown in gastrointestinal cell lines promotes vacuolisation, with electron microscopy showing evidence of autophagosome formation which is inhibited by 3-methyladenine (3MA; pan-PI3K and autophagy inhibitor) co-treatment (Comes *et al.*, 2007). Curiously, in Comes' study, prevention of autophagy lead to an apoptotic response. The interplay between autophagy and apoptosis was further investigated in 5-Flurouracil (5-FU) treatment where p38 activity determines whether cells enter an apoptotic (p38 activation) or autophagic response (p38 inhibition) (de la Cruz-Morcillo *et al.*, 2012). Z-VAD-FMK, a broad-spectrum inhibitor of caspase activity and apoptosis, promoted an autophagic response to 5-FU in HCT-116 cells (de la Cruz-Morcillo *et al.*, 2012). ZKSCAN3 (Zinc finger protein with KRAB and SCAN domains 3) is a transcriptional repressor of autophagy and lysosomal biogenesis, opposing the action of TFEB (Chauhan *et al.*, 2013). JNK and p38 phosphorylate ZKSCAN3 promoting its cytoplasmic localisation, relieving its repression of autophagic genes (Li et al. 2016). Finally, JNK has been shown to phosphorylate the apoptosis regulator BCL2 preventing its association with Beclin1, enabling Beclin1 to carry out its autophagic role as part of the VPS34 complex (Wei *et al.*, 2008).

There are multiple mechanisms by which the ERK1/2 and mTORC1 signalling pathways interact. RAS activation is known to stimulate both the RAF/MEK/ERK and PI3K/AKT/mTOR signalling pathways. RAS co-immunoprecipitates with PI3K, and RAS overexpression in cells results in an increase in PIP_3 levels (Rodriguez-Viciana *et al.*, 1994).

Whilst PI3K is activated directly in response to RTK activation, which is mediated by p85 interaction with phosphotyrosine, RAS activates PI3K through interaction with the p110 catalytic domain (Pacold *et al.*, 2000). *PIK3CA* mutations represent an intrinsic resistance mechanism to MEK1/2 pathway inhibition in *KRAS* tumours, likely due to sustained cyclin D1 (Halilovic *et al.*, 2010). Our research group has found that SW620 cells which have acquired resistance to the mTOR inhibitor AZD8055 by upregulating eIF4E and maintaining cap-dependent translation (SW620:8055R), are cross-resistant to MEK1/2 pathway inhibition, where cyclin D1 levels were now more stable upon MEK1/2 inhibition (Cope *et al.*, 2014). Thus, PI3K and RAF, both effectors of RAS, can converge on the same downstream targets. In addition to RAS-mediated activation of PI3K, ERK1/2 and RSK1/2 directly phosphorylate RAPTOR to increase mTORC1 signalling, as discussed previously (Section 1.3.1.4). ERK1/2 phosphorylation of TSC2 at S664 promotes dissociation of TSC1/2 complex and activation of mTORC1 signalling (Ma *et al.*, 2005). In addition, RSK1/2 phosphorylates TSC2 at S1798 to inhibit its activity and promote mTORC1 signalling (Roux *et al.*, 2004). Furthermore, both the ERK1/2 and mTORC1 pathways feed into shared effector functions. RSK directly phosphorylates 40S ribosomal protein S6 (Roux *et al.*, 2007), and mice deficient in S6K1 and S6K2 still undergo phosphorylation of S235 and S236 which was abolished with the MEK inhibitor PD184352, showing that both the RSK and S6K pathways independently feed into translational control (Pende *et al.*, 2004). ERK1/2 phosphorylates and activates MNK1/2, which in turn phosphorylates eIF4E (the translation factor that 4E-BP1 interacts with) at S209 (Waskiewicz *et al.*, 1997). It has been shown that phosphorylation at S209 promotes dissociation of eIF4E from the RNA cap and it is speculated that this enables ribosome migration and translation initiation after it has completed its role in the eIF4F initiation complex (Scheper *et al.*, 2002).

1.3.6 Oncogene induced senescence and autophagy

Cells have an intrinsic tumour suppressor mechanism against oncogenic mutations within the MAPK cascade, in that they undergo senescence in response to chronic stimulation. This has been extensively studied using overexpression systems of the RAS oncoprotein in fibroblasts (Serrano *et al.*, 1997), but can also be observed in other settings such as drug-withdrawal from COLO205 cells which have been made resistant to AZD6244, such that they have amplification of the *BRAF* V600E oncoprotein (Sale *et al.*, 2019). Young and colleagues described how retroviral transduction of $HRAS^{V12}$ into IMR90 fibroblasts led to oncogene induced senescence (OIS), via an ATG5/ATG7-dependent mechanism (Young *et al.*, 2009). Supporting this data, Nam and colleagues demonstrated that chronic mTOR inhibition, stimulating autophagy, alongside radiation treatment was sufficient to induce increased levels of senescence (Nam *et al.*, 2013). Furthermore, knockdown of

ATG5 impaired oncogene induced senescence in melanocytes, induced by overexpression of $BRAF^{V600E}$ or $HRAS^{G12V}$ (Liu *et al.*, 2013). Explaining the paradoxical findings that autophagy is induced yet protein synthesis is maintained in senescent cells, mTOR was found to be localised to distinct compartments termed TOR-autophagy spatial coupling compartment (TASCC) separating active mTOR from the autophagy machinery (Narita *et al.*, 2011).

Curiously it has been shown that the E3 ubiquitin ligase STUB1 impairs the autophagic degradation of Δ133p53α. Δ133p53α is an isoform of p53 that lacks the N-terminus preventing its interaction with MDM2 and causing it to inhibit full-length p53. Loss of STUB1 is observed in senescent cells, leading to a loss of Δ133p53α by autophagy (Horikawa *et al.*, 2014). Since the overexpression of Δ133p53α is sufficient to prevent senescence induced by STUB1 knockdown, this study provides a possible mechanism by which autophagy promotes senescence (Horikawa *et al.*, 2014). Surprisingly, STUB1 is found to preferentially target TFEB for degradation, such that loss of STUB1 promotes accumulation of inactive TFEB and a reduction in overall TFEB activity (Sha *et al.*, 2017). Furthermore, this study showed that macroautophagy was attenuated in STUB1 -/- MEFs (Sha *et al.*, 2017). In contrast, elevated nuclear TFEB levels have been observed in response to RAS transfection (Urbanelli *et al.*, 2014). One potential possibility for reconciling Horikawa, Urbanelli and Sha's findings is that Δ133p53α is regulated by selective autophagy. Indeed, it has been shown that oncogene induced senescence drives a selective form of nucleophagy, whereby Lamin B is exported from the nucleus to the cytoplasm before undergoing autophagic degradation (Dou *et al.*, 2015).

Conversely, autophagy has also been shown to be repressed during senescence. For example, depletion of ATG7, ATG12 or Lamp2 in fibroblasts promotes premature senescence (Kang *et al.*, 2011). Likewise, shATG5 has been shown to promote senescence both in basal conditions and in response to oxidative stress (H_2O_2) (Tai *et al.*, 2017). These results are in direct contrast to that by the Narita group (Young *et al.*, 2009). A potential reason for this discrepancy is the underlying type of autophagy being explored, where generally OIS is observed with elevated autophagy, whilst other forms of senescence are observed with decreased autophagy. This was recently suggested in a review article by Kwon and colleagues (Kwon *et al.*, 2017), and requires further experimentation.

1.4 TFEB

Transcription Factor EB is a member of the MITF (Microphthalmia-Associated Transcription Factor) family of transcription factors, and has critical roles in lysosomal biogenesis (Sardiello *et al.*, 2009; Zhou *et al.*, 2013) and autophagy (Settembre *et al.*,

2011). TFEB's structure consists of highly conserved basic Helix-loop-helix (bHLH) and leucine zipper domains (Steingrímsson, Copeland and Jenkins, 2004). All the MITF family, like other bHLH transcription factors, recognise the E-box sequence CACGTG (Hemesath *et al.*, 1994), and this has subsequently been extended to comprise an eight base sequence comprising the 'coordinated lysosomal expression and regulation' (CLEAR) element (TCACGTGA) (M. Palmieri *et al.*, 2011). Developing animal models to study TFEB functions was initially impaired, since it is required for VEGF (Vascular Endothelial Growth Factor) secretion by placental labyrinthine cells meaning that TFEB null mice were not viable past 9.5 days (Steingrímsson *et al.*, 1998). Therefore, TFEB studies to date mainly involve overexpression and genetic silencing in cell lines. Tissue-specific and conditional knockout models do exist; for example, knockout of TFEB in the intestinal epithelium increased the severity (reduced body weight) of dextran sodium sulfate (DSS)-induced colitis, potentially due to reduced transcription of apolipoprotein A1 (Murano *et al.*, 2017).

1.4.1 Clinical implications of TFEB

MITF family translocations are present in a small subset of Renal Cell Carcinoma (RCC) patients (Argani, 2015). MALAT1-TFEB (Metastasis Associated Lung Adenocarcinoma Transcript 1-TFEB) translocations result in an overexpression of wild-type TFEB due to enhanced activity of the MALAT1 promoter relative to the TFEB promoter (Argani *et al.*, 2016). Due to TFEB's role in RCC and MITF's essential role in melanomas, there is interest in identifying any potential oncogenic role of TFEB in other malignancies. Investigations of patient derived samples showed TFEB expression levels had no correlation with grade or stage of lung carcinomas, and whilst univariate analysis suggested high TFEB expression levels correlated with a poor prognosis, this did not hold up in multivariate analysis (Giatromanolaki *et al.*, 2015). The authors did find that TFEB siRNA significantly impaired a migratory phenotype in a scratch assay. Conversely, data exists that suggests TFEB may be a favourable prognostic marker, with high TFEB mRNA levels associated with favourable prognosis in both renal and pancreatic cancers (Human protein atlas using data derived from TCGA).

1.4.2 Regulation of TFEB

TFEB localisation is responsive to a range of physiological stimuli including: starvation (Settembre *et al.*, 2011), endoplasmic reticulum stress (Martina *et al.*, 2016) and lysosomal dysfunction (Settembre *et al.*, 2012). Furthermore, mass spectrometry indicates that TFEB could have as many as 20 phosphorylation sites (Dephoure *et al.*, 2008; Olsen *et al.*, 2010). There is therefore interest in identifying the signalling pathways that regulate TFEB localisation. A summary of kinases found to phosphorylate TFEB, as well as ULK1 and ATG13, is provided in Figure 1.5.

1.4.2.1 Regulation of TFEB by mTOR signalling

Under normal growth conditions with sufficient nutrients, TFEB has a predominantly cytosolic localisation; conversely, nutrient starvation results in rapid nuclear localisation and upregulation of CLEAR genes (Settembre *et al.*, 2011). Whilst mTOR is a starvation-responsive kinase, initial evidence suggested that mTOR had either a negligible (Settembre *et al.*, 2011) or a promoting (Peña-Llopis *et al.*, 2011) role in TFEB dynamics. This early work was carried out using rapamycin, an mTOR inhibitor that does not target the catalytic domain but instead complexes with FKBP12 and causes only a partial inhibition of mTOR signalling. The use of Torin1, a catalytic inhibitor of mTOR, has revealed rapamycin resistant functions of mTOR (Thoreen and Sabatini, 2009; Thoreen *et al.*, 2009). In the case of TFEB, Torin1 causes rapid nuclear accumulation and upregulation of autophagic and lysosomal genes regulated by CLEAR elements (Martina *et al.*, 2012; Roczniak-Ferguson *et al.*, 2012; Settembre *et al.*, 2012). Rag-GTPases target TFEB to lysosomes, via the N-terminal first 30 residues, where it undergoes phosphorylation on S211 by mTOR (Martina and Puertollano, 2013). Interestingly, MITF-M which is a melanocyte specific isoform of MITF has a truncated N terminus (Levy, Khaled and Fisher, 2006), such that it is predominantly nuclear in basal conditions (Roczniak-Ferguson *et al.*, 2012). Phosphorylation of S211 mediates TFEB's sequestration by 14-3-3 proteins as evidenced by immunoprecipitation and mass spectrometry (Roczniak-Ferguson *et al.*, 2012). In this study, S142 mutation had no effect on 14-3-3 binding (Roczniak-Ferguson *et al.*, 2012). Therefore whilst follow up work by the Ballabio group showed S142 phosphorylation by mTOR, which was essential for cytoplasmic retention of TFEB (Settembre *et al.*, 2012), the mechanism was unclear. It has recently been demonstrated that mTORC1 mediated phosphorylation of both S138 and S142, but not S211, is required for CRM1-dependent nuclear export of TFEB (Napolitano *et al.*, 2018). Curiously, it was observed that the Nuclear Export Signal (NES) mutant M144A was phosphorylated at S138 and S142 more rapidly upon re-feeding than wild-type, leading the authors to conclude that these sites are phosphorylated in the nucleus (Napolitano *et al.*, 2018). One model that therefore incorporates these findings together is that S211 dephosphorylation in the cytoplasm promotes TFEB nuclear localisation, whereas S138 and S142 phosphorylation in the nucleus promotes its export. The localisation of mTORC1 to the nucleus is a matter of debate and is discussed further in Section 3.3.1. The nutrient responsive regulation of TFEB is summarised in Figure 1.7.

Recent evidence has also suggested a multistep mechanism for mTOR dependent regulation of TFEB. TFEB^{S211A}-GFP was observed to have a dispersed cytosolic and nuclear signal, in comparison to TFEB-GFP which was excluded from the nucleus (Vega-

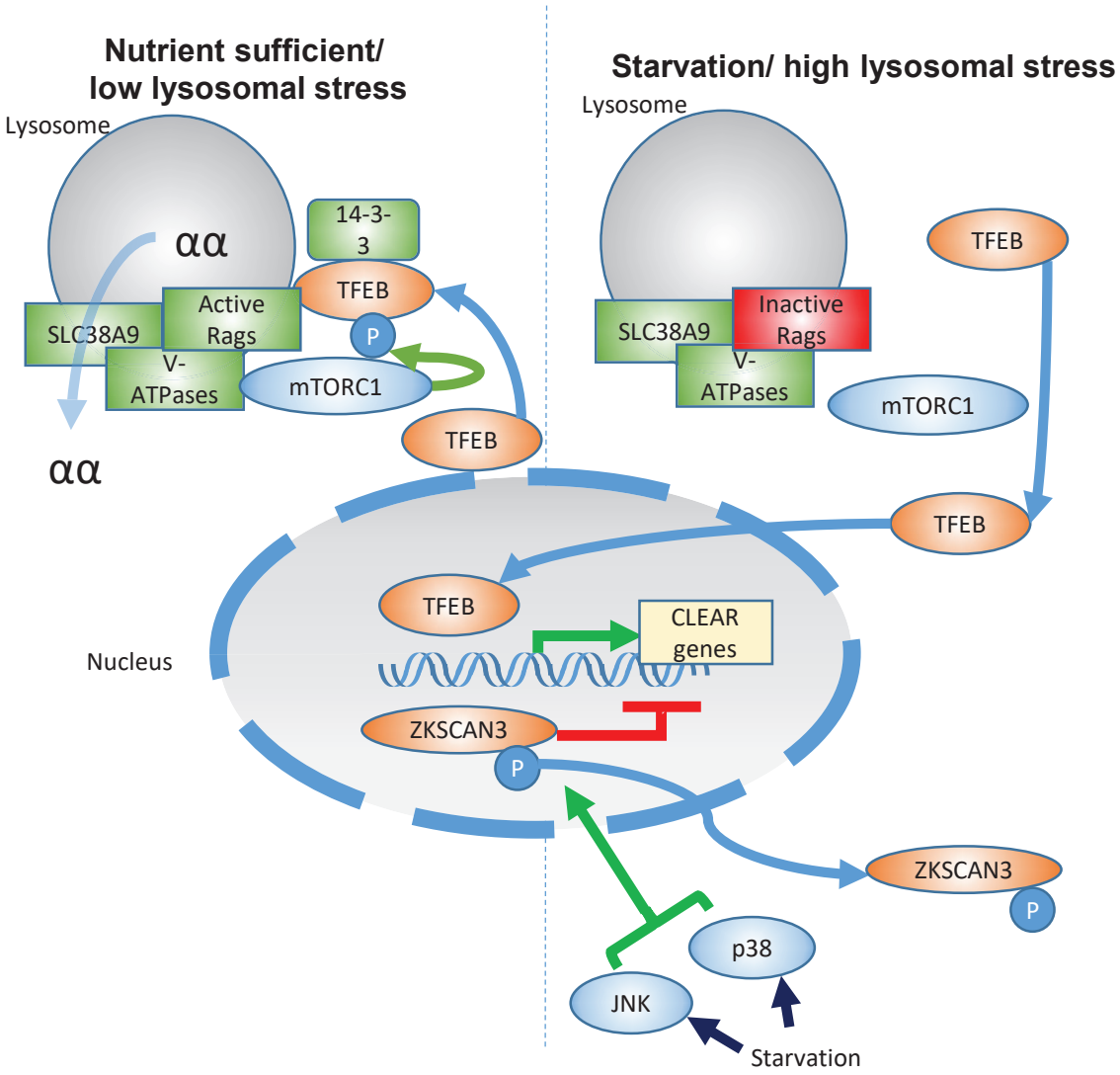

Figure 1.7: Lysosome transcriptional programs are upregulated during starvation.
In nutrient sufficient conditions TFEB is sequestered in the cytosol by binding 14-3-3 chaperone proteins. In starvation or lysosomal stress (i.e Salicylihalamide A treatment), loss of S211 phosphorylation due to mTORC1 inactivation releases TFEB from sequestration, enabling its nuclear localisation and upregulation of CLEAR genes. Conversely, ZKSCAN3 is present in the nucleus during nutrient sufficient conditions, acting as a repressor of CLEAR gene transcription. However, starvation stimulates JNK and p38 activity which phosphorylates ZKSCAN3, promoting its expulsion from the nucleus. αα = amino acids.

Rubin-de-Celis *et al.*, 2017). Furthermore, the authors found that TFEB^{S211A} continued to exhibit regulation by mTOR, and that S122 dephosphorylation was an essential step in TFEB nuclear localization (Vega-Rubin-de-Celis *et al.*, 2017). Rapid dephosphorylation of TFEB is presently thought to occur via Calcineurin, with inhibition of calcineurin catalytic isoform beta (PPP3CB) preventing starvation-induced nuclear translocation of TFEB (Medina *et al.*, 2015).

Scant evidence exists for mTOR-mediated influences on TFEB protein expression level. Semi-quantitative western blotting of HeLa cells suggested prolonged exposure to Torin1 caused a transient increase in TFEB protein levels at a 3 hour time point, returning to basal levels at 5 hours (Marin Zapata *et al.*, 2016). Conversely, in the same study, fresh media resulted in an initial dip in TFEB protein levels at the 1, 1.5 and 3 hour time point, before returning to basal levels (Marin Zapata *et al.*, 2016). Whilst the study examined mTOR activity via phospho-4E-BP1 immunoblotting, no other signalling pathways were investigated. TFEB is already suggested to transcribe its own promoter forming an auto-regulatory feed-forward mechanism (Settembre *et al.*, 2013), Marin and colleagues found that the increase in TFEB concentration was not perturbed by either Actinomycin D (an inhibitor of transcription) or epoxomicin (a proteasome inhibitor). Regardless, mTORC1 may have a transient and minor role in the regulation of TFEB protein levels.

1.4.2.2 Regulation of TFEB by the ERK1/2 pathway

ERK2 signalling was one of the first pathways implicated in TFEB regulation. Initial data from the Ballabio group suggested that ERK2 was responsible for phosphorylating S142, which maintained cytosolic localisation of TFEB, with MEK inhibition resulting in nuclear accumulation of TFEB (Settembre *et al.*, 2011). S142 corresponds to a PNSP motif, which is a conserved ERK1/2 target in MITF (Hemesath *et al.*, 1998; Wu *et al.*, 2000; Weilbaecher *et al.*, 2001) and is conserved throughout evolution (Consurf evaluation; Ashkenazy et al. 2016). Subsequent studies have shown variable results concerning the role of ERK1/2 in TFEB localisation. RIP1-mediated suppression of autophagy was suggested to be via ERK1/2-mediated phosphorylation of TFEB (Yonekawa *et al.*, 2015). Furthermore, ERK1/2-mediated S142 phosphorylation, alongside GSK3 mediated phosphorylation of S138, was suggested to be responsible for the nuclear export of TFEB (L. Li *et al.*, 2018). A number of studies have shown that ERK1/2 pathway inhibition has little or no effect on TFEB localisation (Martina *et al.*, 2012; Settembre *et al.*, 2012), whilst others have suggested that decreased ERK1/2 activity results in decreased TFEB nuclear localisation (or increased ERK1/2 activity leads to increased nuclear TFEB) (Martinez-Lopez *et al.*, 2013; Urbanelli *et al.*, 2014). In one of these studies, the decreased ERK1/2

activity was a consequence of ATG5 knockout and therefore allows for other effects of ATG5 knockout (Martinez-Lopez *et al.*, 2013).

It has been suggested that a minimum threshold of ERK1/2 signalling is required for it to exhibit an effect on TFEB localisation, since melanoma cells exhibiting the *BRAF* V600E mutation, such that the ERK1/2 signalling pathway is constitutively active, display ERK1/2-regulated localisation of TFEB (S. Li *et al.*, 2019). Specifically, Li and colleagues proposed that ERK1/2, via S142 phosphorylation, mediated lysosomal localisation of TFEB enabling it to be phosphorylated by mTOR (S. Li *et al.*, 2019). The mechanism by which this occurs was not elucidated.

Whilst TFEB expression is ubiquitous, RNA datasets show variable mRNA expression, with enrichment of TFEB mRNA in lymphoid tissues and especially EBV-transformed lymphocytes (GTEX dataset evaluation; Lonsdale et al. 2013). cAMP response element binding protein (CREB) is a transcription factor which has been shown to upregulate *TFEB* mRNA (Seok *et al.*, 2014). Conversely, a weak inverse correlation between *KRAS* mRNA and *TFEB* mRNA levels has been observed and *KRAS* silencing lead to increased TFEB protein levels (Klein *et al.*, 2016). Therefore, ERK1/2 signalling may play a role in TFEB regulation at the mRNA level.

1.4.2.3 Regulation of TFEB by the GSK3 pathway

mTOR- and ERK1/2-independent mechanisms of TFEB nuclear localisation are beginning to emerge. Both selective GSK3 inhibitors (Parr *et al.*, 2012; Marchand *et al.*, 2015) and the natural compound HEP14, which was found to inhibit GSK3β via PKC3 (Li et al. 2016), have been shown to induce TFEB nuclear localisation without impairing mTOR activity. GSK3 phosphorylates TFEB at S134 and S138 in vitro (Li et al. 2016). Curiously, inhibition of GSK3 by CHIR99021 resulted in TFEB hypophosphorylation relative to mTOR inhibition (Marchand *et al.*, 2015). It has been proposed that GSK3 enables targeting of TFEB to lysosomes for phosphorylation by mTORC1 with TFEB (S134A/S138A) failing to localise to lysosomes during Torin1 treatment (Y. Li *et al.*, 2016), and treatment with CHIR99021 impairing TFEB's interaction with the mTOR-associated proteins LTOR1 and RRagC (Marchand *et al.*, 2015). Regardless, there is clear evidence that GSK3 plays a role in TFEB cytosolic localisation.

It has been proposed that GSK3 and ERK2 co-operate to enable TFEB nuclear export, with ERK2-mediated S142 phosphorylation enabling GSK3-catalysed S138 phosphorylation (L. Li *et al.*, 2018). Similarly, ERK and GSK3 co-operate to mediate MITF nuclear export by phosphorylation of the equivalent sites (Ngeow *et al.*, 2018). However, this has been disputed by other findings that show that mTORC1 and not ERK2 or GSK3

is primarily responsible for TFEB phosphorylation (Napolitano *et al.*, 2018). Napolitano did not find that S138 was phosphorylated by GSK3 in cells. It is also important to note that the mTORC1 and GSK3 pathways can exhibit several mechanisms of negative crosstalk (see section 1.3.4.1), a complication that at present is not currently reconciled in models of TFEB regulation by these two protein kinases.

1.4.2.4 Regulation of TFEB by Protein Kinase C

TFEB is required for osteoclast development secondary to RANKL signalling (Ferron *et al.*, 2013). TFEB protein levels were stabilised via PKCβ-dependent multisite phosphorylation at S462, S463, S466 and S467 (Ferron *et al.*, 2013). Curiously, RANKL favoured only accumulation of TFEB and not MITF, despite both containing the PKC motif (Ferron *et al.*, 2013). Furthermore, PKC has been shown to inactivate GSK3, thus promoting TFEB nuclear localisation (Y. Li *et al.*, 2016).

1.4.2.5 Regulation of TFEB by MAP4K3

The N-terminus of TFEB is required for its cytosolic localisation and either truncation of the first 30 amino acids, or mutation of either S3 or R4 results in constitutive nuclear localisation of TFEB (Roczniak-Ferguson *et al.*, 2012). MAP4K3 has been shown to be critical for mTORC1 activation in response to nutrient availability, but not growth factor signalling (Findlay *et al.*, 2007). Subsequently, it was shown that MAP4K3 phosphorylation of TFEB at S3 was required for TFEB's interaction with and phosphorylation by mTORC1 (Hsu *et al.*, 2018).

1.4.2.6 Regulation of TFEB by Endoplasmic Reticulum (ER) stress

In addition to starvation, TFEB and TFE3 are implicated in the ER stress response. Martina and colleagues demonstrated that 16 hours of tunicamycin treatment, an inducer of ER stress due to activation of the Unfolded protein response, promoted nuclear localisation of TFEB (Martina *et al.*, 2016). This was demonstrated to be via PERK activation of calcineurin promoting dephosphorylation of TFEB. Curiously, this paper also identified a potential role for TFEB in driving apoptosis, with $TFEB^{S211A}$ upregulating PUMA mRNA levels 11-fold.

1.4.2.7 Other post-translational modifications of TFEB

Whilst the primary regulation of TFEB appears to be a result of mTORC1-mediated phosphorylation, other post-translational modifications have been implicated in TFEB's regulation. Four lysines have been shown to be acetylated (K91, K103, K116, K430), and mutation of these sites reduces TFEB transcriptional activity (Zhang *et al.*, 2018). In contrast with these results, deacetylation of K116R was found to stimulate TFEB activity and lysosomal biogenesis (Bao *et al.*, 2016). Therefore, there may be variability as to how

acetylation at different sites affects TFEB transcriptional activity. Little is known about the protein turnover of TFEB; however, the ubiquitin ligase STUB1 preferentially ubiquitinates phosphorylated TFEB leading to its turnover and this paper suggested that TFEB is primarily regulated via the proteasome (Sha *et al.*, 2017).

1.5 MIT/TFE family of transcription factors

1.5.1 MITF

MITF whilst ubiquitously expressed is critical to differentiation programs in melanogenesis and osteoclastogenesis. This appears to be mediated by different splice variants, with MITF-E linked with osteoclastogenesis (Lu, Li and Lin, 2010) and MITF-M with melanogenesis. MITF has been linked to the lineage-specific regulation of pro-survival factors in melanocytes with both BCL2 (McGill *et al.*, 2002) and BCL2A1 (Haq *et al.*, 2013) under direct transcriptional regulation, with inhibition of the latter being sufficient to increase apoptosis in combination with BRAF inhibitors (Haq *et al.*, 2013). MITF has also been shown to directly regulate p21, controlling melanocyte entry into cell cycle (Carreira *et al.*, 2005) and regulating the DNA damage response to UV radiation (Liu *et al.*, 2010). Furthermore, knockdown of MITF has been shown to cause a number of mitotic defects such as development of multinucleated cells and prolonged mitosis (Strub *et al.*, 2011). Overall, MITF plays a critical role in a number of processes in melanocytes.

1.5.2 TFE3

TFE3 has been implicated in many functions regulated by TFEB and MITF, such as autophagy and lysosomal biogenesis (Martina *et al.*, 2014), demonstrating redundancy amongst the MITF family of proteins. Like TFEB and MITF, TFE3 is ubiquitously expressed throughout all tissues (Kauffman *et al.*, 2014), with differential expression between lineages. It has been suggested that the MITF family only heterodimerise with each other; however, TFE3 has been shown to interact with E2F3, promoting transcription of p68 (Giangrande *et al.*, 2003) suggesting this model may be overly simplistic. TFE3 shares many of the regulatory mechanisms observed for TFEB. AKT phosphorylation of TFEB at S467 promotes TFEB cytosolic localisation (Palmieri *et al.*, 2017); likewise, AKT catalyses phosphorylation of TFE3 at S565 (the homolog to TFEB S467) and this also mediates cytosolic localisation (Pi *et al.*, 2019). Furthermore, mTORC1 phosphorylates TFE3 at S321 (with the caveat it was not formally validated *in vitro*), corresponding to TFEB S211, mediating 14-3-3 binding (Martina *et al.*, 2014).

1.5.3 Importin 8

It has been widely reported that certain pancreatic adenocarcinoma cell lines have nuclear localisation of TFEB and other MITF family members, even under normal growth conditions (Marchand *et al.*, 2015; Perera *et al.*, 2015; Klein *et al.*, 2016). This was shown not to be due to either the mTOR or MAPK pathways, but TFE3 localisation was abolished by knockdown of Importin 8 (IPO8) (Perera *et al.*, 2015). Whether regulation of IPO8 has any role to play in normal physiological control of TFEB has not been investigated.

1.6 Interpreting autophagy assays

'Autophagic flux' describes the flow of autophagic processing from the synthesis of autophagosomes to fusion with lysosomes resulting in substrate degradation. Interpreting 'autophagic flux' can be challenging as it involves observation of numerous stages along the autophagic pathway. Electron microscopy allows confident detection of autophagosomes as well as the sequestered contents (reviewed: Klionsky *et al.*, 2016); however, it is expensive, dependent upon sufficient expertise and not readily available to many researchers. Therefore, detection of lipidated LC3B (LC3B-II), either via immunoblotting or immunofluorescence, is readily used for estimation of autophagosome number (Mizushima, Yoshimori and Levine, 2010). An alteration in the number of autophagosomes can result from a change in the rate of their synthesis or degradation. Furthermore, interpretation of LC3 assays can be misleading with non-canonical autophagy (Jacquin *et al.*, 2017), transient GFP-LC3 (Green fluorescent protein-LC3) expression (Kuma et al. 2007), and protein aggregates (Kuma et al. 2007) all leading to autophagy-independent LC3 lipidation/ puncta.

To investigate whether an increase in LC3B lipidation is due to an increase in autophagosome synthesis, pan-PI3K inhibitors such as 3-Methyladenine or wortmannin, can be utilised which inhibit the VPS34 complex thereby preventing autophagosome assembly and LC3B lipidation. By comparison, investigation of autophagosome degradation can be achieved by use of lysosomal inhibitors and p62 (SQSTM1) immunoblotting (reviewed: Mizushima, Yoshimori and Levine, 2010; Klionsky *et al.*, 2016). Lysosomal inhibition should result in an increase in markers of LC3B lipidation if lysosome function is intact. Complicating interpretation of these experiments, many lysosomal inhibitors used to study canonical autophagy can lead to LC3 lipidation via non-canonical autophagy, with the exception of bafilomycin A which appears to inhibit non-canonical autophagy (Jacquin *et al.*, 2017). A decrease in p62 protein levels is indicative of an increase in autophagic flux (Mizushima, Yoshimori and Levine, 2010). However, p62 protein levels can vary during the induction of autophagy; for example, it's transcription is

upregulated by TFEB (Settembre *et al.*, 2011). A further system which can be utilised is RFP-GFP-LC3 (Red fluorescent protein-GFP-LC3), whereby acidic compartments will lose GFP but not RFP signal, enabling relative evaluation of autophagosome-lysosome fusion (Kimura et al. 2007). RFP puncta can be highly stable, with accumulation in lysosomes occurring over time such that there are numerous RFP puncta in conditions without substantial autophagy (Nicholas Ktistakis and Oliver Florey, personal communication). It has been suggested that the turnover of RFP-LC3 is governed by proteolytic activity within the lysosomes since it is able to withstand the acidity of both autophagolysosmes and lysosomes (reviewed: Yoshii and Mizushima, 2017). Overall, there is no single assay which is caveat-free and it is advised that multiple assays are employed when interpreting changes in autophagic flux (reviewed Klionsky *et al.*, 2016).

1.6.1 Experimental manipulations of mTORC1 signalling

It is well established that inhibition of mTORC1 promotes autophagy. Rapamycin (sirolimus) is a macrocyclic antibiotic produced by Streptomyces hygroscopicus and is a selective mTORC1 inhibitor due to its interaction with FKBP12 (reviewed: Ballou and Lin, 2008). Due to not being ATP-competitive, it has the significant advantage of being highly selective. Several mTORC1 substrates have been identified which are insensitive to rapamycin, i.e., 4E-BP1 (T37) and ULK1 (S758) (Kang *et al.*, 2013). Curiously, this has been proposed to be a result of the properties of the phosphorylation sites themselves. Sites which exhibit a relatively high phosphorylation by mTORC1 *in vitro*, such as 4E-BP1 (T37) and ULK1 (S758) are rapamycin insensitive, whilst sites with low *in vitro* phosphorylation such as S6K1 (T389) are rapamycin sensitive (Kang *et al.*, 2013). The exact mechanism by which rapamycin mediates these differential effects is unclear. Structural analyses of mTORC1 has suggested that prolonged exposure to rapamycin *in vitro* promotes mTORC1 disassembly, including of the mTOR-RAPTOR interaction (Yip *et al.*, 2010) and this has also been observed in cells (Kim *et al.*, 2002). Indeed, prolonged exposure to rapamycin both in cells and *in vitro* did eventually block 4E-BP1 phosphorylation, in contrast to S6K phosphorylation which is blocked rapidly. Surprisingly, S6K can be phosphorylated by free mTOR dissociated from RAPTOR suggesting this is not the mechanism by which Rapamycin blocks S6K phosphorylation (Yip *et al.*, 2010). Instead, Yip and colleagues propose the FKBP12-Rapamycin prevents binding to a comparatively large substrate during the initial phase (S6K compared to 4E-BP1) (Yip *et al.*, 2010), though this seems unlikely given that ULK1 (150 kDa) is also a rapamycin-insensitive substrate of mTORC1.

By contrast, catalytic inhibitors of mTOR such as Torin1 abolish phosphorylation of all mTORC1 sites rapidly and with similar dynamics (within 30 minutes) (Kang *et al.*, 2013). Due to being an ATP-competitive inhibitor targeting the catalytic domain of mTOR, Torin1 (Thoreen *et al.*, 2009), PP242 (Feldman *et al.*, 2009) and AZD8055 (Chresta *et al.*, 2010) inhibit both mTORC1 and mTORC2 with similar IC_{50} profiles, providing no means to distinguish between these two different complexes. Therefore, more recent studies have utilised these catalytic inhibitors, combined with different genetic approaches to distinguish between the two complexes. For example, TFEB underwent nuclear localisation in response to Torin1 and siRNA against RAPTOR, Rag-GTPases and components of regulator (p18) (Martina and Puertollano, 2013). As such, a combination of small molecule and genetic approaches is usually required when identifying novel substrates of either mTOR complex.

1.7 The mammalian cell cycle

The cell cycle encompasses the entire process of a diploid interphase cell replicating its genomic contents and critical organelles, right through to its bisection and production of two equal daughter cells. As such, this is a tightly regulated process and fluctuations in activity in different cyclin-CDK complexes determine the chronological order of events. Cyclin-dependent kinases (CDKs) belong to the CMGC kinase family and are all proline-directed serine/threonine kinases. Cyclins act as regulatory subunits mediating substrate specificity. Inhibition of CDK1 whether by expression of a dominant-negative kinase (van den Heuvel and Harlow, 1993) or small molecule inhibition (Vassilev *et al.*, 2006) promotes a G2 arrest. Only CDK1 is believed to be critical for the cell cycle, with mice mutant in CDK2 (Berthet *et al.*, 2003), CDK4 (Rane *et al.*, 1999) or CDK6 (Malumbres *et al.*, 2004) being viable. Whilst CDK4 -/-; CDK6 -/- mice are not viable due to late stage anaemia, they do undergo organogenesis and fibroblasts can be acquired from these mice with replicative capability (Malumbres *et al.*, 2004). By contrast, CDK1 -/- mice cannot establish mitotic cell division and thus are lethal from onset such that no homozygous knockout embryos are detected (Diril *et al.*, 2012). CDK1 is the only CDK absolutely required for the mammalian cell cycle, with CDK2 -/-; CDK4 -/-; CDK6 -/- mice undergoing organogenesis and developing till midgestation (Santamaría *et al.*, 2007). Tissue specific functions of CDKs have been suggested, for example CDK4 -/- mice develop diabetes as a result of decreased pancreatic beta cells (Rane *et al.*, 1999). These findings of tissue-specific functions for CDK4/6 has stimulated the notion of CDK4/6 inhibitors being selective to certain cancers. Whilst many cyclins have been identified and various functions attributed to them, only cyclin A2 (Murphy *et al.*, 1997) and CCNB1 (cyclin B1) knockouts are embryonically lethal (Brandeis *et al.*, 1998). Overall, whilst there is several cyclin-CDK

complexes that are co-ordinately regulated during the cell cycle, there appears to be significant redundancy to ensure the cell cycle is completed.

All of the cell cycle CDKs (1,2,4,6) require activation by CDK-activating kinase (CAK), which consists of CDK7, cyclin H and MAT1. CDK7 has two known functions: CDK activation and transcriptional regulation, via its recruitment into the general transcription factor TFIIH and phosphorylation of RNA polymerase II. Concerning the cell cycle, Inhibition of CDK7 in mammalian cells in either G1 or G2 results in cell cycle arrest at this point (Larochelle *et al.*, 2007). Importantly, this study inhibited CDK7 by genetic manipulation altering the kinase domain, such that it could be selectively inhibited with introduction of a non-hydrolysable analog which did not affect its roles in global transcription, likely as a result of compensatory phosphorylation of S5 on Pol II (Larochelle *et al.*, 2007). Thus, CDK7 inhibition, leads to the respective CDK inhibition at any given point in the cell cycle.

1.7.1 Mitosis

1.7.1.1 Timing of mitotic events is controlled by CCNB1-CDK1

Mitosis is a highly evolutionary conserved process involving the duplication and subsequent bifurcation of a cell's genomic content. In addition, many of the cells organelles will also divide between the two daughter cells, with lysosomes splitting in an apparently ordered process despite their mostly stochastic distribution (Bergeland *et al.*, 2001). The process of mitosis can be subdivided into distinct stages: prophase, prometaphase, metaphase, anaphase, telophase, and cytokinesis. During prophase, nuclear envelope breakdown and chromosome condensation occur as a result of increasing CCNB1-CDK1 activity. Cells then proceed through prometaphase where chromosomes progress to line on the metaphase plate. During metaphase, chromatid pairs must be securely connected to microtubules originating from both spindles, termed the spindle assembly checkpoint (reviewed: Lara-Gonzalez, Westhorpe and Taylor, 2012). Satisfaction of the spindle assembly checkpoint, enables CDC20-mediated activation of the ubiquitin ligase APC/C, which in turn leads to degradation of Cyclin B1 which triggers anaphase onset (Chang, Xu and Luo, 2003). It should be noted that there is some residual APC/C activity even when the SAC has not been satisfied. This residual activity can degrade CCNB1 levels below the threshold required for mitotic exit, leading to a failure of cell division prior to cytokinesis termed 'mitotic slippage' (Brito and Rieder, 2006). Thus, cells post-slippage are tetraploid and can subsequently go on to a number of cell fates including further cell division, cell cycle arrest or apoptosis (Balachandran and Kipreos, 2017)

A rapid alteration in the post-translational modifications of CDK1 enables entry into mitosis. Prior to the initiation of mitosis, CCNB1 levels steadily increase during the G2 phase of the cell cycle (Pines and Hunter, 1989). The CCNB1-CDK1 complex is held in an inactive state by phosphorylation of Tyrosine 15 by WEE1 (Gould and Nurse, 1989; Lundgren *et al.*, 1991). The switch to mitotic progression is achieved by the phosphatase CDC25 causing dephosphorylation of CDK1 T15, thereby activating CDK1 (Gautier *et al.*, 1991). CDK1 can then phosphorylate WEE1 at S123, which enables PLK1 to phosphorylate Wee1 at S53 promoting Wee1's degradation via a β-TrCP dependent mechanism (Watanabe *et al.*, 2005), and promoting a feed-forward activation loop; though it has been demonstrated that WEE1 can still be phosphorylated and inactivated *in vitro* by mitotic lysates depleted of cdc2 (Tang, Coleman and Dunphy, 1993).

CCNB1-CDK1 activity is observed to increase approximately 27 minutes prior to nuclear envelope breakdown in HeLa cells (Gavet and Pines, 2010b). This is complemented by a decrease in activity of key phosphatases, such as the PP2A-B55 family, that usually acts to oppose phosphorylation of CDK1 substrates (reviewed: Nasa and Kettenbach, 2018). PP2A-B55 activity increases in response to PP1 activity in a phosphatase signalling cascade (Grallert *et al.*, 2015). CCNB1-CDK1 phosphorylates PP1 to repress its phosphatase activity (Dohadwala *et al.*, 1994), thus PP2A-B55 is inactivated in response to increased CCNB1-CDK1 activity. Curiously, B55-dependent phosphatase activity is found to occur at a minimum S/T-P CDK1 consensus motif flanked by basic residues, whereby the composition of flanking basic residues determines dephosphorylation dynamics, thereby enabling differential temporal regulation of CDK1 phosphosites where the most basic are dephosphorylated more rapidly (Cundell *et al.*, 2016). Overall, CCNB1-CDK1 activity, counterbalanced by PP1 and PP2A-B55 activity is critical in determining the timing of mitotic onset and exit (Figure 1.8).

Metazoan cells undergo an 'open mitosis' whereby nuclear envelope breakdown occurs during the separation of chromosomes (Güttinger, Laurell and Kutay, 2009). Nuclear envelope status is dynamically regulated by CDK1 activity, with nuclear envelope breakdown occurring during prometaphase in conjunction with high CDK1 activity (Heald and McKeon, 1990) and re-envelopment occurring during anaphase when cyclin B is degraded inactivating CDK1 (Chang, Xu and Luo, 2003). In addition, the phosphatase PP2A-B55 works to promote nuclear envelope reformation by dephosphorylating envelope components such as BAF, Lamin and Nup107 in Drosophilia (Mehsen *et al.*, 2018), whilst PP1 has been found to dephosphorylate AKAP149 in vitro, resulting in nuclear reassembly (Steen *et al.*, 2000). Thus, nuclear envelope dynamics are modulated by Cyclin B1-CDK1

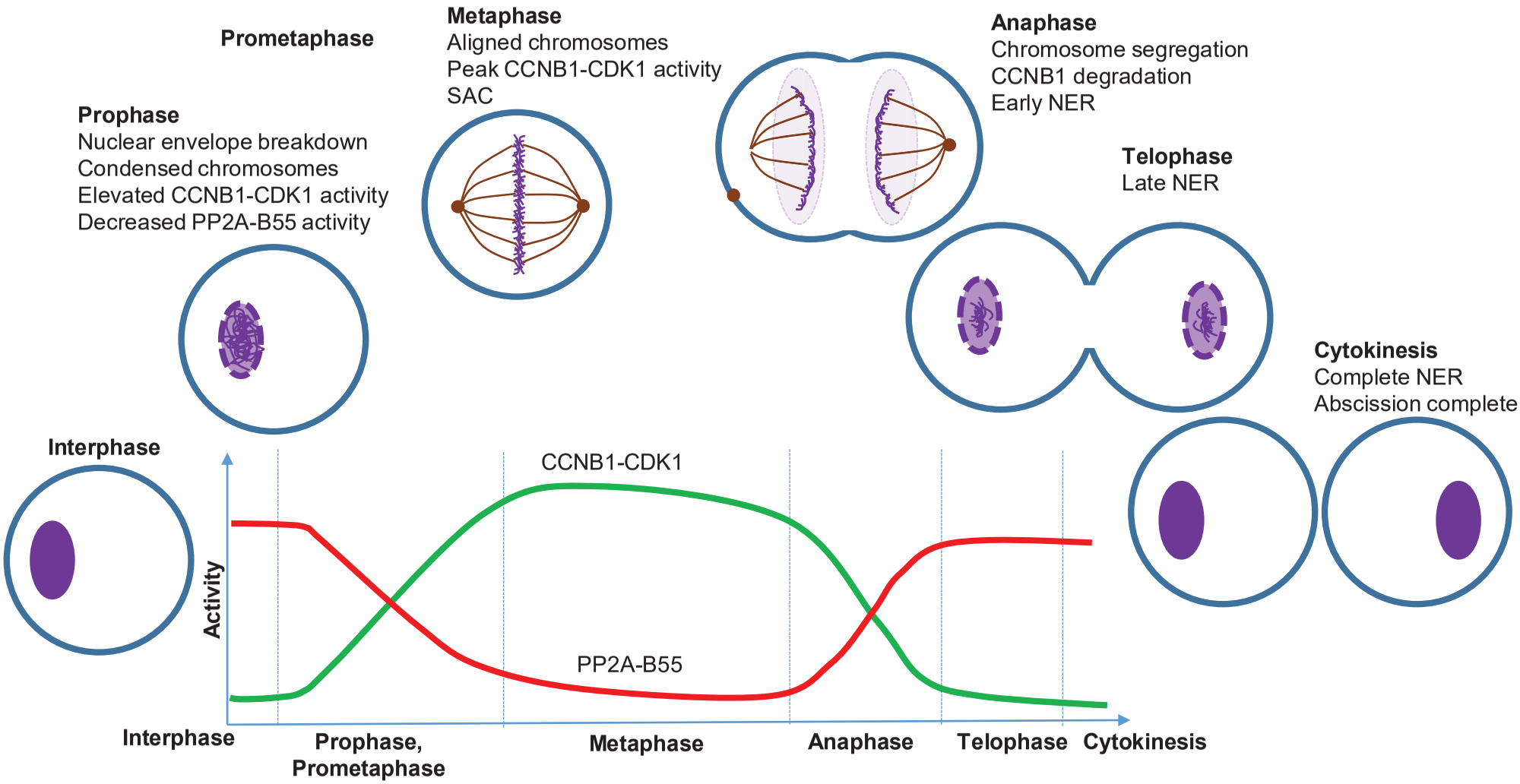

Figure 1.8: Stages of mitosis and relative CCNB1-CDK1 activity.
The stages of the mitotic cycle are represented. Abbreviations used: CCNB1 (Cyclin B1), SAC (Spindle assembly checkpoint), NER (nuclear envelope reformation). Relative CCNB1-CDK1 and PP2A-B55 activity are shown for each stage of the cycle. Adapted from Nasa *et al*., 2018, and Gavet and Pines, 2010

through either its direct phosphorylation of nuclear envelope proteins or modulating relevant phosphatases.

1.7.2 mTORC1 signalling during mitosis

Curiously, CDK1 is observed to substitute for mTOR during mitosis for certain substrates. It has been suggested that mTOR is hyperactivated during mitosis due to RAPTOR hyperphosphorylation, with *in vitro* kinase assays showing that phosphomimetic mutations of the RAPTOR sites promoted mTOR activity (Ramírez-Valle *et al.*, 2010). Furthermore, immunoprecipitated mitotic mTORC1 possessed enhanced activity in an *in vitro* kinase assay with S6K as a substrate (Ramírez-Valle *et al.*, 2010). CDK1 has been shown to phosphorylate TSC1, though TSC2 binding to TSC1 appeared to prevent its phosphorylation by CDK1 (Astrinidis *et al.*, 2003). A phospho-null mutant of the CDK1 putative sites on TSC1 had an increased inhibitory effect on P-S6K (T389) phosphorylation relative to wild-type, but this was performed in interphase cells (Astrinidis *et al.*, 2003). Therefore, the Astrinidis and Ramirez-Valle studies suggest that mTORC1 is activated during mitosis. However, the mitotic hyperphosphorylation of mTOR substrates in cells was resistant to mTOR inhibitors and RAPTOR shRNA (Ramírez-Valle *et al.*, 2010). Consistent with this, paclitaxel induced hyperphosphorylation of 4E-BP1 was attenuated by rosocvitine and purvalanol A, two CDK1 inhibitors, but not rapamycin or wortmannin (Greenberg and Zimmer, 2005). *In vitro* kinase assays have suggested that 4E-BP1 can act as a direct substrate of CDK1, and that CDK1 phosphorylation of 4E-BP1 promotes its dissociation from eIF-4E (Heesom *et al.*, 2001) and enables cap-dependent translation during mitosis (Shuda *et al.*, 2015). Furthermore, CDK1 additionally phosphorylates 4E-BP1 at serine 83, which is not phosphorylated by mTORC1, leading to translation-independent functions (Velásquez *et al.*, 2016). CDK1 mediated signalling appears to upregulate p70 S6 Kinase Threonine 389 phosphorylation (Greenberg and Zimmer, 2005; Ramírez-Valle *et al.*, 2010) These findings are not supported in other studies where P-S6K (T389) is shown to be reduced in mitotic cells (Shah, Ghosh and Hunter, 2003; Ruf *et al.*, 2017). Instead microtubule inhibitors promoted phosphorylation at Threonine 421 and Serine 424 by JNK (Le *et al.*, 2003) and CDK1 (Shah, Ghosh and Hunter, 2003). CDK1 has also been shown to directly phosphorylate S6K at Serine 411 (Papst *et al.*, 1998; Shah, Ghosh and Hunter, 2003). It is important to note that P-S6K (T389) is not a proline-directed site and would not be expected to be phosphorylated by CDK1.

Several phosphorylation events within the PI3K/PDK1/AKT signalling cascade are absent during mitosis, including P-AKT (T308), P-AKT (S473), P-PRAS (T246) (Ramírez-Valle *et al.*, 2010). Cells expressing constitutively active PI3K class I (p110CAAX) have, via

AKT signalling, inactivated forkhead transcription factors, preventing the transcription of cyclin B and PLK1, resulting in failure of cytokinesis (Alvarez *et al.*, 2001). Thus, it appears PI3K signalling is disabled during mitosis to enable forkhead transcription of mitotic regulators.

Whilst the majority of research has focused on mTORC1's inhibition leading to a G1 arrest some G2/M-specific functions of mTOR signalling components have also emerged. Inhibition of mTOR promotes an accelerated mitotic entry in both fission yeast (Petersen and Nurse, 2007) and mammalian cells (via a decrease in WEE1) (Atkin *et al.*, 2014). A number of publications have suggested that mTORC1 is active during mitosis due to immunofluorescence of the autophosphorylation site S2481 being increased during mitosis (Vazquez-Martin *et al.*, 2009, 2011; Lopez-Bonet *et al.*, 2010). It has also been suggested that mTORC1 signalling regulates both Aurora A and PLK, with Mio (GATOR2 component) siRNA causing loss of P-mTOR (2481) at mitotic centrosomes (immunofluorescence), delayed bipolar spindle formation and loss of P-Aurora A (T288) (western blot) (Platani *et al.*, 2015). S2481 phosphorylation is usually attributed with mTORC2 (Copp, Manning and Hunter, 2009). These results are discussed further in Section 4.3.2 but should be treated with caution given the phospho-antibody is not approved for immunofluorescence use.

1.8 Autophagy and the cell cycle

1.8.1 G1/S phase

For a cell to be able to progress through the G1 restriction point, it must have sufficient nutrients to proceed. mTOR functions as a central control, coupling nutrient signalling to cell cycle progression (Fingar and Blenis, 2004). Inhibition of mTOR can promote a G1 phase arrest (Gao *et al.*, 2003), which is partially ameliorated by overexpression of its substrates 4E-BP1 and S6K (Fingar *et al.*, 2004). In addition, components of the PI3K/AKT/mTOR signalling axis also interact with cell cycle components. For example, AKT phosphorylates the CDK inhibitor p21 at T145/S146, mediating its increased stability though in the cell lines tested this had little effect on the cell cycle (Li, Dowbenko and Lasky, 2002). Other nutrient-sensitive pathways also interact with cell cycle progression. For example, the CDK inhibitor $p27^{KIP1}$ is phosphorylated by AMPK on Threonine 198, increasing its stability and promoting autophagy (Liang *et al.*, 2007).

Evidence also exists of autophagy being regulated by cell cycle components. Agents which induced G1 cell cycle arrest such as mimosine, hydroxyurea and aphidicolin increased LC3B lipidation (Liang *et al.*, 2007). Overexpression of CDK inhibitors p16, p19, p21 also promoted autophagy and senescence in fibroblasts (Capparelli *et al.*, 2012). Cyclin A-CDK2 phosphorylates AKT at 477/479, which enables AKT phosphorylation at T308 and

S473 thus promoting AKT activation, although the functional consequences on autophagy were not assessed (Liu *et al.*, 2014). It was previously shown that CDK2 knockdown resulted in modest upregulation of autophagy (Liang *et al.*, 2007).

There are currently no known links between the cell cycle and TFEB. CDK4/6 inhibition has been associated with enrichment of lysosomal and fatty acid metabolism gene sets, with a concurrent increase in lysosome number over 24 hours (Franco *et al.*, 2016). Furthermore, the CDK4/6 inhibitor PD0332991 promoted LC3B protein expression in a dose-dependent manner (Capparelli *et al.*, 2012). The Narita group has previously shown that autophagy induction is associated with senescence, an irreversible cell cycle arrest, but is not a general consequence of cell cycle arrest. For example, quiescent cells generated by total confluence possess no increase in total LC3B or LC3B lipidation (Young *et al.*, 2009). Cyclin D1-CDK4/6 phosphorylates LKB1 at S325, leading to its inactivation, impairment of AMPK signalling and thus reduced autophagy (Casimiro *et al.*, 2017). Overall, there is little consensus on a direct link between cell cycle regulators and autophagy.

1.8.1.1 CDK4/6 inhibitors

Aberrant regulation of cyclin D-CDK4/6 is a key feature of many cancers (Musgrove *et al.*, 2011) and, as a result, CDK4/6 inhibitors have been developed such as PD0332991 (Palbociclib) and LY2835219 (abemaciclib). Gelbert and colleagues' pre-clinical characterisation of LY2835219 showed that it produced marked G1 arrest at doses above 320 nM in COLO205 (Gelbert *et al.*, 2014). Supplemental data within this study suggested that at these doses PIM1 kinase was also inhibited as indicated by the dephosphorylation of the substrates BAD (S112) and 4E-BP1 (T37/46). PIM1 was also identified in the study's *in vitro* kinase screen with a Ki less than 100nM, alongside HIPK2 and DYRK2. However, the panel of kinases did not include mTOR and 4E-BP1 is a well-established mTOR substrate. Recently, LY2835219 was found to synergise with mTOR inhibitors in head and neck squamous cell carcinoma (Ku *et al.*, 2016). Whilst this study showed that phosphorylation of mTOR was not impaired by LY2835219, it did not evaluate mTOR substrate phosphorylation.

1.8.2 Mitosis

It has been postulated that autophagy should be repressed during mitosis in mammalian cells, since the nuclear envelope is disintegrated exposing vulnerable nuclear contents to the autophagic machinery (Eskelinen *et al.*, 2002). Eskelinen and colleagues first observed that there was reduced autophagy during mitosis by observing, via electron microscopy, few autophagosomes being present in either nocodazole-arrested

prometaphase-like cells, or metaphase and anaphase cells released from nocodazole block relative to interphase cells (Eskelinen *et al.*, 2002). Furthermore, they observed that autophagosomes only began to form upon nuclear envelope closure during telophase (Eskelinen *et al.*, 2002). Subsequent studies have generally supported the observed reduction in autophagosomes by observation of reduced lipidated LC3B in mitotic cells (Liu *et al.*, 2009; Furuya *et al.*, 2010; Veldhoen *et al.*, 2013; Z. Li *et al.*, 2016; Lu *et al.*, 2019). Debate has arisen as to whether the reduction in autophagosome number is a result of reduced autophagosome synthesis or increased autophagosome degradation. Treating cells with lysosomal inhibitors causes an accumulation of autophagosomes in mitotic cells (Liu *et al.*, 2009; Z. Li *et al.*, 2016); however, since lysosomal inhibitors are added for prolonged time periods (between 1 and 16 hours), these autophagosomes may be accumulated from interphase. Liu and colleagues tried to address this issue by treating mitotic cells, harvested by shake off, with ammonia and showing that LC3B could still be lipidated Ammonia is known to cause non-canonical L3B lipidation (Jacquin *et al.*, 2017) and this is independent of the ULK1/2 complex (Cheong *et al.*, 2011). It is also worth noting that it has previously been observed that LC3 puncta can remain for approximately 30 minutes (Axe *et al.*, 2008); therefore, even in the absence of lysosomal inhibitors, it is entirely possible that LC3 puncta observed during early mitosis are inherited mature autophagosomes from interphase. A recent paper further tried to address this issue by treating cells with nocodazole, prior to the treatment with lysosomal inhibitors and showed that both chloroquine and bafilomycin A1 failed to cause an increase in lipidated LC3, supporting a suppression of autophagy (Lu *et al.*, 2019). Furthermore, the widespread use of microtubule inhibitors in many of these studies could easily provide misleading results given the implication of microtubules in autophagosome transport (Mackeh *et al.*, 2013). It is therefore currently still unknown whether the reduction in autophagosome number is as a result of repression of macroautophagy.

Independent studies have also established roles for autophagy in outcomes post-mitotic slippage (Sorokina *et al.*, 2017; Jakhar *et al.*, 2018). Curiously, in the Jakhar study they concluded that mTOR signalling was increased in mitosis due to increases in P-ULK 757 relative to total ULK levels. Specifically, they observed that total ULK levels had decreased (to the point of not being detectable) with stable phospho-757 signal. Furthermore, the phospho-757 signal was band-shifted suggesting that other post-translational modifications of ULK1 maybe occurring during nocodazole-induced mitotic arrest of U20S cells (Jakhar *et al.*, 2018).

On the basis that macroautophagy is repressed during mitosis, mechanistic detail is limited, though beginning to emerge. VPS34 is phosphorylated at T159 by CDK1,

promoting dissociation from Beclin-1 and reduction in autophagosome number (Furuya *et al.*, 2010). Supporting these findings, cells treated with paclitaxel, known to increase CDK1 activity due to holding cells in a prometaphase-like state (Chadebech *et al.*, 2000), exhibit loss of LC3B puncta, as well as phosphorylation of VPS34 at T159 (Veldhoen *et al.*, 2013). Whilst evidence exists that CDK1 also phosphorylates p62 (Linares *et al.*, 2011), no role in autophagy has been identified or investigated.

It has also been suggested that autophagy plays critical roles in cytokinesis (Pohl and Jentsch, 2009; Belaid *et al.*, 2013; Matsui *et al.*, 2013) and midbody degradation (Kuo *et al.*, 2011). Whilst LC3-dependent, the machinery involved in autophagosome synthesis, UNC-51 and EPG-8 (homologs of ULK1 and ATG14 respectively), are not required for *Caenorhabditis elegans* midbody degradation, again demonstrating the difficulty in dissecting macroautophagy with non-canonical causes of LC3B puncta formation (Fazeli *et al.*, 2016). Instead, the midbody appears to be directly recruited to LC3 structures by FYCO1 (Dionne *et al.*, 2017) and selective autophagy receptor NBR1 binding to midbody protein CEP55 (Kuo *et al.*, 2011). Furthermore, CDK1 activity does not persist into cytokinesis, with cyclin B degradation being essential for progression through anaphase (Chang, Xu and Luo, 2003). Indeed, no VPS34 T159 phosphorylation is seen in cells undergoing telophase or cytokinesis (Furuya *et al.*, 2010). Thus, it is possible that CDK1-mediated repression of autophagy terminates by cytokinesis.

Other forms of selective autophagy have also been implicated during mitosis. Cyclin A2 has been proposed to be degraded during metaphase by selective autophagy, whereby cyclin A2 directly interacts with p62 and LC3B (Loukil *et al.*, 2014). Whether other components of the autophagy machinery are required is not known.

It has been shown that autophagy is required for the progression through mitosis in nitrogen-starved conditions in budding yeast (Matsui *et al.*, 2013). It has been postulated that this is to return cells to a G1 arrest in starvation conditions (Mathiassen, De Zio and Cecconi, 2017). Crucially, these studies have been conducted in yeast which do not undergo open mitosis (reviewed: Güttinger, Laurell and Kutay, 2009). mTOR appears to maintain regulation of autophagy during mitosis in yeast since rapamycin induces autophagy in nocodazole arrested mitotic yeast cells (Noda and Ohsumi, 1998), in contrast to the findings of Eskelinen in mammalian cells (Eskelinen *et al.*, 2002).

1.8.3 Miscellaneous CDK interactions with autophagy

Whilst CDK5 is not part of the cell cycle, it has been demonstrated to interact with autophagy initiation via its repressive phosphorylation of VPS34 (Furuya *et al.*, 2010). Conversely CDK5 has been suggested to promote basal autophagy by phosphorylating

acinus at S437, which has been shown to induce basal starvation-independent autophagy in drosophila (Nandi *et al.*, 2017). The relevance in mammalian systems has not been explored. Supporting a stimulatory role in autophagy, CDK5 has been shown to phosphorylate endophilin B1 (also referred to as Bif-1) (Wong *et al.*, 2011). Endophilin B1 binds to UVRAG and enhances VPS34 activity; however, it is implicated in stimulating autophagosome formation as opposed to maturation (Takahashi *et al.*, 2007). CDK5-mediated phosphorylation of endophilin B1 at T145 increased lipidated LC3 in response to starvation (Wong *et al.*, 2011). The reasons behind the discrepancy in Furuya and Wong's findings are unclear.

Knockdown of CDK11 in mammalian cells promotes increased autophagic flux; however, after prolonged periods of knockdown there appears to be an impairment in lipidated LC3 turnover (Wilkinson *et al.*, 2011). Very little is known about the function of CDK11. Homozygous null mice are embryonically lethal, with blastocysts arresting in mitosis as measured by P-H3 (S10) (Li *et al.*, 2004). Both the p110 and the p58 isoforms have a conserved kinase domain at their C-terminus. Whilst CDK11^{p110} is expressed uniformly across the cell cycle, CDK11^{p58} is expressed via an IRES site which is solely translated during mitosis (Cornelis *et al.*, 2000). Despite this, Wilkinson and colleagues concluded that the autophagy inhibition mediated by CDK11 was not linked to its role in mitosis, since the proportion of cells displaying elevated autophagosomes was far higher than the numbers in mitosis. Overall, the mechanism by which CDK11 regulates autophagy has not been elucidated.

1.9 Selective autophagy

Selective autophagy for several cargoes has been identified but the signalling required to direct them is poorly understood. Cargo is generally agreed to be sequestered by cargo receptors which, via LC3-interaction region (LIR) motifs, are recruited to the developing phagophore (reviewed: Johansen and Lamark, 2019). But how then is the phagophore initiated? Direct recruitment of ULK1 by cargo receptors to enable phagophore initiation has been proposed, for example NDP52 via its SKICH domain, can directly interact with the ULK1 complex via FIP200 during mitophagy (Vargas *et al.*, 2019) and xenophagy (Ravenhill *et al.*, 2019). In both cases this appears to be mediated by TBK, and overexpression of mTOR leading to enhanced P-ULK1 (S757) failed to prevent mitophagy (Vargas *et al.*, 2019). Likewise, p62 directly interacts with the c-terminus of FIP200, though curiously ULK1 can still be recruited to p62-ubiquitin condensates when FIP200 is knocked down, though ATG16L1 fails to be recruited (Turco *et al.*, 2019). Overall, it would appear that selective cargo receptors are responsible for recruiting both the ULK1 complex and the targeted cargo; therefore, it is perhaps unsurprising that phagophore extension is in close

proximity to the cargo, excluding other contents (reviewed: Johansen and Lamark, 2019). What is less clear is whether mTORC1-catalysed repressive phosphorylation events on the ULK1 complex have to be removed to enable selective autophagy. Whilst data from the Randow group would suggest not (Vargas *et al.*, 2019), it does not rule out potential possibilities such as localised phosphatase activity mediating localised de-repression of the ULK1 complex. Another potential possibility is that high concentrations of localised ULK1 complex, mediated by the recruitment by selective cargo receptors, effectively promote trans-autophosphorylation and shield the ULK1 complex from mTORC1 activity (reviewed: Turco, Fracchiolla and Martens, 2019), a theory derived from observations of yeast Atg1 during selective autophagy of damaged peroxisomes and cvt (Kamber, Shoemaker and Denic, 2015; Torggler *et al.*, 2016). It is worth noting that it has been proposed that mTORC1 does play a role in xenophagy. *Salmonella enterica* infection does lead to activation of AMPK, and subsequent inhibition of mTORC1, and AMPK knockout MEFs showed significantly decreased lipidation of bacteria (Losier *et al.*, 2019). Overall, how mTORC1-mediated repression is overcome during selective autophagy requires further investigation.

The selectivity of starvation-induced autophagy is also a matter of debate. Originally thought of as a non-selective bulk degradative process, more recent studies have suggested a degree of selectivity. Proteomic analysis from cells suggested that cytosolic proteins were preferentially lost earlier than those proteins associated with organelles during prolonged starvation (Kristensen *et al.*, 2008). Separately to the well characterised mTORC1-regulated bulk autophagy, amino acid starvation also promotes microautophagy of well characterised selective autophagy receptors such as p62, NBR1, NDP52 (Mejlvang *et al.*, 2018). This requires further investigation.

1.10 Aims

Whilst mTORC1 is widely viewed as the master regulator of autophagy, there is keen interest in the identification of novel regulatory mechanisms which may open therapeutic avenues from which to modulate autophagy with less toxic effects. Since the seminal work of Settembre and colleagues identifying TFEB as a transcriptional regulator of autophagy and lysosomal biogenesis, there has been increasing efforts to identify novel regulatory mechanisms. Whilst S142 was identified as an ERK2 phosphorylation site which mediated cytosolic retention, this site has also been identified as an mTORC1 site. Since ERK1/2 often phosphorylates multiple proline directed sites in close proximity to each other and that 15 serine or threonine proline-directed sites exist in the TFEB amino acid sequence, we set out to investigate if TFEB was regulated by ERK1/2 and to identify if there were other ERK1/2 target sites on TFEB.

The question of autophagy during mitosis has been a source of ongoing debate over the last two decades. Much of this debate appears to be due to the methodologies used not being appropriate for the study of autophagy during mitosis, such as LC3 lipidation. Work by a collaborating lab (Ktistakis) has detailed the recruitment of the ULK1 complex to the omegasome intermediate structure, enabling a more transient and direct readout of autophagy initiation. Therefore, a second objective was to re-evaluate the status of autophagy during mitosis. Given we hypothesised that autophagy is repressed during mitosis, clarifying the status of the canonical regulatory mechanism, mTORC1, during mitosis would be critical. Indeed, the status of mTORC1 activity during mitosis is as controversial as the status of autophagy. Given that mTORC1 signalling has been shown to be subverted by CDK1 in the case of S6K and 4E-BP1 during mitosis, we wanted to investigate the phosphorylation status of ULK1, ATG13, ATG14 and TFEB in mitotic cells. It is curious that the key regulatory sites of mTOR-mediated phosphorylation on these proteins (TFEB:S142 (Settembre *et al.*, 2012), ULK1: S758 (Kim *et al.*, 2011), and ATG13: S258 (Puente, Hendrickson and Jiang, 2016)) are all proline-directed serine sites. Therefore, there is a possibility that proline-directed serine/threonine kinases, such as CDK1, phosphorylate these proteins during mitosis. Since these phosphorylation events are well known to repress autophagy regulators, it might provide a mechanism by which the reported reduction in autophagosome number during mitosis occurs.

2 Materials and methods

2.1 General reagents

Supplier	Reagents
BioRad	20% Sodium dodecyl sulphate (SDS) 30% v/v acrylamide/bis solution Bradford reagent (Protein assay reagent) Precision Plus protein markers
Hoefer	Gel casting apparatus
Marvel	Milk powder
Melford	Tris
New England Biolabs	BL21(DE3) competent cells DH5α competent cells Lambda Phosphatase
Life technologies/ Gibco	Dulbecco's Modified Eagles Medium L-15 media (Leibovitz) Geneticin (G418) IMDM L-glutamine OptiMEM Penicillin/Streptomycin RPMI SYBR green PCR master mix TrypLE Trypsin-EDTA
Perkin-Elmer	Cell-Carrier 96 well imaging plates
Qiagen	Miniprep and Midiprep kits
Roche	Epidermal Growth Factor (EGF)
Sigma	4-hydroxytamoxifen (4HT) Aprotinin Bovine serum albumin (BSA) Coomassie brilliant blue Dimethyl sulphoxide (DMSO) Ethylene glycol bis(2-aminoethyl ether)- N,N,N'N'-tetraacetic acid (EGTA) Ethylenediaminetetraacetic acid (EDTA) Leupeptin Magnesium chloride β-Mercaptoethanol Phenylmethylsulfonyl fluoride (PMSF) Propidium iodide Ribonuclease A

	Sodium fluoride Sodium orthovanadate Triton X-100 Tween-20
Thermo	Nunc Tissue culture plasticware
Thistle Scientific	µ-Dish 35 mm, high Glass Bottom
Vectorlabs	Vectashield hardset with DAPI
VWR	Acetic acid Calcium chloride Ethanol Glycerol Haemocytometer Magnesium chloride Methanol Propan-2-ol Potassium chloride Potassium dihydrogen phosphate Sodium azide Sodium bicarbonate Sodium chloride Sodium hydroxide Trichloroacetic acid

Table 2.1: List of general reagents used within this thesis, with the respective manufacturer.

2.2 Cell culture

Cell line	Media
A549, CO115, HCT116, HEK293, HeLa (ATCC CCL-2), HeLa Dox:KRAS^{G12D}, PANC-1, HeLa Tet-CDC2, HEK293 mRFP-EGFP-LC3	DMEM 10% FBS (v/v) Penicillin 100 µgml^{-1} Streptomycin 100 µgml^{-1} L-glutamine 2 mM
HM3 (HEK293 ΔMEKK3:ER), HeLa HA-RAPTOR (WT, A7, D7)	DMEM 10% FBS (v/v) Penicillin 100 µgml^{-1} Streptomycin 100 µgml^{-1} L-glutamine 2 mM Puromycin 4 µgml^{-1}
HR1 (HEK293 ΔRAF-1:ER), HeLa Δ30TFEB-GFP,	DMEM 10% FBS (v/v)

HEK293 GFP-ATG13, HEK293 GFP-ATG13 H2B-mCherry, HeLa TFEB-GFP, HeLa TFEB-GFP H2B-mCherry, A549 TFEB-GFP	Penicillin 100 $\mu g ml^{-1}$ Streptomycin 100 $\mu g ml^{-1}$ L-Glutamine 2 mM G418 400 $\mu g ml^{-1}$
COLO205	RPMI 10% FBS (v/v) Penicillin 100 $\mu g ml^{-1}$ Streptomycin 100 $\mu g ml^{-1}$ L-Glutamine 2 mM
HT-29	McCoys 10% FBS (v/v) Penicillin 100 $\mu g ml^{-1}$ Streptomycin 100 $\mu g ml^{-1}$ L-glutamine 2 mM
SW620 (SW620:8055R have media supplemented with 2 µM AZD8055)	Leibovitz's L-15 10% FBS (v/v) Penicillin 100 $\mu g ml^{-1}$ Streptomycin 100 $\mu g ml^{-1}$ L-Glutamine 2 mM 7.5% sodium bicarbonate
HAP1 parental, HAP1 RAPTOR-GFP (endogenous CRISPR)	IMDM 10% FBS Penicillin 100 $\mu g ml^{-1}$ Streptomycin 100 $\mu g ml^{-1}$

Table 2.2: Cell line culture media.

2.3 Small interfering RNA

Target	Sequence/ Category number
TFEB	M-009798-02 (Dharmacon) pooled siRNA: D-009798-02 Target sequence: CUACAUCAAUCCUGAAAUG Antisense: CAUUUCAGGAUUGAUGUAG D-009798-03 Target sequence: AGACGAAGGUUCAACAUCA Antisense: UGAUGUUGAACCUUCGUCU D-009798-04 Target sequence: CAAGUUUGCUGCCCACAUC Antisense: GAUGUGGGCAGCAAACUUG

	D-009798-18 Target sequence: CGGGAGUACCUGUCCGAGA Antisense: UCUCGGACAGGUACUCCCG

Table 2.3: siRNA used within this study.

2.4 Drugs

Drug	Mechanism of action	Target used to validate
4-Hydroxytamoxifen	Activation of ER constructs	Relevant downstream substrate of induced kinase
AZD8055	ATP competitive mTOR inhibitor	P-S6K (T389); P-ULK1 (S758); 4E-BP1 or TFEB dephosphorylation
Bafilomycin A1	Vacuolar-type H+ ATPase inhibitor (lysosomal acidification inhibitor)	LC3B-II accumulation
BI 6727	PI3K inhibitor	Mitotic arrest with distinct chromosome morphology
BIRB-796	p38 inhibitor	P-MAPKAPK2 (T222)
Camptothecin	Topoisomerase I inhibitor	P-Chk1 (S317)
CHIR99021	GSK3 inhibitor	P-β-Catenin (Ser33/37/Thr41)
Dimethylenastron	Eg5 inhibitor	P-Histone H3 (S10) 4E-BP1 δ isoform
Doxycycline		Induction of relevant signalling pathway
Etoposide	Topoisomerase II inhibitor	P-Chk1 (S317)
GSK1120212 (Trametinib)	Allosteric MEK1/2 inhibitor	P-ERK1/2 (T202/Y204)
JNK-IN-8	JNK inhibitor	P-c-JUN (S63)
LY2835219 (abemaciclib)	CDK4/6 inhibitor	P-Rb (S795)
Nocodazole	Microtubule destabilising. Arrests cells in prometaphase-like state with upregulation of Cyclin B/CDK1 activity	P-Histone H3 (S10), 4E-BP1 δ isoform
NU6102	Pan-CDK inhibitor (1 and 2)	P-Histone H3 (S10), 4E-BP1 δ isoform
Paclitaxel	Taxol compound. Microtubule stabilising. Similar to Nocodazole.	P-Histone H3 (S10), 4E-BP1 δ isoform

PD0332991	CDK4/6 inhibitor	P-Rb (S795)
PP242	mTOR inhibitor	P-S6K (T389)
RO-3306	Reversible CDK1 inhibitor	FACS PI stain, 4E-BP1 δ isoform
Roscovitine	Pan-CDK inhibitor (1,2 and 5)	P-Histone H3 (S10), 4E-BP1 δ isoform
SCH772984	ERK1/2 inhibitor	P-RSK (T359, T380)
Torin1	mTOR inhibitor	P-S6K T389
Wortmannin	Pan-PI3K inhibitor	Absence of ATG13 puncta
ZSTK474	Class I PI3K inhibitor	P-AKT (S473)

Table 2.4: Compounds used within this thesis, along with the read-out used to validate target engagement.

2.5 Solutions

Solution	Components
TG lysis buffer	20 mM Tris-HCl pH 7.6; 137 mM NaCl; 1% v/v Triton X-100; 10% glycerol; 1 mM EGTA; 1.5 mM $MgCl_2$; 50 mM NaF; 1 mM Na_3VO_4; 1 mM PMSF; 10 $\mu g ml^{-1}$ leupeptin; 5 $\mu g ml^{-1}$ aprotinin
RIPA buffer	50 mM Tris-HCl pH 8.0; 150 mM NaCl; 1% v/v Triton X-100; 1% Sodium deoxycholate (w/v); 0.1% SDS; 50 mM NaF; 1 mM Na_3VO_4; 1 mM PMSF; 10 $\mu g ml^{-1}$ leupeptin; 5 $\mu g ml^{-1}$ aprotinin
IP extraction buffer	50 mM Tris pH 7.5; 150 mM NaCl; 0.1% NP-40; 20 mM EGTA; 50 mM NaF; 1 mM Na_3VO_4; 1 mM PMSF; 10 $\mu g ml^{-1}$ leupeptin; 5 $\mu g ml^{-1}$ aprotinin
CDK1 IP wash buffer	50 mM Tris pH 7.5; 500 mM NaCl; 0.1% NP-40; 20 mM EGTA; 50 mM NaF; 1 mM Na_3VO_4; 1 mM PMSF; 10 $\mu g\ ml^{-1}$ leupeptin; 5 $\mu g ml^{-1}$ aprotinin
0.3% CHAPS buffer	40 mM HEPES pH 7.4; 120 mM NaCl; 0.3% CHAPS, 1mM EDTA, 50mM NaF; 1 mM Na_3VO_4; 1 mM PMSF; 10 $\mu g ml^{-1}$ leupeptin; 5 $\mu g ml^{-1}$ aprotinin
4 x Laemmli buffer (sample buffer)	200 mM Tris-HCl pH 6.8; 8% w/v SDS; 40% v/v glycerol; 4% v/v β-mercaptoethanol; 0.04% w/v bromophenol blue
Phosphatase buffer	50 mM HEPES pH 7.4; 100 mM NaCl; 2 mM DTT; 0.1% NP-40; 1 mM PMSF; 10 $\mu g ml^{-1}$ leupeptin; 5 $\mu g ml^{-1}$aprotinin; 1mM $MnCl_2$
REAP (cytosolic) buffer	PBS; 0.1% NP-40; 50mM NaF; 1 mM Na_3VO_4; 1 mM PMSF; 10 $\mu g ml^{-1}$ leupeptin; 5 $\mu g ml^{-1}$aprotinin

Isotonic buffer	20 mM HEPES pH 7.4, 250 mM sucrose, 0.5 mM EDTA, 50 mM NaF; 1 mM Na_3VO_4; 1 mM PMSF; 10 μgml^{-1} leupeptin; 5 μgml^{-1} aprotinin
Dialysis buffer	50 mM Tris pH 7.6, 150 mM NaCl, 2 mM DTT
Kinase assay buffer	50 mM Tris pH 7.6, 100 µM EGTA, 10 mM $MgCl_2$, 100 µM ATP Where applicable: 2 µCi [γ-^{32}P] ATP
Running buffer	192 mM glycine; 25 mM Tris base; 0.1% v/v SDS
Transfer buffer	192 mM glycine; 25 mM Tris base; 20% v/v methanol
Tris-buffered saline with Tween (TBST)	50 mM Tris-HCl pH 7.6; 150 mM NaCl; 0.1% Tween 20
5% Milk/TBST	5% Milk (Marvel; w/v); TBST
5% BSA/TBST	5% Bovine Serum Albumin (w/v); TBST
Luria Broth (LB)	10 gL^{-1} Tryptone 10 gL^{-1} NaCl 5 gL^{-1} Yeast extract
Phosphate-buffered saline (PBS)	137 mM NaCl 2.7 mM KCl 1.47 mM KH_2PO_4 8.1 mM Na_2HPO_4

Table 2.5: Composition of solutions.

2.6 Antibodies

Antibody	Company	Catalogue number	Species	Solution (For Western blot)	Dilution
4E-BP1	Cell Signalling Technologies (CST)	#9452 /RRID: AB_331692	Rabbit	5% BSA/TBST	1:1000
ATG13	CST	#13468 /RRID: AB_2797419	Rabbit	5% BSA/TBST	WB: 1:1000 IP: 1:250 IF: 1:100
ATG14	CST	#96752 /RRID: AB_2737056	Rabbit	5% BSA/TBST	1:1000

CDK1	Santa Cruz	#SC747 /RRID: AB_631206	Rabbit	5% Milk/TBST	1:1000
Cyclin B1	Thermo	#MS-868-P1ABX/ #SC747 /RRID: AB_145331	Mouse		IP: 1:100
Cyclin B1	Santa Cruz	#sc-245 /RRID: AB_627338	Mouse		IP: 1:20
Cyclin B1	CST	#12231 /RRID: AB_2783553	Rabbit	5% Milk/TBST	1:1000
ERK1/2	CST	#9102 /RRID: AB_330744	Rabbit	5% Milk/TBST	1:2000
GFP	Roche	#11814460001 /RRID: AB_390913	Mouse	5% Milk/TBST	1:1000 IP: 1:100
GST	Santa Cruz	#SC138 /RRID: AB_627677	Mouse	5% Milk/TBST	1:10000
HA	Roche	#11867423001/ RRID: AB_390918	Rat		IF: 1:200
HA	Santa Cruz	#SC805 /RRID: AB_631618	Rabbit	5% Milk/TBST	1:1000
HA	Santa Cruz	#SC7392 /RRID: AB_627809	Mouse		IP: 1:200
Lamin A/C	Santa Cruz	#sc-7292 /RRID: AB_627875	Mouse	5% Milk/TBST	1:100
Lamp2	Abcam	#25631 /RRID: AB_470709	Mouse	5% Milk/TBST	WB: 1:1000 IF: 1:200
LC3B	CST	#2775 /RRID: AB_915950	Rabbit	5% Milk/TBST	WB: 1:1000
MEK1/2	CST	#9122 /RRID: AB_823567	Rabbit	5% Milk/TBST	1:1000
mTOR	CST	#2983 / RRID: AB_2105622	Rabbit	5% BSA/TBST	WB: 1:1000 IF: 1:200

P-4E-BP1 (S65)	CST	#9451 /RRID: AB_330947	Rabbit	5% BSA/TBST	1:1000
p70 S6 Kinase	CST	#9202 /RRID: AB_331676	Rabbit	5% BSA/TBST	1:1000
P-AKT (473)	CST	#4060 /RRID: AB_2315049	Rabbit	5% BSA/TBST	1:1000
P-AKT (473)	CST	#4060 /RRID: AB_2315049	Rabbit	5% BSA/TBST	WB: 1:1000
P-ATG14 (S29)	CST	#13155 /RRID: AB_2798133	Rabbit	5% BSA/TBST	1:1000
P-cJUN (S63)	CST	#9261/ RRID: AB_2130162	Rabbit	5% Milk/TBST	1:1000
P-ERK1/2 (T202/Y204)	CST	#9101 /RRID: AB_331646	Rabbit	5% Milk/TBST	1:2000
P-ERK1/2 (T202/Y204)	CST	#4370 /RRID: AB_2315112			IF: 1:500
P-Histone H3 (S10)	Santa Cruz	#sc-8656 /RRID: AB_2233067	Rabbit	5% Milk/TBST	1:1000 IF: 1:200
P-Histone H3 (S10)	CST	#9706 /RRID: AB_331748	Mouse		IF: 1:200 HCM: 1:1000 FC: 1:200
P-JNK1/2 (T183/Y185)	CST	#4668 /RRID: AB_823588	Mouse	5% Milk/TBST	1:1000
P-MAPKAPK2 (T222)	CST	#3044 /RRID: AB_330728	Rabbit	5% Milk/TBST	1:1000
P-p38 MAPK (T180/Y182)	CST	#9211S /RRID: AB_331641	Rabbit	5% BSA/TBST	1:1000
P-p70 S6 Kinase (T389)	CST	#9205 /RRID: AB_330944	Rabbit	5% BSA/TBST	1:1000

P-Rb (S795)	CST	#9301 /RRID: AB_330013	Rabbit	5% BSA/TBST	1:1000
P-TFEB (S122)	Bethyl	#A300-BL13169 /RRID: AB_2797420	Rabbit	5% Milk/TBST	1:1000
P-TFEB (S142) Note: marketed as P-MITF (S73)	Sigma	#SAB4503940 /RRID: AB_2797421	Rabbit	5% Milk/TBST	1:1000
P-ULK1 (S758)	CST	#6888 /RRID: AB_10829226	Rabbit	5% BSA/TBST	1:1000
P-ULK1 (S758)	CST	#14202 /RRID: AB_2665508	Rabbit		FC: 1:200 HCM: 1:1000
RagA	CST	#4357 /RRID: AB_10545136	Rabbit	5% BSA/TBST	1:1000
RagC	CST	#3360 /RRID: AB_2180068	Rabbit	5% BSA/TBST	1:1000 IF: 1:200
RAPTOR	CST	#2280 /RRID: AB_561245	Rabbit	5% BSA/TBST	1:1000
TFE3	CST	#14779 /RRID: AB_2687582	Rabbit	5% BSA/TBST	1:500
TFEB	CST	#4240 /RRID: AB_11220225	Rabbit	5% BSA/TBST	1:500 IP: 1:200
ULK1	Santa Cruz	#33182 /RRID: AB_2214706	Rabbit	5% BSA/TBST	1:1000
WIPI2	Bio-rad	#MCA5780GA /RRID: AB_10845951	Mouse		IF: 1:200
β-actin	Sigma	#A5441 /RRID: AB_476744	Mouse	5% Milk/TBST	1:10000
Secondary Antibodies					

anti-mouse (secondary)	BioRad	#170-6516/ RRID: AB_11125547	Goat	5% Milk/TBST	1:3000
anti-rabbit (secondary)	BioRad	#170-6515 / RRID: AB_11125142	Goat	5% Milk/TBST	1:3000
anti-rabbit 488	Invitrogen	#A11034/ RRID: AB_2576217	Goat		IF: 1:500
anti-mouse 488	Invitrogen	#A11029/ RRID: AB_2534088	Goat		IF: 1:500
anti-rabbit 568	Invitrogen	#A11011/ RRID: AB_143157	Goat		IF: 1:500
anti-mouse 568	Invitrogen	#A11004/ RRID: AB_2534072	Goat		IF: 1:500
anti-mouse 647	Invitrogen	#A21235/ RRID: AB_2535804	Goat		IF: 1:500
Highly cross-absorbed anti-mouse 647	Invitrogen	#A21236/ RRID: AB_2535805	Goat		IF: 1:500
anti-rat 488	Invitrogen	#A11006/ RRID: AB_2534074	Goat		IF: 1:500
Anti-mouse (Dylight 800)	CST	#5257/ RRID: AB_10693543	Goat	5% Milk/TBST	1: 30000
Anti-Rabbit (Dylight 800)	CST	#5151/ RRID: AB_10697505	Goat	5% Milk/TBST	1: 30000

Table 2.6: Antibodies used throughout thesis.

2.7 qRT-PCR

Primer Target	Oligo sequences
TFEB (validated by siRNA)	Fwd: 5'-CAGATGCCCAACACGCTAC-3' Rev: 5'-TTGTCTTTCTTCTGCCGCTC-3'
YWHAZ	Fwd: 5'-ACTTTTGGTACATTGTGGC-3' Rev: 5'- CCGCCAGGACAAACCAGTAT-3'
B2M	Fwd: 5'-TGCTGTCTCCATGTTTGATG-3' Rev: 5'-TCTCTGCTCCCCACCTCTAA-3'

Table 2.7: Primers used in qRT-PCR.

2.8 DNA Oligos used in PCR subcloning

Oligo	Sequence (note all have a 4 nucleotide TAAC which is cleaved off)
ATG13 194-282	Fwd (BamHI): TAACGGATCCGCATTCATGTCTACCAGG Rev (EcoRI, stop codon): TAACGAATTCTCAGTCAGCTGATCCAACGCC
ATG14 348-470	Fwd (EcoRI): TAACGAATTCGTGAAGAAACTGAATGC Rev (XHOI, stop codon): TAACCTCGAGTCATGCACTGCTGCTCGCGATG
TFEB 76-160	Fwd (BamHI): TAACGGATCCCTGGAGAATCCCACATCC Rev (EcoRI, stop codon): TAACGAATTCTCAGACATCATCCAACTCCCTCT
ULK1 706-827	Fwd (BamHI): TAACGGATCCGCGTTTGGGACACAAGCC Rev (EcoRI, stop codon): TAACGAATTCTCAGGCCTCGAAGGTCACAGC

Table 2.8: Oligos used for PCR subcloning.

2.9 DNA Oligos used in Sanger sequencing reactions

Oligo	
GEX-4T1 vectors (TFEB, ATG13, ULK1, ATG14)	Fwd: 5'- GGGCTGGCAAGCCACGTTTGGTG -3' Rev: 5'- CCGGGAGCTGCATGTGTCAGAGG -3'
pBabe-RAPTOR (WT, A7, D7)	Fwd primers: 5'- CTTTATCCAGCCCTCAC -3' 5'- ACCTCCTGCCTCACCACC -3' 5'- ACATGCCAGCTGAACACC -3' 5'- AGCATATCCTGTCCTTCG -3' 5'- CGAGGGTCACTGCCATGG -3' Rev primers: 5'- ACCCTAACTGACACACATTCC -3' 5'- CAGTGACCCTCGTGTACC -3' 5'- TGTTGAGTACTTTCATGG -3' 5'- TCTCATGAGCGCTGTCCC -3' 5'- CTAGCCACCAGCAAGTCC -3'

Table 2.9: Primers used for sanger sequencing of indicated constructs.

2.10 Plasmids

Plasmid	Reference	Source
FH-pBabe-Raptor(A7)	(Ramírez-Valle *et al.*, 2010)	Gift from Robert Schneider
FH-pBabe-Raptor(D7)	(Ramírez-Valle *et al.*, 2010)	Gift from Robert Schneider

FH-pBabe-Raptor(WT)	(Ramírez-Valle *et al.*, 2010)	Gift from Robert Schneider
pCDNA3 H2B-mCherry	(Nam and Benezra, 2009)	Addgene #20972
pEGFP-C1-hAtg14	(Itakura *et al.*, 2008)	Addgene #24295
pEGFP-N1-delta30-TFEB	(Roczniak-Ferguson *et al.*, 2012)	Addgene #44445
pEGFP-N1-TFEB	(Roczniak-Ferguson *et al.*, 2012)	Addgene #38119
pGEX-4T1-ATG13 (194-282)	This study	
pGEX-4T1-ATG14 (348-470)	This study	
pGEX-4T1-TFEB (76-160)	This study	
pGEX-4T1-ULK1 (706-827)	This study	
pmRFP-EGFP-rLC3		Gift from Tamotsu Yoshimori
pOPH10-ATG13	(Karanasios *et al.*, 2013)	
pPOM121-mCherry	(Dultz *et al.*, 2008)	EUROSCARF #P30554
pRK5-HA GST RagB Q99L (GTP)	(Sancak et al., 2008)	Addgene #19303
pRK5-HA GST RagB WT	(Sancak et al., 2008)	Addgene #19301
pRK5-HA GST RagD S77L (GDP)	(Sancak et al., 2008)	Addgene #19308
pRK5-HA GST RagD WT	(Sancak et al., 2008)	Addgene #19307
pRK5-HA-hULK1	(Jung *et al.*, 2009)	Addgene #31963

Table 2.10: Plasmids used within this thesis.

2.11 Tissue culture

All cells were raised in an atmosphere of 37°C, 5% CO_2, 95% humidity. Cells were split at approximately 80% confluency, every 3-4 days. Cell media was aspirated and then cells were washed in Trypsin-EDTA or TrypLE. Cells were then incubated at 37°C in fresh Trypsin-EDTA or TrypLE until detached. Displaced cells were then diluted with appropriate

amounts of fresh media, from which 1 ml was transferred to a new culture flask. For storage of cells, cells were suspended in freezing medium (90% FBS, 10% DMSO) prior to transfer to a -80°C freezer. Frozen vials were then transferred and stored in vapor phase liquid nitrogen for long-term storage.

2.12 Transfection

Cells were cultured to approximately 60% confluency. Constructs were then transfected using JetPrime polyplus transfection reagent (HeLa; A549) or lipofectamine 2000 (HEK293) as per manufacturer's instructions. The Rag WT duplex consisted of $RagB^{WT}$ and $RagD^{WT}$, whilst the active Rag heteroduplex consisted of $RagB^{GTP;\ Q99L}$ and $RagD^{GDP;\ S77L}$.

2.13 Generation of stable cell lines

For the generation of HeLa cells stably expressing TFEB-GFP and Δ30-TFEB-GFP, HeLa cells were transfected with constructs using JetPrime as per manufacturer's instructions. After 48 hours, cell media was then supplemented with G418 (400 $\mu g ml^{-1}$). Cells were then cultured for one week, before undergoing limiting dilution to generate single-cell derived clones. Clonal populations were then screened for GFP expression by western blot and confocal imaging.

For generation of HEK293 GFP-ATG13 or HeLa TFEB-GFP cells stably expressing H2B-mCherry. Cells were transfected as per manufacturer's instructions (HEK293, Lipofectamine 2000; HeLa, JetPrime). After 24 hours, cells were incubated in fresh media and cultured for two weeks. Cells were then single-cell sorted by flow cytometry for positive mCherry expression, using the TFEB-GFP or GFP-ATG13 parental cells as a negative control. After two weeks, 96 well plates were screened for mCherry expression using an InCell 6000, with parental TFEB-GFP or GFP-ATG13 parental cells as a negative control. Clones deemed to have both GFP and mCherry expression were taken forward.

For generation of A549 TFEB-GFP, A549 cells were transfected with constructs using JetPrime as per manufacturer's instructions. After 48 hours, cell media was then supplemented with G418 (400 $\mu g ml^{-1}$). Cells were then cultured for a further two weeks prior to single-cell sorting by flow cytometry. Clonal populations were then screened for GFP expression by high-content microscopy.

Generation of HeLa cells stably expressing HA-RAPTOR constructs was performed by Rebecca Gilley. pBabe-Raptor (WT, A7, D7) vectors were kind gifts from Robert Schneider (Ramírez-Valle *et al.*, 2010). Briefly, these were transfected into Phoenix ampho cell lines (a kind gift from Garry Nolan) according to protocols outlined on the Nolan website

https://web.stanford.edu/group/nolan/_OldWebsite/protocols/pro_helper_dep.html. 48 hours after transfection the retroviral supernatant was used to infect Hela cells. The following day the cells were passaged and 24 hours later selected with puromycin (2 μgml^{-1}) for 2 weeks. Cells were maintained as a polyclonal population. Expression of constructs was checked by immunofluorescence and western blot.

2.14 Treatments

Cells were treated with indicated compounds as outlined. For RO-3306 release experiments, cells were treated with RO-3306 (9 μM) for 20 hours prior to being washed with PBS and released into fresh pre-warmed media. For starvation media treatment, cells were washed with pre-warmed starvation media (Hanks Balanced Salt Solution (Sigma #H8264) supplemented with 1% BSA w/v) and then incubated in starvation media which, where indicated, was supplemented with indicated compounds.

2.15 Cell lysis for western blots

Adherent cells were washed with ice-cold PBS. For experiments with high numbers of floating cells (i.e. mitotic cells), suspension cells were also collected. After aspiration of PBS, cells were lysed in an appropriate volume of RIPA or TG lysis buffer and left on ice for 5 minutes. At this stage, lysates could be snap-frozen and stored at -80°C. Lysates were then transferred to eppendorf tubes and underwent centrifugation at 13,000g for 10 minutes at 4°C. The supernatant was collected and 20 μl added to 180 μl of BCA working reagent (ThermoScientific), as per manufacturer's instructions, for protein quantification. The remaining sample was added to 4x Laemmli sample buffer and boiled at 95°C for 10 minutes. Samples were then diluted such that they had equal protein concentration with 1x sample buffer.

For mitotic shake off experiments, culture flasks were vigorously tapped to dislodge mitotic cells. The media and subsequent PBS wash were then collected, and the pelleted cells lysed; this lysate represented the mitotic fraction. Adherent cells were directly lysed and this represented the interphase-enriched fraction. Subsequent stages were performed as above.

2.16 Western blot

Samples were loaded on to 10 or 15-well acrylamide gel (Separating acrylamide percentage was either 8%, 10% or 14% depending upon the protein being detected) and ran at 100 volts until the dye front reached the bottom. For optimal resolution of band-shifts some gels were ran for longer periods of time, until maximal separation was achieved. Gels then underwent wet transfer onto methanol-activated PVDF membranes at 300 mA for 100

minutes. Membranes were then blocked in 5% milk/TBST for 1 hour at room temperature. Membranes were then incubated in primary antibodies, diluted in 5% milk or BSA as per antibody guidelines, overnight at 4°C. Primary antibody was washed off with TBST three times for five minutes each. Secondary antibodies were then added for 1 hour at room temperature. Membranes were then washed twice for 5 minutes in TBST, with a final 15-minute wash in TBST (ECL detection) or distilled water (LiCOR and Immobilon detection). ECL (GE healthcare) or Immobilon HRP Western HRP chemiluminescent substrate (Millipore) was then added for 1 minute prior to detection, as per manufacturer's guidelines.

Figure preparation of western blots was performed in Adobe Illustrator. Figures contain blots from a single experiment representative of the indicated number of independent biological experiments. Weight markers to the right of blots are in kDa. Separation lines, where included, are to help with visualisation of the experiment, and do not represent splicing.

2.17 Immunoprecipitation

Cells were either lysed in IP extraction buffer or TG lysis buffer as described previously. Lysates then underwent centrifugation at 13,000g for 10 minutes at 4°C. Protein quantification of clarified lysates was performed by Bradford assay as per manufacturer's instructions. After equilibrating protein concentrations between samples, approximately 90% of the lysate was pre-cleared by incubation with protein A sepharose for 30 minutes 4°C. The lysate was then transferred to fresh protein A sepharose and incubated with indicated antibodies for 2 hours at 4°C in the presence of washed protein A/G sepharose beads. The remaining 10% of lysate was reserved for input blots.

For immunoprecipitation of RAPTOR-GFP, cells were lysed in 0.3% CHAPS buffer. Lysates were passed through a 25G needle five times prior to clarification (13,000g for 10 minutes at 4°C). Protein quantification was performed by Bradford Assay. Lysate was then incubated with GFP-Trap agarose (Chromotek) for 1 hour at 4°C. Beads were then washed three times and resuspended in Laemmli sample buffer.

2.18 Phosphatase treatment

For phosphatase treatment of immunoprecipitated proteins, immunoprecipitation of lysates was performed as previously described. Beads were then washed twice with IP extraction buffer and then twice with PBS to remove any residual phosphatase inhibitors. Beads were then resuspended in 150 µl phosphatase buffer and split into two 75 µl aliquots. One aliquot had 1.5 µl (600 units) of lambda phosphatase added to it, the other was left as a negative control. Reactions were subsequently performed for 30 minutes at 30°C, after

which beads were collected and boiled with 4x sample buffer for 10 minutes before being ran on SDS-PAGE gels as outlined previously.

For phosphatase treatment of whole cell lysates, cells were directly lysed in phosphatase buffer. Lysates were clarified by centrifugation and protein quantification performed by Bradford assay (as per manufacturer's instructions). 2000 U of lambda phosphatase were then added to 70 µl of lysate and incubated for 1 hour at 30°C. The phosphatase reaction was then terminated by the addition of hot 4x sample buffer, and then boiled for 10 minutes at 95°C.

2.19 Membrane-cytosol crude fractionation

Cells were collected and resuspended in isotonic buffer and subsequently lysed by passing through a 25G needle 10 times. Lysates then underwent centrifugation at 900g for 1 minute at 4°C, to clear unlysed cells and interphase nuclei. Supernatant was then transferred to fresh tubes and underwent centrifugation at 21,000g for 15 minutes at 4°C. The supernatant was then transferred to fresh tubes and kept as the cytosolic fraction. For the membranous fraction, the pellet was resuspended in isotonic buffer supplemented with 1% Triton X-100 (v/v) and 0.1% SDS (w/v). Whole cell lysates were acquired by direct lysis of cells in TG lysis buffer. All lysates were then equilibrated for protein concentration within their respective fraction after BCA assay, and boiled in sample buffer, prior to SDS-PAGE as described previously.

2.20 RNA extraction

Cell media was aspirated, and cells subsequently washed with 2 ml of ice-cold PBS. After aspiration of PBS, cells were lysed in an appropriate volume of Trizol, and left on ice for 5 minutes before transfer to a pre-chilled eppendorf. 200 µl of chloroform for every ml of Trizol originally used was then added. Samples were then vigorously shaken for 15 seconds and incubated at room temperature for 5 minutes. They then underwent centrifugation at 13,000g for 15 minutes at 4°C. The resulting clear supernatant, representing the RNA fraction, was then transferred to a clean Eppendorf. 500 µl of isopropanol per a ml of Trizol originally used was then added to samples, with vortexing to mix. Samples were then left at room temperature for 5 minutes, before undergoing centrifugation at 13,000g for 10 minutes at 4°C. The resulting supernatant was aspirated and discarded, leaving the RNA pellet. This was then washed in 75% ethanol, vortexed and centrifuged at 7500g for 5 minutes at 4°C. Ethanol was then aspirated, and the pellet air-dried. The pellet was then resuspended in an appropriate volume of nuclease-free water and heated for 10 minutes at 65°C to solubilise the RNA. RNA concentration was then evaluated on a Nanodrop 2000,

and only samples with a 260/280 value greater than 1.8 used for further experiments. 1 µg of RNA was then diluted in 12 ul of nuclease-free water.

2.21 qRT-PCR

cDNA synthesis was achieved by using Qiagen reverse transcriptase kit as per manufacturer's instructions. Briefly, 2 µl of gDNA wipeout was added to the 1 µg of RNA diluted in 12 µl of water previously recovered. This solution was incubated for 3 minutes at 42ºC, and then returned to ice. 6 µl of reverse transcriptase admixture (4 µl 5xRT buffer; 1 µl RT mastermix; 1 µl RT primer mix) was then added, and the mixture incubated for 15 minutes at 42ºC. The reverse transcriptase was then denatured by incubation of the Eppendorf for 3 minutes at 92ºC. Samples were then either stored at -20ºC or used immediately. Wells were loaded with 12.5 µl SYBR green reagent, 2.5 µl 3µM forward primer, 2.5 µl 3 µM reverse primer and 7.5µl generated cDNA. Samples were performed in technical triplicate. PCR were performed on a Bio-Rad FX96 using the following protocol: 95ºC for 10 minutes; 95ºC for 15 seconds; 60ºC for 10 seconds; repeat steps two and three for 40 cycles; 70ºC for 5 seconds, with incremental increases of 1ºC every cycle till 90ºC. Only those primers with efficiency greater than 80% and a single identifiable melting curve were taken forward. B2M and YWHAZ were used as loading controls.

2.22 Double thymidine block

Twenty-four hours after seeding, culture medium was supplemented with thymidine at a final concentration of 2 mM and cells incubated for 16 hours. Cells were released from G1/S block by washing in PBS and incubation in pre-warmed media for 8 hours. The second block was then initiated for 16 hours. Cells were then released as before for 10 hours. Two hours prior to lysis/ fixation treatments were added to culture medium as indicated.

2.23 Flow Cytometry- Propidium iodide and antibody stain

Propidium Iodide staining was performed as previously described (Garner *et al.*, 2002). Briefly, adherent and suspension cells were collected and fixed in 70% ethanol/PBS. Cells were then incubated in PI stain (50 µg ml^{-1} PI, 0.1 mg ml^{-1} RNAse, PBS) for 30 min at 37ºC.

For immunostaining, cells were collected and fixed in 70% ethanol/PBS. Permeabilization was performed by resuspension of cells in 0.2% Triton X-100/PBS for 10 minutes at room temperature. P-ULK (758) and P-H3 (S10) were diluted 1:200 in 1% BSA/PBS and cells incubated for 1 hour at room temperature. Cells were subsequently incubated in secondary antibodies (1:500) for 30 minutes. Cells were resuspended in 1% BSA/PBS prior to analysis. All flow cytometry was performed on a LSRII (BD Biosciences).

Analysis was performed using FlowJo version 10. To calculate P-ULK1 (S758) intensity, mean intensity of the relevant subpopulation from the P-H3 (S10) antibody-only control was subtracted from the mean intensity of the same subpopulation within the sample.

2.24 Plasmid DNA purification

DH5α bacteria (New England Biolabs) were transformed with relevant constructs, as per manufacturer's instructions. Single bacterial colonies were picked from streaked agar plates, incubated at 37°C overnight and used to inoculate an appropriate amount of LB media as outlined in the relevant Qiagen plasmid DNA purification protocol (either miniprep or midiprep). Bacterial cultures were then processed as outlined in the manufacturer's protocol, and the subsequent purified DNA stored at -20°C.

2.25 Polymerase Chain Reaction

PCR reactions were carried out using Pfu Turbo DNA polymerase as per manufacturer's (Agilent) instructions. Briefly, the reaction mixture (10 ng DNA template, 5% DMSO, 10% 10x pfu turbo buffer, 235 nM forward and reverse primers, 200 µM DNTPs) was then incubated in the a BioRad thermocycler at 94°C for 3 minutes, at which point 1 µl of DNA Turbo polymerase was added. Reaction conditions consisted of 30 cycles (94°C for 30 seconds, 60°C for 1 minute and 72°C for 2 minutes). DNA products were verified by agarose gel electrophoresis.

2.26 Restriction Digest and ligation

DNA products were incubated with restriction enzymes for 2 hours at 37°C. Products were either then ran on agarose gels, where they were extracted with Qiagen DNA gel extraction kit as per manufacturer's instructions or purified with Qiagen PCR purification or miniprep kits. For sub-cloning, ligation was performed using a Rapid DNA ligation kit (Roche #11635379001) with a molar ratio of vector DNA to insert DNA of 1:3.

2.27 Bacterial protein expression

Fragments were PCR amplified from pEGFP-N1-TFEB, pOPH10-ATG13, pEGFP-C1-hAtg14 and pRK5-HA-hULK1, and sub-cloned into GEX-4T1 vector using the previously outlined protocols. Primers used for PCR amplification are outlined in Table 2.8. Constructs were verified by Sanger sequencing (Genewiz).

GEX constructs were then used to transform BL21 (DE3) cells as per manufacturer's instruction (New England Biolabs). At OD600 = 0.6, cells were induced with 0.3 mM IPTG and maintained for 16 hours at 21°C. Cells were lysed in bacteria lysis buffer (1% Triton, 2 mM EDTA, 2 mM DTT, 200 µM PMSF, 5 $\mu g ml^{-1}$ aprotinin, PBS). Recombinant

proteins were then purified from bacterial lysates with glutathione-sepharose beads (GE healthcare). Elution was performed by glutathione competition (10 mM reduced glutathione, 50 mM Tris-HCl pH 8), and eluates were dialysed using a 20kDa cut-off Slide-A-lyzer cassette (Thermo). Protein concentration was performed by Bradford assay against a BSA standard curve.

2.28 Kinase assay

HAP-1 cells were treated with paclitaxel (50 nM) for 16 hours prior to lysis in IP extraction buffer. Lysates were then clarified by centrifugation at 13,000g for 10 minutes at 4°C. Lysates were then pre-cleared with protein A sepharose for 30 minutes at 4°C, with subsequent immunoprecipitation of CCNB1 (using clone GNS1 antibody). Immunoprecipitates were washed twice with high-salt wash buffer and once with 50 mM Tris-HCl pH 7.6. Immunoprecipitated CDK1 was then incubated in kinase buffer (50 mM Tris-HCl pH 7.6, 100 µM EGTA) in the presence or absence of RO-3306 (300 nM) for 15 minutes on ice. 300 ng of substrate, $MgCl_2$ (10 mM) and ATP (100 µM) were then added, and the reaction mixture incubated in a shaking incubator for 15 minutes at 30°C. Where indicated, 2µCi [γ-^{32}P] ATP was also added at this stage. The reaction was terminated by the addition of 4X sample buffer, with subsequent steps performed as above (western blot).

2.29 Fixed cell imaging

Cells were cultured in CellCarrier-96 plates (PerkinElmer) or on 22 mm glass coverslips. Two hours prior to fixation, cells were treated with indicated compounds or starvation media. Cells were then fixed in 4% Paraformaldehyde for 15 minutes at room temperature. Permeabilization was performed with ice-cold methanol for 10 minutes at -20°C (ATG13, WIPI2, P-H3 (S10)), or 0.2% TritonX-100/PBS for 5 minutes at room temperature (mTOR, Lamp2, HA, P-ULK1 (S758), P-H3 (S10)). After two washes in PBS for 5 minutes, cells were then incubated in blocking buffer (1% BSA, 0.02% Triton X-100, 5% goat serum, PBS) for one hour at room temperature. Incubation with ATG13 (1:100), WIPI2 (1:200), P-H3 (S10) (1:200; HCM:1:1000), P-ULK1 (S758) (1:1000), mTOR (1:200) or Lamp2 (1:200) primary antibodies were added overnight at 4°C, with subsequent incubation with Alexa Fluor secondary antibodies (1:500) for one hour at room temperature. Finally, DAPI was added at a concentration of 1 ugml^{-1} or coverslips were mounted in VectaShield Hardset onto glass slides. Cells were then imaged using a 40x or 60x oil immersion objective on a Nikon A1R confocal microscope. Z-stacks were acquired covering the entire cell volume at a spacing of 1 µM. Quantification of ATG13 and WIPI2 puncta was performed using Imaris spot counting function. Figures were prepared using ImageJ, with the same brightness/contrast across all conditions within an experiment.

High content microscopy (HCM) images were acquired using an InCell 6000 system with a 20x air objective (open aperture). Analysis of images was performed using InCell 1000 analyser software (GE). A dedicated algorithm was developed whereby cells (determined by a multiscale top-hat) were divided into P-H3 (S10) positive and negative populations based on cell intensity. P-ULK1 (S758) intensity from the P-H3 (S10) only control was then subtracted from average P-ULK1 (S758) within a condition to calculate the total value for that condition.

For analysis of TFEB nuclear/cytoplasmic localisation, acquired images were analysed by Cell analyser 1000 software. TFEB-GFP was used to generate a cytoplasmic mask, and DAPI stain was used to generate a nuclear mask.

2.30 Live cell imaging

HEK293 GFP-ATG13 H2B-mCherry or HEK293 mRFP-EGFP-LC3 cells were cultured in Ibidi 35mm high glass bottomed dishes (Thistle) for 24 hours. Four hours prior to imaging, cell media was replaced with fresh media. Cells were then treated as indicated prior to cells being transferred to a live-cell imaging stage where they were maintained in an atmosphere of 37°C, 5% CO_2. Images were acquired using a spinning disk confocal microscope, comprising Nikon Ti-E stand, Nikon 60x 1.45 NA oil immersion lens, Yokogawa CSU-X scanhead, Andor iXon 897 EM-CCD camera, Andor laser combiner and OKO lab incubation. GFP and mCherry images were acquired with an exposure time of 100 ms (GFP-ATG13) or 150 ms (mRFP-EGFP-LC3), with z-stacks comprising 45 and 50 images with 0.5 µm spacing (GFP-ATG13) or 30 images with 1 µm spacing (mRFP-EGFP-LC3). New image stacks were acquired every 3 minutes (GFP-ATG13) or 10 minutes (mRFP-EGFP-LC3). For GFP-ATG13, raw confocal images were deconvolved with Huygens Professional software (Scientific Volume Imaging), using the Classic Maximum Likelihood Estimation algorithm and a calculated point spread function (Performed by Simon Walker).

HeLa TFEB-GFP H2B-mCherry cells were cultured in CellCarrier-96 plates (PerkinElmer) and treated with AZD8055 (1 µM) 1 hour prior to imaging. Images were acquired using a Nikon Ti-E based wide-field imaging system equipped with a 20x 0.75 NA air lens, Hamamatsu Flash 4.0 camera, Lumencor Spectra-X LED illuminator and OKO lab incubator. Images were acquired every minute. All images were processed in ImageJ.

2.31 Mass spectrometry (performed by David Oxley)

GFP-ATG13 was immunoprecipitated from HEK293 GFP-ATG13 lysates as above. Coomassie-stained GFP-ATG13 or GST-tagged protein fragment gel bands were excised, destained, reduced, carbamidomethylated, and proteolytically digested (with trypsin or AspN) essentially as previously described (Webster and Oxley, 2009).

Digests were either analysed directly or were first enriched for phosphopeptides using titanium dioxide beads (Titansphere, GL Sciences). Peptides were separated on a reversed-phase column (0.075 x 150mm, Reprosil-Pur C18AQ, 2.1um particles) with a 30min linear gradient from 2 to 40% acetonitrile (containing 0.1% formic acid) at a flow rate of 300nl/min, using an UltiMate 3000 nanoHPLC (Thermo Scientific). The column was interfaced to a Q-Exactive mass spectrometer (Thermo Scientific) operating in either data-dependent MS2 mode (for peptide identification), or parallel reaction monitoring mode (for targeted peptide quantitation).

Mass spectral data were processed using Proteome Discoverer 1.4 (Thermo Scientific) and submitted to Mascot (Matrix Science) for database searching. All identified phosphopeptides were manually validated. Quantitative information from targeted runs was extracted from the MS1 and MS2 data using Skyline software (MacCoss Lab, University of Washington).

2.32 Statistical analysis

One-way and Two-way Anova (Tukey) were performed on paired raw-values as indicated using Graphpad Prism 8. For the purposes of figures $P<0.05$ (*), $P<0.01$ (**), $P<0.001$ (***), $P<0.0001$ (****). For the purposes of graphical representation, raw values were made relative to the untreated control sample.

3 ERK1/2 and TFEB: a complicated relationship

3.1 Introduction

TFEB is the master transcriptional regulator of lysosomal biogenesis via its upregulation of CLEAR genes (Sardiello *et al.*, 2009). In addition, it has been suggested to promote some autophagy initiation genes and LC3 lipidation (Settembre *et al.*, 2011), though its key role is in underpinning the degradative part of autophagic flux. Consistent with this, mTORC1 has been found to directly regulate TFEB via multisite phosphorylation at S122, S142 and S211 (Martina *et al.*, 2012; Roczniak-Ferguson *et al.*, 2012; Settembre *et al.*, 2012; Vega-Rubin-de-Celis *et al.*, 2017). mTORC1 was not the only kinase suspected of regulating TFEB in a nutrient-dependent manner and inhibition of ERK2 was found to cause TFEB nuclear localisation in response to amino acid deprivation (Settembre *et al.*, 2011). Evidence indicating that ERK2 phosphorylated TFEB at S142 mediating its cytoplasmic localisation came from a peptide *in vitro* kinase assay (Settembre *et al.*, 2011; L. Li *et al.*, 2018; S. Li *et al.*, 2019), ERK2 siRNA (Settembre *et al.*, 2011), co-immunoprecipitation of overexpressed ERK2 and TFEB (Settembre *et al.*, 2011), and inhibition of MEK with U0126 (Settembre *et al.*, 2011, 2012; L. Li *et al.*, 2018). However, it was observed that TFEB nuclear localisation only occurred at high doses of U0126, with an EC_{50} of 80 μM (Settembre *et al.*, 2012). Indeed, ERK2 regulation of TFEB nuclear/ cytoplasmic localisation has proved controversial. Martina and colleagues failed to observe any differences in TFEB localisation or phosphorylation upon treatment with U0126 in HeLa cells (Martina *et al.*, 2012). By contrast, the Goding group found that U0126 did promote TFEB nuclear localisation, and concluded that ERK1/2 phosphorylated TFEB at S142 to promote its nuclear export (L. Li *et al.*, 2018). The reason for this discrepancy in findings is unclear. One possibility is the cell lines used. HeLa cells have no constitutive activation of the ERK1/2 pathway (20% P-ERK1/2 relative to HCT116; Kidger, personal communications). However, HT29 (*BRAF* V600E; 50% P-ERK1/2 relative to HCT116; Kidger, personal communications) used in Li and colleagues' study do, although they also observed their findings in MCF7 (WT; 15% P-ERK1/2 relative to HCT116; Kidger, personal communications). A recent study found that $BRAF^{V600E}$ mutant melanoma exhibited ERK1/2-dependent regulation of TFEB localisation, whilst $BRAF^{WT}$ melanoma did not (S. Li *et al.*, 2019). Regardless, the further understanding of ERK1/2 regulation of TFEB could lead to potential therapeutic modulation of autophagy in cancers with ERK1/2 pathway mutations.

In addition, whilst there has been significant investigation of TFEB's regulation in response to acute administration of ERK1/2 pathway modulators and their effects on TFEB

phosphorylation, less is known about potential alterations in TFEB in response to prolonged stimulation of ERK1/2 signalling. Urbanelli and colleagues showed that TFEB levels in the nucleus appeared to increase in response to KRAS induction (Urbanelli *et al.*, 2014). Reagents previously developed by the Cook group, including HR1 cells (HEK293 *ΔCRAF:ER*) cells and HM3 cells (HEK293 *ΔMEKK3:ER*), meant we were well positioned to investigate this further. This could be of potential significance given that autophagy has been implicated in oncogene-induced senescence (Young *et al.*, 2009), a process mediated by the hyperactivation of the ERK1/2 pathway.

3.2 Results

3.2.1 ERK1/2 has minimal effect on TFEB's nuclear/ cytoplasmic localisation in unstimulated conditions

Since U0126 is known to have a plethora of off-target effects (Dokladda *et al.*, 2005; Freeman *et al.*, 2011; Evans *et al.*, 2013; Ripple, Kim and Springett, 2013; Wauson *et al.*, 2013; Ong *et al.*, 2015), we first wanted to assess if selective inhibition of ERK1/2 signalling did cause TFEB nuclear localisation. In order to directly compare our results to Settembre's work we elected to use HeLa cells, which were used in the original studies implicating ERK1/2 regulation of TFEB. Cells were treated with either the highly-selective MEK1/2 inhibitor Trametinib or the selective ERK1/2 inhibitor SCH772984. In addition, we used the ATP-competitive mTOR inhibitor AZD8055 as a positive control. For these experiments, we performed sub-cellular fractionation isolating nuclear and cytoplasmic fractions. As expected, AZD8055 promoted an increase in nuclear TFEB, as well as its dephosphorylation (Figure 3.1.A). Both Trametinib and SCH772984 failed to induce robust nuclear localisation of TFEB or cause any apparent dephosphorylation.

Since ERK1/2 signalling is relatively weak in HeLa cells, due to their lack of a mutation in the pathway causing its constitutive activation (i.e. $KRAS^{G12D}$ or $BRAF^{V600E}$), we postulated that mTOR would play a dominant role. Therefore, to further evaluate the contribution of the ERK1/2 pathway we repeated the experiment in A549 cells which harbour a $KRAS^{G12S}$ mutation, thereby activating both the ERK1/2 and PI3K signalling pathways. Like HeLa cells, AZD8055 resulted in robust TFEB nuclear localisation and dephosphorylation (Figure 3.1.B). Furthermore, MEK1/2 pathway inhibitors failed to induce robust nuclear localisation of TFEB. Thus, mTOR, not ERK1/2, appears to be the dominant regulator of TFEB nuclear/cytoplasmic localisation in both HeLa and A549 cells.

To further interrogate these findings, we established a clonal HeLa TFEB-GFP cell line, since in our hands we failed to achieve specific detection of endogenous TFEB via

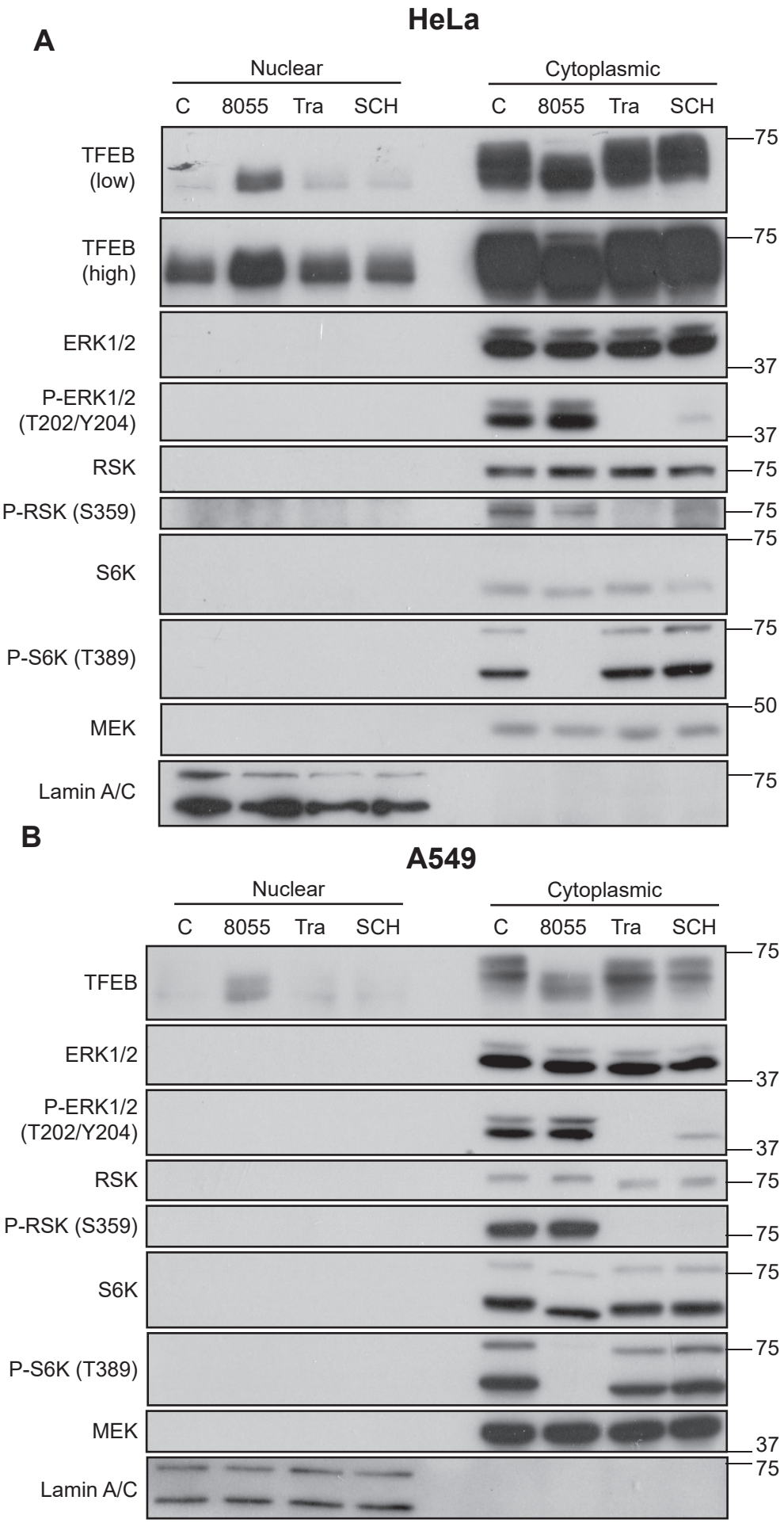

Figure 3.1: Loss of ERK1/2 activity is not sufficient to drive TFEB nuclear localisation.
(A) HeLa cells were treated with indicated compounds for two hours prior to lysis. Compounds: DMSO (0.1%; C), AZD8055 (1 μM; mTOR inhibitor; 8055), Trametinib (1 μM; MEK inhibtor; Tra), SCH772984 (1 μM; ERK inhibitor; SCH). Nuclear and cytoplasmic fractions are indicated. **(B)** Experiment performed as in (A) with A549 cells. Western blots are from a single experiment representative of results from three independent experiments. Molecular weight markers (kDa) are indicated to the right of each blot.

immunofluorescence. Use of TFEB-GFP enabled high-content microscopy to evaluate TFEB nuclear/cytoplasmic localisation in response to inhibitor treatment and was the same methodology employed in Settembre and colleague's work (Settembre *et al.*, 2012). Replicating Settembre's findings, TFEB was localised to the nucleus in response to AZD8055 or high-dose U0126 (80 μM) (Figure 3.2.A/B). In addition, TFEB was localised to the nucleus in response to nutrient deprivation (HBSS + 1% BSA). Treatment with low dose U0126 (10 μM), Trametinib or SCH772984 failed to induce robust nuclear localisation of TFEB in the HeLa TFEB-GFP cell line. These results correlated with the phosphorylation status of endogenous TFEB in the parental HeLa line (Figure 3.2.C), whereby hypophosphorylated TFEB was nuclear localised. Curiously, high dose U0126 appeared to inhibit mTORC1 signalling, with dephosphorylation of both 4E-BP1 and S6K. It is therefore most likely that U0126 was acting off-target on mTORC1 to induce TFEB nuclear localisation in both our results and Settembre's study.

We performed further imaging analysis of a clonal A549 cell line stably expressing TFEB-GFP. Unlike HeLa cells, only relatively low expressing clones were able to be generated, though this still represented a substantial fold increase over endogenous levels (Figure 3.3.C). Of note, TFEB localisation in basal conditions was much more heterogenous in A549 TFEB-GFP cells than in HeLa TFEB-GFP, such that neighbouring cells could have cytoplasmic or nuclear localisation. The mTOR inhibitor AZD8055 promoted consistent nuclear localisation of the TFEB-GFP protein (Figure 3.3.A/B). Like the endogenous protein (Figure 3.1.B), Trametinib and SCH772984 failed to induce robust nuclear localisation of TFEB-GFP (Figure 3.3.B); any changes were relatively minor compared to AZD8055 treatment. Furthermore, it was clear that TFEB localisation remained heterogenous throughout the population upon treatment with ERK pathway inhibitors, such that neighbouring cells showed distinct localisation patterns (Figure 3.3.A). Curiously, nutrient deprivation promoted a consistent and homogeneous cytoplasmic, not nuclear, localisation of TFEB. This was also observed in a second clone (Figure 3.3.B). Since it has been established that a number of cancer lines can maintain mTORC1 signalling during nutrient starvation, for example as a result of mutations in GATOR1 (Bar-Peled *et al.*, 2013), it was important to clarify whether starvation of A549 cells lead to mTORC1 inhibition. HBSS starvation of both parental A549 cells and A549 TFEB-GFP (Clone 2H1) lead to the complete absence of P-S6K (T389), confirming mTORC1 was inhibited (Figure 3.3.C). Unexpectedly, yet in concordance with the microscopy findings, neither endogenous TFEB or TFEB-GFP was hypophosphorylated in response to HBSS starvation. This is despite AZD8055 causing hypophosphorylation. Therefore, two potential lines of investigation arise from the results so far. The first, is whether a minimum threshold of ERK1/2 signalling is

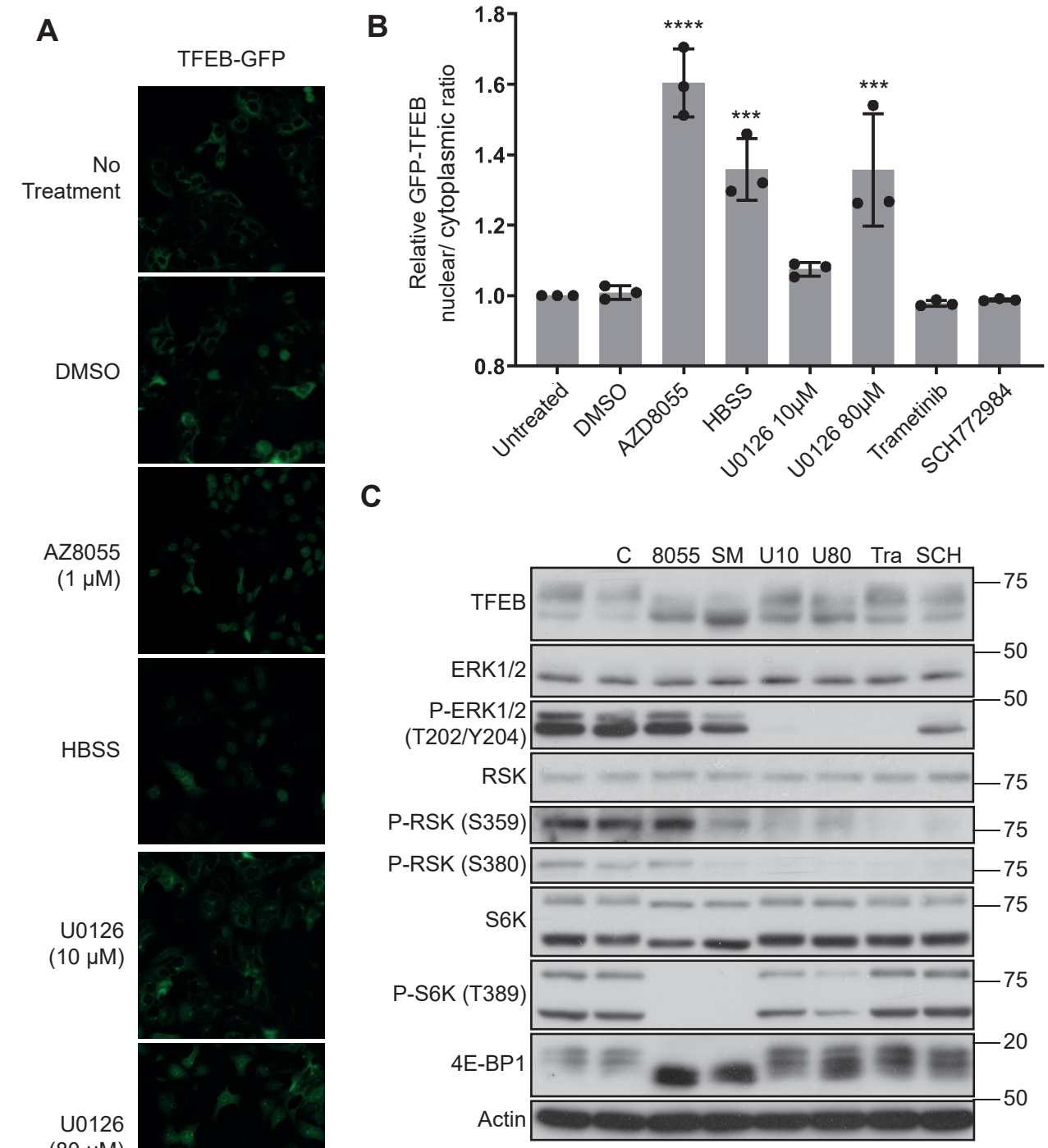

Figure 3.2: U0126 promotes TFEB nuclear localisation correlating with mTORC1 inhbition.
(A) HeLa cells stably expressing TFEB-GFP were treated with indicated compounds or HBSS + 1% BSA for two hours prior to fixation. **(B)** Quantification of (A) where GFP nuclear/ cytoplasmic ratio is shown. Graph shows mean +/- SD across three independent biological experiments relative to untreated control. P-values calculated from Two-way Anova (Tukey). * p<0.05; ** p<0.01; *** p<0.001. **(C)** HeLa cells were treated with indicated compounds for two hours prior to lysis. Compounds: DMSO (0.1%; C), AZD8055 (1μM; mTOR inhibitor), Starvation media (HBSS + 1% BSA; SM), U0126 (10 μM; MEK inhibitor; U10), U0126 (80 μM; U80), Trametinib (1 μM; MEK inhibitor; Tra), SCH772984 (1 μM; ERK inhibitor; SCH). Western blots are from a single experiment representative of results from three independent experiments. Molecular weight markers (kDa) are indicated to the right of each blot.

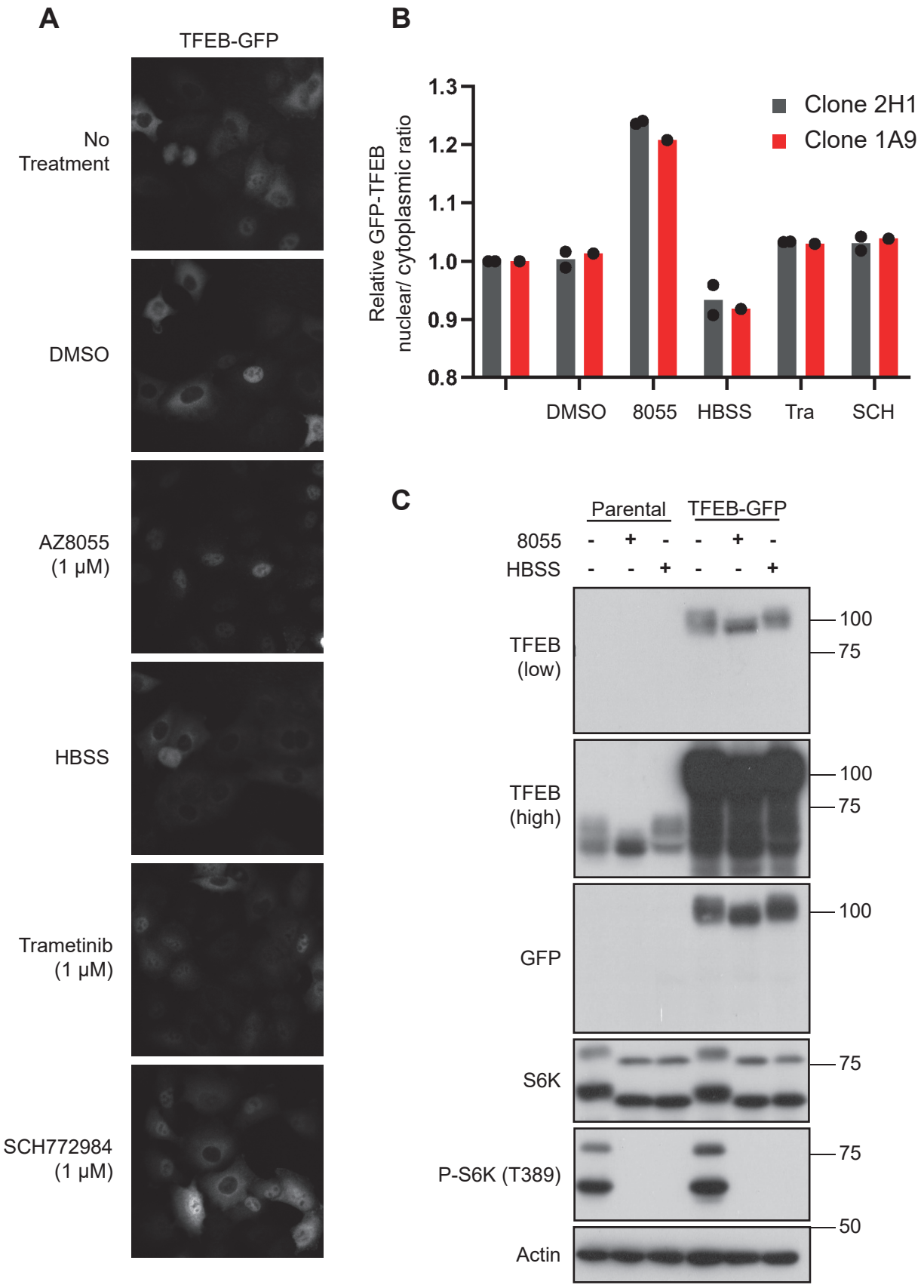

Figure 3.3: TFEB remains hyperphosphorylated and localised to the cytosol upon nutrient starvation in A549.
(A) A549 cells stably expressing TFEB-GFP were treated as indicated for two hours prior to fixation. **(B)** Quantification of relative nuclear/ cytoplasmic GFP values from (A). Graph shows mean for two independent biological experiments for clone 2H1 and a single experiment for clone 1A9. **(C)** Parental A549 and A549 GFP-TFEB (2H1) were treated with either AZD8055 (1 μM) or HBSS + 1% BSA for two hours prior to lysis. Western blots are from a single experiment. Molecular weight markers (kDa) are indicated to the right of each blot.

required for it to have an appreciable effect on TFEB localisation, thus explaining the slight discrepancies between HeLa and A549 cells in terms of their response to inhibition of ERK1/2 signalling. The second, which is not further explored here but is discussed as a potential future direction is why does amino acid deprivation in A549 cells promote cytoplasmic, not nuclear, localisation of TFEB?

3.2.2 EGF stimulation promotes TFEB's localisation to the cytoplasm

To test whether high levels of ERK1/2 signalling were required to modulate TFEB nuclear/ cytoplasmic localisation, we utilised epidermal growth factor (EGF), which promotes a strong activation of the ERK1/2 signalling cascade. We performed a time-course of stimulation with EGF in the stable HeLa TFEB-GFP cell line, both in the presence and absence of amino acids. Furthermore, cells were pre-treated with either DMSO or Trametinib so that phenotypic effects could be attributed to ERK1/2 stimulation or other effects of EGF. Stimulation with EGF promoted a rapid (5-15 minutes) increase in P-ERK1/2 (T202/Y204) which then gradually reduced over the course of the 2-hour stimulation (Figure 3.4.A). This occurred in the presence or absence of amino acids and was blocked in the cells pre-treated with Trametinib. TFEB underwent a nuclear to cytoplasmic localisation that closely correlated with P-ERK1/2 dynamics, with low TFEB nuclear/ cytoplasmic localisation being observed with the highest P-ERK1/2 levels (Figure 3.4.B). Likewise, Trametinib completely blocked the EGF-induced TFEB cytoplasmic localisation. This therefore supports the hypothesis that acute stimulation of ERK1/2 can promote TFEB nuclear to cytoplasmic translocation. The fact that the magnitude of change in TFEB localisation upon EGF stimulation was similar between the nutrient-rich and -depleted conditions, suggests that this mechanism is independent to the nutrient-regulated mechanism of TFEB localisation. This experiment will require repeating before any firm conclusions can be made.

3.2.3 EGF-stimulation does not promote phosphorylation of TFEB at S142

ERK2 is suggested to phosphorylate TFEB at S142, promoting its cytoplasmic localisation (Settembre *et al.*, 2011). This phosphorylation was subsequently suggested in a recent report to regulate its nuclear export (L. Li *et al.*, 2018). We therefore set out to establish whether modulating ERK2 activity altered phosphorylation at S142. TFEB phosphorylation was assessed by multiplex quantitative fluorescent western blotting in HeLa TFEB-GFP cells. As expected, and in concordance with our immunofluorescence data, S142 phosphorylation was decreased in HeLa TFEB-GFP cells starved of amino acids or treated with AZD8055 (Figure 3.5). Trametinib did not decrease S142 phosphorylation in unstimulated conditions. Furthermore, EGF did not alter S142

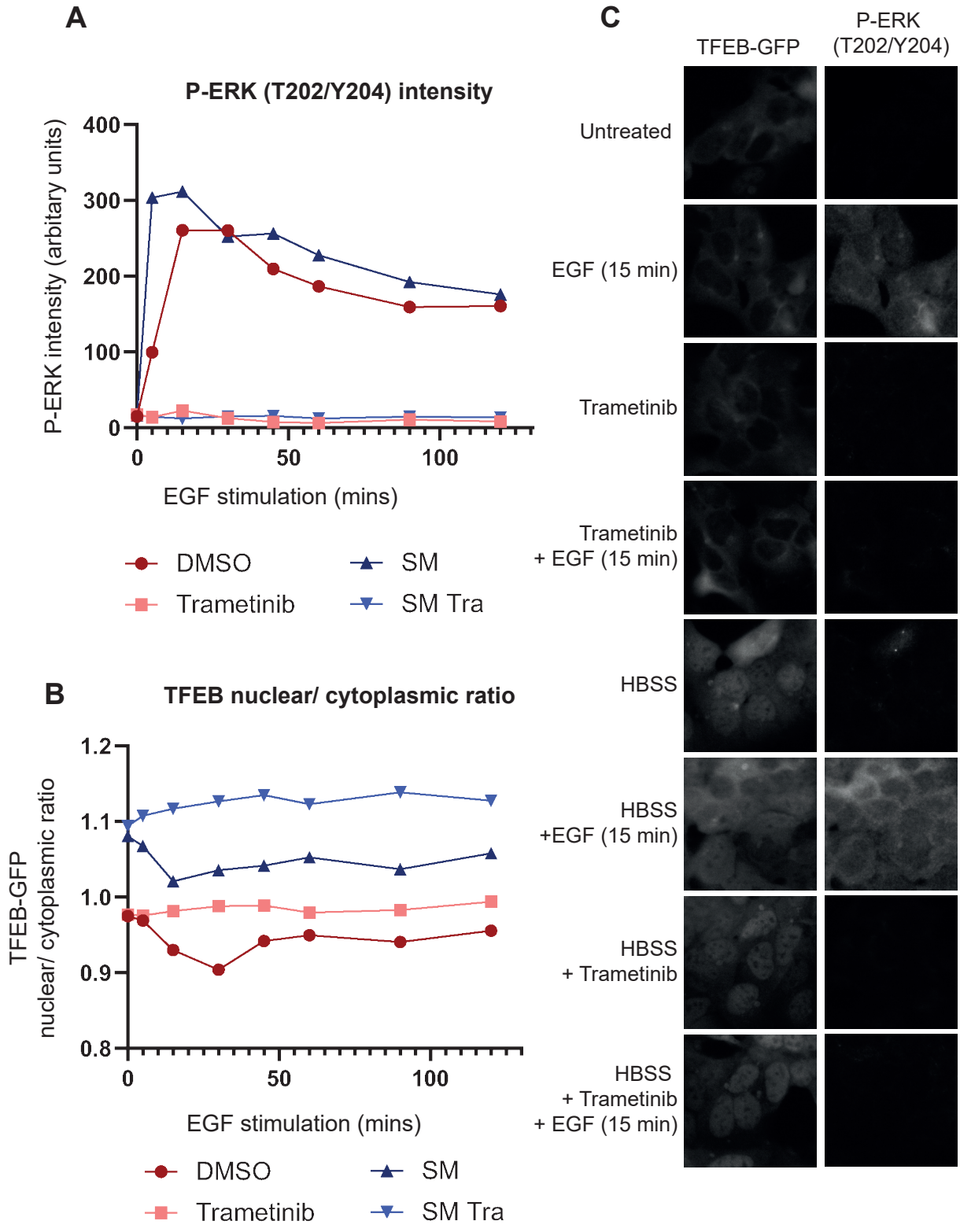

Figure 3.4: EGF promotes cytoplasmic localisation of TFEB in an ERK1/2 dependent manner.
HeLa TFEB-GFP cells were treated as indicated (DMSO; Trametinib (1 μM); HBSS + 1% BSA + DMSO (SM); HBSS + 1% BSA + Trametinib (1 μM) (SM Tra)) for 3 hours. Within this 3 hours, EGF (10 $ngml^{-1}$) was added for indicated times prior to fixation. Cells were stained for P-ERK1/2 (T202/Y204). Quantification from high content microscopy for a single experiment are shown for: **(A)** P-ERK (T202/Y204) intensity **(B)** TFEB-GFP nuclear/ cytoplasmic ratio. **(C)** Example images from indicated treatments

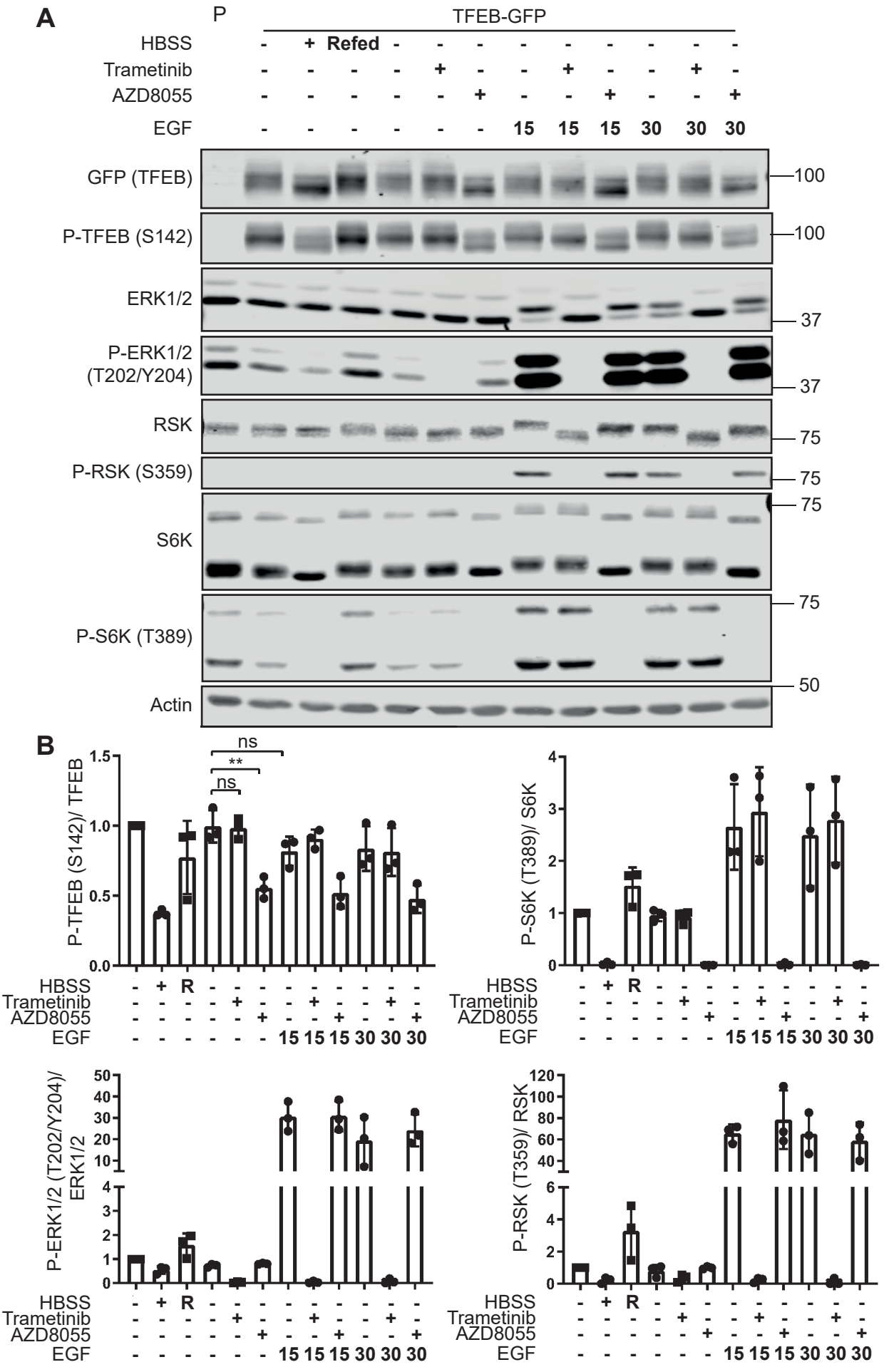

Figure 3.5: TFEB S142 phosphorylation is dependent on mTORC1 signalling but not ERK1/2.(A) HeLa GFP-TFEB cells were treated as follows: HBSS + 1% BSA (t=2 hrs), Refed (R; HBSS +1%BSA t=2 hrs, complete media t=30 min), AZD8055 (1μM; t=1 hr), Trametinib (1 μM; t=1 hr), EGF (10 $ngml^{-1}$; t= indicated mins). Fluorescent western blots are from a single experiment representative of three independent experiments. Molecular weight markers (kDa) are indicated to the right of each blot. **(B)** Quantification of (A). Mean +/- SD from three independent experiments. P-values calculat-ed from One-way Anova (Tukey). ns $p>0.05$; ** $p<0.01$.

phosphorylation, despite causing substantial increases in P-ERK1/2 (T202/Y204) (Approximately 30-fold at 15 minutes), and the ERK1/2 substrate P-RSK (T359) (Approximately 70-fold at 15 minutes). Therefore, despite S142 being a conserved site, analogous to S73 in MITF which is known to be phosphorylated by ERK1/2 (Hemesath *et al.*, 1998), this does not support the hypothesis that TFEB is phosphorylated by ERK1/2 in cells, despite several groups showing that ERK1/2 can phosphorylate this site *in vitro*. Interestingly, EGF also promoted small increases in P-S6K (T389) which were also not reflected in P-TFEB (S142). This suggests that increases in mTORC1 activity in response to EGF stimulation, do not result in increases of P-TFEB (S142). Overall, we found no evidence that EGF-stimulation was mediating changes in TFEB nuclear/ cytoplasmic localisation via S142 phosphorylation.

3.2.4 Dephosphorylation of TFEB in A375 cells correlates to cell cycle arrest and not ERK1/2 pathway inhibition

It has recently been proposed that ERK1/2 regulates TFEB localisation and phosphorylation in melanoma lines with mutations in ERK1/2 pathway proteins, but not in wild-type lines (S. Li *et al.*, 2019). These findings fit with our data presented thus far that high levels of ERK1/2 signalling are required to mediate TFEB localisation changes. Curiously, they suggested the ERK1/2 promoted the lysosomal localisation of TFEB and its phosphorylation by mTORC1. Thus, ERK1/2 pathway inhibition lead to complete collapse of the phosphorylation of TFEB, observed as a hypophosphorylated band similar to treatment with mTORC1 inhibitors or nutrient starvation. Such observations were only made at 12 hours after treatment with a BRAF inhibitor and these correlated with inhibition of mTORC1 itself at this time point. Whilst the authors demonstrated that mTORC1 activation could not rescue this hypophosphorylation, the prolonged periods of time required for the effect caused us to question if this was a direct effect of ERK1/2 inhibition. To investigate this further we performed a time course with the highly selective inhibitors Trametinib (MEK1/2) and Vemurafenib ($BRAF^{V600E}$ inhibitor), both clinically approved for melanoma treatment. We selected A375 cells as this was $BRAF^{V600E}$ mutant and the same cell line used in Li and colleagues study (S. Li *et al.*, 2019). Both P-ERK1/2 (T202/Y204) and P-RSK (T359) signals were lost within an hour of treatment (Figure 3.6). TFEB remained in a hyperphosphorylated state until 16-hours and 24-hours, when a greater proportion of TFEB was observed in a hypophosphorylated state; however, a complete collapse of TFEB phosphorylation was never observed, contrasting with Li's study. The delayed dephosphorylation of TFEB correlated with loss of P-Rb (S795), suggesting the cells had undergone cell cycle arrest. Overall, it would appear that dephosphorylation of TFEB was

A

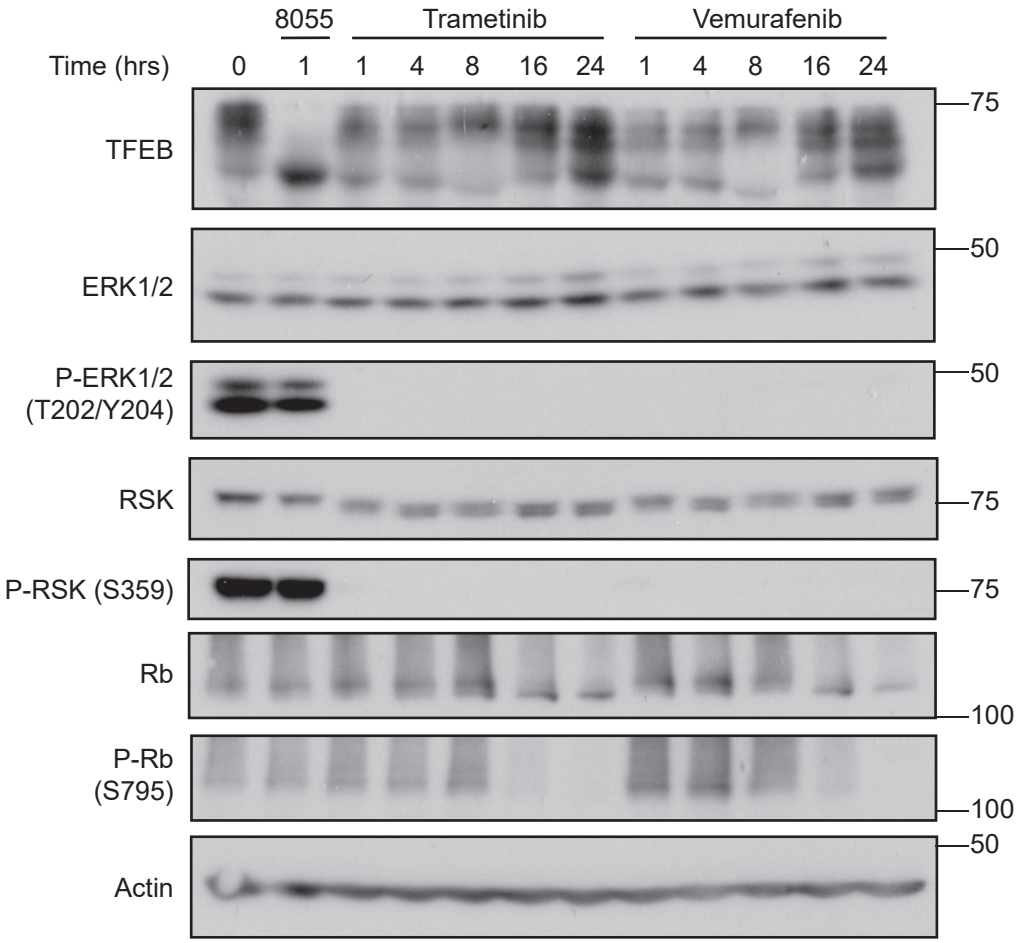

Figure 3.6: A375 cells do not exhibit TFEB dephosphorylation in response to ERK1/2 path-way inhibition.
(A) A375 cells were treated with either trametinib (100 nM) or vemurafenib (2 μM) for indicated times prior to lysis. As a positive control, AZD8055 (1 μM; t=1 hr) was added. Western blots are from a single experiment, representative of two independent experiments. Molecular weight markers (kDa) are indicated to the right of each blot.

not a direct result of ERK1/2 inactivation in A375 cells, and it is more likely that differences in TFEB phosphorylation observed were a consequence of the G1 cell cycle arrest elicited by these drugs (Sale *et al.*, in press), but this requires further investigation.

3.2.5 Sustained ERK1/2 activation increases TFEB abundance in HEK293 cells.

Since transient alterations in ERK1/2 signalling failed to consistently regulate TFEB nuclear/cytoplasmic regulation and phosphorylation, we did not pursue this further. We next wanted to investigate whether prolonged ERK1/2 hyperactivation led to alterations in TFEB abundance, since Urbanelli and colleagues (Urbanelli *et al.*, 2014) had reported increases in nuclear TFEB in response to transfection of oncogenic *KRAS*. HR1 cells possess a *ΔCRAF:ER* construct, whereby the isolated kinase domain is fused to ER; this represses the kinase domain but addition of 4-hydroxytamoxifen (4-HT) promotes de-repression and activation of the CRAF kinase (Boughan *et al.*, 2006). This leads to rapid and selective activation of the ERK1/2 signalling cascade upon 4-HT treatment (Figure 3.7.A/B). Curiously, we found that TFEB protein levels were markedly raised from 8 hours after ERK1/2 signalling activation, and this was sustained for at least 48 hours (Figure 3.7.B). This increase in protein level was not reflected in TFE3, suggesting the regulation mechanism was selective for TFEB and not conserved across TFEB family members, though we did not assess MITF. To evaluate whether this increase in TFEB protein levels was specific to the activation of the ERK1/2 signalling cascade or due to other effects of 4-HT, we pre-treated HR1 cells with DMSO or the MEK1/2 inhibitor Trametinib, prior to stimulation with 4-HT. The addition of Trametinib completely abolished 4-HT induced increases in TFEB protein levels (Figure 3.7.C), thus suggesting this was a result of ERK1/2-dependent signalling.

Protein kinase C has previously been shown to increase TFEB protein levels by phosphorylating the C-terminus resulting in TFEB's stabilisation (Ferron *et al.*, 2013). Curiously, the C-terminal site S467 is conserved in MITF (S409). MITF S409 is known to be phosphorylated by RSK-1, which in combination with S73 phosphorylation by ERK1/2 promotes its degradation via the proteasome (Wu *et al.*, 2000). Since RSK is a well validated substrate of ERK1/2, we hypothesised that RSK phosphorylation at S467 could be altering the rate of degradation of TFEB (though this would be the opposite of MITF). To test this, we treated HR1 cells with 4-HT, activating the ERK1/2 signalling pathway and activating RSK, as measured by P-YB1 (S102) (Stratford *et al.*, 2008). Treatment with the RSK inhibitor LJH685 failed to reverse 4-HT-induced increases in TFEB protein levels (Figure 3.7.D). Curiously, LJH685 appeared to promote feedback activation of the ERK1/2 signalling pathway, as measured by increases in P-ERK (T202/Y204) in the absence of 4-

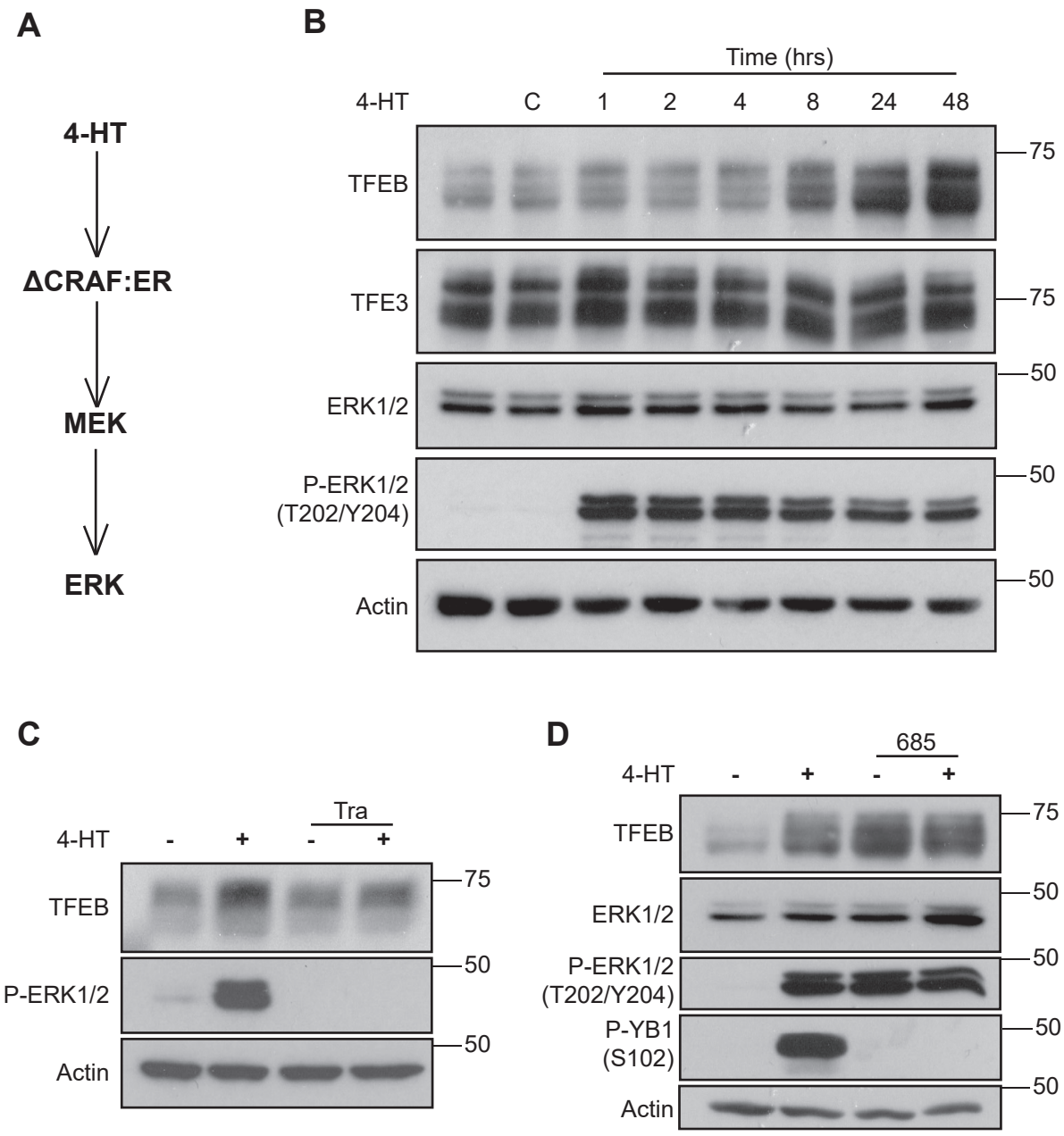

Figure 3.7: Prolonged 4-HT treatment in HR1 cells leads to increased TFEB protein levels in an ERK1/2 dependent manner.
(A) Schematic of CRAF signalling pathway **(B)** HR1 cells were treated with 4-HT (100 nM) for indicated time. **(C)** HR1 cells were pre-treated with either DMSO or Trametinib (1 μM) for 1 hour, and subsequently treated with EtOH or 4-HT for 8 hours. **(D)** HR-1 cells were treated with 4-HT (100 nM) or LJH685 (3 μM; RSK inhibitor) for 8 hours. All western blots are from a single experiment representative of three experiments showing similar results. Molecular weight markers (kDa) are indicated to the right of each blot.

HT. Like 4-HT treatment, LJH685 promoted increases in TFEB protein level, supporting the hypothesis that prolonged ERK1/2 signalling was driving increases in TFEB protein level.

It was noticeable that TFEB was hyperphosphorylated to a greater extent within 2 hours of 4-HT treatment in HR1 cells. Based on our previous data which found no clear links between ERK1/2 activity and TFEB phosphorylation status, we queried whether this was more likely a result of downstream mTORC1 activation, since it is known that ERK1/2 stimulates mTORC1 activity (Introduction; Figure 3.8.A). Indeed, *ΔCRAF:ER* activation increased S6K phosphorylation, and this was reversed by the MEK1/2 inhibitor Trametinib (Figure 3.8.B). As previously observed, 4-HT treatment led to TFEB hyperphosphorylation; however, combining 4-HT treatment with either the mTOR inhibitor AZD8055 or nutrient depletion completely prevented the hyperphosphorylation of TFEB, despite active ERK1/2 signalling. Therefore, the hyperphosphorylation of TFEB in HR1 cells upon 4-HT treatment is likely a result of mTORC1 activation downstream of ERK1/2.

In order to evaluate the contribution of other MAP kinases, we utilised HM3 cells which stably express a ΔMEKK3:ER construct, such that treatment with 4-HT promotes activation of the JNK, p38 and ERK1/2 pathways (Todd *et al.*, 2004) (Figure 3.9.A). Like HR1 cells, treatment of HM3 cells with 4-HT promoted increases in TFEB protein levels at 8-hours of treatment (Figure 3.9.B). Curiously, the increase in TFEB protein level was not reversed by any single agent inhibitor, suggesting there may be redundancy in MAPK signalling and increases in TFEB protein levels (Figure 3.9.C). To test this, combinations of inhibitors should be tested.

We next wanted to evaluate whether TFEB protein levels correlated with mRNA levels. As observed previously, 4-HT treatment stimulated increases in TFEB protein levels (Figure 3.10.A). In parallel, we performed qRT-PCR on mRNA extracts. qRT-PCR showed high variability between independent biological samples (Figure 3.10.B), despite small technical replicate variability, and we speculate this is likely a result of TFEB's low expression. Regardless, there was no obvious increase in TFEB mRNA levels upon 4-HT treatment. Treatment with the translation inhibitor emetine (40S ribosomal subunit inhibitor) did prevent 4-HT-induced increases in TFEB protein level (Figure 3.10.C). This suggests that whilst increases in TFEB protein levels are not a result of increased transcription, it does depend upon de-novo translation. These results must be treated with caution. TFEB responds to numerous and varied stress inducers, and it is apparent that emetine has promoted TFEB dephosphorylation. Therefore, alterations in TFEB's response to 4-HT may be affected by a global stress response to emetine treatment. In addition, it may be that increases in TFEB protein level are a downstream effect, with ERK signalling promoting the

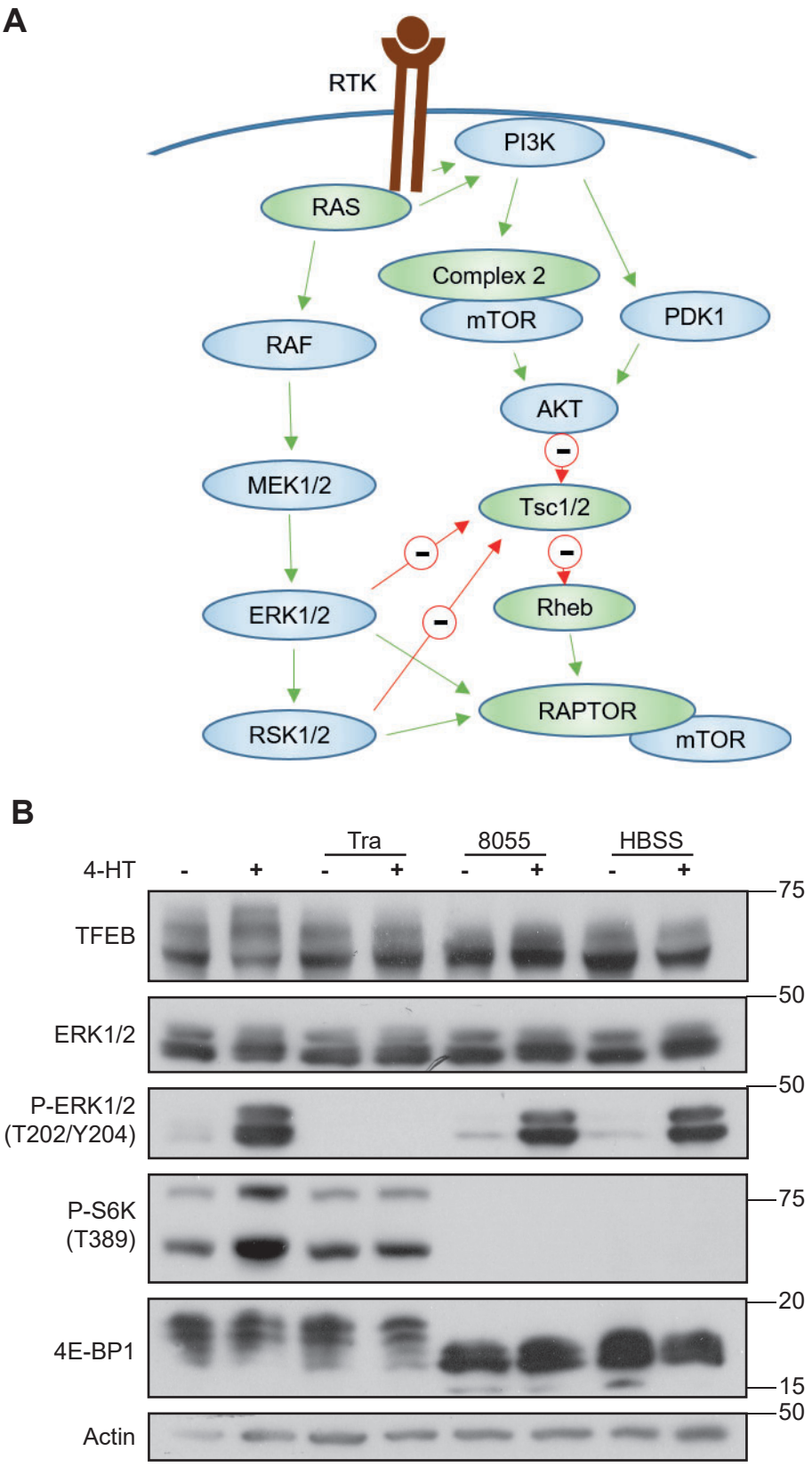

Figure 3.8: Hyperphosphorylation of TFEB observed upon 4-HT treatment in HR1 cells is responsive to mTORC1 inhibition.
(A) Schematic representation of interactions between the ERK1/2 and mTORC1 signalling pathways. **(B)** HR1 cells were treated with 4-HT (100 nM), Trametinib (1 μM; MEK inhibitor), AZD8055 (1 μM; mTOR inhibitor) or HBSS + 1% BSA for two hours. All western blots are from a single experiment. Molecular weight markers (kDa) are indicated to the right of each blot.

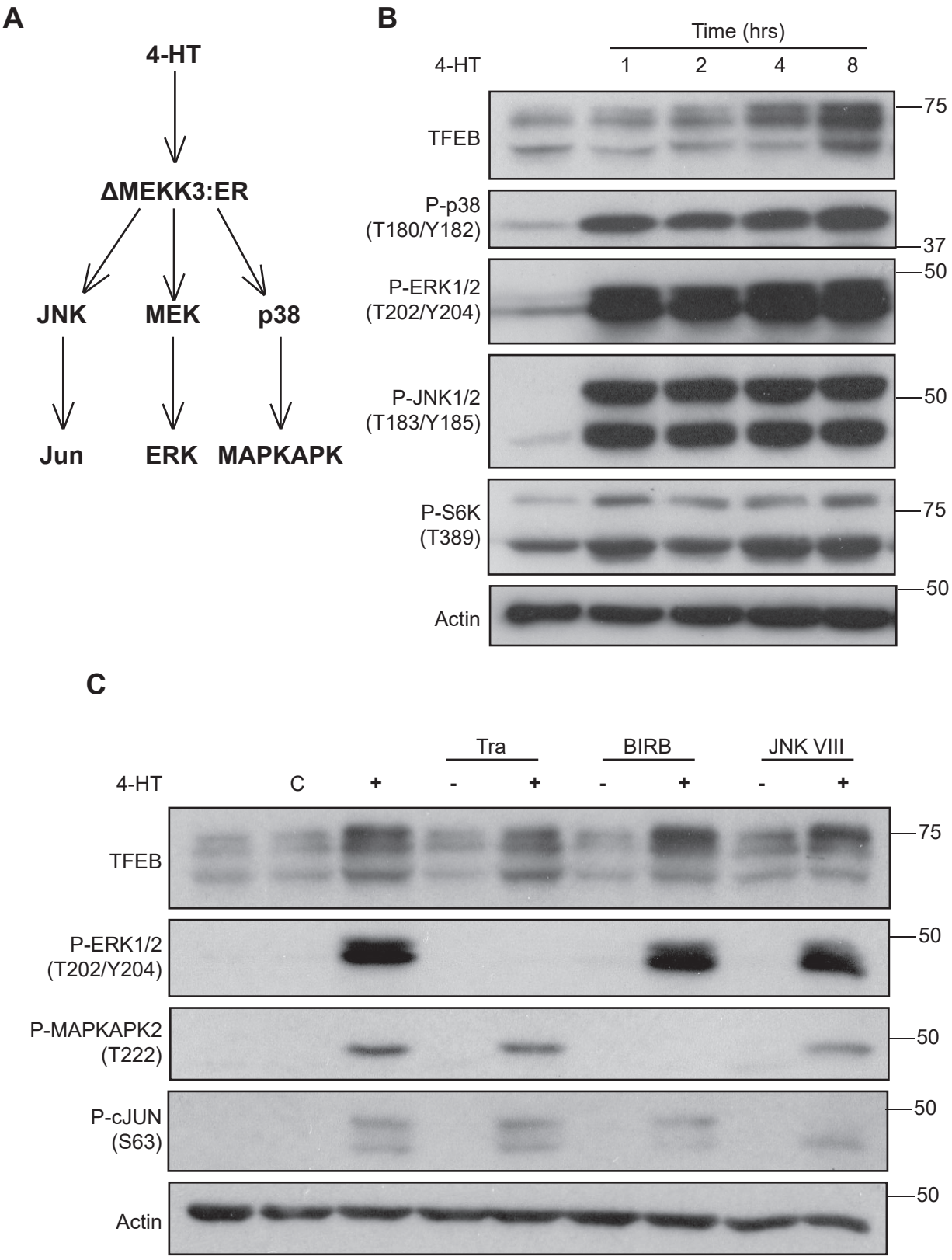

Figure 3.9: Prolonged treatment of HM3 cells with 4-HT leads to increased TFEB protein levels, but this is not solely dependent on ERK1/2.
(A) Schematic of MEKK3 signalling pathway **(B)** HM3 cells were treated with 4-HT (100 nM) for indicated time. **(C)** HM3 cells were pre-treated for 1 hour with either DMSO, Trametinib (1 μM; MEK inhibitor), BIRB796 (1 μM; p38 inhibitor) or JNK VIII (10μM; JNK inhibitor). Cells were subsequently treated with either EtOH or 4-HT (100 nM) for 8 hours. All western blots are from a single experiment representative of three experiments showing similar results. Molecular weight markers (kDa) are indicated to the right of each blot.

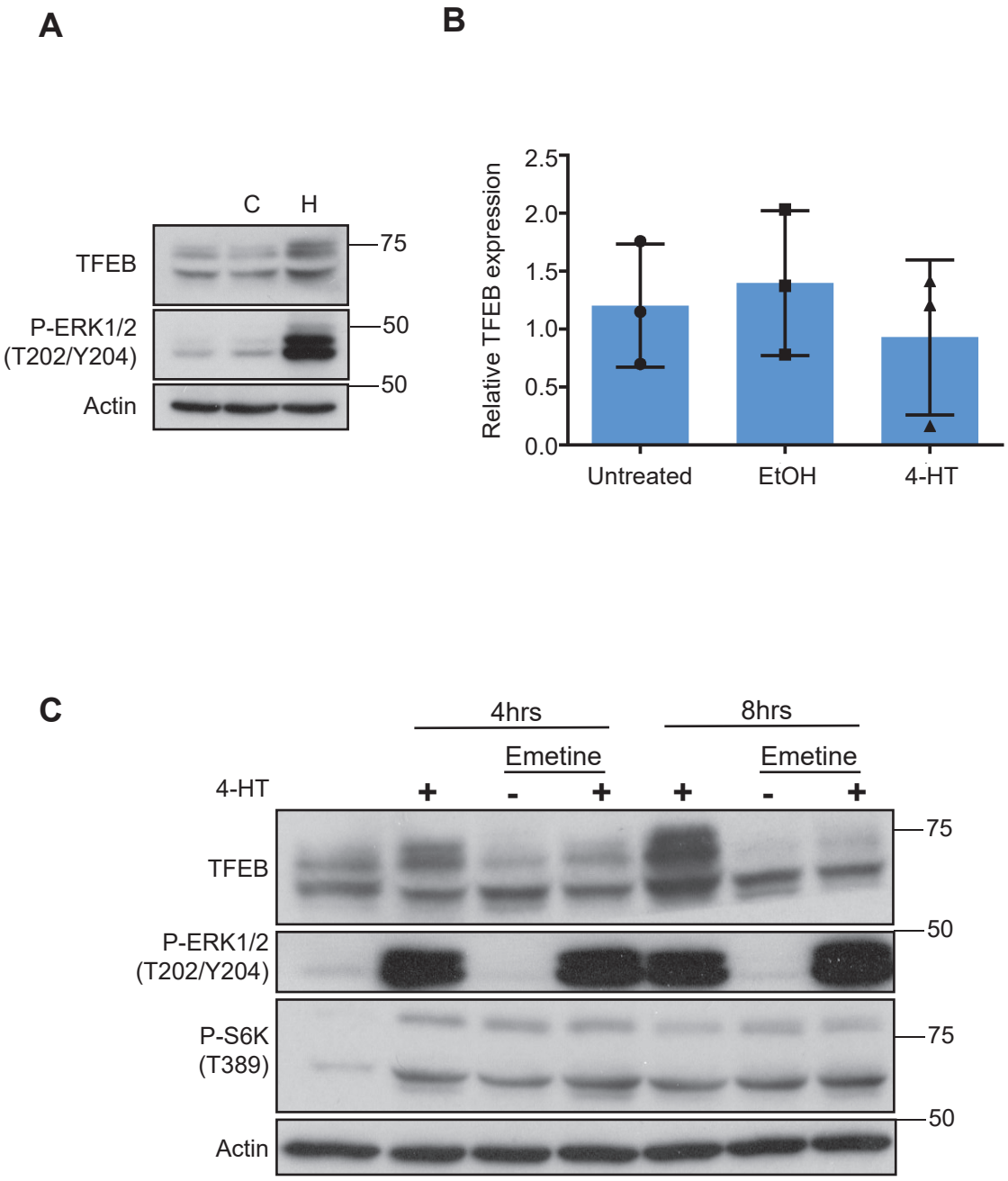

Figure 3.10: TFEB mRNA levels are stable upon prolonged 4-HT treatment; however, increases in TFEB protein level do depend upon de novo translation.

HR1 cells were treated with either EtOH (C) or 4-HT (H; 100 nM) for 8 hours. **(A)** Western blots were performed to validate ERK1/2 pathway activation. Western blots are from a single experiment repre-sentative of three experiments showing similar results. **(B)** qRT-PCR of TFEB mRNA was used to quantify transcript levels. qRT-PCR data is mean +/- SD from three independent experiments. **(C)** HR1 cells were treated with 4-HT (100 nM) and/or emetine (10 μm) for 8 hours. We stern blots are from a single experiment. Molecular weight markers (kDa) are indicated to the right of each blot.

transcription and translation of another protein which then has an effect on TFEB at the protein level. The fact that alterations in TFEB protein level took 8 hours to occur points towards this. Therefore, we cannot conclude from this dataset that alterations in the translation of TFEB transcript are responsible for alterations in TFEB protein level.

3.2.6 Inhibition of ERK1/2 in cancer cell lines with ERK1/2 pathway mutations, does not consistently lead to TFEB protein level reductions.

We next wanted to establish whether alterations in TFEB protein level occurred upon inhibition of endogenous ERK1/2 signalling. To test this, we treated four cancer cell lines harbouring mutations of either *KRAS* (A549 and HCT116) or *BRAF* (COLO205 and HT29) with Trametinib over 48 hours. Whilst there was variability between experiments, there was a relatively consistent decrease in TFEB protein levels in HCT116, whilst TFEB protein levels were relatively stable in the other cell lines tested (Figure 3.11 and 3.12). We also observed dephosphorylation of TFEB in HCT116, COLO205 and HT29 cells. In the case of COLO205 and HT29, this clearly correlated with a reduction in mTORC1 activity (Figure 3.12). In HCT116 cells no such correlation was apparent.

Based on the temporal dynamics of the dephosphorylation in HCT116 cells, we hypothesised that it might be a result of cell cycle arrest. To test this hypothesis, we incubated HCT116 cells for 24 hours with various doses of either the mTOR inhibitor AZD8055, or the CDK4/6 inhibitors LY2835219 or PD0332991. As expected, AZD8055 promoted dephosphorylation of TFEB correlating with reductions in P-S6K (T389) (Figure 3.13.A). In addition, there was loss of p62 and the unlipidated form of LC3B (LC3B-I), indicative of an increase in autophagic flux. The reason that AZD8055 promoted loss of LC3B-I, as opposed to increases in LC3B-II, is likely because of the long treatment time (24 hours) relative to a majority of studies which add mTOR inhibitors for a short time (1-4 hours). This prolonged treatment time was used due to the inclusion of CDK4/6 inhibitors, which would be expected to affect the G1 phase of the cell cycle, meaning that sufficient time is required to enable all cells to pass through to G1. As expected, PD0332991 promoted dephosphorylation of Rb (S795) from 200 nM but did not promote changes in autophagy proteins except at 5 μM, at which it was most likely exerting off-target effects (Figure 3.13.B). By comparison, LY2835219 promoted a dose dependent reduction in P-Rb (S795) and P-S6K (T389), suggesting inhibition of both CDK4/6 and mTORC1 (Figure 3.13.C). Comparisons of the cell cycle arrest caused by PD0332991 and LY2835219, as assessed by EdU staining (Figure 3.14) and P-Rb (S795) (Figure 3.13) demonstrated that TFEB dephosphorylation was not a result of cell-cycle arrest. This is because a dose of 1 μM PD0332991 and 500 nM LY2835219 both caused approximately similar decreases in

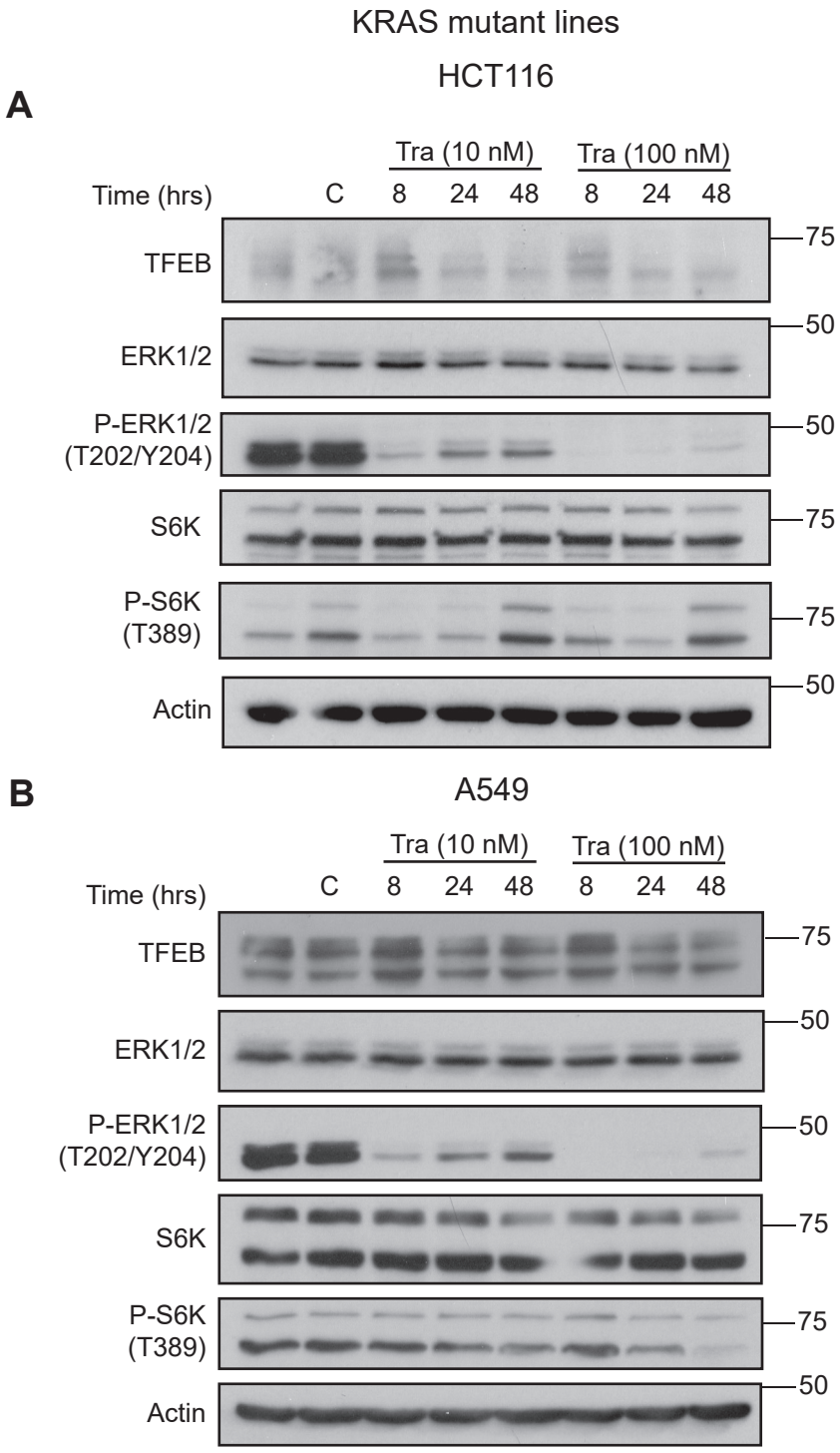

Figure 3.11: Inhibition of ERK1/2 signalling does not directly regulate TFEB protein levels in KRAS mutant cell lines.
HCT116 **(A)** and A549 **(B)** cells were treated with either 10 or 100 nM Trametinib for up to 48 hours. All western blots are from a single experiment representative of three independent experiments. Molecular weight markers (kDa) are indicated to the right of each blot.

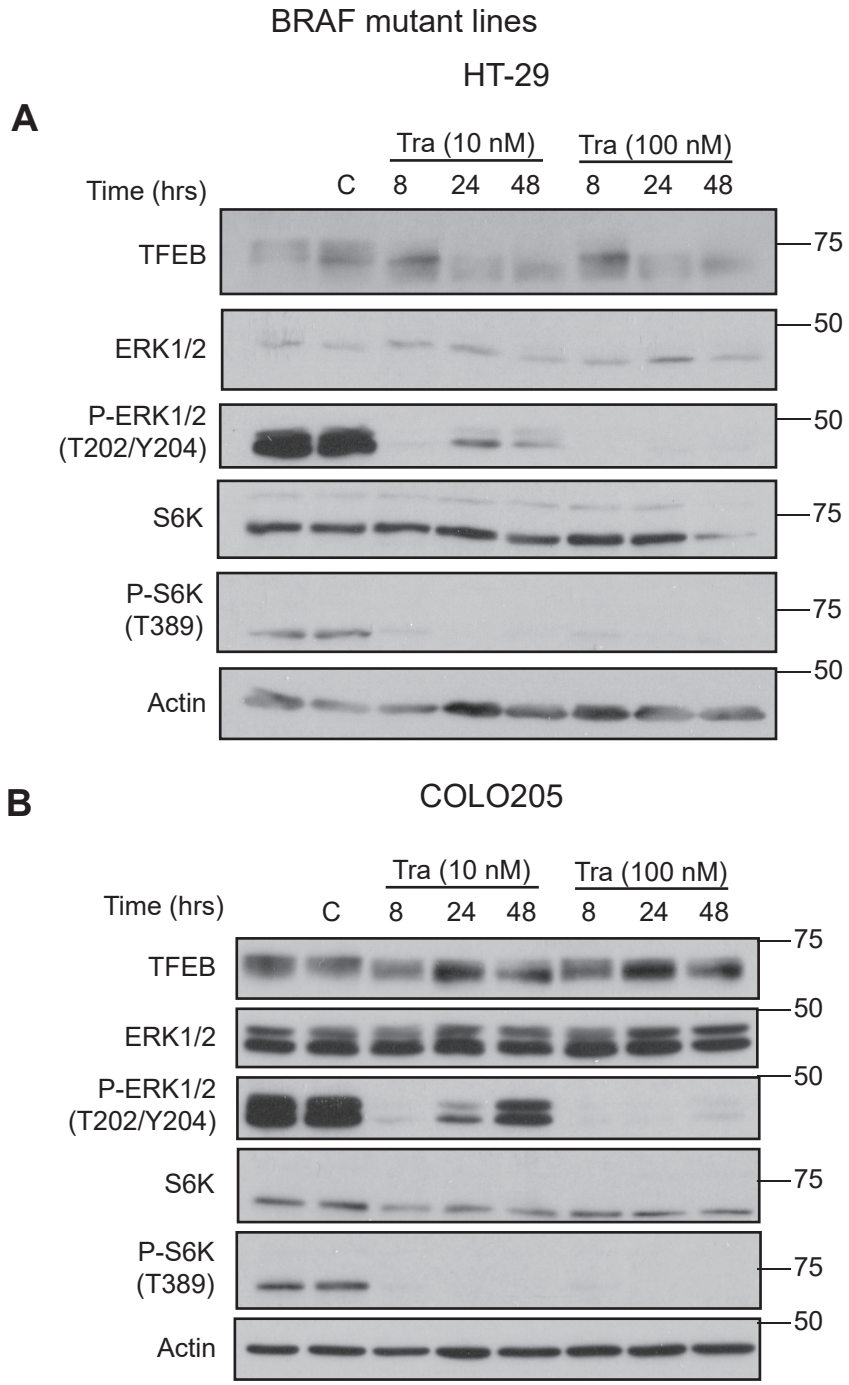

Figure 3.12: Inhibition of ERK1/2 signalling does not directly regulate TFEB protein levels in BRAF mutant cell lines.
HT-29 **(A)** and COLO205 **(B)** cells were treated with either 10 or 100 nM Trametinib for up to 48 hours. All western blots are from a single experiment representative of three independent experiments (though it is noted one replicate of HT29 did show reduced TFEB levels upon trametinib treatment). Molecular weight markers (kDa) are indicated to the right of each blot.

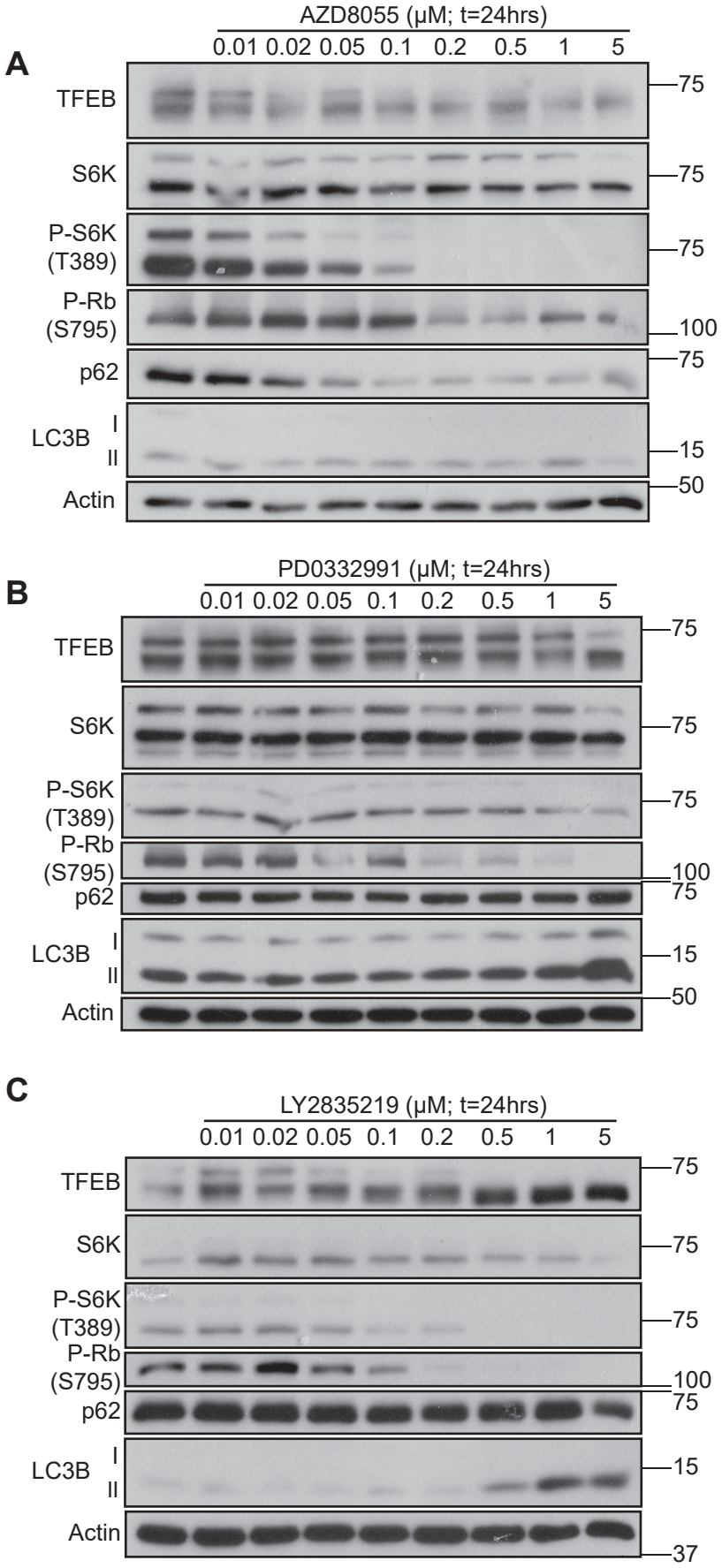

Figure 3.13: TFEB protein levels do not vary with cell cycle arrest. **(A-C)** HCT116 cells were treated with compounds at indicated doses for 24 hours. **(A)** AZD8055 (mTOR inhibitor), **(B)** PD0332991 (CDK4/6 inhibitor), **(C)** LY2835219 (CDK4/6 inhibitor). Western blots are from a single experiment representative of three independent experiments. Molecular weight markers (kDa) are indicated to the right of each blot.

A

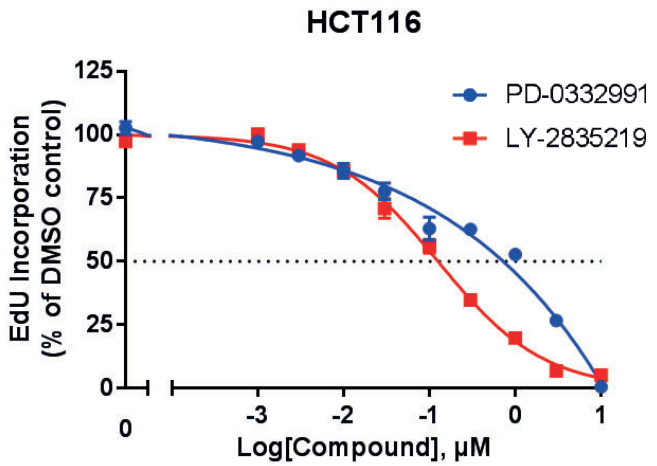

Figure 3.14: CDK4/6 inhibitors prevent EdU incorporation, indicating cell cycle arrest, in a dose dependent manner.
(A) HCT116 cells were treated with either PD0332991 or LY2835219 for 24 hours. One hour prior to fixation they were pulsed with EdU (10 µM). Data represents mean +/- SEM from three independent experiments. Experiments performed and data provided by Andrew Kidger.

EdU incorporation, but whilst LY2835219 caused pronounced TFEB dephosphorylation, PD0332991 did not. Treatment with LY2835219, in comparison to AZD8055, caused no change in p62. Furthermore, LY283219 treatment was associated with an accumulation of the lipidated form of LC3B (LC3B-II), with no concurrent loss of unlipidated LC3 (LC3B-I). These alterations in LC3 are in stark contrast to the findings for AZD8055, where loss of unlipidated LC3 (LC3B-I) was the predominant feature. Furthermore, TFEB dephosphorylation appeared to occur to a greater extent than AZD8055. Therefore, TFEB dephosphorylation was likely mediated by factors in addition of mTORC1 inhibition. It was therefore important to assess the temporal dynamics of TFEB and S6K dephosphorylation upon LY2835219 treatment. Whilst we observed that P-S6K (T389) reduced slowly over time, suggesting that LY2835219 was not directly inhibiting mTORC1 (Figure 3.15.A), TFEB dephosphorylation occurred within the first hour of LY2835219 treatment. This suggests that the dephosphorylation of TFEB was occurring through another mechanism.

It is known that mTORC1 activity and TFEB phosphorylation status is dependent upon lysosomal integrity (Settembre *et al.*, 2012). Therefore, defects in the lysosome could result in mTORC1 inactivity, dephosphorylation of TFEB and inhibition of autophagic flux. To test whether autophagic flux was impaired, we treated cells with each of the indicated compounds for 24 hours, and then in the last hour treated them with the vacuolar H^+-ATPase inhibitor bafilomycin A1, which impairs lysosomal acidification and autophagosome-lysosomal fusion (reviewed: Klionsky *et al.*, 2008). As expected, bafilomycin A1 promoted the accumulation of LC3-II in cells treated with either AZD8055, PD0332991, or DMSO control; showing that autophagic flux was still active in these cells (Figure 3.15.B). Bafilomycin had no effect on cells pre-treated with LY2835219, suggesting that this compound had already impaired lysosome function, thereby preventing the degradation of autophagosomes.

Further supporting the hypothesis that lysosomes were defective, cells treated with LY2835219 exhibited vacuoles observable by light microscopy, whilst cells treated with AZD8055 and PD0332991 exhibited no alterations in morphology (Figure 3.16.A). Immunofluorescence of LY2835219-treated cells revealed that these vacuoles stained positive for Lamp2 but not LC3 (Figure 3.16.B). This suggested a failure in fusion of the autophagosome with the lysosome as the principle mechanism behind the blockade of autophagic flux. After we collected these results, it was demonstrated by another group that LY2835219 promoted lysosomal membrane permeabilization (Knudsen *et al.*, 2017), and our findings are consistent with this hypothesis. It has also been demonstrated that both PD0332991 and LY2835219 undergo ‘lysosomal trapping’ whereby the drugs, with a relatively basic pKa (above 8), are protonated within the acidic lysosome; however, this

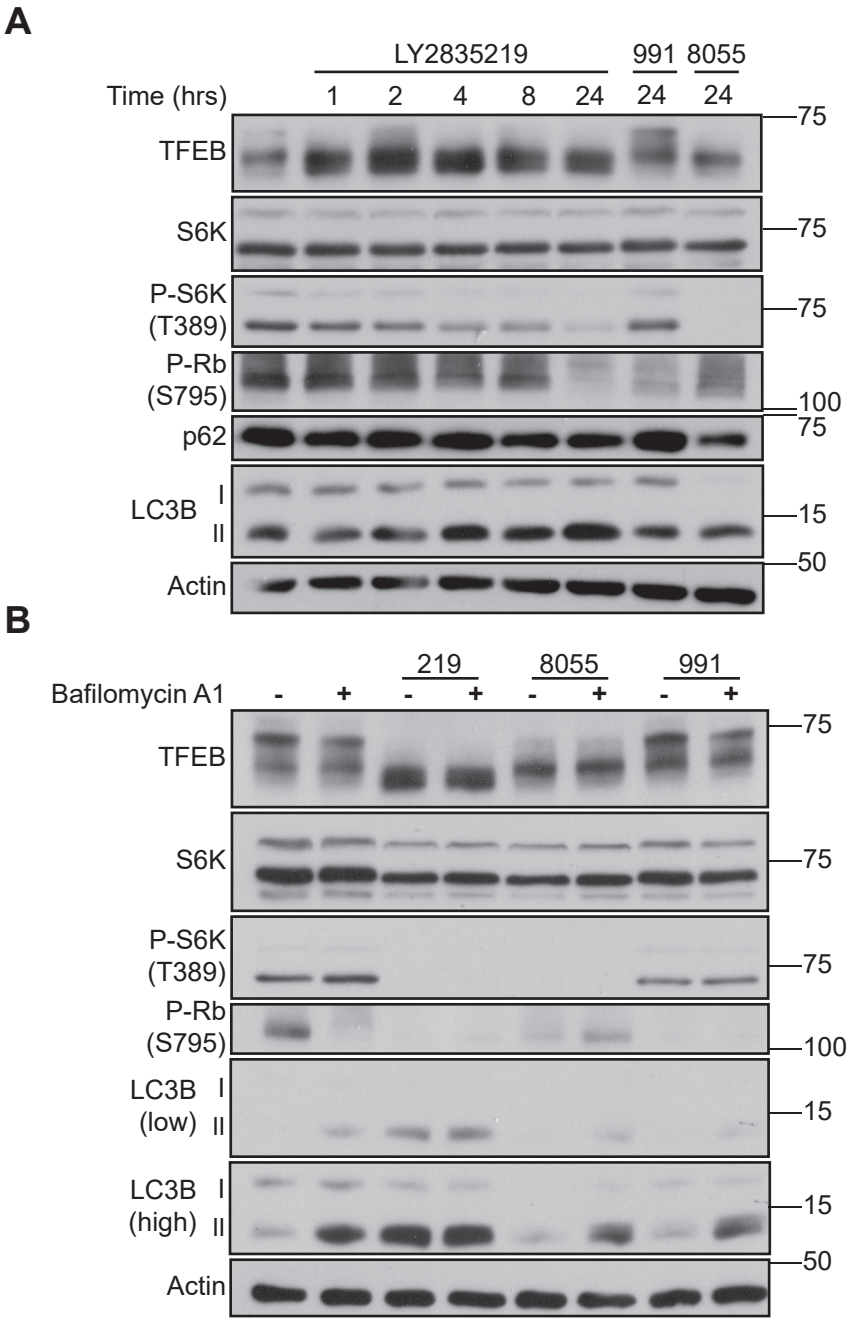

Figure 3.15: LY2835219 inhibits autophagic flux.
(A) HCT116 cells were treated with compounds for indicated times. **(B)** HCT116 cells were treated with compounds for 24 hours. One hour prior to lysis, cells were treated with Bafilomycin A1 (100 nM). Concentrations of compounds in both experiments were as follows: LY2835219 (500 nM), PD0332991 (1 μM) or AZD8055 (200 nM). Western blots are from a single experiment representative of three independent experiments. Molecular weight markers (kDa) are indicated to the right of each blot.

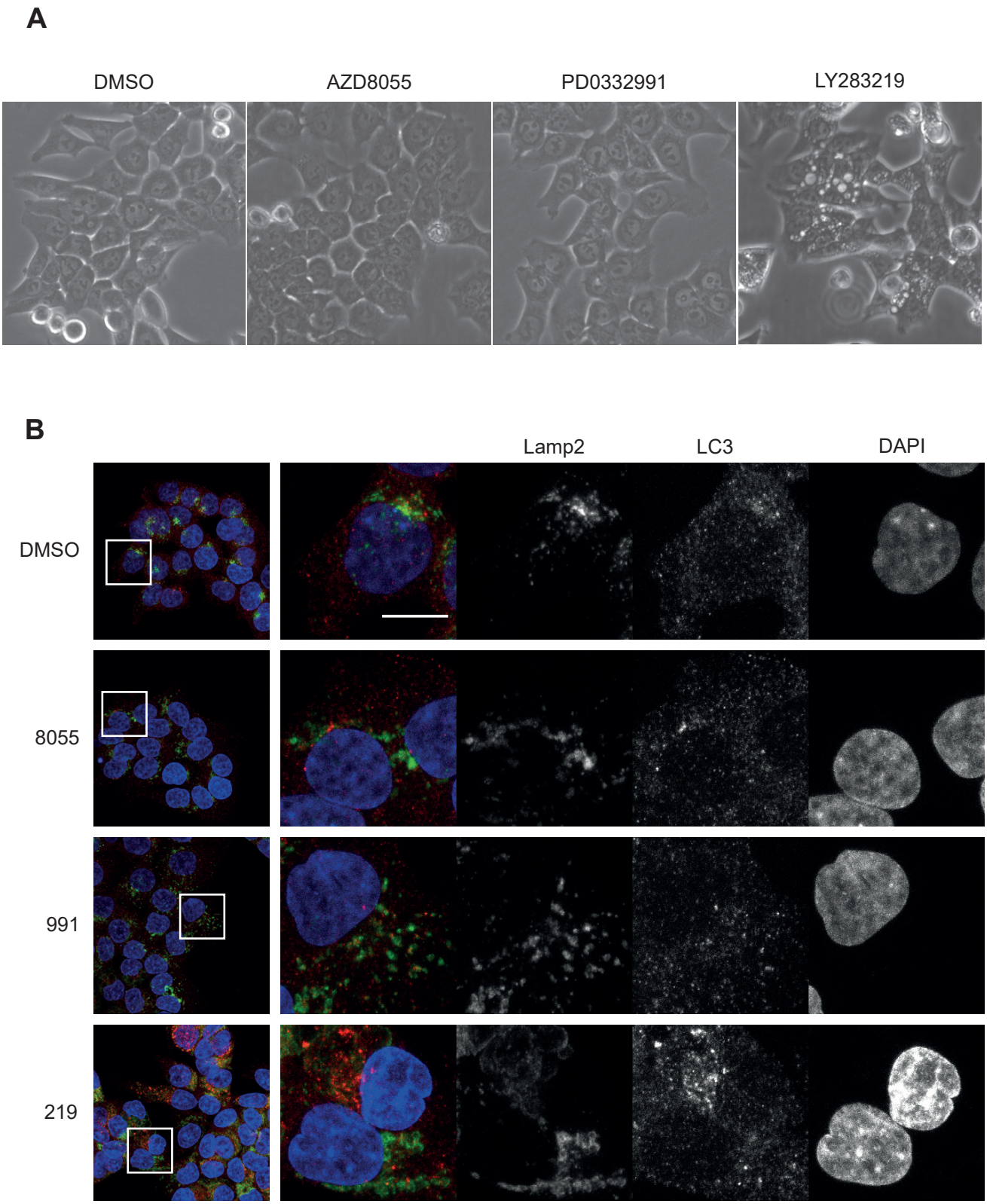

Figure 3.16: LY2835219 induces vacuolation which is Lamp2 positive.
(A) HCT116 cells were treated with LY2835219 (500 nM), PD0332991 (1 μM) or AZD8055 (200 nM) for 24 hours prior to image acquisition. **(B)** HCT116 cells were treated with LY2835219 (500 nM), PD0332991 (1 μM) or AZD8055 (200 nM) for 24 hours prior to fixation. Primary antibodies: Lamp2 (green), LC3B (red) Images are from a single experiment. Scale bar: 20 μm.

study found no effect on lysosomal pH or p62 levels upon treatment with PD0332991 for 24 hours (Llanos *et al.*, 2019). Whilst PD0332991 did impair autophagic flux after seven days of treatment, this was in common with other methods of inducing senescence. It is important to note that we decided the doses of LY2835219 and PD0332991 based on readouts of CDK4/6 activity (P-Rb (795)) and cell cycle activity (EdU activity) at 24 hours. It may be the case that if doses were selected based on the degree of lysosomal entrapment, then similar effects may have been observed. Whether this would be achievable given that LY2835219 did not have the same fluorescent properties as PD0332991 is another matter. Regardless, these studies would have to be conducted before concluding whether lysosomal entrapment was the main mechanism responsible for the inhibition of autophagic flux we observed.

We had previously found that emetine halted TFEB protein level increases but could not readily interpret this result as emetine also caused prominent dephosphorylation of TFEB (Figure 3.10.C). Since we had found that LY2835219 promoted dephosphorylation of TFEB to a greater extent than AZD8055, we utilised this compound in combination with 4-HT to observe if increases in protein levels observed in HR1 cells could be reversed. As previously observed, 4-HT treatment of HR1 cells caused increases in TFEB protein level, whilst LY2835219 caused TFEB dephosphorylation (Figure 3.17). LY2835219 treatment failed to prevent 4-HT induced increases in TFEB protein level. We observed no decreases in P-Rb (S795) upon LY2835219 treatment in HR1 cells, suggesting that HEK293 cells are not dependent upon CDK4/6 for cell cycle progression. Overall, it is most likely that emetine's ability to prevent 4-HT induced increases in TFEB protein level is a result of translation blockade and not TFEB dephosphorylation.

3.2.7 TFEB protein expression is highly variable across cell lines

Given that inhibition of ERK1/2 signalling did not reliably decrease TFEB protein levels, we next wanted to compare TFEB protein levels across a number of tissue types with either WT or mutated BRAF and KRAS proteins. Eight cell lines were selected for this preliminary experiment: two harbouring no ERK pathway mutations (HEK293 and HeLa); two harbouring *BRAF*^{V600E} mutations (HT29 and COLO205); four harbouring constitutively active *KRAS* mutations (A549, HCT116, Panc-1, SW620). Strikingly, HT29 and COLO205 had elevated TFEB protein levels relative to the other cell lines tested (Figure 3.18.A). Since Trametinib had not affected TFEB protein levels in these cells, and the KRAS mutant lines also had low levels of TFEB protein, we found it unlikely that BRAF was driving these changes. Furthermore, both of these cell lines also possessed high TFEB mRNA levels (Figure 3.18.B; Source: CCLE), with COLO205 exhibiting amplification of the TFEB gene

A

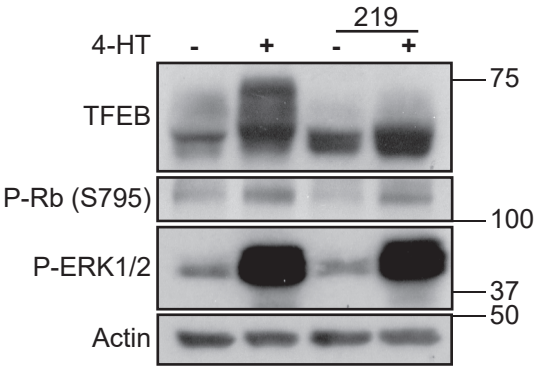

Figure 3.17: LY2835219 does not prevent 4-HT induced increases in TFEB protein levels in HR-1 cells.
(A) HR-1 cells were treated with 4-HT (100 nM) and/or LY2835219 (500 nM) for 24 hours. Western blots are from a single experiment. Molecular weight markers (kDa) are indicated to the right of each blot.

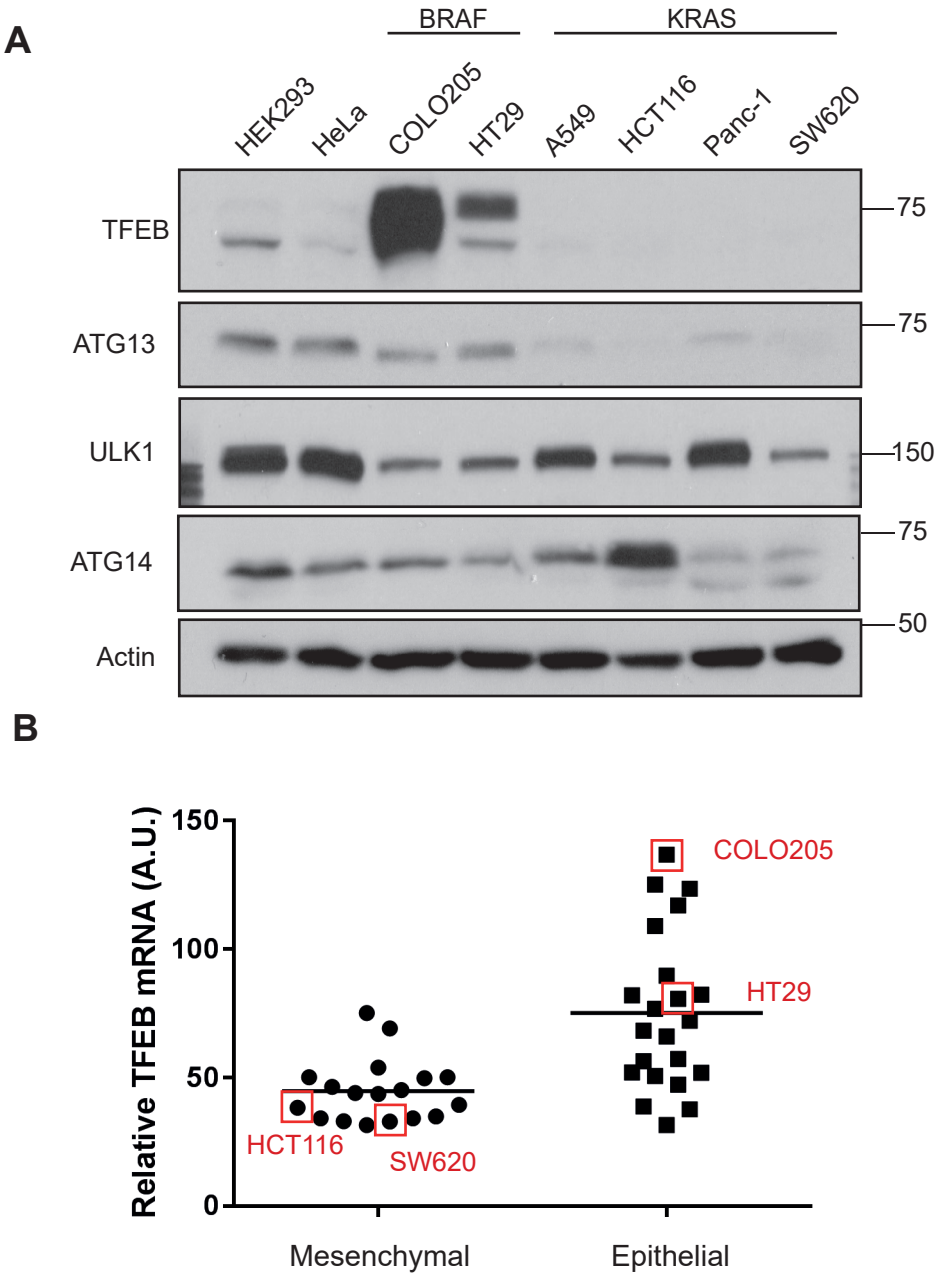

Figure 3.18: Cell lines which are observed to have more epithelial-like properties also have raised TFEB levels.
(A) Comparison of TFEB protein levels across cell lines. Cells were lysed at approximately 70%confluency. Western blot is from a single experiment. Molecular weight markers (kDa) are indicated to the right of each blot. **(B)** Gastrointestinal cell lines were characterised into either mesenchymal or epithelial groups based on Schliker and colleague's classification. TFEB mRNA levels for these cells were retrieved from the CCLE. Colorectal lines used within this thesis are indicated.

(12 copies) (Source: CANSAR4.0). Thus, the mechanism linking these cells to high TFEB protein was unlikely to be the same as in HR1 cells. HT29 and COLO205 cells also possess epithelial-like properties, as compared to more mesenchymal-like cells such as HCT116 and SW620 as defined by Schliker and colleagues characterisation of colorectal cancer cell lines (Schlicker *et al.*, 2012). Indeed, when comparing TFEB mRNA levels from the CCLE database based on Schliker's criteria, it is apparent that epithelial-like cells possess higher TFEB mRNA than mesenchymal like cells (Figure 3.18.B).

It is therefore apparent that the only evidence thus far strongly linking the ERK1/2 pathway to TFEB protein levels was acquired upon hyperactivation of the pathway in HEK293 cells. Our lab possessed other model systems for investigating ERK1/2 hyperactivation. The first were HeLa cells stably transfected with a doxycycline-inducible $KRAS^{G12D}$ construct, such that adding doxycycline promoted activation of the ERK1/2 pathway, as evidenced by increases in P-ERK1/2 (T202/Y204) over time (Figure 3.19.A). No robust increases in TFEB could be observed in this system. Another system we utilised was COLO205 cells which had been made resistant to prolonged exposure of the MEK1/2 inhibitor AZD6244 (Selumetinib), such that they maintain P-ERK1/2 (T202/Y204) levels by amplification of $BRAF^{V600E}$ (Little *et al.*, 2011). As a result of the *BRAF* amplification, washing off inhibitor results in rapid hyperactivation of the pathway (Sale *et al.*, 2019). Whilst there was variability in TFEB protein levels, this appeared to correlate with time of lysis as opposed to the presence or absence of AZD6244. For example, day 2 TFEB protein levels appeared slightly raised in the representative experiment shown regardless of the presence or absence of AZD6244 (Figure 3.19.B). As a side note, it was curious that ULK protein levels appeared to increase with ERK1/2 hyperactivation. This may be of interest to the mechanism of senescence seen in these cells, since autophagy has been implicated in the development of oncogene-induced senescence (Young *et al.*, 2009). We also attempted to investigate TFEB protein levels in response to *ΔCRAF:ER* activation in hTERT MRC5 immortalized fibroblasts, which undergo OIS. Whilst we observed cell morphologies consistent with OIS after 6 days of 4-HT treatment, TFEB's phosphorylation status was highly variable, though protein levels consistently did not increase (data not shown). Overall, none of these systems replicated the findings we observed in HEK293 cells that ERK1/2 hyperactivation lead to increases in TFEB protein levels. It is therefore very unlikely to be a conserved or important mode of regulation and likely represents a cell-type specific downstream consequence of prolonged ERK1/2 signalling.

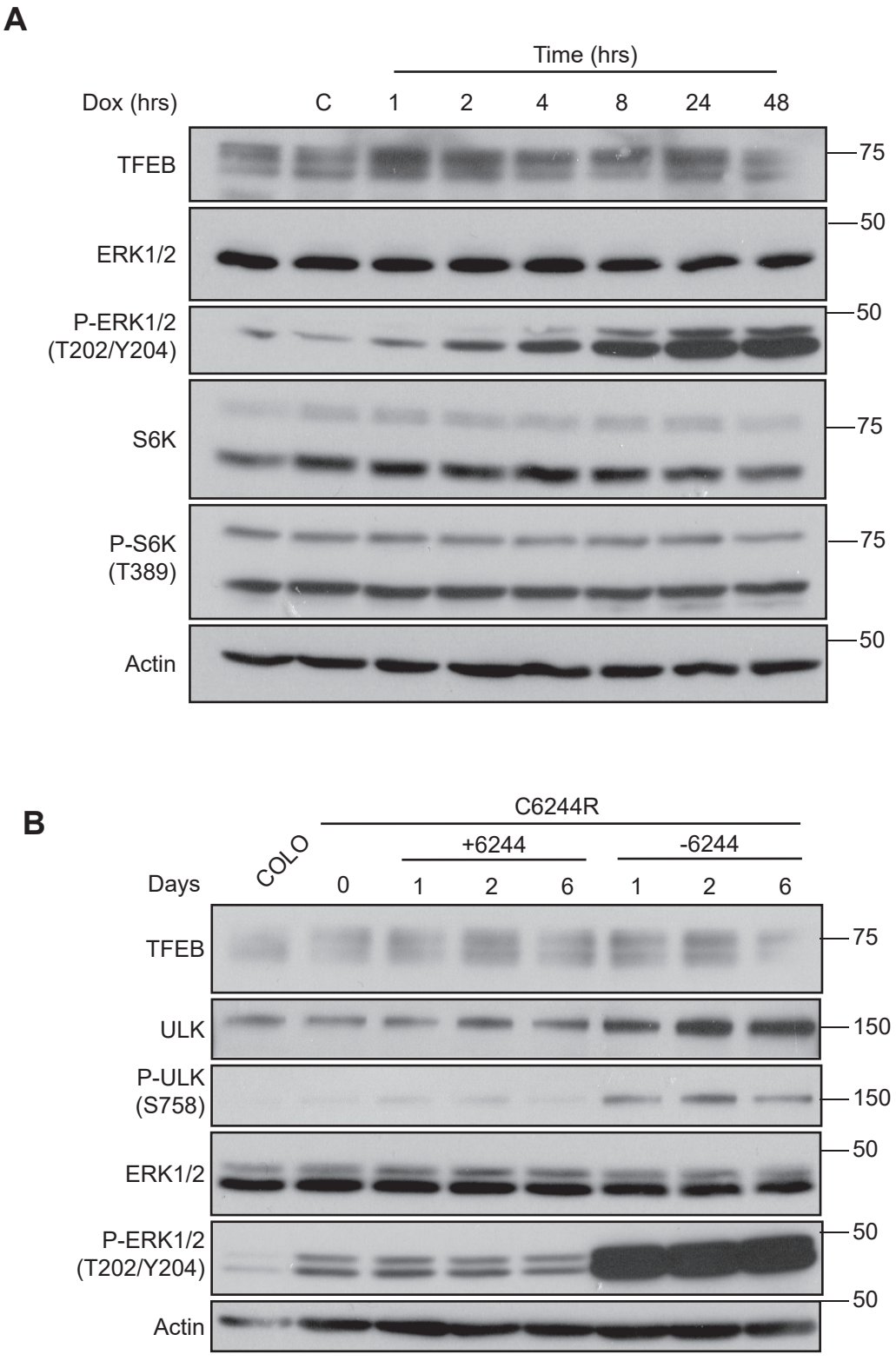

Figure 3.19: Model systems independent of HEK293 cells show no increase in TFEB protein levels with enhanced ERK1/2 activity.
(A) HeLa cells stably expressing a doxycycline-inducible KRAS G12D were treated with doxycy-cline (100 ngml^{-1}) for the indicated time prior to lysis **(B)** C6244R cells were cultured in drug-supple-mented media and then swapped to media with or without AZD6244 (MEK inhibitor) for the indicat-ed time. Western blots are from a single experiment representative of three independent experi-ments. Molecular weight markers (kDa) are indicated to the right of each blot.

3.3 Discussion

3.3.1 ERK1/2 is unlikely to regulate nuclear export of TFEB via direct S142 phosphorylation

Whilst TFEB is known to be regulated by availability of amino acids, the kinases responsible for this have been revised based on methodologies used. Originally, mTORC1 was dismissed as the candidate kinase, since rapamycin failed to cause TFEB hypophosphorylation or nuclear localisation (Settembre *et al.*, 2011). Furthermore, mTORC1 failed to phosphorylate S142 in the peptide-based *in vitro* kinase assay (Settembre *et al.*, 2011), though it was subsequently shown that mTORC1 could phosphorylate full-length TFEB immunoprecipitated from cells at S142 (Settembre *et al.*, 2012). The use of ATP-competitive inhibitors of mTOR, in combination with genetic approaches, then demonstrated that mTORC1 was beyond reasonable doubt the main nutrient-dependent regulator of TFEB (Martina *et al.*, 2012; Roczniak-Ferguson *et al.*, 2012; Settembre *et al.*, 2012).

Given that mTORC1 appears to be the key nutrient-dependent regulator of TFEB, the role that ERK2 plays has been widely debated. More recently, it has been suggested that ERK2 regulates TFEB's nuclear export by S142 phosphorylation (L. Li *et al.*, 2018), though this has been suggested to be mainly regulated by mTORC1 instead (Napolitano *et al.*, 2018). Some groups fail to see any convincing evidence for TFEB's regulation by ERK2 (Martina *et al.*, 2012). Other groups suggest that ERK2 regulation of TFEB is context-dependent, such as a requirement for constitutive pathway activation as is found in melanoma (S. Li *et al.*, 2019). Overall, it is clear no consensus has been reached and further evidence was therefore required to substantiate links between ERK2 and TFEB. My findings exemplify the variability and differing conclusions in the field. Whilst there was little evidence to suggest that TFEB was regulated by ERK2 in basal conditions (Figures 3.1-3.3), EGF promoted TFEB cytosolic localisation in an ERK1/2-dependent manner (Figure 3.4). It is unclear what biological impact such transient modulations in TFEB localisation would have and whether TFEB is important for biological responses to growth factor stimulation should be investigated further. Furthermore, TFE3 and MITF localisation should be observed in response to EGF, given they both have conservation of the PNSP motif. We did not observe ERK-dependent phosphorylation of TFEB S142 (Figure 3.5) and the reason for this is unclear. One possibility is that ERK2 cannot bind to TFEB in cells. ERK-catalysed phosphorylation of MITF requires binding to a 100 amino acid region to the C-terminal side of S73, since it does not possess either a classical FXF or D-site docking domain which ERK usually requires to phosphorylate its substrates (Molina, Grewal and Bardwell, 2005).

There is a poor homology between TFEB and MITF in this region, with the little homology that does exist featuring the transactivation domain (Figure 3.20).

From a conceptual perspective, it easier to reconcile ERK1/2 as a direct regulatory kinase of TFEB in the nucleus than mTORC1. mTORC1 is a 1 MDa complex, yet the maximum size that can appear to passively diffuse into the nucleus is approximately 110 kDa (Wang and Brattain, 2007). Even if mTORC1 was disassembled into its constituent components, diffused into the nucleus, and reassembled, mTOR (250 kDa) and RAPTOR (150 kDa) are both greater than this limit. Thus a nuclear localisation signal and import mechanism would be required and mTOR's primary sequence possesses no such NLS (Bachmann *et al.*, 2006). Despite this, many studies have observed that mTOR can function in the nuclear compartment as assessed by fractionation or immunofluorescence (Zhang *et al.*, 2002; Bachmann *et al.*, 2006; Kazyken *et al.*, 2014; Audet-Walsh *et al.*, 2017). One possibility is that mTORC1 is not localised to the nucleus in basal conditions but can be stimulated in certain conditions. For example, nuclear mTOR has been identified in response to hypoxic conditions (Bernardi *et al.*, 2006) and androgens (Audet-Walsh *et al.*, 2017). Findings in our subsequent studies (Figure 4.10) using both HAP1 RAPTOR-GFP cells and the mTOR antibody both showed exclusive cytosolic localisation regardless of nutrient status. Altogether, our and others results suggest that mTORC1 is not nuclear localised under basal or nutrient-depleted conditions. Since nuclear export of TFEB is rapid, it is unclear how mTORC1 could mediate the nuclear export of TFEB given the differences in localisation. Clearly, the level of confidence surrounding nuclear mTOR needs to be strengthened, and, if verified, mechanisms by which a 1 MDa complex is imported into the nucleus investigated. By contrast, ERK1/2 is well established to shuttle into the nucleus upon its activation (Chen, Sarnecki and Blenis, 1992) thereby acting as an ideal candidate for mediating TFEB nuclear export, by promoting its CRM1-dependent export (L. Li *et al.*, 2018). Indeed, ERK1/2 has been demonstrated to phosphorylate other proteins in the nucleus to alter their CRM1-dependent export, such as class II transactivator (CIITA; ERK1/2 phosphorylation promotes export) (Voong *et al.*, 2008) or HIF-2α (ERK1/2 phosphorylation impairs export) (Gkotinakou *et al.*, 2019).

Recently, it has been suggested that TFEB undergoes ERK1/2 dependent hyperphosphorylation in melanoma with constitutively active mutations of the ERK1/2 signalling cascade but not in wild-type lines (S. Li *et al.*, 2019). Furthermore, TFEB failed to undergo mTORC1-dependent phosphorylation when BRAF was inhibited, leading the authors to conclude that ERK1/2 phosphorylation of S142 promoted TFEB localisation to the lysosome. The data we present here suggests that TFEB hypophosphorylation temporally correlates with cell cycle arrest not ERK1/2 pathway inhibition in A375 cells (the

Figure 3.20: Clustal analysis of TFEB and MITF-M.

TFEB (Uniprot identifier: P19484-1) and MITF-M (Uniprot identifier: O75030-9) were analysed by Clustal Pairwise analysis for homologous regions. Key regulatory sites are indicated. The purple highlighted region indicates the ERK2 binding region identified on MITF-M (Molina, Grewal and Bardwell, 2005). Within this, bold letters indicate the conserved activation domain.

same line used in Li's study (S. Li *et al.*, 2019)). Furthermore, it is difficult to reconcile that if ERK1/2 phosphorylation was a critical event in TFEB's localisation to the lysosome, it would only be applicable in cell lines with mutations of the ERK1/2 pathway and not in wild-type lines, since this would imply that another kinase must be responsible for mediating TFEB's localisation in these lines. Finally, the S142 phosphorylation site in TFEB is highly conserved in TFE3 (S246), and yet this showed no nuclear localisation upon treatment with the BRAF-inhibitor PLX4720 (S. Li *et al.*, 2019). Whilst, the authors introduced a number of mutants to constitutively activate mTORC1 signalling, they did not verify that mTORC1 signalling remained active in the presence of ERK1/2 pathway inhibitors and this would be an important verification. Regardless, we find it hard to reconcile a model whereby ERK1/2 specifically promotes lysosomal localisation of TFEB in select circumstances.

Overall, the only evidence we observed that ERK1/2 activity had a role on TFEB localisation was its partial cytosolic localisation upon EGF treatment. This should be repeated with addition of the CRM1 inhibitor leptomycin B, since it has been demonstrated that TFEB requires CRM1 for nuclear export and that leptomycin B prevents TFEB's export (L. Li *et al.*, 2018). Given Li's findings, it is most likely that EGF does promote TFEB nuclear export. Contrary to Li's hypothesis, we observed no phosphorylation of S142 in cells upon EGF stimulation. This would suggest that S142 phosphorylation is not the main mechanism mediating EGF-induced TFEB export. Whilst we attempted to generate HM3 cells stably expressing TFEB-GFP, thus enabling us to investigate S142 phosphorylation in response to rapid MEKK3 activation, positive clones exhibited high levels of death under normal growing conditions. Therefore, these were not taken further due to the potential impact this would have on results. Similar attempts in HR1 cells or C6244R cells, both of which enable selective activation of the ERK1/2 pathway, could be attempted. Indeed, the higher levels of TFEB in COLO205 cells, may mean they will tolerate overexpression better.

3.3.2 ERK1/2 pathway stimulation can promote increases in TFEB protein abundance

In this work, we consistently found that prolonged hyperactivation of the ERK1/2 signalling cascade in HEK293 cells resulted in elevated TFEB proteins levels. Since this was almost certainly a cell line-specific observation, much of the follow-up and validation work regarding this remains incomplete. It would be important to observe if there was any functional consequence to the observed increases in TFEB protein level. Settembre and colleagues found that overexpression of TFEB resulted in an approximate doubling of LC3B lipidation (Settembre *et al.*, 2011). It is likely that transient overexpression of TFEB was at far higher levels than that observed for 4-HT induced increases. Therefore, more sensitive

approaches for evaluating functional output of TFEB should be considered such as qRT-PCR of known TFEB target genes (i.e. BCL2, LAMP1, p62) (Settembre *et al.*, 2011) or transcriptional reporter assays such as 4X CLEARiLuc (4x TFEB consensus site) (Cortes *et al.*, 2014).

Overall, we could find no consistent evidence that ERK1/2 signalling led to changes in TFEB protein level across cell types. Our rationale for pursuing 4-HT induced increases in TFEB protein level is that it represents a relatively unique form of regulation, with the majority of reports to date focused on alterations in TFEB localisation. Thus, identifying the mechanism of TFEB protein level increases would likely represent a unique finding. However, there was not enough data to warrant further investigation once it was established this was apparently unique to HEK293s. Further work could be to establish how ERK1/2 signalling promotes these increases in HEK293 cells, and then investigate whether this, likely downstream, event is observed in other cell lines as a conserved mechanism.

3.3.3 Nutrient depletion promotes unexpected cytosolic localisation of TFEB in A549 cells

One curious result was the ability of HBSS starvation to promote TFEB cytosolic localisation and hyperphosphorylation in A549 cells (Figure 3.3). This was despite clear mTORC1 inactivation, as assessed by P-S6K (T389). Furthermore, the mTOR inhibitor AZD8055 promoted TFEB nuclear localisation as in other cells. It is not quite apparent how these paradoxical findings can be reconciled; however, it clearly merits further investigation. Initial efforts could be directed towards further characterising the mTORC1 response to HBSS, by evaluating the phosphorylation of other substrates (4E-BP1 and ATG13) and mTORC1 localisation (mTOR immunofluorescence). Identifying other cell lines that show similar findings would also aid further development of model systems in which to study these findings. Since the endogenous TFEB remained hyperphosphorylated, there would be no requirement for overexpression of TFEB and phosphorylation status of TFEB in response to HBSS and AZD8055 could be assessed by SDS-PAGE. Once several cell lines have been identified, then similar characteristics can be identified (i.e tissue type) which may elucidate reasons for this discrepancy in regulation. These findings could provide important insights into how amino acids differentially regulate mTORC1 regulation of different substrates. Further experimentation should interrogate whether TFEB localisation is altered in A549 cells in response to knockdown of various components of nutrient-dependent mTORC1 signalling i.e. RAPTOR, Rag-GTPases, components of Ragulator, etc. What is also unclear is why it would be beneficial for a cell to inactivate TFEB, arguably

a master regulator of catabolic metabolism (Michela Palmieri *et al.*, 2011), during nutrient starvation.

3.3.4 LY2835219 impairs lysosomal function resulting in impaired autophagic flux

During the course of our studies investigating whether cell cycle arrest played a role in either TFEB phosphorylation status or loss of TFEB protein level, we observed that LY2835219 treatment caused pronounced Lamp2 positive vacuolisation (Figure 3.16), suggesting a lysosomal defect. Consistent with this, autophagic flux was impaired as assessed by LC3B-II levels upon bafilomycin A1 treatment. Curiously, TFEB dephosphorylation, known to occur in response to lysosomal defects (Settembre *et al.*, 2012), occurred to a greater extent than with mTOR inhibition alone (Figure 3.15.B). This suggests that LY2835219 treatment is likely inhibiting another kinase. GSK3 inhibition has previously been shown to promote TFEB dephosphorylation beyond that of mTOR inhibition (Marchand *et al.*, 2015); however, we observed that lysosomal localisation was not required for GSK3 phosphorylation since Δ30-TFEB (generation of stable line described in chapter 5), a mutant which fails to localise to the lysosome, still underwent dephosphorylation upon treatment with the GSK3 inhibitor CHIR99021 (Figure 3.21). Therefore, whilst it should be confirmed that LY2835219 does not inhibit GSK3, it is likely that another kinase is responsible for the further dephosphorylation of TFEB. A candidate kinase could be MAP4K3, which is known to phosphorylate TFEB at S3 and is localised to the lysosome (Hsu *et al.*, 2018). Regardless, whilst we were conducting this work another group demonstrated lysosomal membrane permeabilization upon LY2835219 treatment leading to vacuolisation (Knudsen *et al.*, 2017). This did not appear to alter the *in vivo* properties of the drug compared to PD0332991 as assessed by transcriptomics of tissue samples.

A

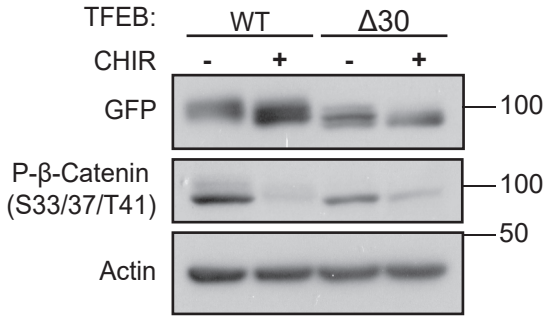

Figure 3.21: GSK3-mediated phosphorylation of TFEB does not require its lysosomal localisation.
(A) HeLa cells stably expressing either WT-TFEB-GFP or Δ30-TFEB-GFP were treated with either DMSO or CHIR99021 (5 μM) for 2 hours prior to lysis. Western blots are from a single experiment. Molecular weight markers (kDa) are indicated to the right of each blot.

4 Macroautophagy and mTORC1 are paradoxically both repressed during mitosis

4.1 Introduction

Macroautophagy is widely appreciated to be a crucial catabolic mechanism cells utilise in times of metabolic stress, especially nutrient starvation. In doing so, the cell maintains an adequate nutrient supply by recycling various macromolecules and organelles. This process is beneficial for longevity, with chronic rapamycin treatment, or genetic stimulation of autophagy extending lifespan in a variety of models (discussed in detail within the introduction). There are times when it would be theoretically damaging for autophagy to occur, such as mitosis. This is due to nuclear envelope breakdown exposing the genome to the cytosolic autophagic machinery. Indeed, autophagosomal engulfment of mitotic chromosomes has previously been observed (Sit *et al.*, 1996), though only under conditions of severe cellular stress.

Since mTORC1 regulates cap-dependent translation, including cell cycle proteins such as cyclin D1 and D3, the cell can arrest prior to the cell cycle's G0/G1 restriction point when mTORC1 is inhibited. Thus, in times of nutrient starvation, the cell switches to a catabolic state, where internal supply of amino acids is increased and demands for protein synthesis are reduced. However, if cells have already passed the G1 restriction point, they are committed to cell cycle progression and completion of mitosis. The time taken for cells to complete the cell cycle from S-phase is several hours, and mitosis itself is approximately 90 minutes (variable between cell lines). By contrast autophagy initiation occurs within minutes of nutrient starvation and mTORC1 inactivation (Axe *et al.*, 2008). Therefore, there is a window of several hours whereby starvation-induced autophagy and mitosis could be occurring simultaneously. It has therefore been hypothesised previously that autophagy should be repressed during times of nuclear envelope breakdown to ensure protection of the genome (Eskelinen *et al.*, 2002).

To investigate the status of autophagy during mitosis, seminal work by Eskelinen and colleagues demonstrated that the number of autophagosomes was strikingly reduced during early mitosis. There has been conflicting evidence as to whether this is due to a decrease in autophagy initiation or an increase in autophagosome degradation. This is likely due to differences in experimental protocol. A conventional approach for assessing autophagic flux is to assess LC3B puncta combined with the use of lysosomal inhibitors to block lysosome-mediated degradation. This enables differences in LC3 lipidation to be attributed to alterations in initiation or degradation, and such approaches have been employed by independent research groups to argue that autophagic flux and initiation is

active during mitosis, despite the reduced autophagosome number (Liu *et al.*, 2009; Z. Li *et al.*, 2016). These studies are complicated due to the duration of lysosomal inhibition likely exceeding the time a cell has spent in mitosis, meaning that an apparent accumulation of autophagosomes during mitosis could simply reflect their 'carry over' from interphase. This is especially true of the study by Liu and colleagues that utilised lysosomal inhibitors for 16 hours (Liu *et al.*, 2009). Even without the use of lysosomal inhibitors, the lifespan of LC3 puncta is approximately 30 minutes (this study; Axe *et al.*, 2008); therefore, observed LC3 puncta could be inherited from interphase cells even in untreated conditions. To try and address this possibility Liu and colleagues treated mitotically-arrested cells with ammonium chloride to demonstrate that autophagic flux was highly active in early mitosis with increases in lipidated LC3B (Liu *et al.*, 2009). It has been demonstrated that ammonia is capable of causing non-canonical LC3B lipidation (Jacquin *et al.*, 2017). Therefore, these results, where autophagosomes could be accumulated from interphase or be a result of non-canonical autophagy, must be treated with caution.

4.2 Results

4.2.1 Autophagy initiation is inhibited during mitosis, in a manner independent of mTOR

To exemplify the complication with using LC3 as a readout of autophagy during mitosis, we utilised a clonal HEK293 line stably expressing the tandem mRFP-EGFP-LC3 reporter (Puncta dynamic shown in Figure 4.1.A). As explained in detail within the thesis introduction, GFP-LC3 is acid-sensitive, whilst RFP-LC3 is acid stable. This construct therefore usually allows the evaluation of autophagic flux by comparing the RFP to GFP ratio (Figure 4.1.B). Due to the concerns with regard to GFP-LC3 carry over into mitosis, we first assessed the stability of LC3 puncta upon entry into mitosis. We performed live-cell imaging of cells, with addition of the mTOR inhibitor AZD8055 and paclitaxel 30 minutes prior to imaging (Figure 4.2). As expected, cells in interphase had abundant GFP-LC3 and RFP-LC3 puncta, consistent with the high autophagic flux induced by mTORC1 inhibition. Consistent with previous publications, cells showed a pronounced decrease in GFP-LC3 upon nuclear envelope breakdown and entry into mitotic arrest. This led to the near absence of GFP-LC3 puncta approximately 30-40 minutes after nuclear envelope breakdown. Since mitosis lasts approximately one hour, it is clear that monitoring GFP-LC3 puncta is not feasible during a normal mitosis, since we cannot establish whether puncta originated from interphase. In addition, RFP-LC3 puncta were highly stable and did not appear to noticeably reduce in number across the three hours of imaging. Upon entry into mitosis, RFP-LC3 accumulated into large and highly stable puncta, which based on later imaging have many

A

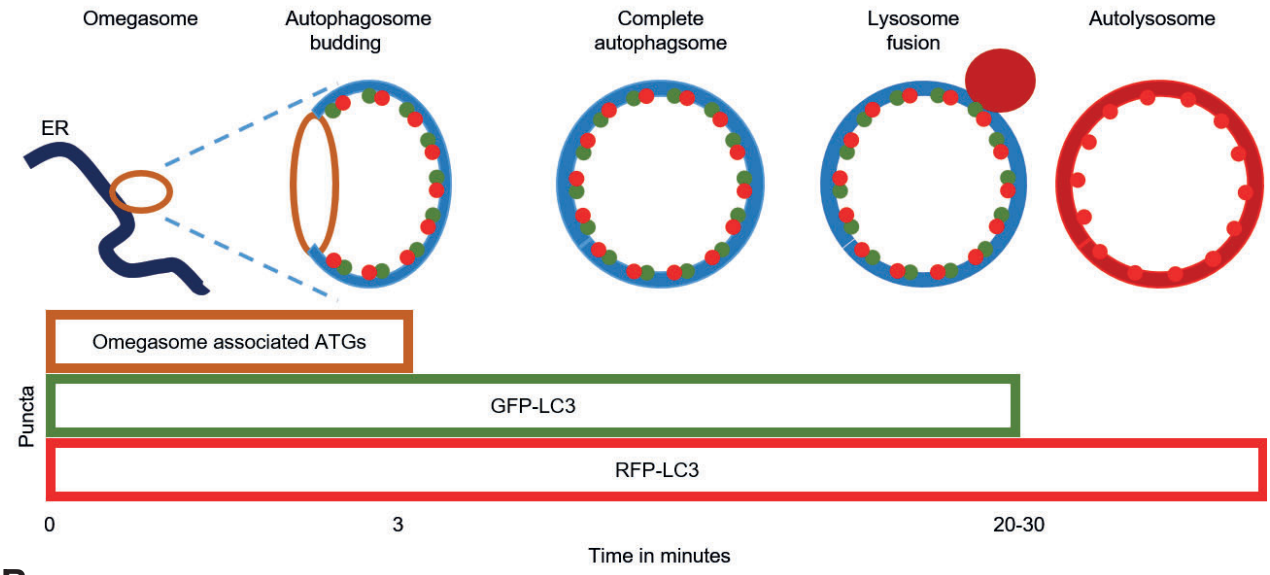

B

	Structures present	Puncta count		
		Omegasome	GFP-LC3	RFP-LC3
Untreated		↔	↔	↔
Increased autophagy initiation (i.e HBSS or AZD8055)		↑	↑	↑
Lysosome blockade (i.e Bafilomycin A1)		↔	↑	↔
Increased autophagosome degradation (i.e Li and Liu's proposed model)		↔	↓	↔
Decreased autophagy initiation (i.e Eskelinen's proposal)		↓	↓	↓

Figure 4.1 Schematic representation of immunofluorescence findings upon variations in auto-phagic flux.
(A) Schematic illustrating how autophagic structures relate to puncta detected by immunofluores-cence. Adapted from Yoshii and Mizushima, 2007. **(B)** How autophagy structures and, by association, puncta counts alter with variations in autophagic flux. Proposed models of alterations to autophagic flux during mitosis are included (Eskelinen et al., 2002; Liu et al., 2009; Li et al., 2016).

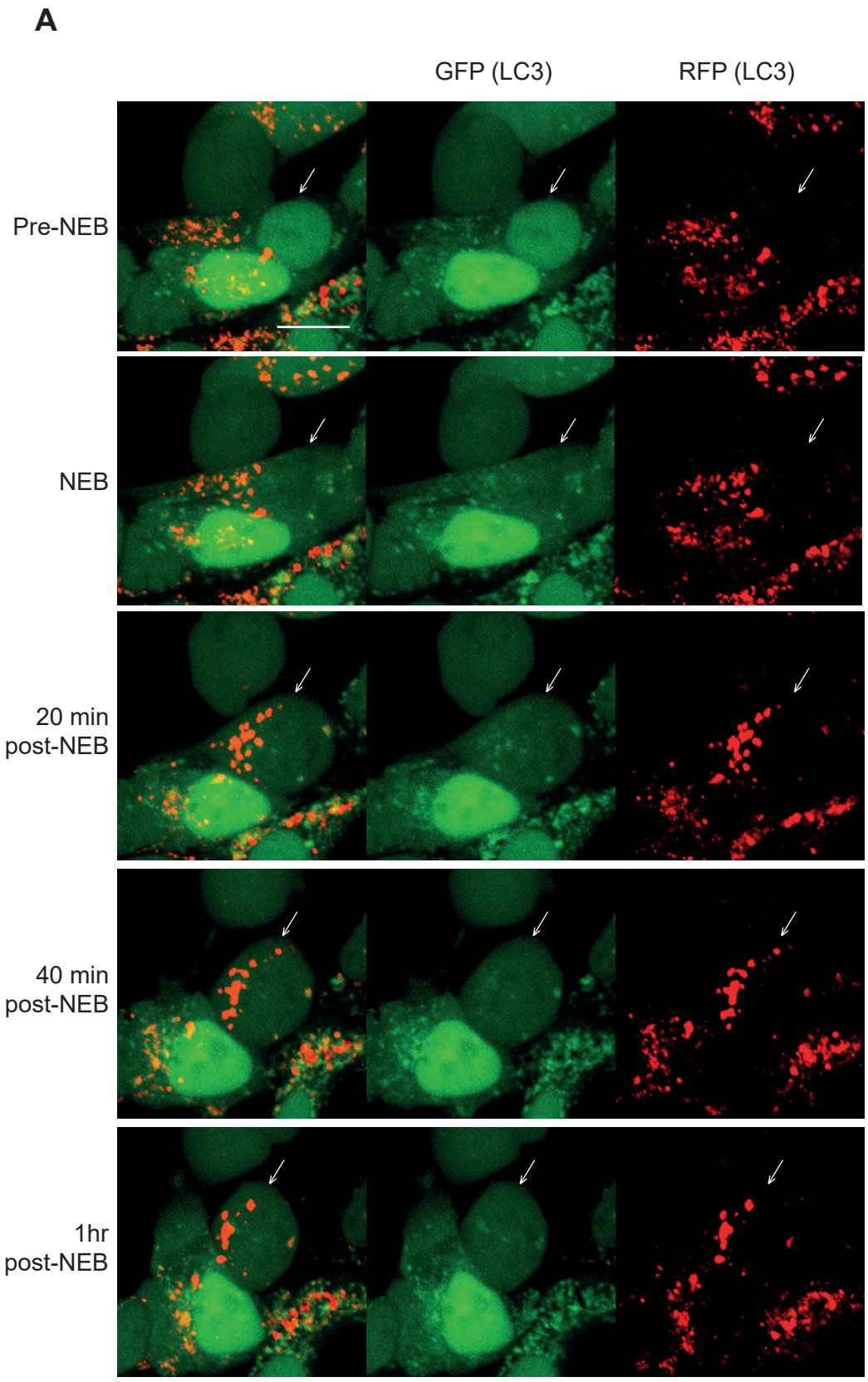

Figure 4.2: mRFP-EGFP-LC3 puncta stability affects its interpretation as a readout of autophagy during mitosis.
(A) HEK293 cells stably expressing mRFP-EGFP-LC3 were treated with AZD8055 (1 μM) and paclitaxel (50 nM) 30 minutes prior to transfer to a live-cell imaging stage. Image acquisition by spinning disc confocal microscopy. Representative images from different time points relative to nuclear envelope breakdown (NEB) are shown. Images from a single experiment. Scale bar: 20 μm. Arrows indicate a mitotic cell.

similarities to the lysosomal stain Lamp2 (i.e. Figure 4.10). As discussed previously, it has been suggested that RFP-LC3 can be resistant to lysosomal acidity and its turnover is governed by proteolytic activity within the lysosome (Yoshii and Mizushima, 2017).

Fixed-cell imaging further supported these findings (Figure 4.3). Interphase cells treated with the mTOR inhibitor AZD8055 consistently showed a higher number of both GFP and RFP puncta, consistent with an increase in autophagy initiation. In contrast, cells arrested in mitosis consistently had fewer GFP and RFP LC3 puncta compared to neighbouring interphase cells consistent with a decrease in autophagy initiation. Some mitotic cells showed a much higher number of RFP-LC3 puncta. Whilst this was almost certainly an accumulation from interphase cells, it was not possible to conclude this from fixed-cell imaging. Based on these findings, we therefore felt the only way to accurately assess autophagic flux utilising this system was to induce autophagy in a cell already shown to be in mitosis and then observe puncta number. To do this, we treated cells with paclitaxel for 3.5 hours prior to transfer to a live-cell imaging spinning disc confocal microscope. Then after 30 minutes of imaging, we added the mTOR inhibitor AZD8055. Unfortunately, AZD8055 appeared to generate an artefact in the blue channel, preventing the use of a DNA marker such as Hoescht; however, condensed chromosome outlines, indicating cells in mitotic arrest, could be visualised in the GFP channel. Consistently, we observed an increase in both GFP and RFP puncta in interphase cells upon addition of the mTOR inhibitor AZD8055; however, no such increase was observed in cells already arrested in mitosis (Figure 4.4). This supports the idea that autophagy induction in response to mTOR inhibition is repressed during mitosis.

4.2.2 Markers of the omegasome reveal that autophagy initiation is inhibited during mitosis

Whilst the preceding results suggested that autophagy initiation was repressed during mitosis, they also highlighted the need for more dynamic and unambiguous readouts of autophagy initiation. ATG13, as part of the ULK1 complex, is recruited to the omegasome intermediate upon mTOR inhibition and appears as distinct puncta upon immunofluorescence (Karanasios *et al.*, 2013). Furthermore, ATG13 puncta disperse prior to autophagosome budding and completion, thereby representing a transient marker of autophagy initiation which is not affected by the rate of degradation (Karanasios *et al.*, 2013; Maday and Holzbaur, 2014). Indeed, the omegasome appears to have a lifespan of approximately 3 minutes and therefore represents a more dynamic and responsive readout of autophagy initiation than LC3 (Axe *et al.*, 2008) (Figure 4.1). Furthermore, imaging of LC3 puncta cannot differentiate between macroautophagy, non-canonical autophagy and

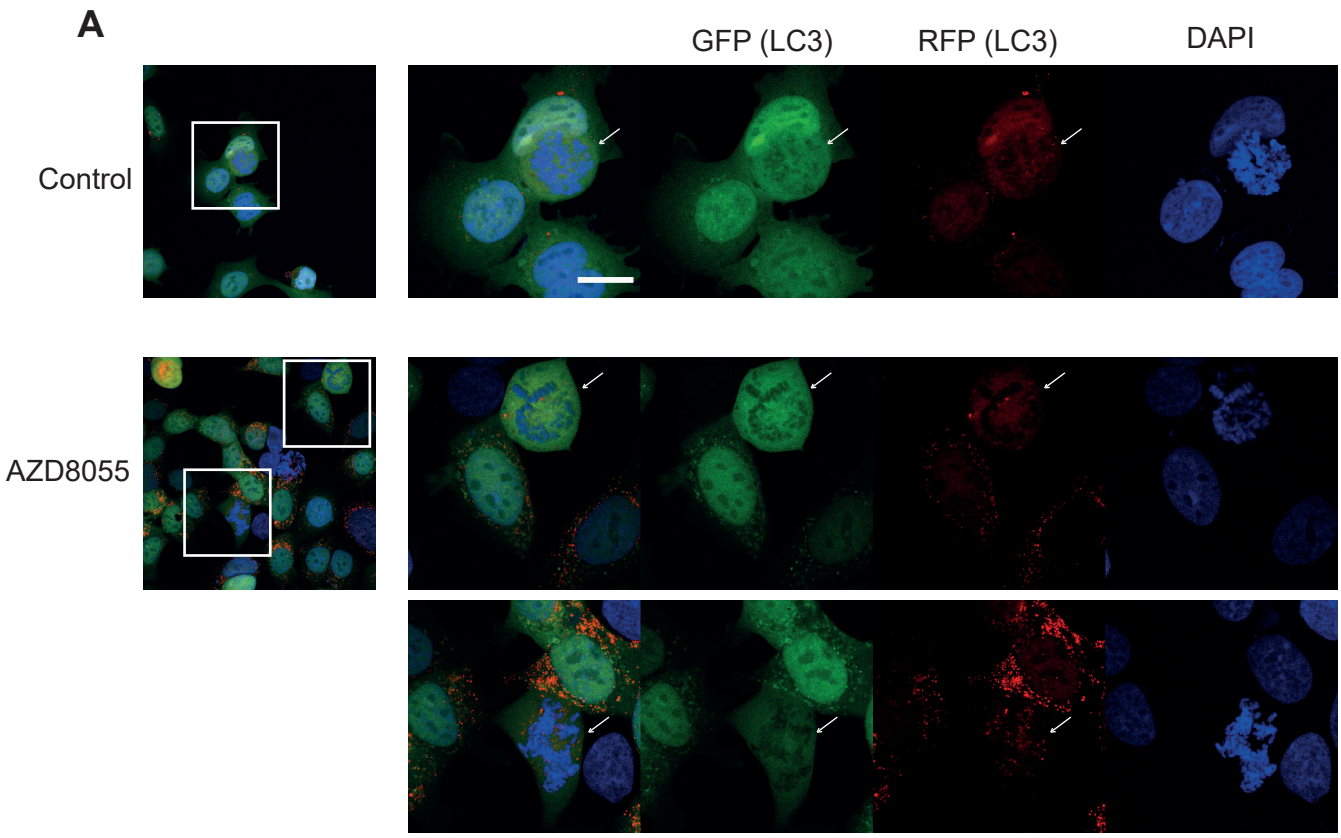

Figure 4.3: Both GFP-LC3 and RFP-LC3 are reduced in mitotically-arrested cells. **(A)** Asynchronous HEK293 cells expressing the tandem LC3 reporter mRFP-EGFP-LC3 were treated with AZD8055 (1 μM) for 2 hours prior to fixation and imaging by confocal microscopy. Images from a single experiment representative of two independent experiments. Scale bar: 20 μm. Arrows indicate mitotic cells.

A

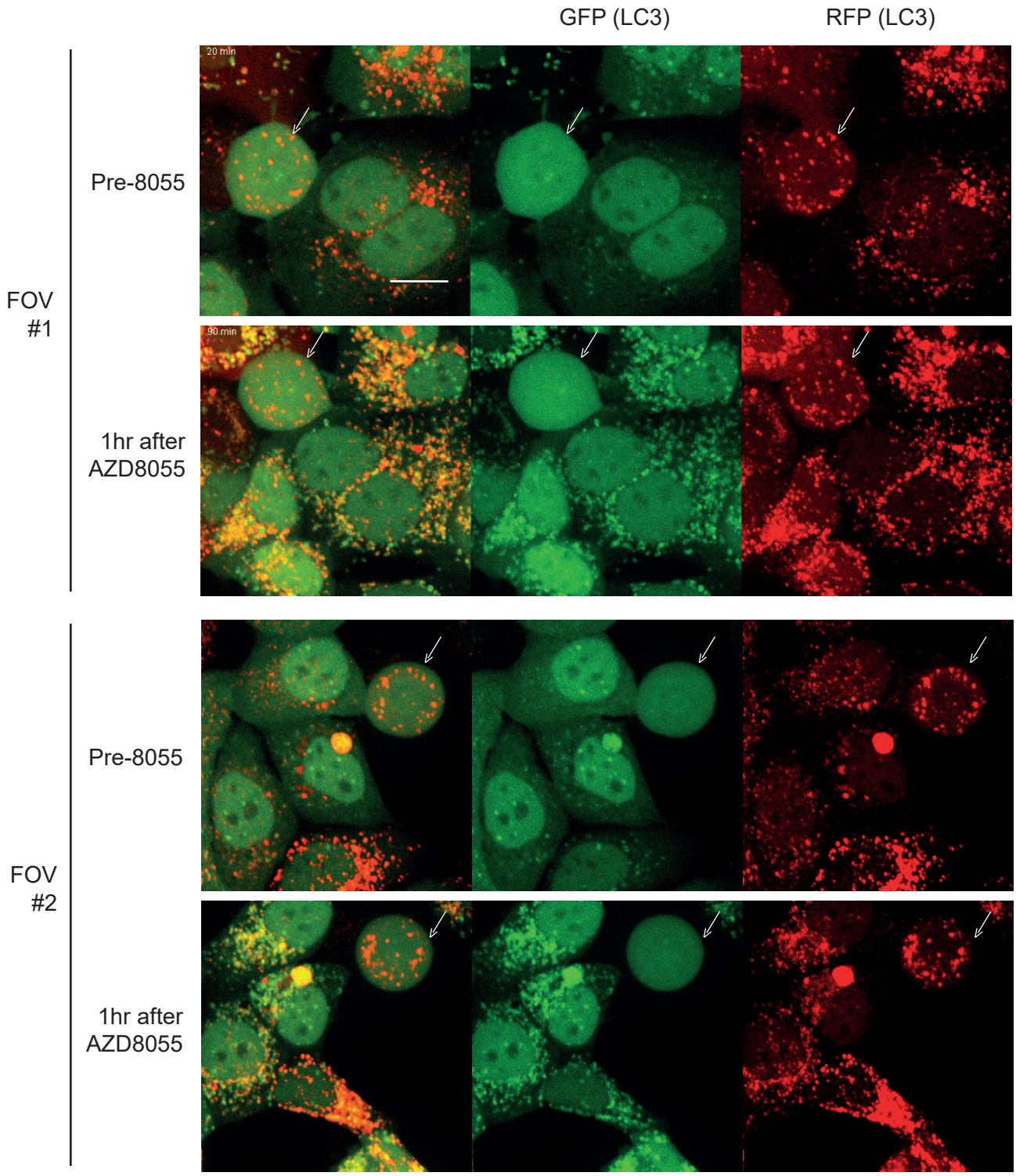

Figure 4.4: Autophagy induction is repressed during mitotic arrest.
(A) HEK293 mRFP-EGFP-LC3 were treated with paclitaxel for 3.5 hours prior to transfer to live-cell imaging stage. Representative images from before and one hour after addition of AZD8055 are shown (1 μM). Images from two fields of view (FOV) are shown, with mitotically arrested cell indicated by arrow. Scale bars: 20 μm. Images from a single experiment representative of three biological replicates.

selective autophagy, though the extent to which components of the omegasome are required for selective autophagy is recently beginning to be elucidated (see introduction). By contrast, since the ULK1 complex is not required for non-canonical autophagy it will not form punctate structures in this setting. Thus, imaging omegasomes have several critical advantages when addressing the question of macroautophagy initiation during mitosis. To investigate whether autophagy initiation was repressed during mitosis, we arrested HeLa cells at the G1/S border with a double thymidine block. The basis of a double thymidine block is by providing the cell with a vast surplus of thymidine, it appears to deplete pools of deoxycytidine triphosphate (dCTP), which in turn inhibits DNA synthesis (Bjursell and Reichard, 1973). As such a single thymidine block will arrest cells either on entry to S phase or cells already in S phase. Since S phase can encompass a several hour window, this would not provide an accurate synchronisation. Cells are therefore released from the first block for 8 hours, such that all cells have exited S phase and made it into G2 or G1 phases of the cell cycle. Since, theoretically, no cells are then left in S phase, a second thymidine block is added, which will synchronously arrest cells at the start of S phase. From this, cells can then be released in a relatively synchronised fashion. We then released cells for 10 hours, such that there was an enrichment in a mitotic population. Two hours prior to fixation we either left cells untreated, treated them with the ATP-competitive mTOR inhibitor AZD8055, or incubated cells in starvation media. As expected, in P-H3 (S10) negative interphase cells the number of ATG13 puncta significantly increased with either AZD8055 treatment or incubation in starvation media (HBSS supplemented with 1% BSA) (Figure 4.5). ATG13 puncta were largely absent in P-H3 (S10) positive cells regardless of treatment. This suggests there was a repression of autophagy initiation during mitosis, and that this was independent of mTORC1 activity.

To further assess the status of the omegasome, we performed immunofluorescence of WIPI2, an autophagy-specific PI(3)P sensor (Dooley *et al.*, 2014). WIPI2 and other PI(3)P-sensing proteins contain FYVE domains, which bind specifically to PI(3)P (Gaullier *et al.*, 1998). Whilst Furuya and colleagues had previously shown that the number of punctate structures of an isolated FYVE domain were reduced during mitosis (Furuya *et al.*, 2010), from approximately 50 to 35 FYVE spots/cell, this experiment could be interpreted as a likely underestimate of autophagy repression. Firstly, no autophagy stimulus was provided, and therefore would have been evaluating low levels of basal autophagy. Secondly, as previously discussed, many FYVE domain containing proteins are localised to the endosomes, not ER, and therefore FYVE structures will act as a readout of all PI(3)P synthesis. Whilst VPS34 is the sole class III PI3K kinase in mammalian cells, VPS34 is found in many complexes involved in a diverse set of functions, with the ATG14-

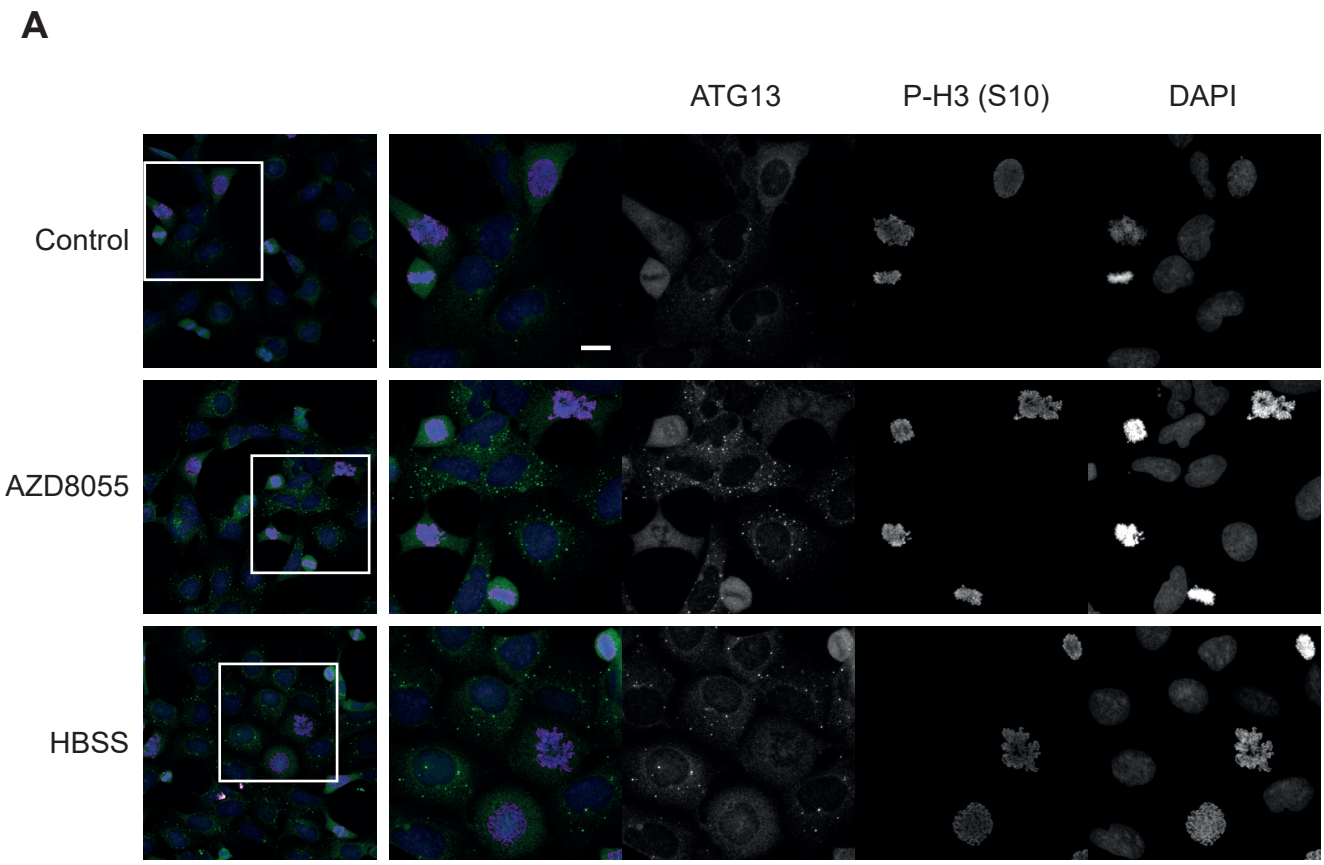

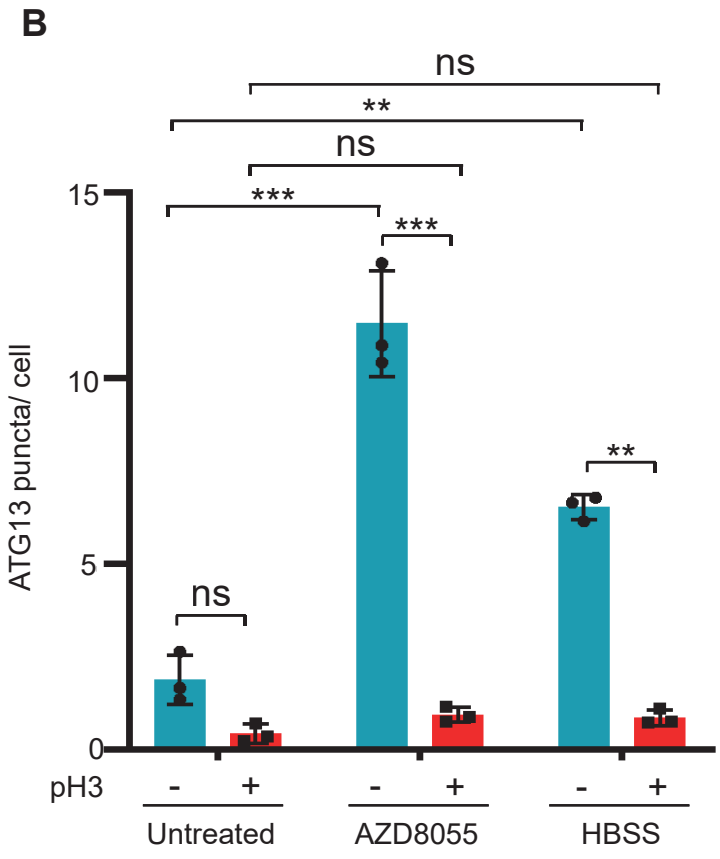

Figure 4.5: ATG13 puncta are significantly reduced in P-H3 (S10) positive mitotic cells compared to interphase cells.
(A) HeLa cells were released from double thymidine block for 10 hours. Two hours prior to fixation, cells were treated with AZD8055 (1 μM) or were incubated in HBSS + 1% BSA for 2 hours. Primary antibodies used: ATG13 (green), P-H3 (S10) (magenta). **(B)** Quantification of (A) showing the average number of ATG13 puncta per a cell in different conditions. Mean +/- SD across three biological replicates. P-values calculated from Two-way Anova (Tukey). * $p<0.05$; ** $p<0.01$; *** $p<0.001$. Scale bars: 20 μm.

containing complex being specific to macroautophagy and in some cell-lines, such as MEFs, only making a small contribution to the total pool of VPS34 complexes (Kim *et al.*, 2013). By contrast WIPI2, which also associates with the omegasome intermediate structure (Polson *et al.*, 2010), is critical for LC3B conjugation in response to PI(3)P, via its recruitment of the ATG16 complex (Dooley *et al.*, 2014). It is therefore a specific marker of autophagy. Reflecting our findings with ATG13, WIPI2 puncta increased in interphase cells upon mTOR inhibition or nutrient starvation, and no such increase occurred in mitotic cells (Figure 4.6). Indeed, WIPI2 puncta were largely absent in mitotic cells regardless of treatment. Overall, markers of the omegasome, which are relatively transient and serve as a direct readout of autophagy initiation (Figure 4.1), were largely absent from mitotic cells regardless of nutrient status.

Since HeLa cells are a cancer line with an abnormal karyotype, we wanted to observe whether mitotic repression of autophagy occurred in diploid fibroblasts. We therefore utilised hTERT-MRC5, a diploid cell line derived from foetal lung fibroblasts (Jacobs, Jones and Baille, 1970) and subsequently immortalised by expression of exogenous hTERT (Lee, Choi and Ouellette, 2004). As expected, treatment of hTERT-MRC5 cells with AZD8055 or starvation of amino acids resulted in pronounced autophagy induction, as judged by ATG13 puncta, in interphase cells but not mitotic cells (Figure 4.7). Therefore, repression of autophagy during mitosis occurs in immortalised diploid fibroblasts, as well as in HeLa cells.

Curiously, throughout these experiments examining omegasome markers there were a few cells which were P-H3 (S10) positive that exhibited robust numbers of ATG13 puncta. These all appeared to have intact nuclear morphology. Consistent with this, P-H3 (S10) phosphorylation occurs during late G2 and prior to nuclear envelope breakdown (Hendzel *et al.*, 1997). We therefore hypothesised that the loss of ATG13 puncta should temporally correlate with the onset of nuclear envelope breakdown and reappear upon the conclusion of mitosis. To address this, we elected to use a clonal population of HEK293 cells stably expressing GFP-ATG13 (previously generated (Karanasios *et al.*, 2013)), enabling live-cell imaging of ATG13 puncta. Fixed-cell imaging confirmed that, like endogenous ATG13, GFP-ATG13 puncta formed in response to treatment with the mTOR inhibitor AZD8055 and starvation media in interphase cells, but no puncta were present in mitotic cells (Figure 4.8.A). We therefore wanted to stably express H2B-mCherry (a histone protein) into these HEK293 GFP-ATG13 cells to enable live-cell imaging throughout mitosis. Whilst DNA stains such as Hoescht can be utilised for live-cell imaging, there were several advantages to utilising H2B-mCherry. As stated earlier, we found that AZD8055 led to an artefact, resulting in a cytoplasmic stain, in the blue (405) channel. Furthermore, DNA

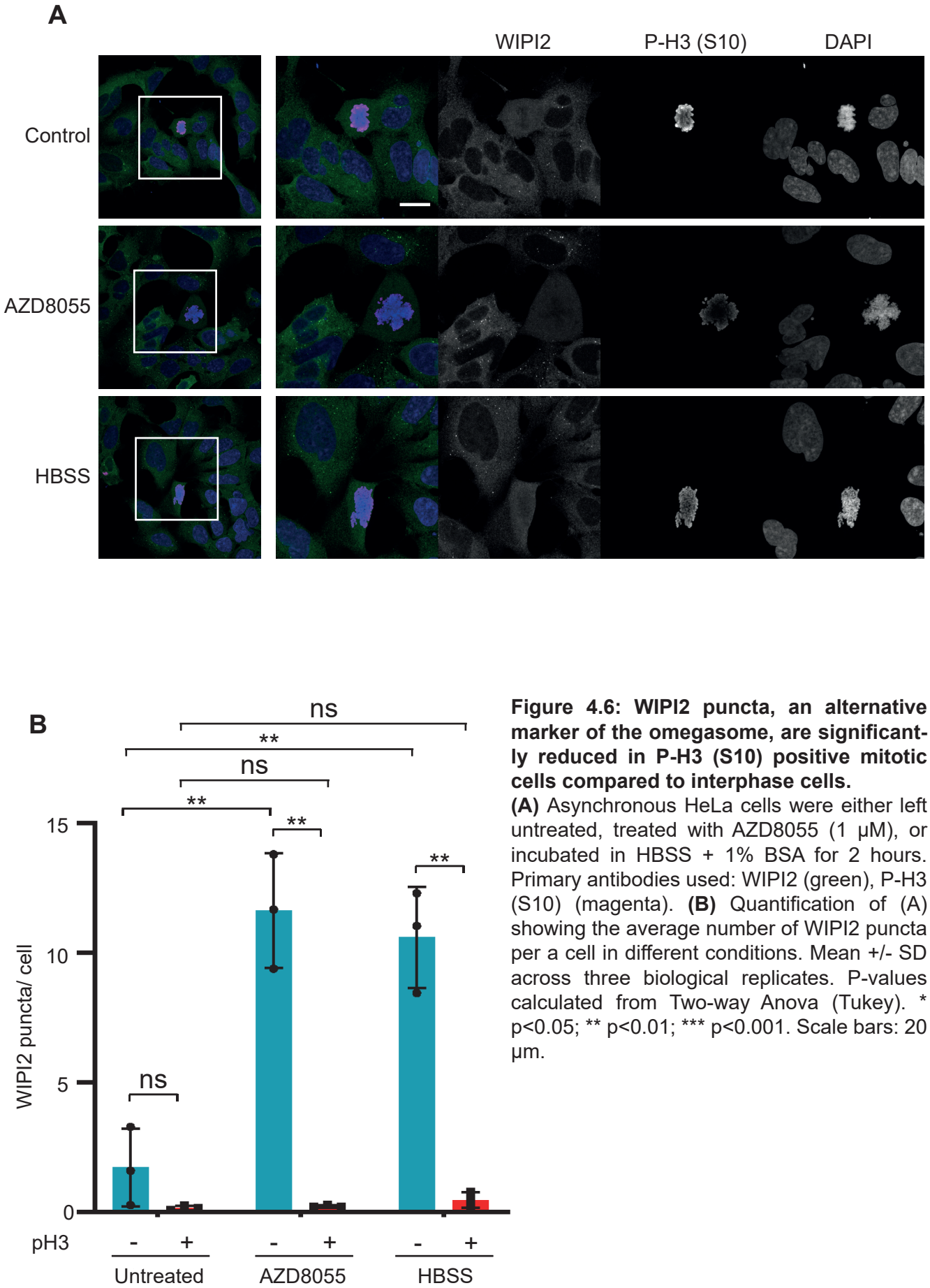

Figure 4.6: WIPI2 puncta, an alternative marker of the omegasome, are significantly reduced in P-H3 (S10) positive mitotic cells compared to interphase cells.
(A) Asynchronous HeLa cells were either left untreated, treated with AZD8055 (1 μM), or incubated in HBSS + 1% BSA for 2 hours. Primary antibodies used: WIPI2 (green), P-H3 (S10) (magenta). **(B)** Quantification of (A) showing the average number of WIPI2 puncta per a cell in different conditions. Mean +/- SD across three biological replicates. P-values calculated from Two-way Anova (Tukey). * p<0.05; ** p<0.01; *** p<0.001. Scale bars: 20 μm.

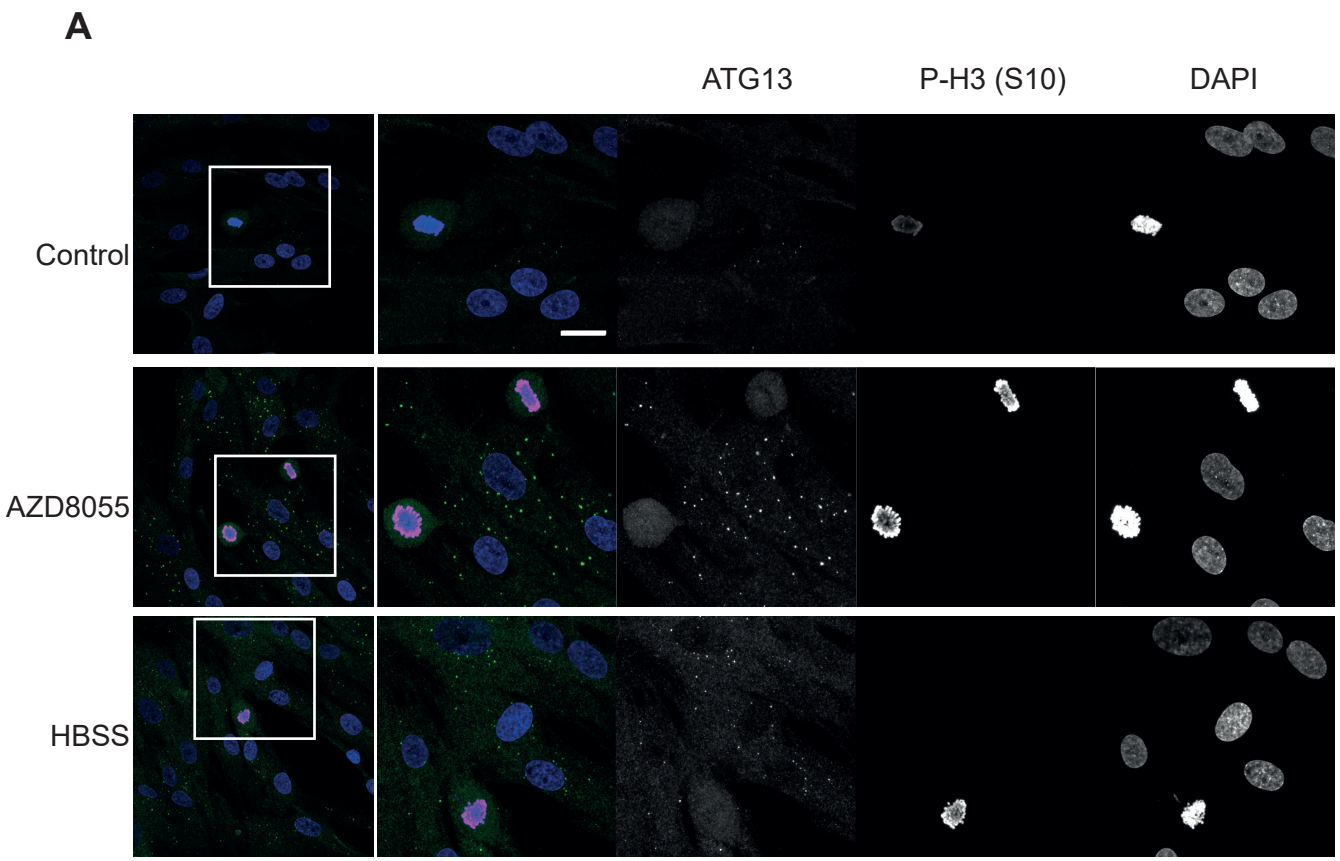

Figure 4.7: Autophagy is repressed in the diploid fibroblast line MRC5.
(A) Asynchronous MRC5 cells were treated with AZD8055 (1 μM) or were incubated in HBSS + 1% BSA for 2 hours. Primary antibodies used: ATG13 (green), P-H3 (S10) (magenta). Images from a single experiment representative of three biological replicates. Scale bar: 20 μm.

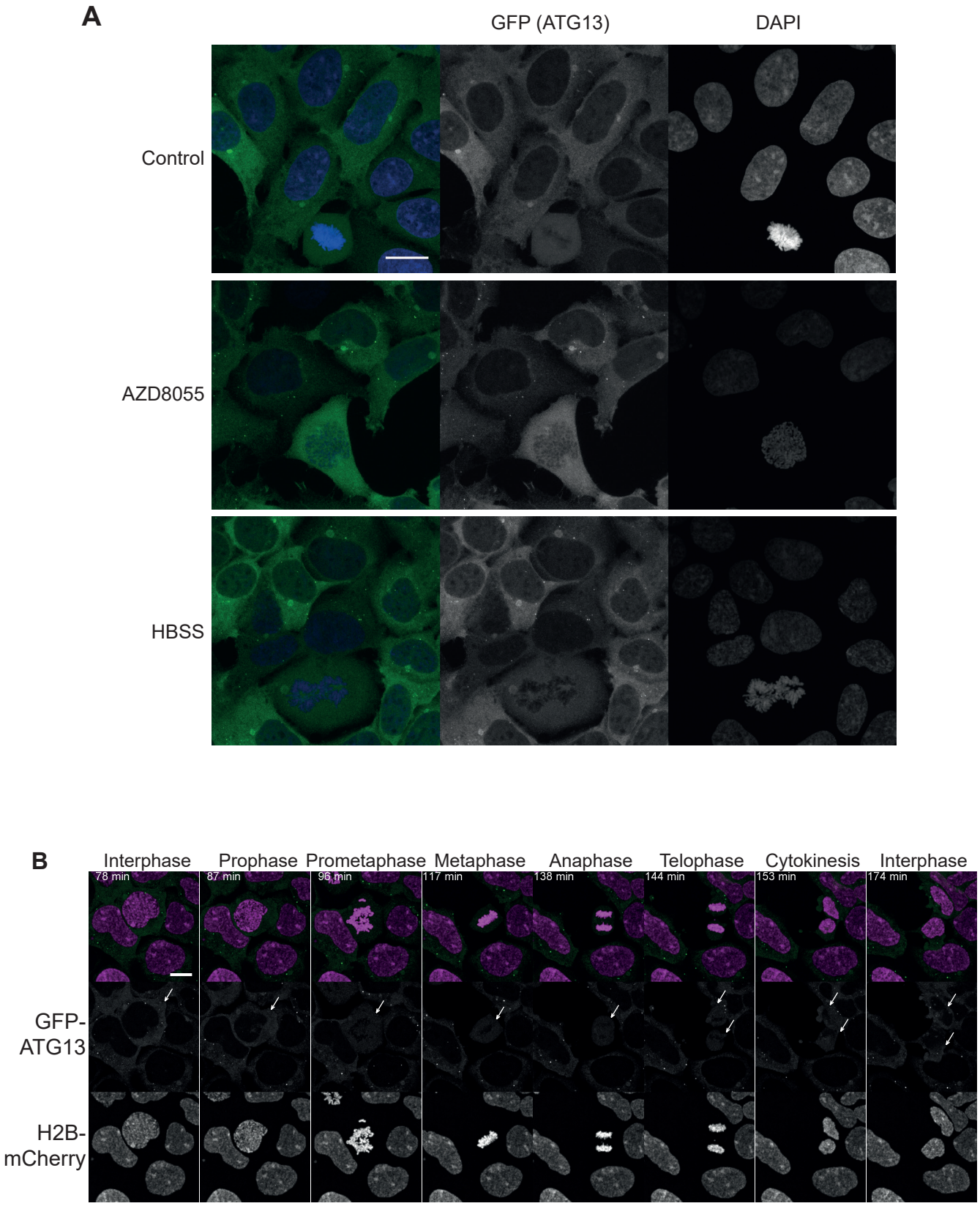

Figure 4.8: Loss of ATG13 puncta temporally correlates with chromosome condensation. **(A)** Asynchronous HEK293 GFP-ATG13 cells were either left untreated, treated with AZD8055 (1 μM), or incubated in HBSS + 1% BSA for 2 hours. **(B)** Asynchronous HEK293 GFP-ATG13 (green) H2B-mCherry (magenta) were treated with AZD8055 (1 μM) for one hour prior to transfer to a live-cell imaging incubator. Mitotic cell indicated by arrow. Scale bars: 20 μm. All images are from a single experiment representative of three independent experiments.

dyes lead to toxicity over time. Given, we were already stressing cells with the addition of an mTOR inhibitor and taking z-stacks over a large range (50 slices at 0.5μM spacing), reducing additional stressors was critical. Importantly, we wanted to perform live-cell imaging on asynchronous samples. Since we could not predict when within an experiment cells would enter mitosis, it was required to image several fields of view for 5 hours to ensure we captured a number of cells which completed mitosis. These factors together made the use of a stably expressed H2B-mCherry superior to Hoescht. Due to the rounded cell morphology of mitotic cells, wide-field imaging, whilst more sensitive, did not provide adequate spatial resolution to ensure puncta detection in interphase and mitotic cells at the same time. Both GFP-ATG13 and H2B-mCherry were detectable on a spinning disk confocal live-cell imaging system, enabling z-stacks to be acquired to ensure full coverage of the mitotic cell. Cells were treated with an mTOR inhibitor AZD8055 to induce autophagy prior to being mounted inside the imaging chamber, where images were captured at 3-minute intervals. Initially, all cells in the field of view were in interphase and had abundant puncta, consistent with induced autophagy initiation (Figure 4.8.B). In cells that underwent mitosis, ATG13 puncta immediately dispersed upon chromosome condensation and onset of prophase. ATG13 puncta were absent throughout mitosis, right through to cytokinesis. The two daughter cells, with reformed nuclear morphology and entry into interphase, then exhibited abundant ATG13 puncta again, similar to neighbouring interphase cells. Thus, autophagy initiation underwent a temporally coordinated repression at the start of and throughout mitosis, where exposed chromatin is contiguous with the cytosol, before returning to apparently normal levels once mitosis was complete.

We further generated a clone from the HEK293 GFP-ATG13 cells stably expressing mCherry-Pom121. Pom121 is a nuclear pore protein, thereby enabling direct monitoring of nuclear envelope breakdown (NEB) and reformation (NER) (Dultz *et al.*, 2008). It forms a punctate structure exclusively localised to the nuclear envelope, except during nuclear envelope breakdown where it disperses into the ER (Daigle *et al.*, 2001). As published, in our experiments POM121 formed a localised pool during anaphase which then dispersed across the reforming nuclear envelope (Daigle *et al.*, 2001). Therefore, it is clear to see that imaging POM121 provides another temporal reference point from which to consider the repression of autophagy during mitosis. Unfortunately, there appeared to be a selection pressure against this construct as few cells expressed the fluorescent protein, even after single cell cloning. Furthermore, many cells which did express this construct appeared to have disrupted nuclear morphology. From the few cells observed with a normal nuclear morphology, it was clear that ATG13 puncta were lost prior to nuclear envelope breakdown and started to reappear upon nuclear envelope reformation, though did not robustly come

back until after cytokinesis (Figure 4.9). Crucially, all of these live-cell experiments were conducted in the absence of mitotic poisons; this was only made possible by the use of omegasome markers rather than LC3. Overall, these results strongly suggest that autophagy initiation is impaired during mitosis.

4.2.3 mTORC1 fails to localise to lysosomes during mitosis, a critical step in its activation during interphase

All of the data generated so far suggested that autophagy was repressed during mitosis. This curiously also appeared to be the case in the presence of the catalytic mTOR-inhibitor AZD8055 or in the absence of amino acids, which would also inhibit mTORC1 signalling. Since mTORC1 is widely considered the master repressor of starvation-induced macroautophagy, its activity during mitosis warranted further investigation. Thus far, research into the status of mTORC1 during mitosis has been controversial. It has been shown by independent research groups that raptor is hyperphosphorylated in a CDK1-dependent manner (Gwinn, Asara and Shaw, 2010; Ramírez-Valle *et al.*, 2010). This has been suggested to promote its activity, and overexpressed RAPTOR immunoprecipitated with overexpressed 4E-BP1 in mitotic lysates, suggesting mTORC1 could continue to associate with its substrates (Gwinn, Asara and Shaw, 2010). However, during mitosis, 4E-BP1 is hyperphosphorylated such that it runs as a mitosis-specific δ isoform on SDS-PAGE, due to CDK1's specific phosphorylation of S83 (Velásquez *et al.*, 2016). Yet in Gwinn's study, the overexpressed 4E-BP1 did not exhibit the mitotic δ isoform in mitotic lysates on SDS-PAGE (Gwinn, Asara and Shaw, 2010), suggesting it was not acting like the endogenous protein. In contrast, another research group suggested that mTORC1 was inactive during mitosis, as the previously reported S6K T389 phosphorylation during mitosis, could not be reversed by shRAPTOR (Ruf *et al.*, 2017). Likewise, Shah and colleagues found that whilst S6K was phosphorylated on other sites by CDK1, T389 was dephosphorylated during mitosis (Shah, Ghosh and Hunter, 2003). Multiple groups have shown that the δ isoform of 4E-BP1 is resistant to ATP-competitive mTOR inhibitors (Ramírez-Valle *et al.*, 2010; Shuda *et al.*, 2015; Velásquez *et al.*, 2016).

mTORC1 is usually activated in response to nutrients. This occurs by Rag GTPase sensing of amino acid status and recruitment of mTORC1 to lysosomes through RAPTOR binding to Rag GTPases (Sancak *et al.*, 2008, 2010; Manifava *et al.*, 2016). We therefore wanted to investigate whether mTORC1 continued to be recruited to lysosomes during mitosis. Fixed-cell confocal immunofluorescence showed co-localisation of mTOR with Lamp2 in interphase cells (Figure 4.10.A), in concordance with previous reports (Sancak *et al.*, 2010). However, cells undergoing mitosis showed minimal co-localisation Lamp2 and

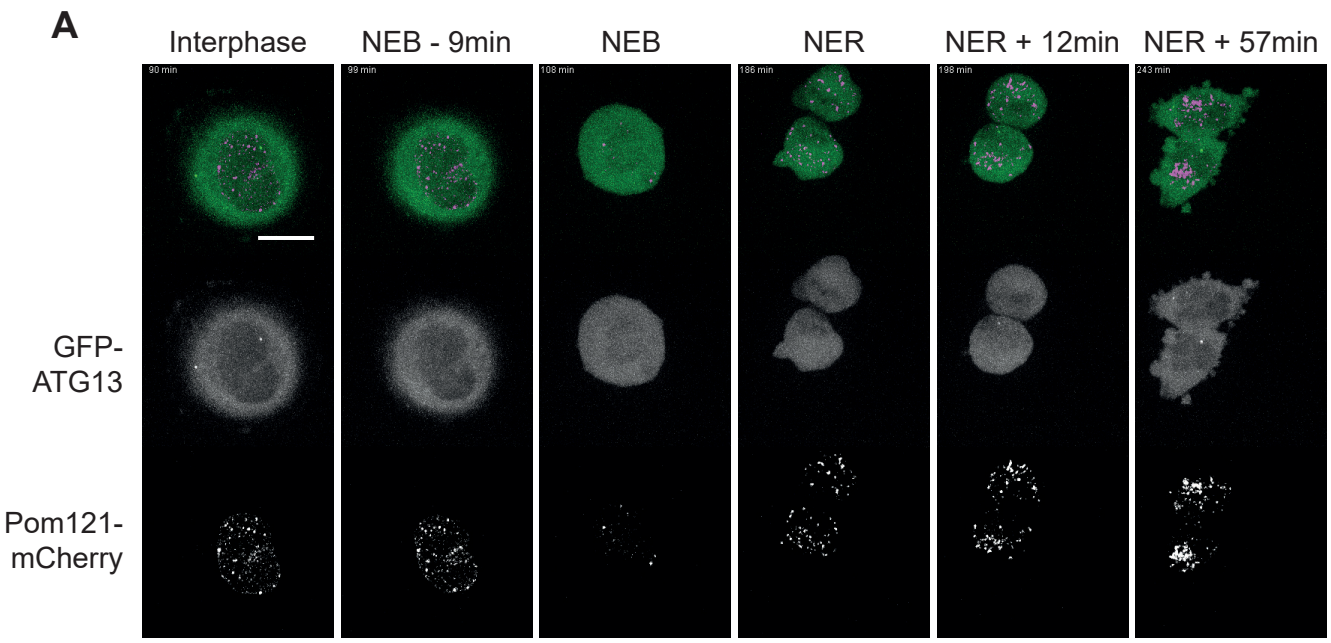

Figure 4.9: Loss of ATG13 puncta temporally correlates with nuclear envelope breakdown.
(A) Asynchronous HEK293 GFP-ATG13 (green) Pom121-mCherry (magenta) were treated with AZD8055 (1 μM) for one hour prior to transfer to a live-cell imaging incubator. NEB: Nuclear envelope breakdown. NER: Nuclear envelope reformation. Scale bars: 20 μm. Images representative from two independent biological experiments.

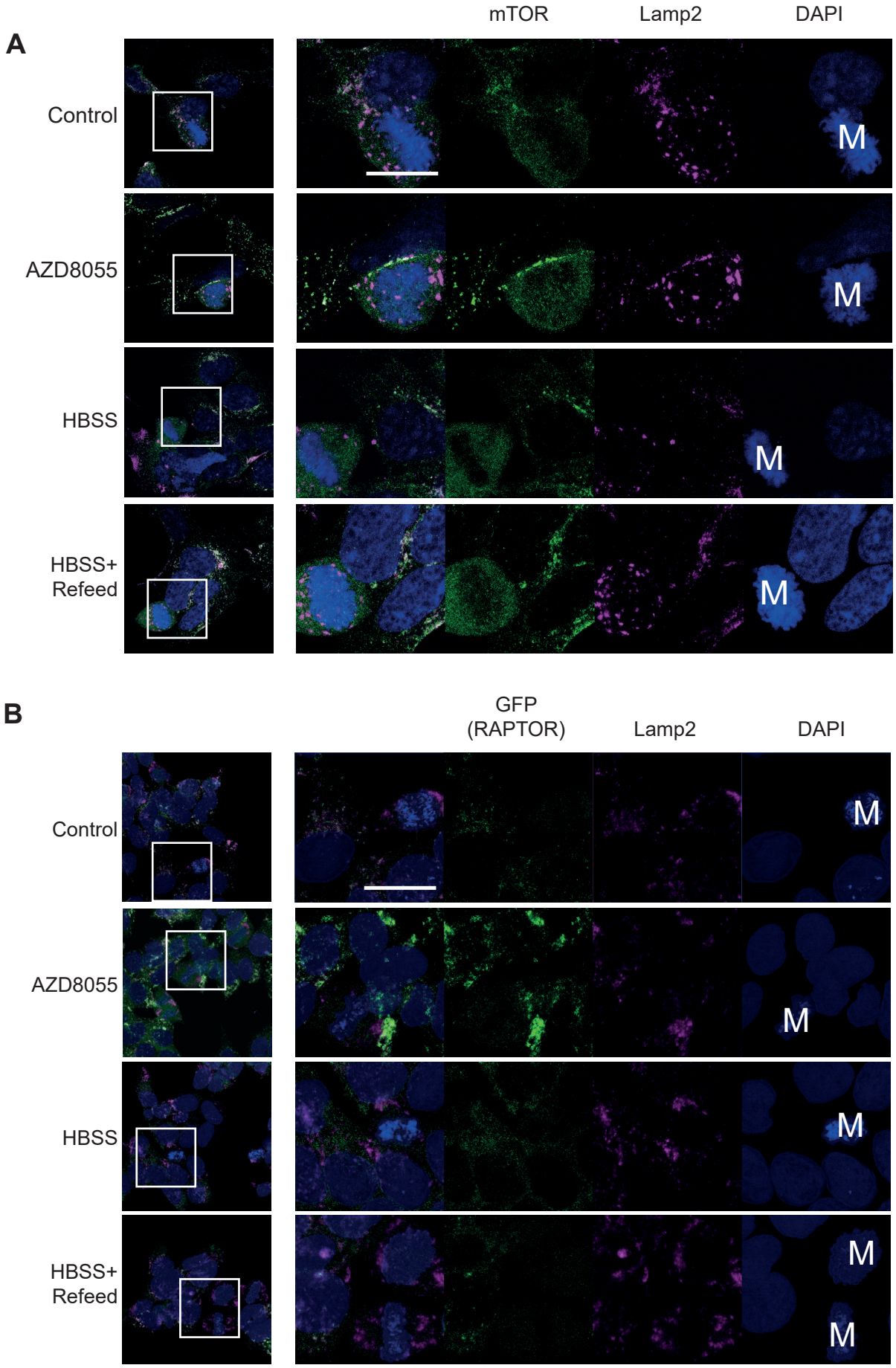

Figure 4.10: mTORC1 fails to localise to lysosomes during mitosis.
(A) Asynchronous HeLa cells were treated with AZD8055 (1 μM) or incubated in HBSS + 1% BSA for 2 hours. For refeed, cells were starved for 2 hours, and their media then switched to complete growth media for 5 minutes. Primary antibodies: Lamp2 (magenta) and mTOR (green). **(B)** HAP1 RAPTOR-GFP cells were treated as per (A). Primary antibody: Lamp2 (magenta). Mitotic cells are indicated (M) in the DAPI channel. All images are 2-dimensional max-intensity projections of z-stacks encompassing the whole cell volume. Images representative of mitotic cells across three biological replicates. Scale bar: 20 μm.

mTOR, suggesting that mTORC1 was not recruited to lysosomes during mitosis. AZD8055, in common with another ATP-competitive mTOR inhibitor Torin1 (Ohsaki *et al.*, 2010), drives mTOR to lysosomes via an unknown mechanism. AZD8055 had minimal effect in mitotic cells where the mTOR signal was still mostly diffuse with minimal foci, supporting our findings in untreated cells (Figure 4.10.A). Whilst it has been shown that mTOR dissociates from lysosomes in response to the absence of amino acids in HeLa cells (Sancak *et al.*, 2010), this has subsequently been shown to be controversial, with several groups showing at least a degree of colocalization persists during amino acid starvation (Korolchuk *et al.*, 2011; Manifava *et al.*, 2016). In concordance with these later findings, we found minimal difference in the colocalization patterns of mTOR and Lamp2 during amino acid starvation or refeeding in HeLa cells. In all treatment conditions, mitotic cells showed minimal co-localisation between mTOR and Lamp2.

We next wanted to validate these findings through complementary approaches. Overexpressed RAPTOR has been shown to have aberrant localisation and confers phenotypes not consistent with those observed for the endogenous protein (Manifava *et al.*, 2016). Furthermore, no RAPTOR antibodies currently available are suitable for immunofluorescence (Ktistakis, personal communication). To circumvent these problems, our colleagues in the Ktistakis group have previously performed CRISPR-Cas9 gene editing to tag the endogenous RAPTOR protein with GFP. To do this, they utilised the near haploid cell line HAP-1. This means that all of the RAPTOR protein within the cells is GFP-tagged, as evidenced by the complete shift on SDS-PAGE of the total protein by approximately 25kDa (Figure 4.12; Manifava *et al.*, 2016). Supporting our findings with the mTOR antibody in HeLa cells, RAPTOR-GFP showed colocalization with Lamp2 in untreated interphase cells but not in mitotic cells (Figure 4.10.B). Likewise, AZD8055 intensified RAPTOR-GFP localisation to Lamp2 in interphase cells but not in mitotic cells. In the original publication describing these cells, RAPTOR-GFP exhibited a pronounced dissociation from lysosomes in the absence of amino acids (Manifava *et al.*, 2016). In addition, reintroduction of amino acids promoted rapid recruitment of RAPTOR-GFP to lysosomes. Replicating these findings, in interphase cells, RAPTOR-GFP dissociated from lysosomes in starvation media, and this was reversed upon addition of complete media. In mitotic cells, there was no observable focal recruitment of RAPTOR-GFP to lysosomes when cells were re-incubated in complete media. Thus, mTORC1 failed to be recruited to lysosomes in a nutrient-dependent manner during mitosis.

To validate these immunofluorescence findings by an alternative methodology, we performed membrane-cytosolic fractionation (Figure 4.11). Whilst HeLa cells do not perfectly arrest in mitosis upon treatment with the microtubule inhibitor paclitaxel, mitotic

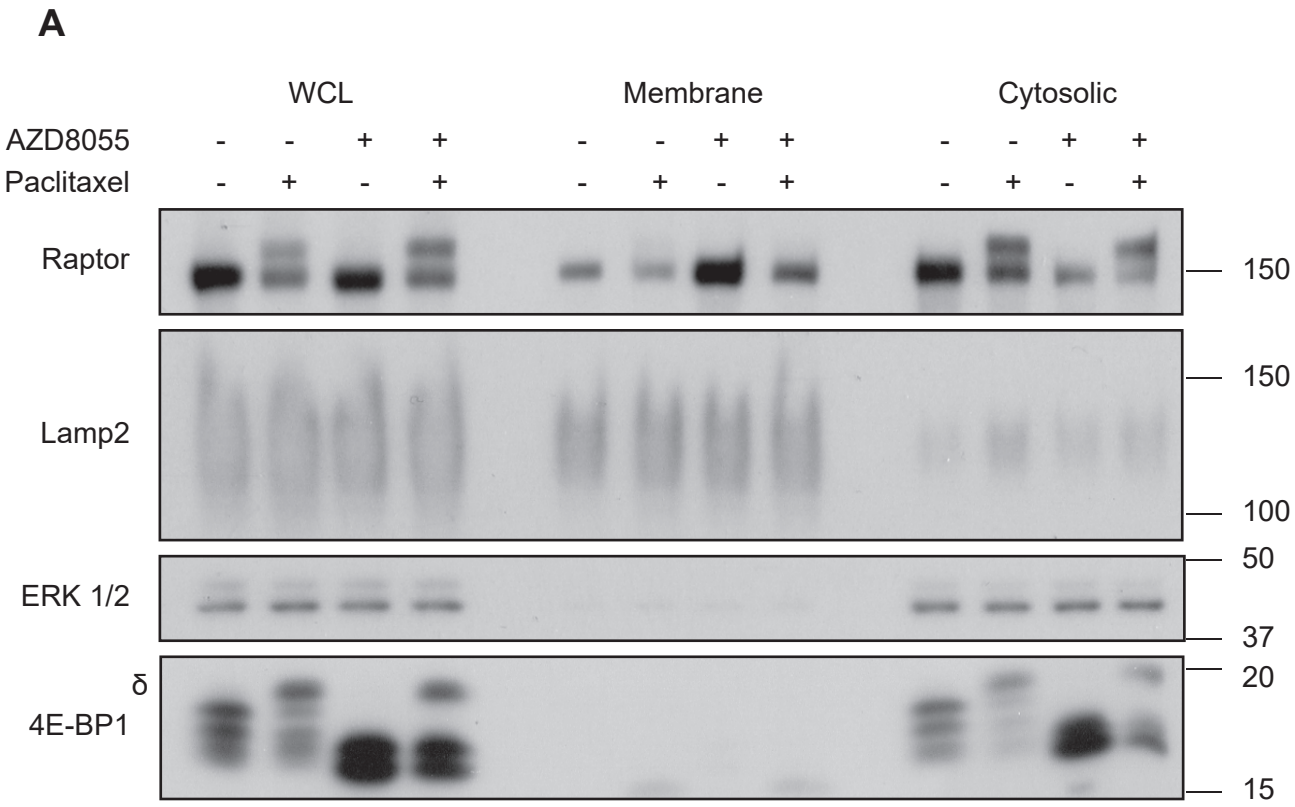

Figure 4.11: Mitotic-RAPTOR is localised to the cytosol not membranous fraction of cell lysates.
(A) HeLa cells were treated with paclitaxel (t=16 hrs; 50 nM) and/ AZD8055 (t=2 hrs; 1 μM). Lysates were then fractionated into membrane and cytosol enriched fractions, with Lamp2 and ERK1/2 serving as the respective loading controls. Western blots are from a single biological replicate representative of three independent experiments. Molecular weight markers (kDa) are indicated to the right of each blot.

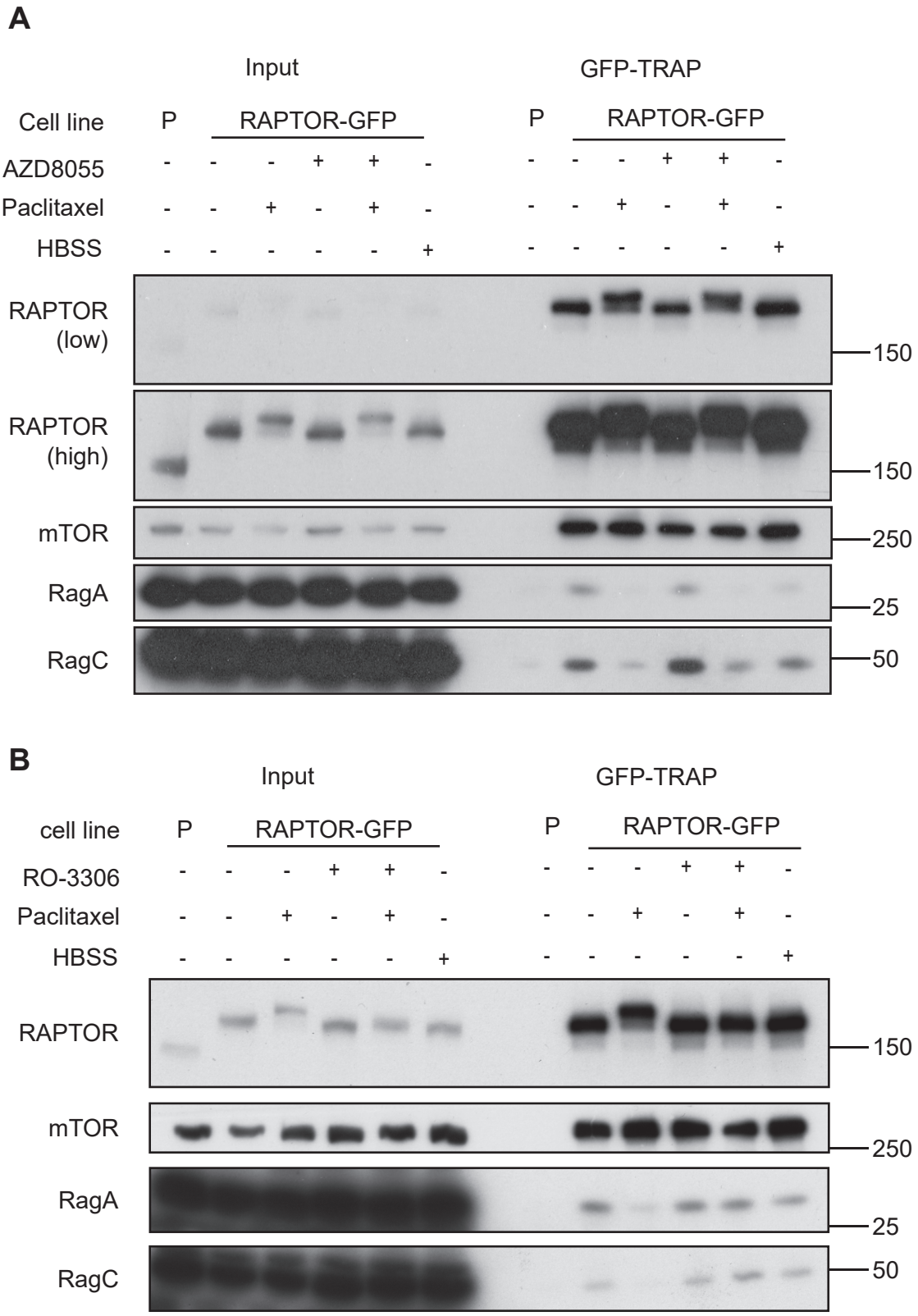

Figure 4.12: Mitotic-RAPTOR fails to interact with Rag-GTPases in a CDK1-dependent manner.

(A) HAP1 RAPTOR-GFP cells were treated with paclitaxel (50 nM; t=16 hrs), AZD8055 (1 μM; t=2 hrs) or HBSS + 1% BSA (t=2 hrs) prior to immunoprecipitation with GFP-TRAP (Chromotek). HAP1 parental cells were included as a negative control (P). **(B)** HAP1 RAPTOR-GFP cells were treated with paclitaxel (50 nM; t=16 hrs), RO-3306 (2 μM; t=2 hrs) or HBSS + 1% BSA (t=2 hrs) prior to immunoprecipitation with GFP-TRAP. Western blots are from a single biological replicate representative of three independent experiments. Molecular weight markers (kDa) are indicated to the right of each blot.

RAPTOR can be readily distinguished from interphase since it undergoes a considerable SDS-PAGE mobility shift due to CDK1-dependent phosphorylation (Ramírez-Valle *et al.*, 2010). Immunoblotting of Lamp2 and ERK1/2 confirmed that there was considerable enrichment for lysosomal and cytosolic proteins within the membranous and cytosolic fractions respectively. 4E-BP1 (cytosolic protein) further validated this fractionation, as well as the degree of mitotic arrest (δ isoform). As expected, in asynchronous lysates, the mTOR inhibitor AZD8055 promoted an accumulation of non-phosphorylated RAPTOR in the membranous fraction (Figure 4.11). In contrast, paclitaxel treatment, which promotes mitotic arrest, increased the fraction of Raptor in the cytosol. Furthermore, very little hyperphosphorylated mitotic-RAPTOR was detected in the membranous fraction and this was the case even with AZD8055. The increase in membranous RAPTOR observed in paclitaxel-treated samples in response to AZD8055 was most likely from interphase contamination. Therefore, these results support the immunofluorescence findings that mTORC1 was not recruited to lysosomes during mitosis. It is worth noting that immunoblotting of RAPTOR was performed as it is a selective marker of mTORC1, whereas immunoblots of mTOR cannot distinguish between the complexes.

Since mTORC1 did not localise to lysosomes during mitosis we wanted to examine the RAPTOR-Rag interaction in mitotic cells. To do this, we utilised GFP-TRAP immunoprecipitation from the HAP1 RAPTOR-GFP cells. GFP-TRAP involves the conjugation to agarose beads of a recombinant variable domain derived from alpaca antibodies against GFP. Alpacas produce a heavy chain antibody which is devoid of a light chain and can bind an antigen through a single variable domain. This single variable domain can then be recombinantly expressed such that GFP-TRAP does not contain either a heavy or light chain. This enables detection of endogenous RagC at 50 kDa, which would usually be obscured by the heavy chain. In both asynchronous and mitotically-arrested lysates, mTOR co-immunoprecipitated with RAPTOR-GFP, suggesting the mTORC1 complex was intact during mitosis. By contrast, whilst in asynchronous lysates RagA and RagC were successfully coimmunoprecipitated with RAPTOR-GFP (Figure 4.12.A), this interaction was lost in paclitaxel-treated samples. This occurred regardless of the presence or absence of AZD8055, correlating with our findings that hyperphosphorylated RAPTOR is not localised to the membranous fraction. The CDK1 inhibitor RO-3306 completely reversed the dissociation of RAPTOR-GFP from Rag-GTPases (Figure 4.12.B), demonstrating that this loss of interaction was dependent upon CDK1 activity in paclitaxel-treated samples. Overall, this data strongly suggests that mTORC1 cannot be recruited to lysosomes during mitosis and this correlated with CDK1-dependent RAPTOR phosphorylation. Since this is a critical step in its activation in interphase cells, it is likely that mTORC1 is inactive and would not

be capable of phosphorylating its canonical substrates. This supports our hypothesis that mTORC1 is not the master regulator of autophagy during mitosis.

Since the RAPTOR-Rag interaction governs mTORC1's localisation to lysosomes, we hypothesised that the alterations affecting mTORC1 localisation during mitosis must be directly impacting Rag-GTPases and/or RAPTOR. Since Rag-GTPases are tethered to the lysosome via the Ragulator complex, we first investigated the localisation of RagC by immunofluorescence. This showed strong colocalization of RagC and Lamp2 in both interphase and mitotic cells, suggesting there was no alteration to Rag-GTPase localisation (Figure 4.13.A). It has previously been shown that overexpression of Rag GTPases in an active conformation ($RagB^{GTP}$, $RagD^{GDP}$) can promote mTORC1 localisation to lysosomes, regardless of nutrient status. Whilst we observed prominent mTOR localisation to lysosomes in interphase cells overexpressing the active heteroduplex, no such localisation was observed in mitotic cells (Figure 4.13.B). Therefore, whilst upstream activation pathways have effectively been bypassed by overexpressing this construct, mTORC1 still failed to be recruited to lysosomes. This suggested that alterations in the activity of Rag-GTPases were not mediating the alterations in mTORC1 localisation during mitosis.

It is an attractive hypothesis that CDK1-dependent phosphorylation of RAPTOR is what mediates its dissociation from Rag-GTPases. Indeed, treatment with the CDK1 inhibitor RO-3306 completely reversed the dissociation of RAPTOR-Rag (Figure 4.12.B). The Schneider group previously identified seven sites by mass spectrometry that were phosphorylated in a CDK1-dependent manner (Ramírez-Valle *et al.*, 2010), and it was subsequently demonstrated that at least some of these were directly phosphorylated by CDK1 (Gwinn, Asara and Shaw, 2010). Some of these sites are not proline directed (S722, S855, S859) and therefore do not fit a CDK1 consensus motif. Whilst it has been shown that RAPTOR is phosphorylated by PLK1 during interphase, no changes in S722 or S859 phosphorylation was detected with PLK1 overexpression or PLK1 inhibition (Ruf *et al.*, 2017). However, it was observed that PLK1 overexpression promoted mTORC1 dissociation from lysosomes in interphase (Ruf *et al.*, 2017). Regardless, PLK1 inhibition did not promote mTORC1's localisation to lysosomes during mitosis (Figure 4.14).

To further explore whether these seven sites in RAPTOR were responsible for mTORC1's failure to localise to the lysosome, we infected HeLa cells with retrovirus expressing constructs containing the seven mutated sites as either phospho-null (A7) or phospho-mimetic (D7). As observed in the original publication, whilst both the A7 and D7 mutant strikingly dampens the electrophoretic-shift upon paclitaxel treatment, it still persists to a degree suggesting that other mitotic phosphorylation sites are present (Ramírez-Valle

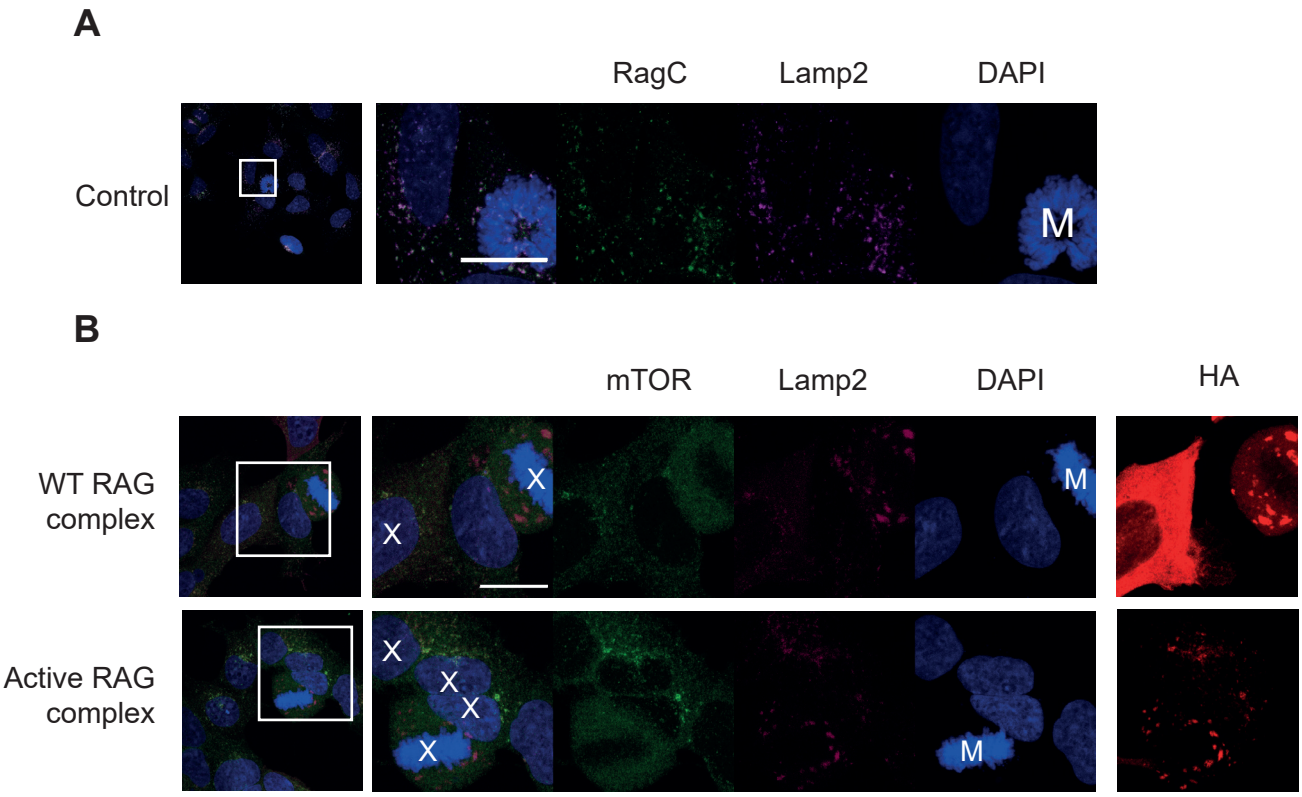

Figure 4.13: Alterations in Rag-GTPase duplex activity is not responsible for mTORC1 dissociation from the lysosome during mitosis.
(A) Asynchronous HeLa cells were immunostained for RagC (green) and Lamp2 (magenta). **(B)** Asynchronous HeLa cells were transfected with either WT RagB and RagD (WT RAG complex) or $RagB^{GTP}$ $RagD^{GDP}$ (Active Rag Complex). Transfected cells are indicated with an X in the Merge image (based on HA immunostain). Images are representative of three independent biological experiments. Scale bars: 20 μm.

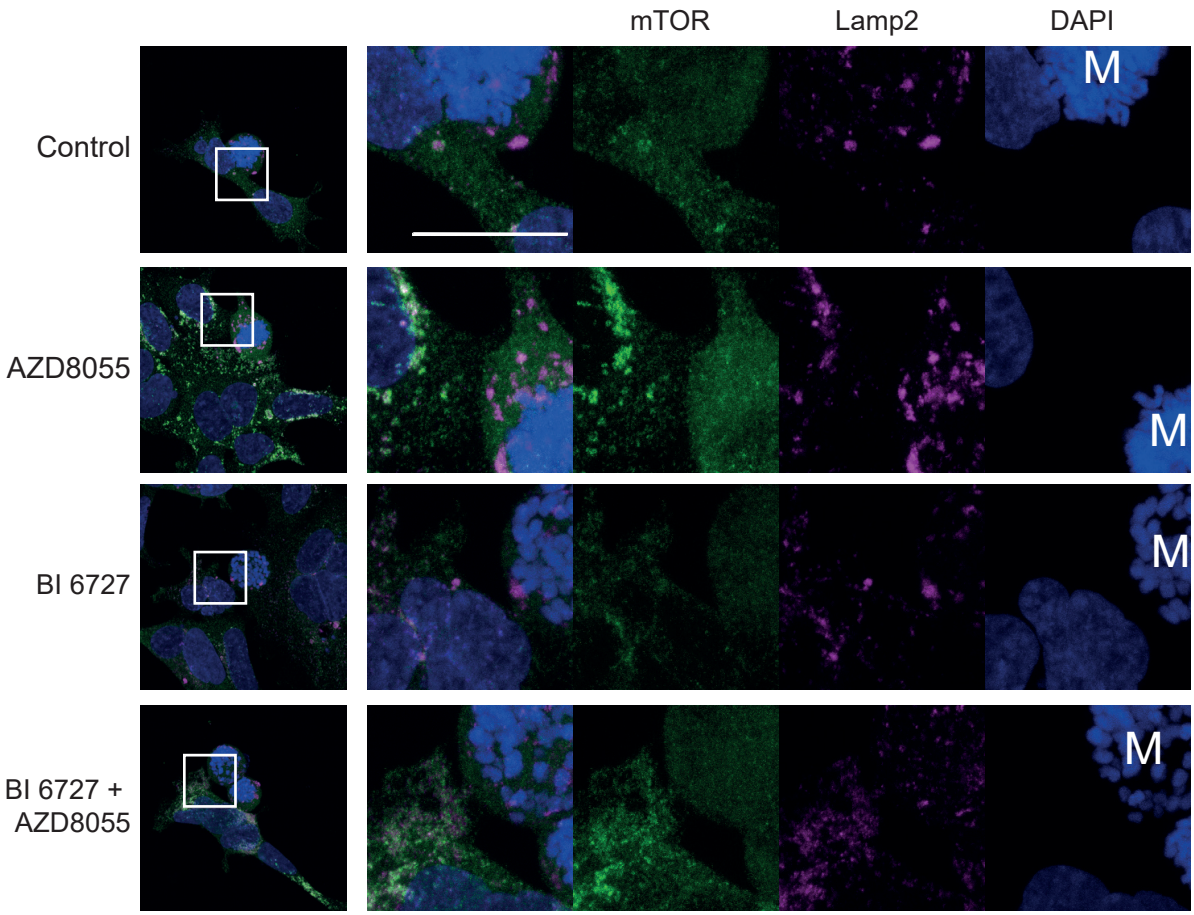

Figure 4.14: PLK1 does not mediate mTORC1 dissociation from the lysosome during mitosis.
(A) HeLa cells were treated with AZD8055 (1 μM) and/or BI 6727 (100 nM) for 2 hours prior to fixation. Primary antibodies: Lamp2 (magenta) and mTOR (green). All images are 2-dimensional max-intensity projections of z-stacks encompassing the whole cell volume. Images representative of mitotic cells from a single experiment. Scale bar: 20 μm.

et al., 2010) (Figure 4.15). There is currently no feasible way to deduce what other sites are phosphorylated during mitosis, since RAPTOR is a large protein (150kDa, 1335 amino acid) with 113 serine and 73 threonine sites (based on FASTA sequence of isoform 1, UNIPROT identifier:Q8N122-1). As previously established (Manifava *et al.*, 2016), immunofluorescence of overexpressed RAPTOR did not show any specific localisation pattern (data not shown). Immunoprecipitation of the HA-tag revealed intact mTORC1 complexes which responded to paclitaxel-treatment like the endogenous protein, with dissociation of phosphorylated RAPTOR from RagA. The most striking difference was the reduction in binding of RAPTOR-D7 to RagA compared to either WT-RAPTOR or RAPTOR-A7 in asynchronous samples. Overall, these results suggest that phosphorylation of these seven sites contribute towards the RAPTOR-Rag disassociation, but it is likely that other sites are also implicated. Therefore, CDK1-mediated phosphorylation of RAPTOR, and its separation from Rag-GTPases, contributes to the inactivation of mTORC1 during mitosis.

4.3 Discussion

4.3.1 Autophagy induction is repressed during mitosis

The field has been debating the status of autophagy during mitosis for 17 years, with a plethora of evidence supporting both sides of the argument. This has likely come as a result of the use of assays which have become gold-standard, such as the use of lysosomal inhibitors with LC3 detection. Here, we demonstrate why the use of these techniques are likely to produce spurious results during mitosis. It is important to note for all of our findings presented in both this and the next chapter, that our results and conclusions are entirely compatible with the results found by other groups, even if their conclusions were different. In contrast to LC3, omegasome markers are a transient, dynamic and direct readout of autophagy initiation, and these are dramatically reduced throughout mitosis. This was the case even when autophagy stimuli such as starvation or mTORC1 inhibitors were introduced. Thus, autophagy initiation is repressed throughout mitosis until cytokinesis. Whilst, ATG13 puncta do not robustly reappear until approximately 30 minutes after nuclear envelope reformation and after cytokinesis, they are visible as early as 12 minutes after nuclear envelope reformation. This gradual return of autophagy is likely to represent the time taken in the switching back of regulation from CDK1 (next chapter) to mTORC1. It is also worth noting that nuclear envelope breakdown and reformation is itself a dynamic process, and whilst the nuclear pore protein POM121 is recruited during anaphase, other components of the nuclear pore complex such as Nup62 and Nup93 are recruited during telophase (Dultz *et al.*, 2008). Likewise, Lamins do not recruit until late telophase/ early cytokinesis (Daigle *et al.*, 2001). Therefore, the delay could

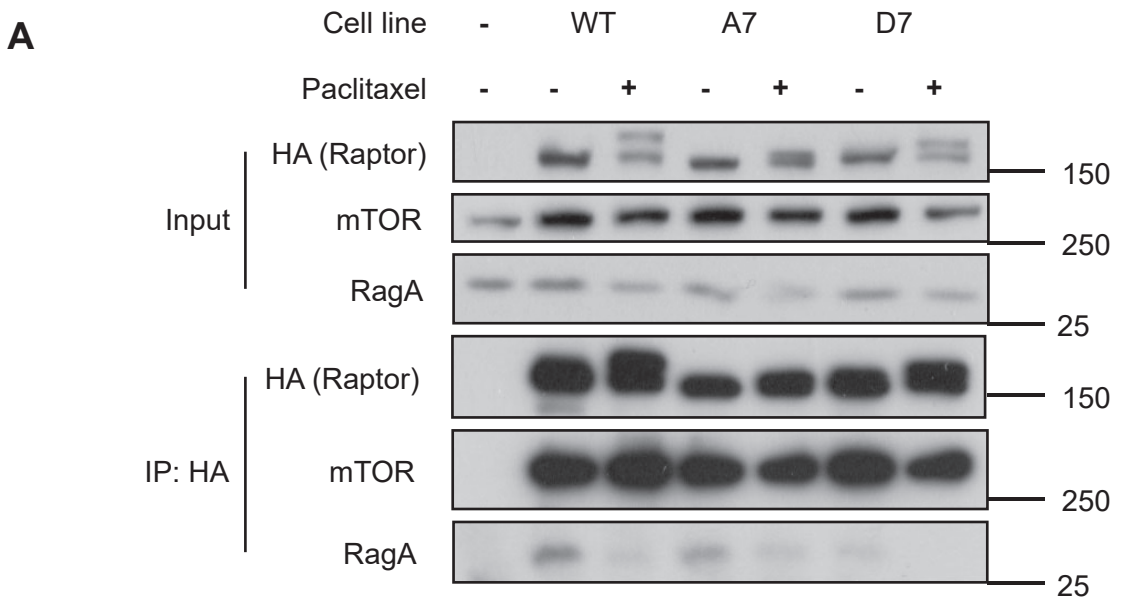

Figure 4.15: Paclitaxel-induced phosphorylation of RAPTOR is the most likely mechanism for the disassociation of RAPTOR from RagA.
(A) HeLa cells stably expressing indicated HA-RAPTOR constructs were treated with paclitaxel (50 nM; t=16 hrs) where indicated prior to immunoprecipitation with HA antibody. Western blots are from a single experiment representative of three independent experiments. Molecular weight markers (kDa) are indicated to the right of each blot.

simply reflect a requirement for complete nuclear envelope reformation. Regardless, there is a strong temporal correlation between loss of ATG13 puncta and nuclear envelope breakdown.

4.3.2 mTORC1 fails to localise to lysosomes during mitosis

Based on previous literature and our findings presented here, it seems most likely that mTORC1 is inactive during mitosis. This is based on several lines of evidence. There is a lack of upstream AKT signalling, meaning that canonical activation pathways are inactive during mitosis (Ramírez-Valle *et al.*, 2010). Whilst studies had initially advocated that mTORC1 was hyperactive, thus enabling it to phosphorylate 4E-BP1 and S6K even in the presence of catalytic mTOR inhibitors (Ramírez-Valle *et al.*, 2010), a more recent study has convincingly shown that 4E-BP1 undergoes a switch in regulation to CCNB1-CDK1 in mitosis (Shuda *et al.*, 2015). We now show that mTORC1 also fails to recruit to lysosomes during mitosis, likely as a result of CDK1-dependent phosphorylation of RAPTOR. Thus, it is highly likely mTORC1 is inactive. By contrast, to present the argument that mTORC1's activity is maintained during mitosis, there would have to be a completely alternative activation pathway to that described during interphase, not involving either AKT signalling or lysosomal localisation of mTORC1. Furthermore, there would have to be an alteration in mTORC1 that made it not susceptible to inhibition by a variety of catalytic inhibitors. No such mechanism has been described in the literature and seems unlikely. It is noteworthy, that whilst the Schneider group's findings suggest mTORC1 kinase activity was increased during mitosis (Ramírez-Valle *et al.*, 2010), this does not necessarily conflict with our findings here. This is because it has previously been shown that ULK1 phosphorylation promotes mTORC1 kinase activity but inhibits mTORC1 signalling in cells (Dunlop *et al.*, 2011). Thus, what we describe here are the paradoxical findings that whilst starvation-induced autophagy is repressed during mitosis, the known master repressor of this process, mTORC1, is inactive. This suggests that a switch in regulation is occurring during mitosis to ensure repression of autophagy. Given the temporal correlation between loss of ATG13 puncta and nuclear envelope breakdown, a process governed by CCNB1-CDK1, we postulated that CCNB1-CDK1 may be regulating autophagy and this is explored in the next chapter.

It is worth noting further experiments that could be performed to further test these findings. Whilst the experiment demonstrating that hyperphosphoylated RAPTOR was localised to the cytosolic and not membranous fraction is clear, it could be argued that a better experiment to perform would be the recently established lysoIP, whereby HA-tagged TMEM192 is overexpressed in cells, enabling immunoprecipitation of intact lysosomes from

cells (Abu-Remaileh *et al.*, 2017). Therefore, this enables a relatively pure immunoprecipitation of lysosomes without contamination from other membranous organelles. Since we observe the shift in localisation being towards the cytosol, this experimental protocol should provide the exact same result and we utilised AZD8055 as a positive control to verify that we could observe shifts in membrane/cytosolic localisations in our protocol. Therefore, whilst LysoIP would be a further way to validate this result, it was not deemed critical.

Finally, it has been suggested that mTORC1 is active during mitosis due to mitotic cells staining positive for P-mTOR (S2481) during mitosis (Vazquez-Martin *et al.*, 2009, 2011; Lopez-Bonet *et al.*, 2010; Platani *et al.*, 2015). Whilst this antibody is not approved for use in immunofluorescence, Platani did show that the centrosomal distribution of this signal during metaphase was reduced with Mios depletion. However, whilst we also observed a centrosomal localisation with this antibody during metaphase, this signal was still present when HAP1 RAPTOR-GFP cells had been treated with the catalytic mTOR inhibitor AZD8055 (data not shown). It has previously been shown that P-mTOR (S2481) is abolished (western blot) by treatment with Torin-1 (Soliman *et al.*, 2010). This suggests that, whilst we cannot rule out differences in protocols leading to altered results, findings from immunofluorescence using this antibody should be treated with caution. Furthermore, RAPTOR-GFP did not colocalise with the S2481 signal, though this alone does not discount the possibility of a subset of mTORC1 being phosphorylated, or mTORC2.

5 An mTORC1-to-CDK1 switch maintains suppression of autophagy during mitosis

5.1 Introduction

Macroautophagy is primarily regulated by mTORC1's phosphorylation of autophagy regulators ATG13, ULK1, ATG14 and TFEB; hereafter these are referred to as ARs. This regulation enables the direct coupling of nutrient availability to macroautophagy, in which nutrient starvation inactivates mTORC1 to de-repress autophagy; this maintains homeostasis and survival during starvation. As discussed in the previous chapter, mitosis represents an example where such homeostatic control may be disadvantageous and temporarily switched off as a result. Given that we had observed the paradoxical findings that mTORC1 was inactive, yet autophagy was repressed during mitosis, an obvious question became whether the repression of autophagy was mediated via the same repressive pathway as in interphase cells or by alternative mechanisms. Much study has gone into identifying alternative mechanisms of mTORC1-mediated repression of autophagy during mitosis. Whilst convincing data exists that CDK1 phosphorylates VPS34 to prevent its association with Beclin-1, the mutation of the putative CDK site did not reverse autophagy inhibition (Furuya *et al.*, 2010), suggesting other mechanisms of autophagy repression during mitosis exist.

Recently, it has been suggested that WIPI2 is degraded during mitosis and that by inhibiting the responsible ubiquitin ligase, autophagy could reinitiate during mitosis leading to senescence (Lu *et al.*, 2019). Many questions arise from the interpretation of this dataset. Most pressing, is that inhibition of the ubiquitin ligases (CUL4) lead to a prominent G1 peak by Propidium iodide flow cytometry, thus it's likely that autophagy regulation was no longer under mitotic control and it is therefore unsurprising that LC3B lipidation was restored. Indeed, on assessment of P-H3 (S10) in cells treated with both nocodazole and the NEDD8-Activating Enzyme inhibitor MLN4924 (which in turn inhibits CUL4), they showed this combination lead to lower P-H3 (S10) than even untreated conditions. The authors attributed this to mitotic slippage caused by mitotic autophagy; however, given that mitotic slippage does not lead to cell division, and as such cells would have a tetradiploid G2 DNA content, it is more likely that these compounds mediated a G1 arrest. Whilst a single experiment did look at LC3 puncta in nocodazole treated cells, this suffered from all the previously listed caveats of LC3 and it was only shown that puncta intensity, not total number increased. Furthermore, they did not stratify cells into mitotic and interphase cells and given their subsequent findings that inhibiting CUL4 and treatment with nocodazole mediates either mitotic exit or G1 arrest, they may again have been observing predominantly interphase cells. Therefore, the authors are much more likely to have

observed autophagy in interphase cells rather than mitotic cells with this combination. This would explain their paradoxical findings that whilst wortmannin had previously been suggested to promote mitotic autophagy (Eskelinen *et al.*, 2002), wortmannin strikingly blocked the senescence phenotype they observed upon combination treatment. The potential way to control for this possibility would have been the addition of a CDK1 inhibitor, such as RO-3306, into the combination since this would have prevented cells entering mitosis in the first place. Thus, RO-3306 should have blocked the senescence phenotype if it was a result of mitotic autophagy. However, without this control there is no way to interpret whether the effects they observe were due to a re-initiation of mitotic autophagy, and it seems highly doubtful given most cells are not in mitosis. Overall, whilst this dataset supports a role for WIPI2 degradation in mitotic regulation of autophagy repression, it does not exclude the possibility of other mechanisms of regulation.

S6K and 4E-BP1 are directly phosphorylated by mTORC1 to mediate a direct control on ribosomal biogenesis and cap-dependent translation respectively. During mitosis both of these proteins have been suggested to be direct substrates of Cyclin B1-CDK1 (Papst *et al.*, 1998; Shah, Ghosh and Hunter, 2003; Shuda *et al.*, 2015). In the case of S6K, this occurs at sites (S371, S411, T421, S424) (Shah, Ghosh and Hunter, 2003) other than the well characterised T389 site which mTORC1 phosphorylates. This is not surprising given that T389 is not proline-directed and therefore would not fit the common consensus motif for CDK1. That being said, S371 is also likely to be a direct mTORC1 target site during interphase (Saitoh *et al.*, 2002). CCNB1-CDK1 also phosphorylates 4E-BP1 at known mTORC1 target sites T37,T46, S65, T70 (Shuda *et al.*, 2015) and all of these are proline-directed sites. Therefore, CDK1 appears to be able to phosphorylate substrates of mTORC1, including on known target sites when they are proline-directed. Curiously, many of the known mTORC1 target sites on ARs are proline-directed including P-ATG13 (S259), P-ULK1 (S758) and P-TFEB (S122, S142). Therefore, an interesting hypothesis to explore was whether an mTORC1-to-CDK1 switch was occurring not just for 4E-BP1 and S6K, but for ARs as well.

It is important to note the differing upstream inputs into the mTORC1 and CCNB1-CDK1 pathways. mTORC1 is nutrient-responsive and inhibition of its activity, whether by nutrient starvation or kinase inhibition, results in rapid autophagy activation. By contrast CCNB1-CDK1 is not nutrient-regulated and thus would remain active even during times of nutrient stress. Whilst it is inactivated in response to some stressors, such as DNA-damage, this occurs prior to the commencement of mitosis. Thus, a switch to CDK1 could sustain autophagy repression, even in the absence of amino acids, making CDK1 an ideal candidate kinase based on the data described in the previous chapter.

5.2 Results

5.2.1 Mitotic arrest upon treatment with microtubule inhibitors promotes CDK1-dependent hyperphosphorylation of TFEB, ULK1, ATG13 and ATG14

Given the apparent inactivation of mTORC1 during mitosis, we would expect all of the known AR substrates to be in a hypophosphorylated state. To investigate the phosphorylation status of mTOR substrates during early mitosis, we utilised the microtubule inhibitor paclitaxel which arrests cells in prometaphase (Chadebech *et al.*, 2000). Reduced protein mobility on SDS-PAGE gels (a 'band shift') can be used as a surrogate marker of phosphorylation. Band shift of ATG13, ATG14, TFEB and ULK1 was first observed within 2 hours of paclitaxel treatment and steadily increased over 16 hours correlating with increases in the mitotic marker phospho-H3 (Ser10) (Figure 5.1.A). All ARs were hypophosphorylated again after 24 hours of paclitaxel treatment. This was likely to be a result of HCT116 cells undergoing mitotic slippage as evidenced by a decrease in P-H3 (S10); this has been observed to occur in HCT116 cells by multiple independent research groups (Andonegui-Elguera *et al.*, 2016; Sloss *et al.*, 2016; Jakhar *et al.*, 2018). Indeed, autophagy is activated during mitotic catastrophe (Sorokina *et al.*, 2017)/slippage (Veldhoen *et al.*, 2013; Jakhar *et al.*, 2018). Since 16 hours of paclitaxel treatment resulted in the greatest mitotic-arrest and hyperphosphorylation of autophagy regulators, this time-point was used for many of the subsequent experiments. Thus, despite the likely inactivation of mTORC1, ARs were hyperphosphorylated during mitotic arrest.

Microtubule inhibitors, in addition to their ability to arrest cells in mitosis, elicit a plethora of pleiotropic effects, including activation of stress kinase signalling (i.e. JNK) (Amato *et al.*, 1998; Wang *et al.*, 1998). Since these kinases, also members of the CMGC family, phosphorylate proline-directed serine/threonine sites, we next evaluated whether CDK1 activity was specifically required for paclitaxel-mediated phosphorylation of these four substrates. We arrested HCT116 cells in prometaphase with paclitaxel treatment for 16 hours and then two hours prior to lysis, we treated cells with increasing doses of RO-3306 (Figure 5.1.B). As previously shown, autophagy regulators were phosphorylated in paclitaxel-treated cells. As expected, 4E-BP1 was also hyperphosphorylated in paclitaxel-treated samples, observed as the mitosis-specific δ isoform, in concordance with published results (Shuda *et al.*, 2015). These phosphorylation events were reversed by addition of RO-3306 in a dose-dependent manner. Dephosphorylation of ATG13, ATG14, TFEB and ULK1 closely correlated with doses required for dephosphorylation of 4E-BP1, and loss of

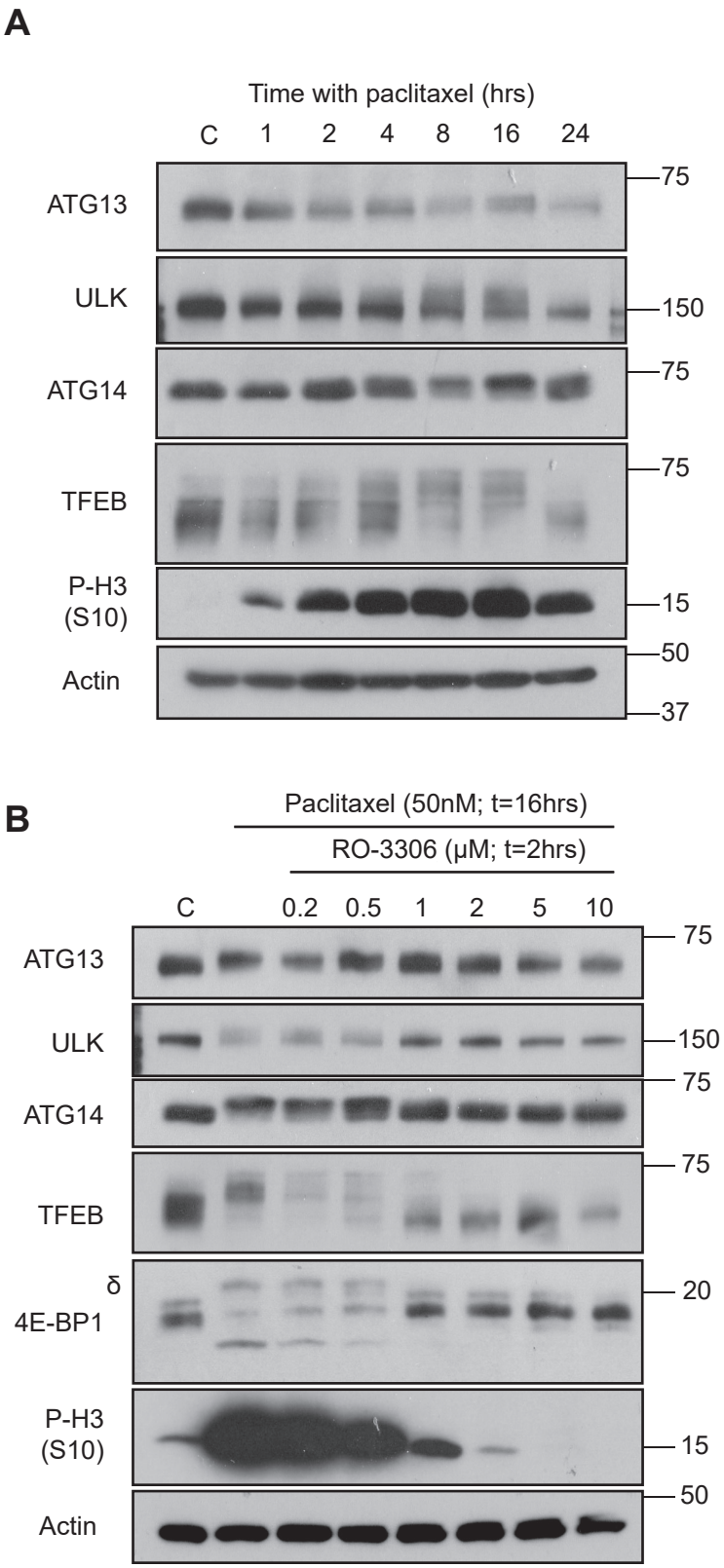

Figure 5.1: ARs band shift upon paclitaxel treatment in a CDK1-dependent manner.
(A) HCT116 cells were treated with paclitaxel (50 nM) for indicated time. **(B)** HCT116 cells were treated with paclitaxel (50 nM) 16 hours. Two hours prior to lysis, cells were treated with indicated doses of RO-3306 (CDK1 inhibitor). Western blots are from a single experiment representative of three independent experiments. Molecular weight markers (kDa) are indicated to the right of each blot.

phospho-H3 (Ser10). It is curious that ULK1 levels appeared to be reduced in paclitaxel-treated lysates compared to unsynchronised samples. This supports findings by Jakhar, which showed reduced ULK1 protein levels in nocodazole-arrested U20S cells, though the level of decrease was much more prominent in their study (Jakhar *et al.*, 2018).

To determine whether the observed band shift was due to phosphorylation or other post-translational modifications, we treated either whole cell lysates (ATG14 and ULK1) or immunoprecipitated proteins (TFEB and ATG13) with lambda phosphatase *in vitro* (Figure 5.2). In the absence of lambda phosphatase, immunoprecipitated proteins from paclitaxel-treated lysates still exhibited a band shift. However, the addition of phosphatase to immunoprecipitated proteins or whole-cell lysates abolished any band shift between untreated and paclitaxel-treated samples. This strongly supported the hypothesis that the band shift of these four proteins reflected their hyperphosphorylation in paclitaxel-treated cells relative to untreated cells. Whilst all these experiments verify this band shift was a result of phosphorylation, it is important to address here the differences in experimental design between the substrates. Namely, that ATG13 and TFEB were immunoprecipitated whilst ATG14 and ULK1 were treated as part of whole cell lysates. Immunoprecipitation of a proposed substrate was beneficial compared to the treatment of whole-cell lysates. This is because it reduces the presence of endogenous enzymes within the lysate which could be active during the 30^{o}C heating stages of the phosphatase protocol. Furthermore, by not purifying the substrate, all other proteins within the lysate will effectively act as a competitive inhibitor of the lambda phosphatase, requiring a greater amount of phosphatase to be added. Therefore, where possible (ATG13 and TFEB), these substrates were immunoprecipitated. Consistently we observed that transiently transfected proteins failed to undergo the same band shift that the endogenous proteins underwent. This is a widely reported complication within the autophagy field and also appears within the literature, i.e. drastically reduced band shifts of overexpressed RAPTOR and 4E-BP1 in mitotic lysates (Gwinn, Asara and Shaw, 2010). As such, transient transfection was utilised as little as possible throughout this study to prevent misinterpretation of overexpression artefacts. As a result, it was critical to observe band shifts in the endogenous protein. Taken together, this meant the experimental protocol required immunoprecipitation of the endogenous protein. As observed in Figure 3.18.A, TFEB protein levels varied drastically between cell lines and were considerably lower in HCT116 cells. To ensure an adequate amount of protein was immunoprecipitated before undergoing phosphatase treatment, we utilised the COLO205 cell line which expresses high levels of TFEB (Figure 5.2.A). Likewise, for ATG13 we utilised HeLa cells (Figure 5.2.B). Unfortunately, whilst we could immunoprecipitate ATG14 and ULK1, the protein was degraded after treatment with lambda phosphatase. The

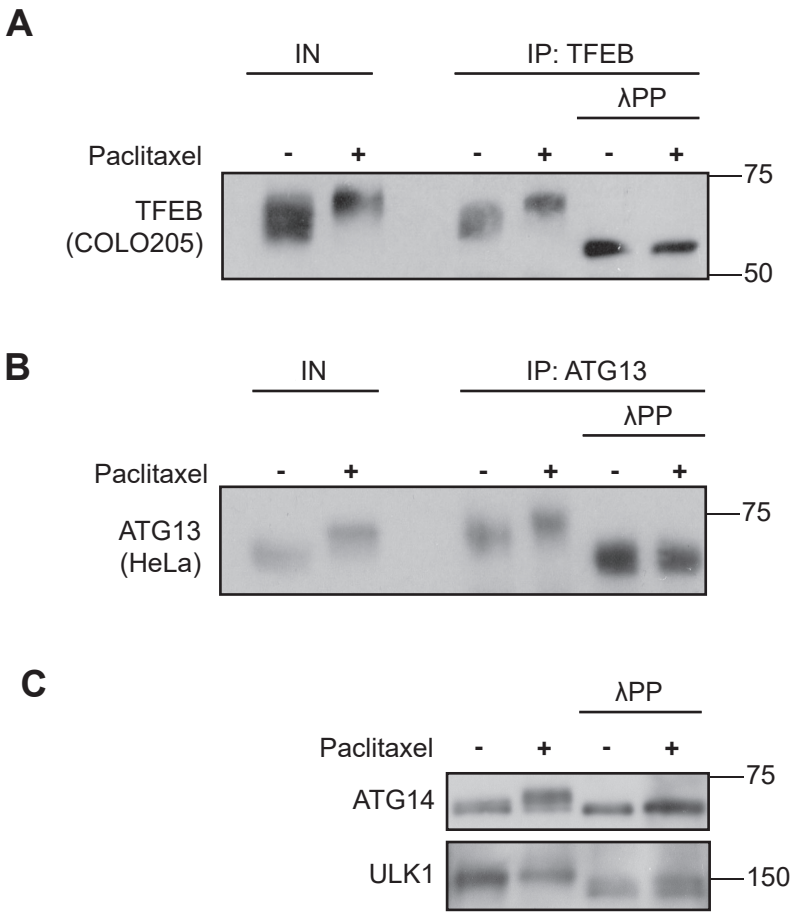

Figure 5.2: Paclitaxel-induced band shifts in ARs are a result of phosphorylation. **(A)** COLO205 cells were treated for 16 hrs with paclitaxel (50 nM) or DMSO control. TFEB was then immunoprecipitated and subsequently treated with lambda phosphatase (λPP) **(B)** Experiment was performed as in (A), except that ATG13 was immunoprecipitated from HeLa cells. **(C)** HCT116 cells were treated with paclitaxel (50 nM) or DMSO control. Whole cell lysates were then incubated in the presence or absence of lambda phosphatase. Western blots are from a single experiment representative of three independent experiments. Molecular weight markers (kDa) are indicated to the right of each blot.

reason for this was unclear, but likely represents the inherent instability these proteins exhibit out of complex *in vitro* due to their highly disordered regions. Therefore, we treated whole-cell lysates with lambda phosphatase (Figure 5.2.C). Regardless, this data strongly suggests that the band shift observed was a result of phosphorylation and later sections of this study further validate this (for ATG13, ULK1 and TFEB) with phospho-specific antibodies and mass spectrometry.

We also wanted to determine if the hyperphosphorylation of autophagy regulators could be recapitulated with other agents that arrest cells in mitosis, and that this could be reversed by distinct CDK1 inhibitors at doses known to inhibit CDK1 (Gilley *et al.*, 2012) (Figure 5.3). As predicted, the microtubule inhibitors nocodazole and paclitaxel both induced hyperphosphorylation of ATG13, ATG14, TFEB and ULK1 which correlated with the previously used mitotic markers (4E-BP1 and P-H3 (S10)) (Figure 5.3.A). This hyperphosphorylation was reversed upon treatment with the CDK1 inhibitors RO-3306 (Vassilev *et al.*, 2006), NU6102 (T. G. Davies *et al.*, 2002) and roscovitine (Meijer *et al.*, 1997). In addition, the Eg5 inhibitor dimethylenastron, which arrests cells in prometaphase due to interference in spindle assembly and maintenance (Liu *et al.*, 2006), also promoted hyperphosphorylation of autophagy regulators which was reversed by RO-3306 (Figure 5.3.B). Altogether, this data strongly suggests that the observed hyperphosphorylation of ARs during mitotic arrest was CDK1-dependent.

5.2.2 Mitotic phosphorylation of autophagy regulators occurs in a manner independent of mTORC1 but dependent on CDK1 activity

It was previously shown that 4E-BP1 and S6K are phosphorylated by CDK1 during mitosis. In the case of 4E-BP1 this is well validated by several groups to occur at both mTORC1 canonical sites (Heesom *et al.*, 2001; Greenberg and Zimmer, 2005; Shuda *et al.*, 2015) and a CDK1 specific site S83 (Velásquez *et al.*, 2016), resulting in the mitosis-specific δ isoform. Since the hyperphosphorylation of these proteins appeared to be independent of mTORC1 during mitosis, we hypothesised that the mitotic hyperphosphorylation of autophagy regulators might also to be independent of mTORC1. In addition, TFEB has been suggested to be an ERK1/2 substrate (Settembre *et al.*, 2011). We therefore treated cells arrested in mitosis with either a CDK1 inhibitor RO-3306, a MEK inhibitor Trametinib or an mTOR inhibitor AZD8055. AZD8055 is an ATP-competitive inhibitor and was selected over rapamycin since it has been revealed that several substrates of mTORC1 are rapamycin insensitive (Thoreen *et al.*, 2009; Kang *et al.*, 2013). Unlike paclitaxel, which was applied for 16 hours, kinase inhibitors were only used for the final 2 hours. This was for two main reasons. Firstly, longer time points enable a larger

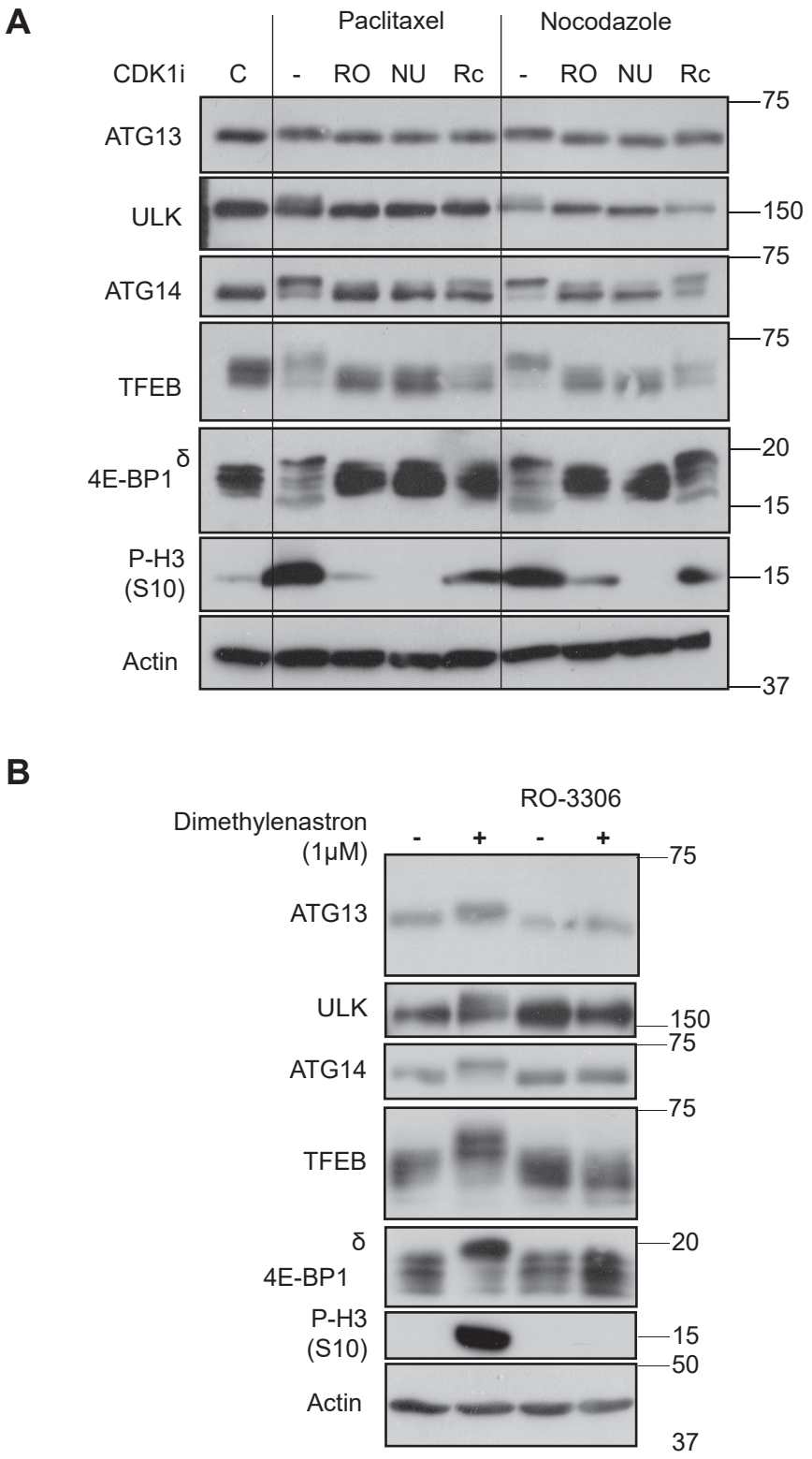

Figure 5.3: Nocodazole (microtubule inhibitor) and Dimethylenastron (Eg5 inhibitor) both promote hyperphosphorylation of ARs in a CDK1-dependent manner. **(A)** HCT116 cells were treated with either paclitaxel (50 nM) or nocodazole (62.5 $ngml^{-1}$) for 16 hours. Two hours prior to lysis, cells were treated with either RO-3306 (2 μM), NU6102 (10 μM) or roscovitine (25 μM). **(B)** HCT116 cells were treated with dimethylenastron (1 μM) 16 hours. Two hours prior to lysis, cells were treated with RO-3306 (2 μM). Western blots are from a single experiment representative of three independent experiments. Molecular weight markers (kDa) are indicated to the right of each blot.

perturbation in the cell's overall signalling network in response to the kinase inhibition. Secondly, if a MEK or mTORC1 inhibitor was applied from the outset, it would likely result in a G0/1-phase arrest, thereby preventing the cells from accumulating in mitosis. This point demonstrates a fundamental advantage of utilising kinase inhibitors over genetic means when addressing the role mTORC1 has during mitosis, since rapid kinase inhibition can ensure that a similar proportion of cells are in mitosis when comparing the effect of different treatments. Cellular phosphatase activity on well validated substrates of mTORC1 is rapid, so that phospho-4E-BP1 (T37/46) and phospho-S6K (T389) were absent after two hours of treatment with AZD8055 in asynchronous lysates (Chresta *et al.*, 2010). In concordance with previously published data, 4E-BP1 remained in the mitotic δ form, even in the presence of mTOR inhibitor AZD8055 (Figure 5.4.A). Strikingly, the mitotic hyperphosphorylation of ARs was also not reversed upon treatment with AZD8055. Furthermore, phosphorylation of ULK1 at S758 was still present in mitotic samples treated with AZD8055, suggesting a kinase other than mTORC1 was responsible for phosphorylating this site during mitosis. Likewise, Trametinib failed to reverse the miotic hyperphosphorylation of ARs including TFEB, suggesting MEK1/2 signalling was not responsible for mitotic phosphorylation of ARs. Finally, RO-3306 reversed the mitotic hyperphosphorylation of ARs, in line with our previous findings. Overall, this data suggested that the hyperphosphorylation of ARs was dependent on CDK1, not mTORC1.

To further validate that the hyperphosphorylation of ARs was independent of mTOR, we performed the same experiment with three independent catalytic inhibitors of mTOR (AZD8055, Torin-1 and PP242) (Figure 5.4.B). As expected, neither 4E-BP1 hyperphosphorylation or the hyperphosphorylation of autophagy regulators in mitotically-arrested cells was reversed upon treatment with the mTOR inhibitors, further suggesting that the mitotic phosphorylation of autophagy regulators was independent of mTORC1. This included the known repressive site P-ULK1 (S758).

Next, we wanted to validate our findings in cell lines from different tissue types and with different mutational statuses. mTOR-independent phosphorylation of ARs was replicated in: A549 (lung; *KRAS*^{mut}), COLO205 (colorectal; *BRAF*^{mut}), HT29 (colorectal; *BRAF*^{mut}), and HEK293 (embryonic kidney) cells (Figure 5.5). Furthermore, different cell lines exhibit different degrees of arrest in prometaphase upon paclitaxel treatment; for example, HEK293 undergo significant rates of mitotic slippage and a relatively small proportion of cells are arrested in mitosis (based on number of cells with rounded morphology). Indeed, HEK293 showed markedly lower levels of hyperphosphorylation of ATG13, ATG14, TFEB and ULK1; correlating with the reduced levels of 4E-BP1 hyperphosphorylation compared to other cell lines (Figure 5.5.C). We found 4E-BP1

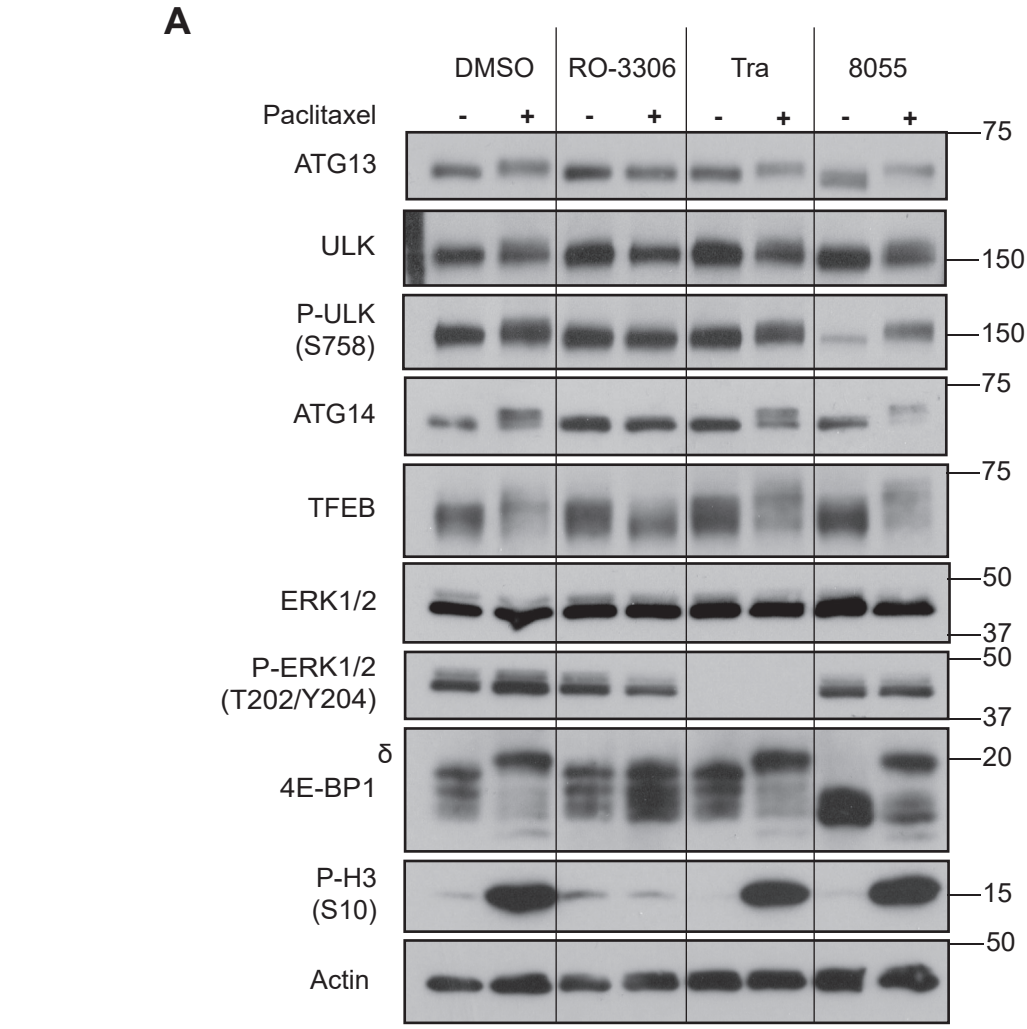

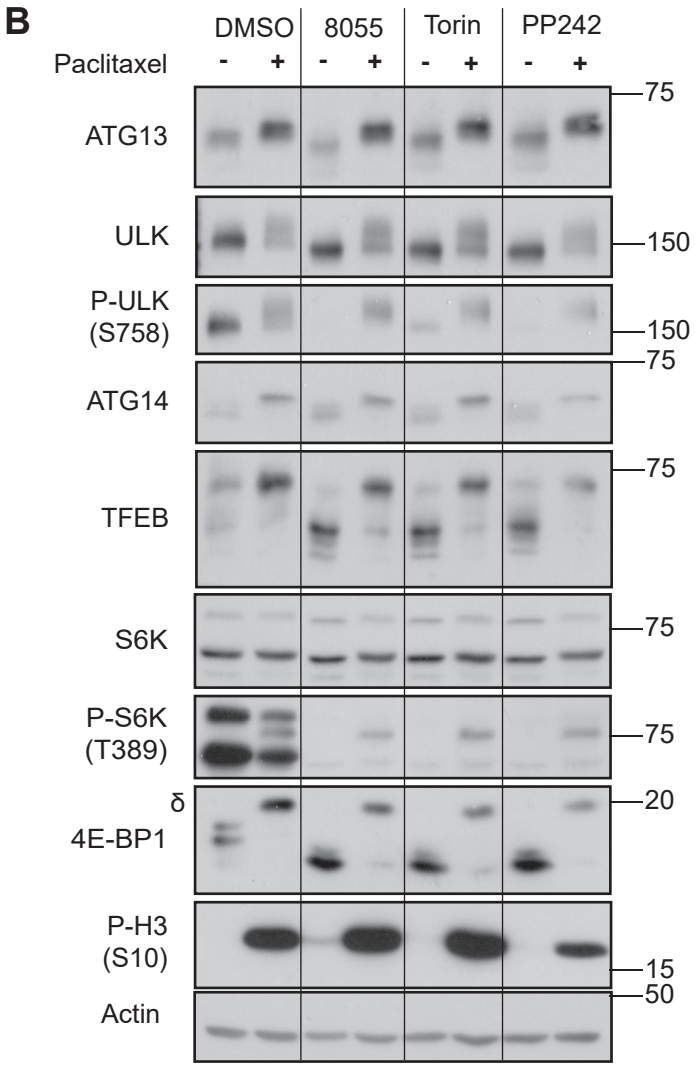

Figure 5.4: Mitotic phosphorylation of ARs is independent of mTORC1.
(A) HCT116 cells were treated with paclitaxel (50 nM) for 16 hrs. Two hours prior to lysis cells were treated with either DMSO, RO-3306 (2 μM; CDK1 inhibitor), Trametinib (1 μM; MEK inhibitor) or AZD8055 (1 μM; mTOR inhibitor) **(B)** HCT116 cells were treated with paclitaxel (50 nM) for 16hrs. Two hours prior to lysis cells were treated with either DMSO, AZD8055 (1 μM), Torin-1 (250 nM) or PP242 (1 μM). Western blots are from a single experiment representative of three independent experiments. Molecular weight markers (kDa) are indicated to the right of each blot.

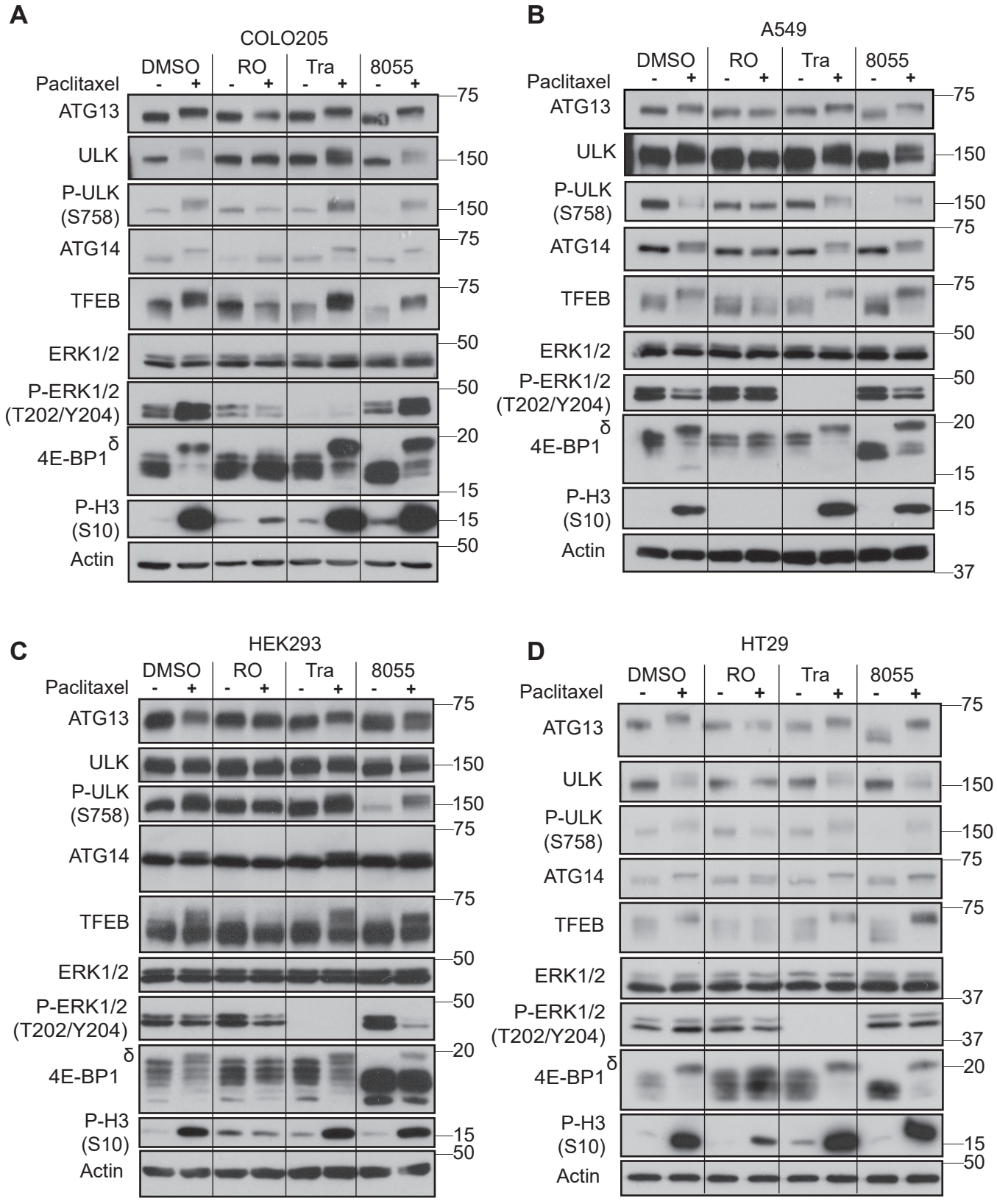

Figure 5.5: Mitotic phosphorylation of autophagy regulators is observed across a diverse panel of cell lines.

Cells were treated with Paclitaxel (50 nM) for 16hrs. Two hours prior to lysis, cells were treated with either DMSO, RO-3306 (2 μM; CDK1 inhibitor), Trametinib (1 μM; MEK inhibitor) or AZD8055 (1 μM; mTOR inhibitor). Cell lines used were as follows: COLO205 **(A)**, A549 **(B)**, HEK293 **(C)**, HT29 **(D)**. Western blots are from a single experiment representative of three independent experiments. Molecular weight markers (kDa) are indicated to the right of each blot.

hyperphosphorylation to be a reliable internal read-out of mitotic arrest across all experiments. In contrast, cancer cells (i.e A549, COLO205, HT-29), many of which show a high-degree mitotic arrest upon paclitaxel treatment, exhibited much higher proportions of hyperphosphorylated ARs than HEK293. Combined, this evidence supports the hypothesis that the hyperphosphorylation of ATG13, ATG14, TFEB and ULK1 was dependent upon CDK1, and not mTOR, during paclitaxel-induced mitotic arrest.

Mitotic shake-off enables the crude separation of mitotic and interphase cells based on their relative adherence to tissue culture plastic. Whilst there was a degree of cross-contamination this enables comparisons of effects in interphase and mitotic cells whilst both are in the presence of paclitaxel. In order to demonstrate that mTORC1-independent phosphorylation of ARs induced by paclitaxel was limited to mitotic cells, HCT116 cells were treated for 6 hours such that approximately 50% of cells possessed a rounded morphology indicative of mitosis. Two hours prior to mitotic shake-off, cells were treated with either DMSO or AZD8055, enabling the comparison of mTOR inhibition in both interphase and mitotic populations. As expected, interphase-enriched cells still underwent hypophosphorylation of 4E-BP1 and ARs (ATG13, ULK1, TFEB), despite the presence of paclitaxel (Figure 5.6). In contrast, lysates from cells enriched for mitosis exhibited mTORC1-independent phosphorylation of both 4E-BP1 and ARs. This confirms that the band-shifts observed were not a generic effect of paclitaxel, but instead were a result of mitotic-arrest.

5.2.3 Mitotic phosphorylation of ARs occurs in SW620:8055R cells

Previous work in the lab has generated a cell line which is entirely resistant to mTORC1 inhibition. SW620:8055R were generated by prolonged culture in 2 μM AZD8055, such that they are routinely cultured in the presence of drug and proliferate at a similar rate to parental cells (Cope *et al.*, 2014). It was previously shown that SW620:8055R cells have amplification of eIF4E, such that translation was maintained even in the absence of mTORC1 signalling as measured by loss of P-S6K (T389) and hypophosphorylation of 4E-BP1 (Cope *et al.*, 2014). As such, they have chronic and sustained inhibition of mTORC1. To verify that SW620:8055R cells still exhibited active autophagic flux, we treated cells both in the presence and absence of AZD8055, with the lysosomal inhibitor Bafilomycin A1. In concordance with previous findings, SW620:8055R had elevated eIF4E protein levels (Figure 5.7). In addition, there was no detectable mTORC1 signalling in either SW620 or SW620:8055R cells treated with AZD8055, as assessed by hypophosphorylation of ATG13, ULK1, S6K and 4E-BP1. As expected, treatment of SW620 cells with AZD8055 promoted increases in lipidated LC3B (LC3B-II). This was further increased by the addition of

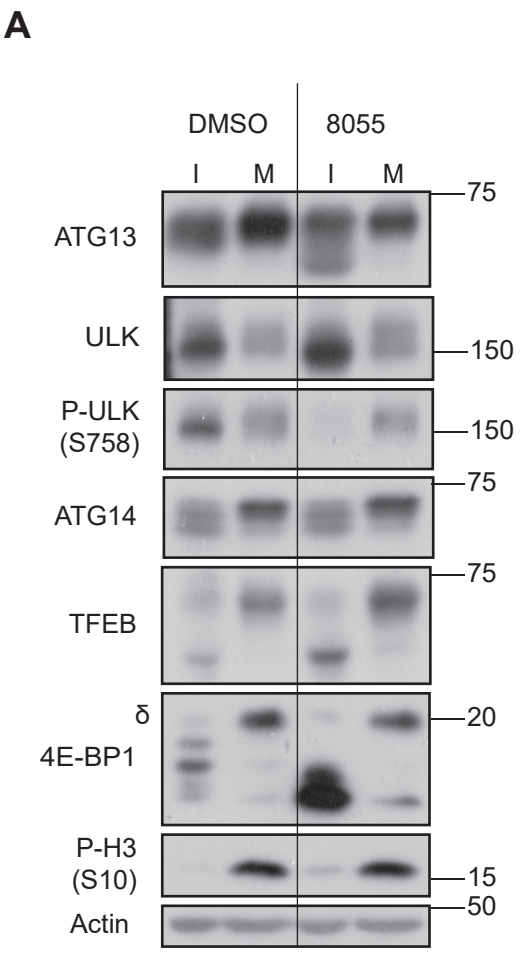

Figure 5.6: Mitotic shake-off confirms that paclitaxel-induced phosphorylation is restricted to mitotic cells.
(A) HCT116 cells were treated with paclitaxel (50 nM) for 6 hours until approximately half of cells were rounded (indicative of mitosis). Two hours prior to lysis, cells were treated with either DMSO or AZD8055 (1 μM). Flasks then underwent mitotic shake-off separating cells into two distinct interphase (I; adherent) and mitosis (M; suspension) enriched fractions. Western blots are from a single experiment representative of three independent experiments. Molecular weight markers (kDa) are indicated to the right of each blot.

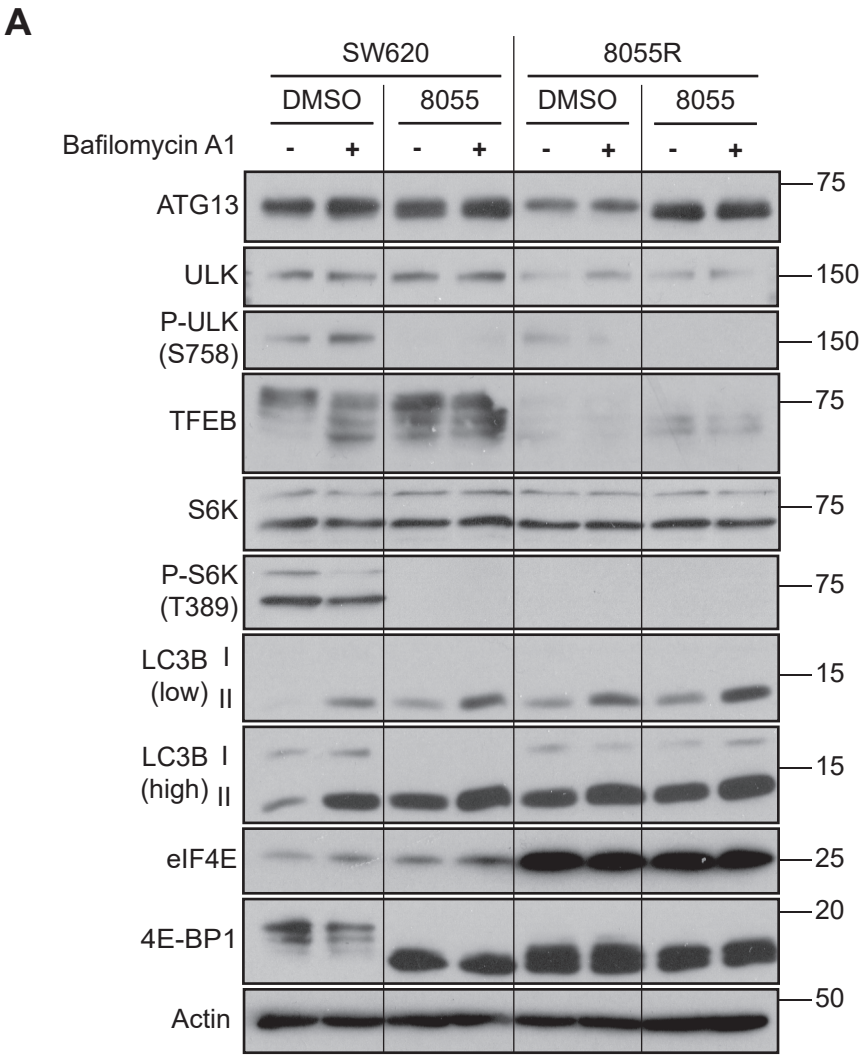

Figure 5.7: SW620:8055R cells exhibit active autophagic flux.
(A) SW620 cells and SW620:8055R cells were cultured in their normal growth medium (either drug-free or supplemented with 2 μM AZD8055). 24 hours prior to lysis, cell media was exchanged for media supplemented with either DMSO or 2 μM AZD8055. Bafilomycin A1 (100 nM) was added 1 hour prior to lysis where indicated. Western blots are from a single experiment representative of two independent experiments. Molecular weight markers (kDa) are indicated to the right of each blot.

Bafilomycin A1, suggesting active autophagic flux with no impairment of lysosomal degradation. SW620:8055R cells showed similar results, though autophagic flux was high in both the presence and absence of AZD8055. Furthermore, there was a striking decrease in the protein level of both TFEB and ULK1, possibly representing negative feedback mechanisms to prolonged autophagy stimulation. We speculate this may be an adaptive mechanism by which cells cope with enhanced autophagy over a prolonged period. When SW620:8055R cells were placed in DMSO-containing media, like previously published findings we saw minimal P-S6K (T389) and no obvious changes in 4E-BP1 banding (Cope *et al.*, 2014). However, phosphorylation of both ATG13 and ULK1 was apparent. We therefore wanted to validate whether mTORC1 signalling was active upon release from AZD8055. We observed that release of SW620:8055R cells into growth media in the absence of AZD8055 caused prominent reactivation of mTORC1 as assessed by phosphorylation of ATG13, S6K and 4E-BP1 (Figure 5.8). Unexpectedly, this occurred even in the absence of amino acids within the first hour, suggesting that the reactivation of mTORC1 upon AZD8055 withdrawal was nutrient-independent.

Amino acids mediate mTORC1 activation through recruitment to the lysosomes, such that starvation inactivates Rag-GTPases resulting in failure of mTORC1 to recruit to the lysosome. Conversely, we and others have previously demonstrated that ATP-competitive mTOR inhibitors, like AZD8055, promote mTORC1's localisation to the lysosome. We therefore hypothesised that AZD8055 may effectively be priming mTORC1's activity by its forced localisation to the lysosome in SW620:8055R cells. To test this, we monitored mTOR localisation by immunofluorescence. In SW620 cells, mTOR showed a weak localisation with lysosomes in basal conditions (Figure 5.9). This was impaired by nutrient depletion and strengthened by treatment with AZD8055. By contrast in SW620:8055R cells, mTOR showed strong co-localisation with the lysosomal marker Lamp2 in all treatment conditions. Thus, mTORC1 is likely primed at the lysosome by chronic AZD8055 treatment, resulting in rapid activation of mTORC1 upon withdrawal of AZD8055 even in the absence of nutrients. Of note, mTOR failed to localise to lysosomes during mitosis in either SW620 or SW620:8055R cells regardless of treatment conditions (example mitotic cells are demonstrated in the 8055 panels of Figure 5.9), supporting our previous findings in HeLa and HAP1 cells. Overall, our results suggested that whilst SW620:8055R cells were a suitable model for assessing the mitotic phosphorylation of autophagy regulators in a background of chronic mTORC1 inhibition, these cells are capable of reactivating the mTORC1 pathway upon drug withdrawal.

Given our findings that 8055R cells do exhibit continued mTORC1 signalling upon drug withdrawal, we treated SW620:8055R cells with paclitaxel in the presence of

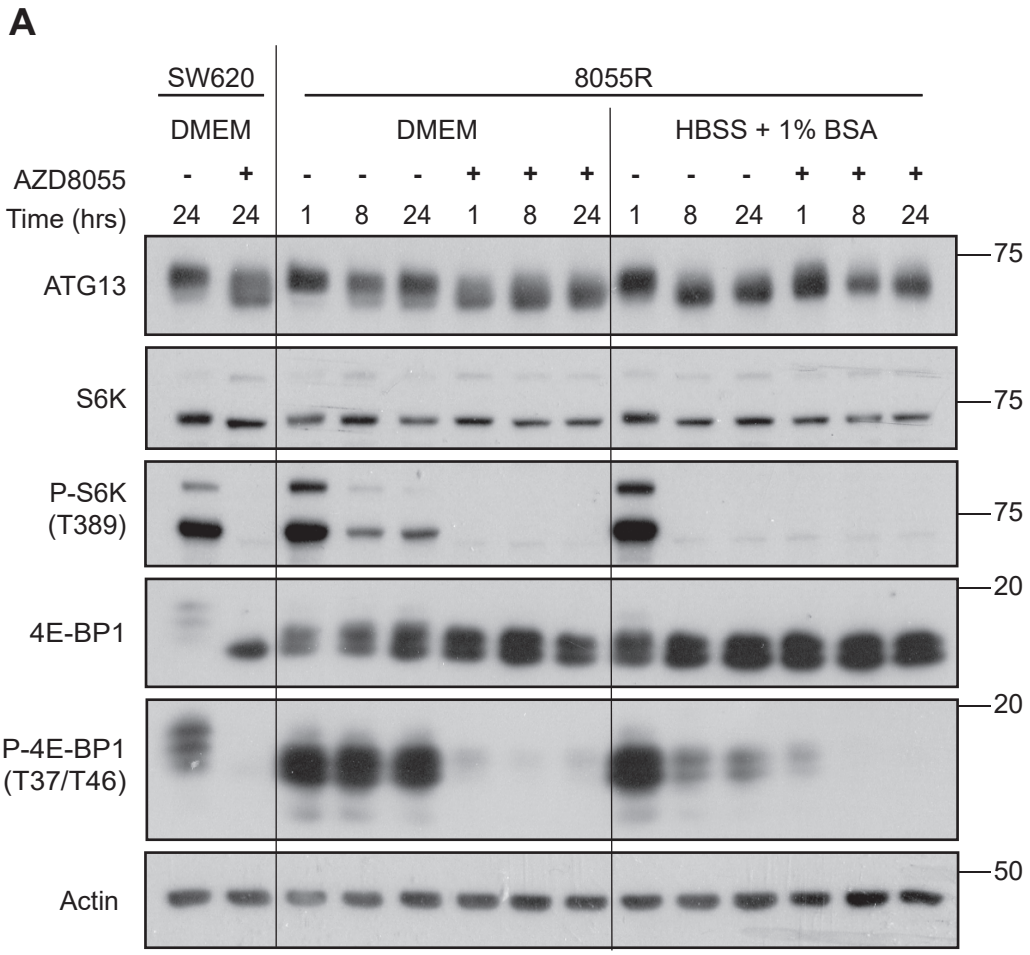

Figure 5.8: SW620:8055R cells have active mTORC1 signalling upon release from AZD8055, even in the absence of amino acids.
(A) SW620 cells and SW620:8055R cells were cultured in their normal growth medium (either drug-free or supplemented with 2 μM AZD8055). For indicated times prior to lysis, cell media was exchanged for either normal growth media or HBSS + 1% BSA, supplemented with either DMSO or 2 μM AZD8055. Western blots are from a single experiment. Molecular weight markers (kDa) are indicated to the right of each blot.

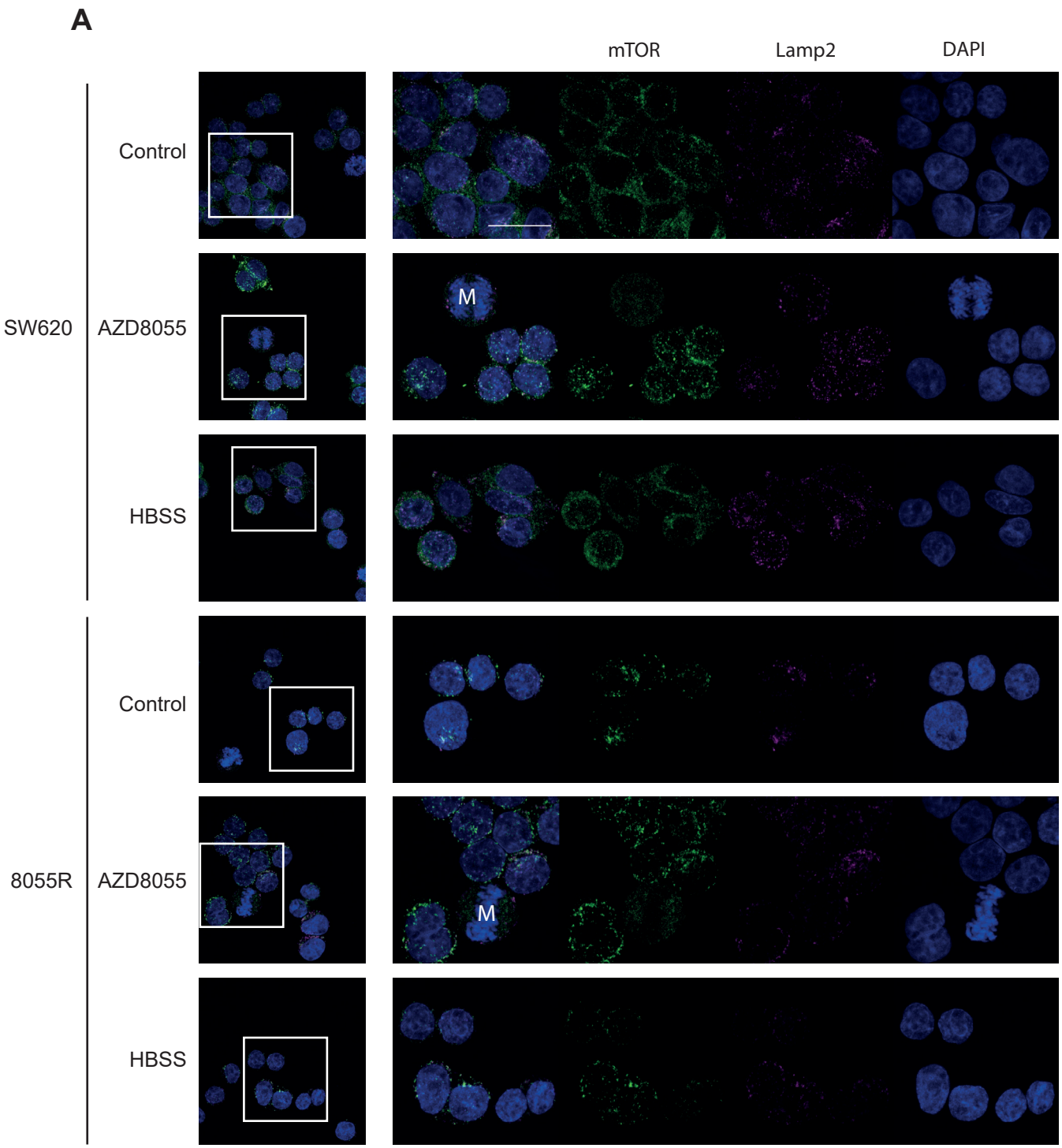

Figure 5.9 SW620:8055R exhibit strong co-localisation of mTORC1 with lysosomal marker Lamp2 in all treatment conditions, except for mitotic cells.
(A) SW620 cells and SW620:8055R cells were cultured in their normal growth medium (either drug-free or supplemented with 2 μM AZD8055). Two hours prior to fixation, media was replaced as indicated. Images are max intensity projections from a single experiment. Mitotic cells are indicated (M). Scale bar: 20 μm.

AZD8055. Whilst this experiment still involves the use of a compound (AZD8055), it does enable verification that mTORC1-independent phosphorylation can be observed in this background and therefore rules out possibilities such as decreased phosphatase activity during mitosis leading to maintained phosphorylation of ARs even after 2 hours of AZD8055 treatment. As expected, SW620:8055R cells showed no active mTORC1 signalling with hypophosphorylation of 4E-BP1 and S6K in asynchronous cells (Figure 5.10). During mitosis, 4E-BP1 was phosphorylated in both SW620 and SW620:8055R cells. Likewise, ARs were also hyperphosphorylated during mitotic arrest in both SW620 and SW620:8055R cells. This further supports the hypothesis that phosphorylation of ARs during mitosis was mTORC1-independent.

5.2.4 A mutant of TFEB which cannot be phosphorylated by mTORC1 (Δ30-TFEB) still undergoes mitotic phosphorylation

Thus far, all the experiments involving the inhibition of mTORC1 have utilised ATP-competitive inhibitors. Genetic manipulation of mTORC1 possesses a number of caveats which made me conclude it was not a feasible approach. CRISPR of mTORC1-specific components has not yet been successful as cells enter a G0/1 arrest with toxicity upon prolonged mTORC1 inhibition (see discussion). Therefore, no-one has successfully grown single cell-clones from this approach. The preferred alternative is shRNA of RAPTOR, which enables a knockdown phenotype but often with residual mTORC1 signalling (Ramírez-Valle *et al.*, 2010; Ruf *et al.*, 2017). The obvious question becomes if there was sufficient mTORC1 signalling to enable continued cell cycling, then mTORC1 activity may not have been reduced enough to rule it out in any process, since translational capacity was clearly maintained. To this end, we decided to direct genetic validation to a specific mTORC1 substrate, TFEB. TFEB has to be recruited to lysosomes to be phosphorylated by mTOR and genetic deletion of the N-terminal 30 amino acids causes its nuclear localisation, non-responsiveness to amino acids and inability to be phosphorylated by mTORC1 (Roczniak-Ferguson *et al.*, 2012; Martina and Puertollano, 2013). We therefore generated a stable cell line with a GFP-tagged N-terminal Δ30 mutant, to compare with WT-TFEB-GFP. In agreement with previous work, this stable cell line showed nuclear localisation of the Δ30-TFEB protein in all treatment conditions (Figure 5.11.A). Furthermore, AZD8055 treatment failed to recruit Δ30-TFEB-GFP to lysosomes, unlike the wild-type protein, demonstrating that Δ30-TFEB failed to locate to lysosomes. On SDS-PAGE, Δ30-TFEB-GFP exhibited no band shift in response to amino acid starvation, nutrient replenishment (refeed) or AZD8055, validating that it was not phosphorylated by mTORC1 (Figure 5.12.A). However, like the wild-type protein, Δ30-TFEB-GFP was

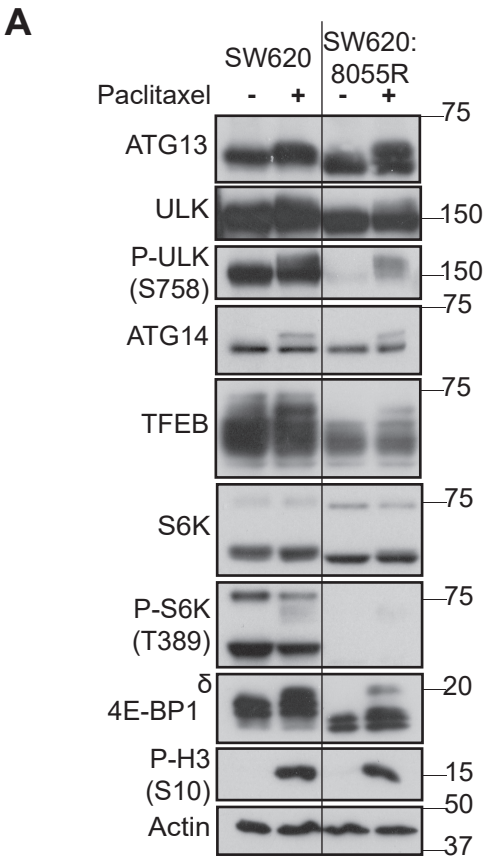

Figure 5.10: SW620:8055R cells exhibit paclitaxel-induced hyperphosphorylation of ARs.
(A) SW620 and SW620:8055R cells were cultured in their respective media and treated with paclitaxel (16 hrs; 50 nM). Western blots are from a single experiment representative of three independent experiments. Molecular weight markers (kDa) are indicated to the right of each blot.

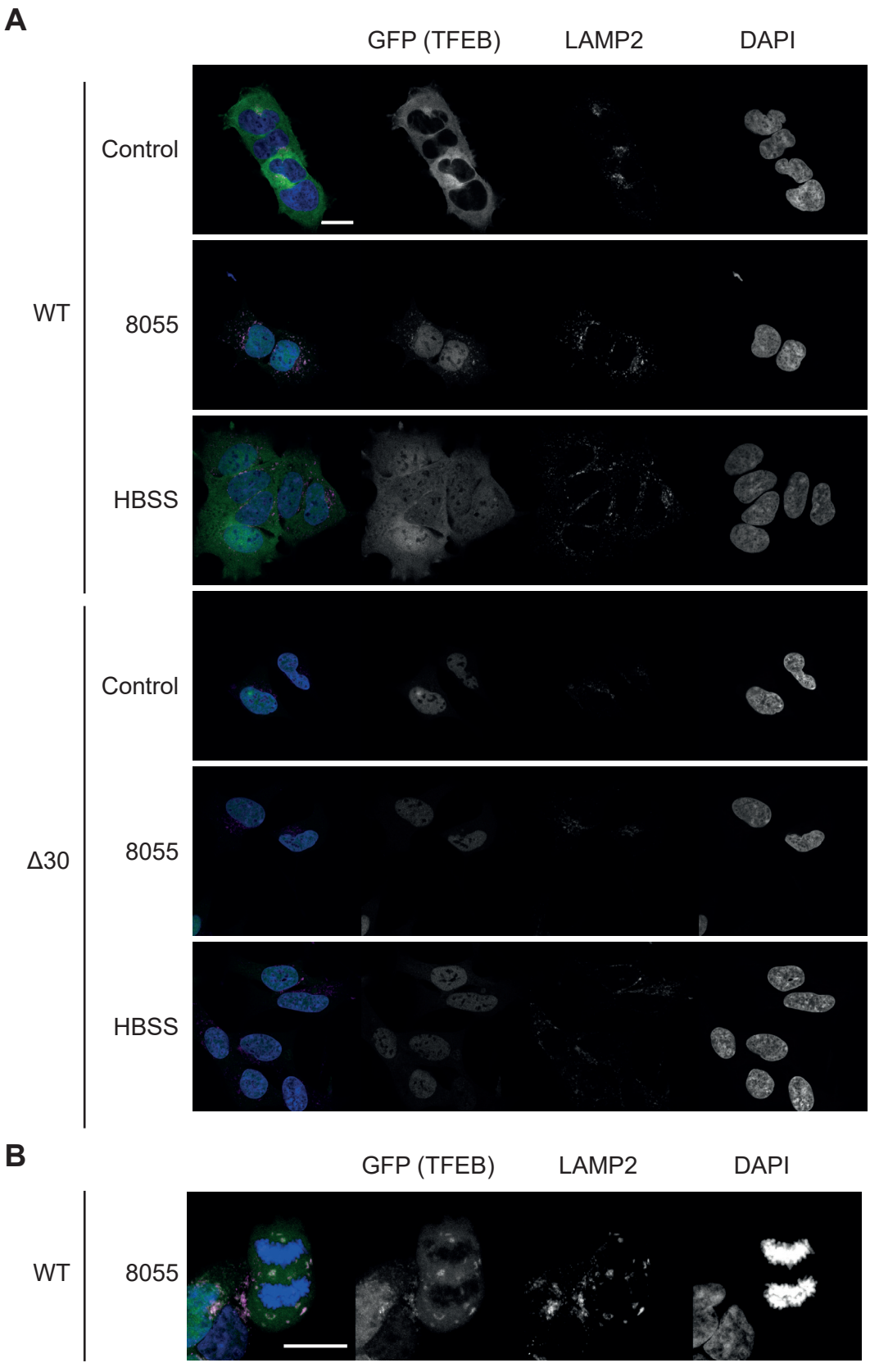

Figure 5.11: A genetic mutant of TFEB (Δ30-TFEB-GFP) is incapable of localising to lysosomes and thus is constitutively nuclear.
(A) HeLa cells stably expressing either WT-TFEB-GFP or Δ30-TFEB-GFP were treated as indicated: HBSS + 1% BSA (2 hrs), AZD8055 (1 μM; t=2 hrs). **(B)** A representative mitotic WT-TFEB-GFP cell from the AZD8055 treatment arm of (A). Scale bars: 20 μm. Images are from a single experiment representative of two independent experiments.

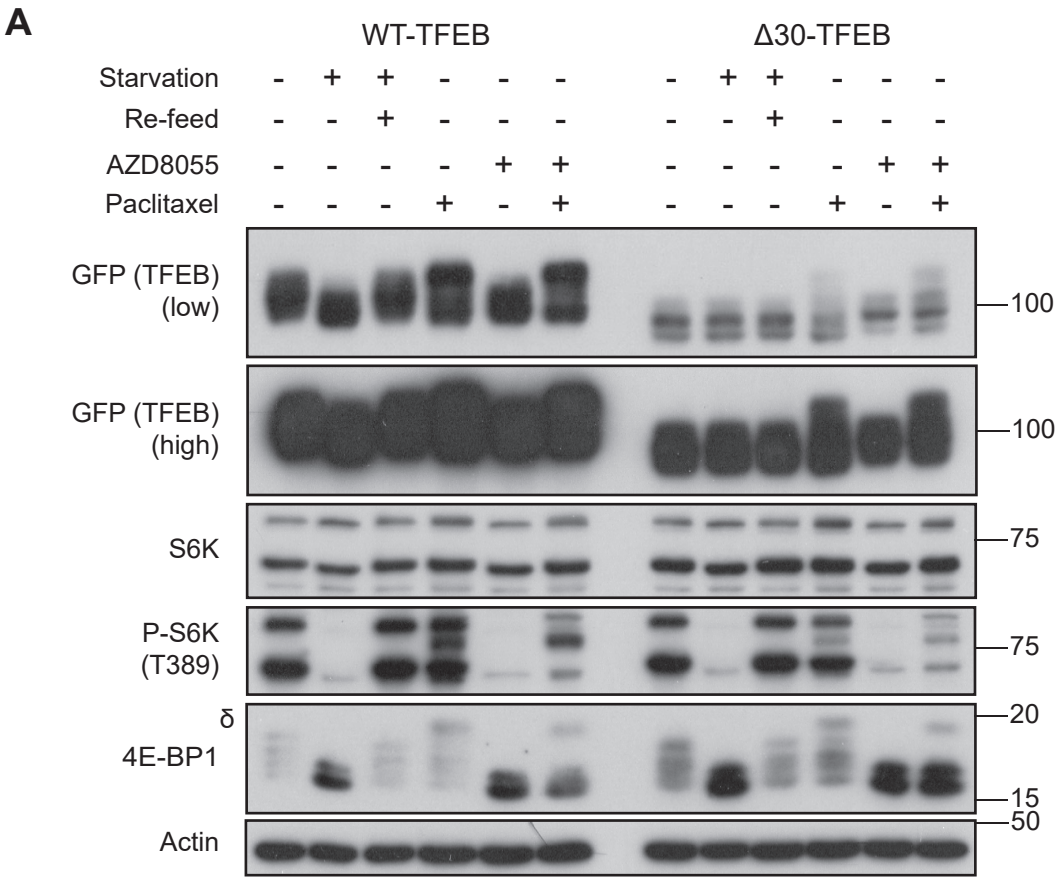

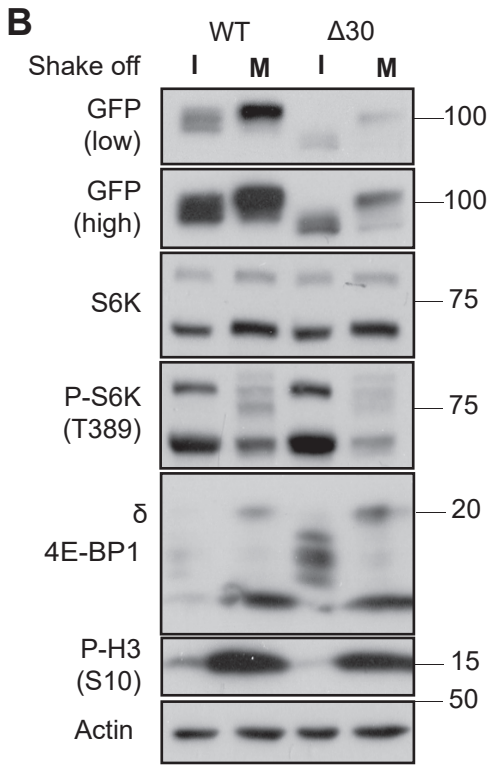

Figure 5.12: Δ30-TFEB-GFP, which cannot be phosphorylated by mTORC1, is phosphorylated upon paclitaxel treatment.
(A) HeLa cells stably expressing either WT-TFEB-GFP or Δ30-TFEB-GFP were treated as indicated: HBSS + 1% BSA (2 hrs), re-feed (HBSS + 1% BSA, 2 hrs; Complete medium, 1 hr), paclitaxel (50 nM; t=16 hrs), AZD8055 (1 μM; t=2 hrs). **(B)** HeLa cells stably expressing either wild-type (WT) or Δ30-TFEB-GFP were treated with paclitaxel (50 nM; t=16 hrs) prior to mitotic shake-off. Adherent interphase-enriched (I) and suspension mitosis-enriched (M) fractions are indicated. Western blots are from a single experiment representative of three independent experiments. Molecular weight markers (kDa) are indicated to the right of each blot.

hyperphosphorylated in response to paclitaxel, and this was unaffected by AZD8055. Whilst this was to a lesser degree than the WT protein, this was almost certainly a result of reduced mitotic arrest, as observed by a lower proportion of 4E-BP1 in the hyperphosphorylated form (note the increased total amounts of 4E-BP1 in the Δ30 line) and a reduced mitotic phospho-S6K (T389) band. We have not verified that the mitotic phospho-S6K (T389) band was S6K specific, and this would be required given there is no corresponding total S6K band at this position. Regardless, it was consistently induced during mitosis across all experiments and therefore was another surrogate readout of mitotic arrest. It was not surprising that the Δ30 line had a slower proliferation rate, given this cell line was likely to have a much higher level of catabolic activity compared to either parental or WT-TFEB cell lines, due to the constitutive activation of CLEAR genes and lysosomal biogenesis (Michela Palmieri *et al.*, 2011). Regardless, to confirm that hyperphosphorylation of both WT and Δ30-TFEB was to the same extent during mitosis, we performed a mitotic shake-off to enrich for the mitotic populations in both cell lines. This verified that the mitotic hyperphosphorylation of both TFEB constructs was to a similar extent in both cell lines (Figure 5.12.B). These results provided genetic evidence that TFEB was phosphorylated in mitosis by a kinase other than mTORC1.

It is important to note that AZD8055 treatment promoted lysosomal localisation of WT-TFEB in both interphase and mitotic cells (Figure 5.11.B). TFEB's recruitment to lysosomes is mediated by its association with Rag-GTPases, as evidenced by expression of dominant-negative Rag heteroduplexes abolishing Torin-1 induced TFEB lysosomal localisation (Martina and Puertollano, 2013). Thus, the finding that TFEB continued to associate with the lysosome was further evidence that alterations in Rag-GTPase activity was not mediating the dissociation of mTORC1 from the lysosome during mitosis (discussed in Chapter 4).

5.2.5 Mitotic phosphorylation of ARs is independent of nutrient availability or class I PI3K

In Eskelinen's original study of the inhibition of autophagy during mitosis, she observed that autophagosome number was paradoxically increased during mitosis in the presence of wortmannin (Eskelinen *et al.*, 2002). Wortmannin is a pan-PI3K inhibitor and has been known to repress autophagy for a number of decades due to VPS34 inhibition. Neither neutralising VPS34 antibodies (PI3K class III inhibition), nor p85 -/- cells (PI3K class I inhibition) could restore autophagy during mitosis (Eskelinen *et al.*, 2002). Treatment of HEK293 GFP-ATG13 cells with wortmannin failed to induce ATG13 puncta in mitotic cells, even in starvation conditions (Figure 5.13). Given that it is was previously published

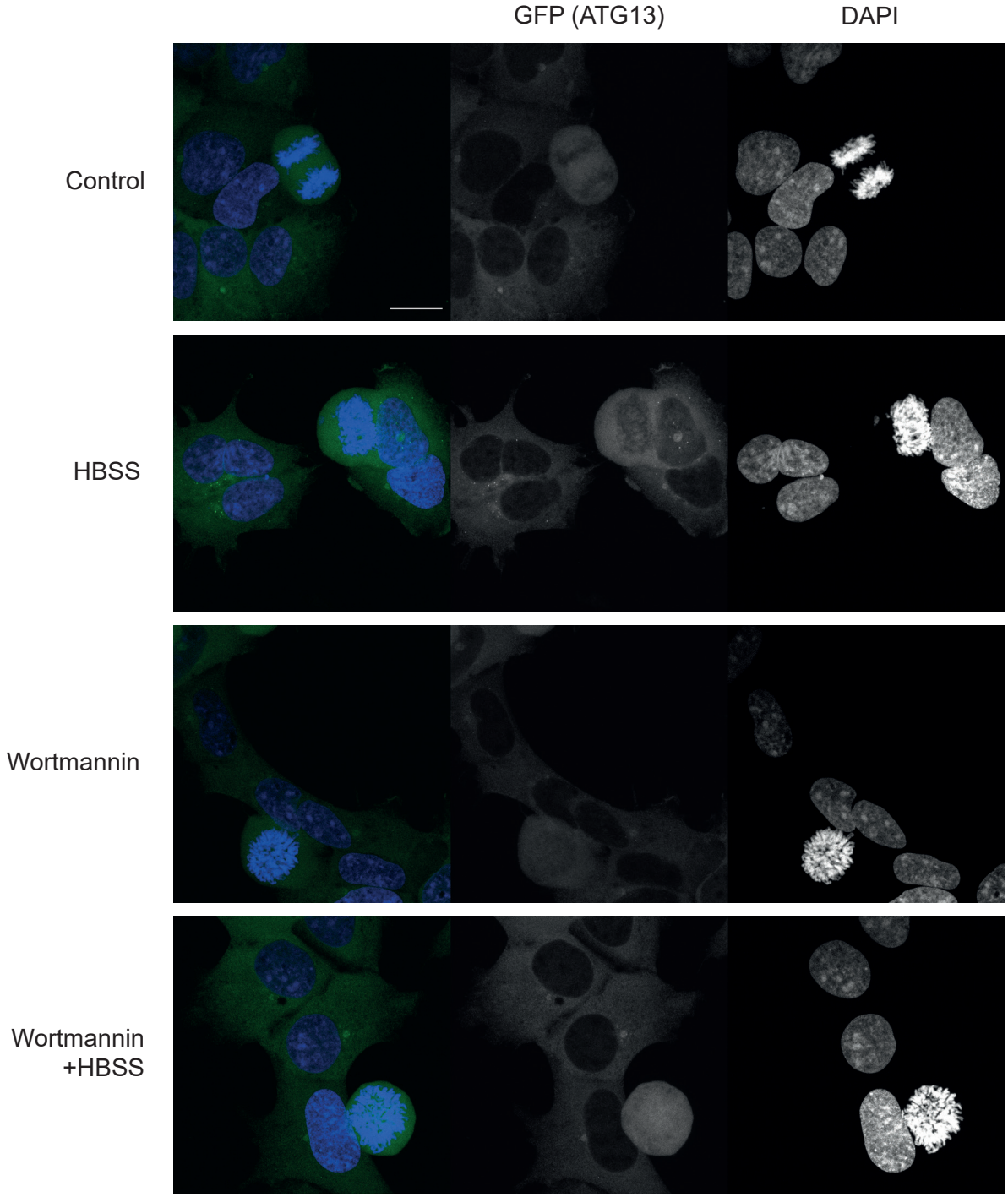

Figure 5.13: Wortmannin treatment does not induce GFP-ATG13 puncta in mitotic cells.
(A) HEK293 GFP-ATG13 cells were treated with either Wortmannin (10 nM) and/or HBSS + 1% BSA. Scale bars: 20 µm. Images are from a single experiment.

that the VPS34 complex is inactive during mitosis, we next used the PI3K class I-selective inhibitor ZSTK474 to see if it could reverse hyperphosphorylation of ARs. Neither ZSTK474 nor nutrient starvation could reverse hyperphosphorylation of ARs (Figure 5.14). This further supports the suggestion that hyperphosphorylation of ARs was independent of mTORC1, since ZSTK474 inhibits the upstream activation of mTORC1.

5.2.6 Mitotic phosphorylation of ARs occurs in the absence of microtubule inhibitors

It was important to address whether hyperphosphorylation of ARs was also observed during normal mitosis, in the absence of microtubule inhibitors. For this, we utilised two cell synchronisation techniques: double thymidine block and RO-3306 release. Unfortunately, due to the lack of commercially available phospho-specific antibodies for ARs, we relied upon band shifts which required a significant proportion of cells to be in prometaphase arrest with high CCNB1-CDK1 activity. Such levels of synchronisation are difficult to achieve in cycling cells. Furthermore, double thymidine blocks have differing efficacy between cell lines. HeLa cells have previously been shown to synchronise well with double thymidine block, so were selected for use in this protocol. However, this was still not sufficient for the level of synchronisation required to observe band-shift in either autophagy regulators or positive control proteins such as 4E-BP1 (data not shown).

An alternative approach was to combine double thymidine block with mitotic shake-off, whereby the loose adherence of mitotic cells enabled them to be isolated from the rest of the culture. This approach enabled the detection of hyperphosphorylated 4E-BP1 in lysates acquired from mitotically-enriched cells, suggesting a sufficient level of synchronisation had been achieved to observe mitotic band shifts (Figure 5.15.A). Indeed, hyperphosphorylation of ARs was observed in the mitotic lysates. This hyperphosphorylation was independent of mTORC1, as it could not be reversed by AZD8055 treatment. Since this experiment did not involve the use of microtubule inhibitors, yet achieved high levels of mitotic synchronisation, we also assessed LC3 lipidation. Strikingly, lipidated LC3 (LC3B-II) was reduced in mitotic lysates compared to interphase-enriched lysates, further supporting our immunofluorescence findings in the previous chapter. Finally, TFE3 shares many phosphorylation sites with TFEB; for example, the region surrounding S246 is highly conserved with S142 in TFEB. Like TFEB, TFE3 was hypophosphorylated upon treatment with AZD8055 in lysates enriched for interphase cells but underwent mTORC1-independent phosphorylation during mitosis. Importantly, the key finding, that ARs were phosphorylated in an mTORC1-independent manner during mitosis (Figure 5.15.A), was replicated by paclitaxel treatment of HeLa cells (experiment performed

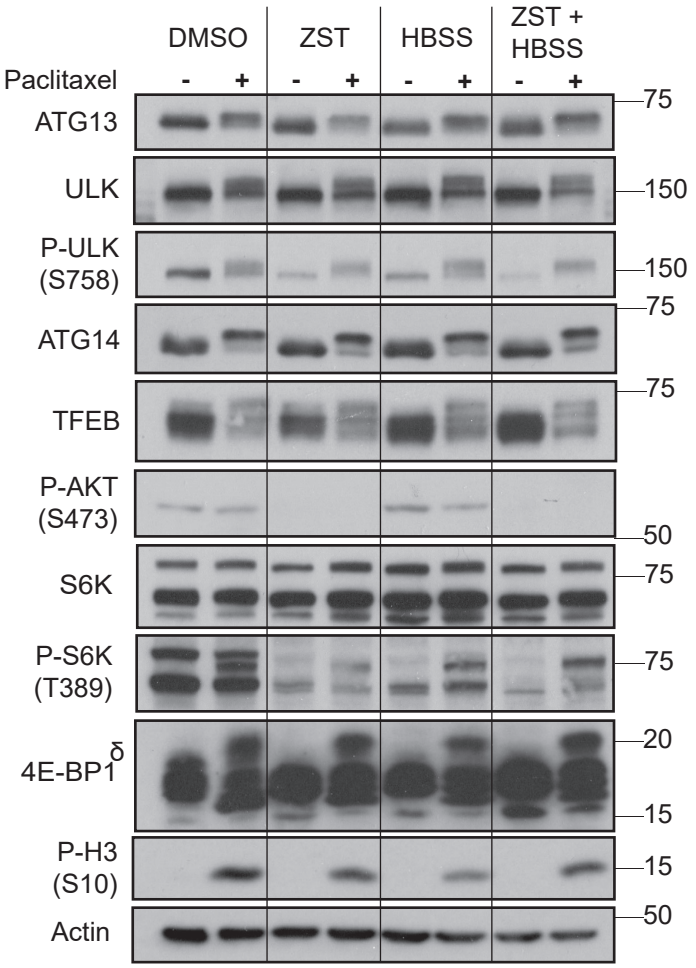

Figure 5.14: Paclitaxel-induced phosphorylation of ARs persists in the absence of amino acids or PI3K signalling.
(A) HCT116 cells were treated with Paclitaxel (50 nM) for 16 hrs. Two hours prior to lysis cells were treated with either DMSO or ZSTK474 (1 μM; PI3K class I inhibitor) and had their media maintained or swapped for HBSS + 1% BSA. Western blots are from a single experiment representative of three independent experiments. Molecular weight markers (kDa) are indicated to the right of each blot.

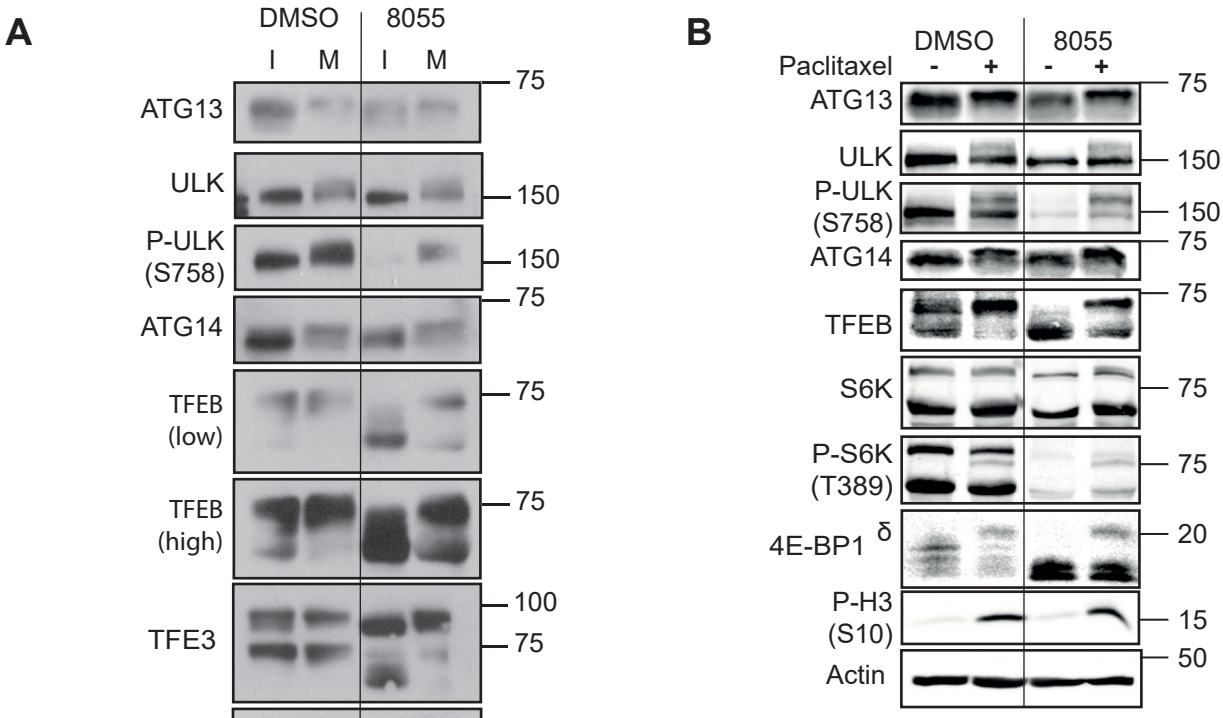

Figure 5.15: Mitotic phosphorylation of ARs occurs during a synchronised mitosis upon release from double thymidine block.
(A) HeLa cells were released from double thymidine block (G1/S border) for ten hours. Two hours prior to lysis, cells were treated with either DMSO or AZD8055 (1 μM). Flasks then underwent mitotic shake-off separating cells into two distinct interphase (I; adherent) and mitosis (M; suspension) enriched fractions. Western blots are from a single experiment representative of three independent experiments. **(B)** HeLa cells were treated with paclitaxel (t=16 hrs; 50 nM) and/ AZD8055 (t=2 hrs; 1 μM). Experiment and analysis was performed by Andrew Kidger. Western blots were acquired using a fluorescent-based LiCOR Odyssey system and are from a single experiment representative of three independent experiments. Molecular weight markers (kDa) are indicated to the right of each blot.

by Andrew Kidger; Figure 5.15.B) and the previous mitotic shake off experiment of HCT116 cells (Figure 5.6). Overall, this experiment (Figure 5.15.A) demonstrated that mitotic hyperphosphorylation of ATG13, ATG14, TFEB and ULK1 took place in normal cycling cells and was not limited to chemically-induced mitotic arrest.

It has been known for over 20 years that inactivation of CDK1 results in a G2 arrest at the G2/M border (van den Heuvel and Harlow, 1993). The development of a reversible catalytic CDK1 inhibitor (RO-3306) enabled cells to be arrested on the G2/M border with RO-3306 treatment and then released into a relatively synchronised mitosis by washing off the drug (Vassilev *et al.*, 2006). Of several cell lines tested, we found HT-29 produced the highest proportion of cells in mitosis upon release from RO-3306 (based on cells with a rounded morphology). HT-29 cells treated with RO-3306 arrested on the G2/M border as assessed by propidium iodide flow cytometry (Figure 5.16.A; G1 – 7%, S – 23%, G2 – 52%). Upon release from RO-3306, cells then underwent a relatively synchronised mitosis with hyperphosphorylation of 4E-BP1 and the ARs (Figure 5.16.B). These phosphorylation events were lost by 4 hours, where PI staining showed a proportion of cells had entered the next G1 (Figure 5.16.A; G1 - 35%, S - 13%, G2 – 41%). Whilst a G2 population did persist at 4 hours, the lack of hyperphosphorylated 4E-BP1, mitotic P-S6K (T389), and reduced P-H3 (S10) means they were not likely to be in mitosis (Figure 5.16.B).

To further assess the phosphorylation of ULK1 at S758 in asynchronous cultures we utilised a different phospho-antibody appropriate for immunofluorescence applications. High-content microscopy with staining for both P-H3 (S10) and P-ULK1 (S758) enables the automated and un-biased segregation of mitotic and interphase cells, and quantification of their respective P-ULK (S758) intensity. HAP1, HeLa, A549 and HT-29 cells were analysed by this methodology (Figure 5.17, 5.18) and have all been used at different points throughout this study. Treatment with AZD8055 or deprivation of nutrients both reduced P-ULK (S758) in interphase cells. It was noticeable that the remaining signal in interphase cells when treated with AZD8055 or HBSS was punctate and likely represents staining of unphosphorylated ULK1. By contrast, mitotic cells showed no noticeable drop in P-ULK (S758) upon mTOR inhibition. Furthermore, paclitaxel addition in the high-content microscopy experiment did not drastically alter results (Figure 5.18), further supporting that its use in previous experiments was justified. Overall, high-content microscopy demonstrated that P-ULK (S758) was largely not responsive to mTOR inhibition during mitosis.

Unfortunately, HCT116 cells could not be analysed by this process; this appeared to be due to a very low number of mitotic cells remaining adherent to the Cell-carrier plates

A

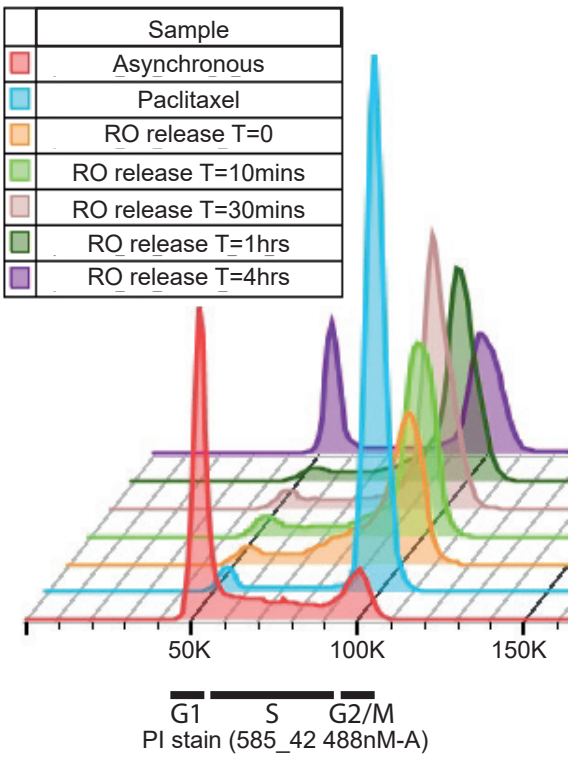

Figure 5.16: Mitotic phosphorylation of ARs occurs during a synchronised mitosis upon release from CDK1-inhbitor (RO-3306) blockade.
(A) Propidium iodide analysis of HT29 cells run in parallel with (B). **(B)** HT29 cells were treated with RO-3306 (9 μM) for 20 hours prior to release into drug-free media for indicated time. For samples treated with AZD8055 (1 μM), drug was added 2 hours prior to release, and cells were released into media supplemented with AZD8055. As a positive control, HT29 cells were treated with paclitaxel (50 nM) for 16 hours (P). Western blots are from a single experiment representative of three independent experiments. Molecular weight markers (kDa) are indicated to the right of each blot.

B

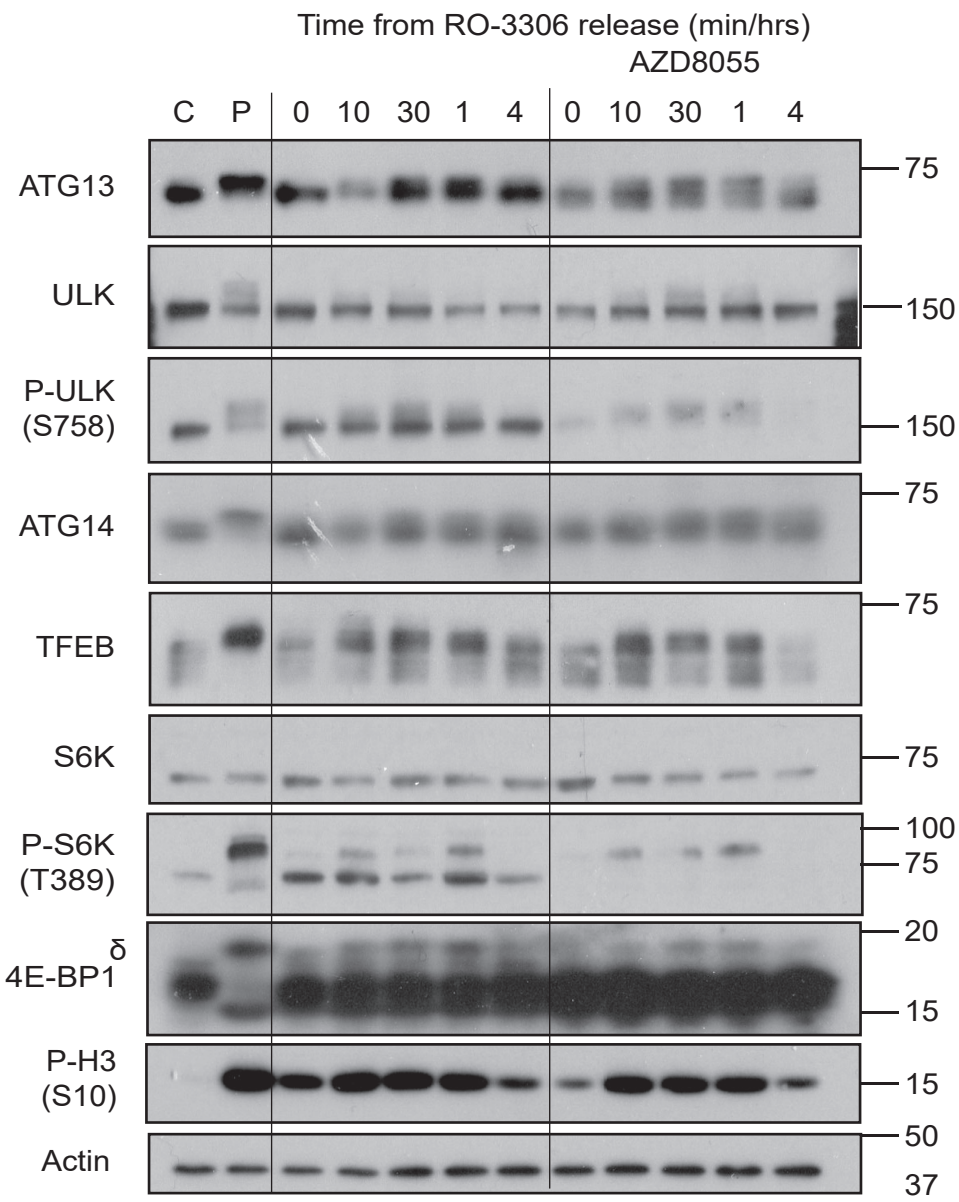

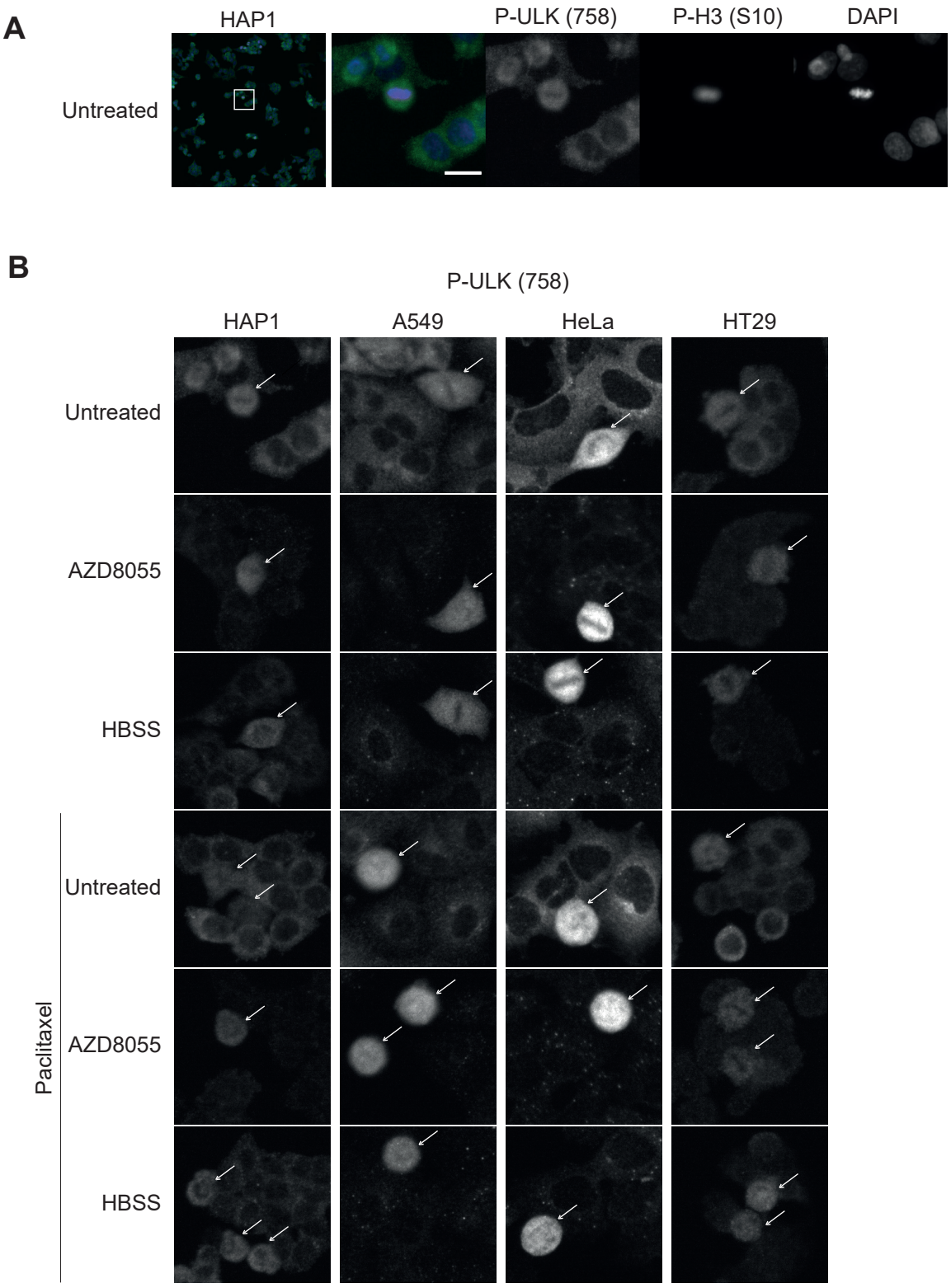

Figure 5.17: High-content microscopy further demonstrates the mTOR-independent phosphorylation of ULK1 in mitotic cells.
Cells were treated as indicated for two hours: paclitaxel (50 nM), AZD8055 (1 μM), HBSS + 1% BSA. Cells were then fixed and immunostained for P-ULK1 (S758) and P-H3 (S10). **(A)** Panel demonstrates an example (Untreated HAP1) of all the parameters utilised for subsequent analysis. **(B)** Representative P-ULK (S758) images from all cell lines and treatment conditions are shown. P-H3 (S10) positive cells are indicated by arrow for the representative images. Images are from a single experiment, representative of three independent experiments. Experiment performed with assistance of Andrew Kidger.

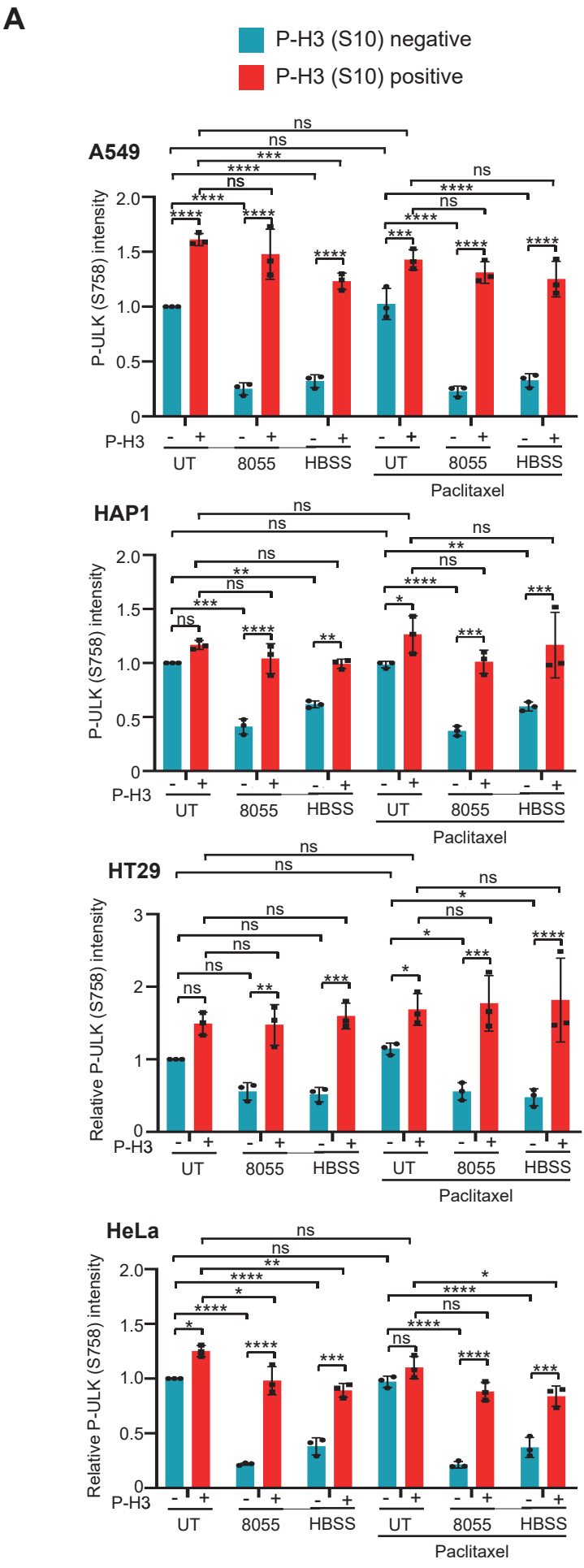

Figure 5.18: Quantification of high-content microscopy.
(A) Quantification of mean P-ULK1 (S758) intensity from (Fig 5.17) for different cell lines is shown. Mean +/- SD from three independent experiments. P-values calculated using Two-way Anova (Tukey). * p<0.05; ** p<0.01; *** p<0.001; **** p<0.0001.

after fixation leading to highly variable data. We therefore also performed flow-cytometry on two cell lines, A549 and HCT116, as an alternative approach. Like high-content microscopy, the use of P-H3 (S10) enabled a gating strategy whereby cells were stratified into interphase (P-H3 (S10) negative) and mitotic (P-H3 (S10) positive) populations (Figure 5.19.A). Plotting P-ULK (S758) intensity as histograms, and stratifying based on P-H3 (S10) staining, revealed that whilst AZD8055 resulted in a striking reduction of P-ULK (S758) in interphase cells, minimal reduction was observed in mitotic cells (Figure 5.19.B). Since P-ULK (S758) intensity showed a normal distribution within any given population or treatment condition, it was appropriate to compare the mean intensity between treatment conditions. This quantitative analysis confirmed that whilst AZD8055 treatment caused significant reductions in P-ULK (S758) within interphase populations, minimal decreases were observed in mitotic cells (Figure 5.19.C). Furthermore, results obtained by both flow cytometry and high content microscopy for A549 cells showed almost identical values, cross validating the analysis methodologies used. HCT116 cells showed almost identical results to A549 cells (Figure 5.19.D). Overall, both techniques strongly supported our findings by western blot, showing that mitotic phosphorylation of P-ULK (S758) was largely independent of mTORC1 (AZD8055 and starvation media). We did observe small but consistent reductions upon inhibition of mTORC1 in most cell lines during mitosis. Indeed, western blot evidence of P-S6K p70 (T389) throughout this chapter showed that whilst phosphorylation was significantly reduced in mitotically-arrested cells (Figure 5.23), there was still residual activity which was responsive to AZD8055 treatment. Therefore, there was likely to be a small fraction of residual mTORC1 activity in mitotic cells. Another possibility was that, as discussed in the previous chapter, not all P-H3 (S10) positive cells have yet entered mitosis and therefore will still be responsive to mTORC1 inhibition. Regardless, the data clearly suggests that P-ULK (S758) is not primarily regulated by mTORC1 in mitotic cells, and these results validate that this was not a result of any synchronisation protocol previously used.

5.2.7 Mitotic phosphorylation of autophagy regulators occurs at known repressive sites which are usually phosphorylated by mTORC1 during interphase

Since we demonstrated that ULK1 was phosphorylated at S758 during mitosis, even in the presence of the mTOR inhibitor AZD8055, we hypothesised that mitotic phosphorylation of autophagy regulators was likely occurring at known mTOR sites. That a majority of these sites are proline-directed made CCNB1-CDK1 a likely candidate and would be consistent with the findings for 4E-BP1. Given the shared similarity of the region surrounding the S142 of TFEB with other MITF family members (S73 for MITF), antibodies

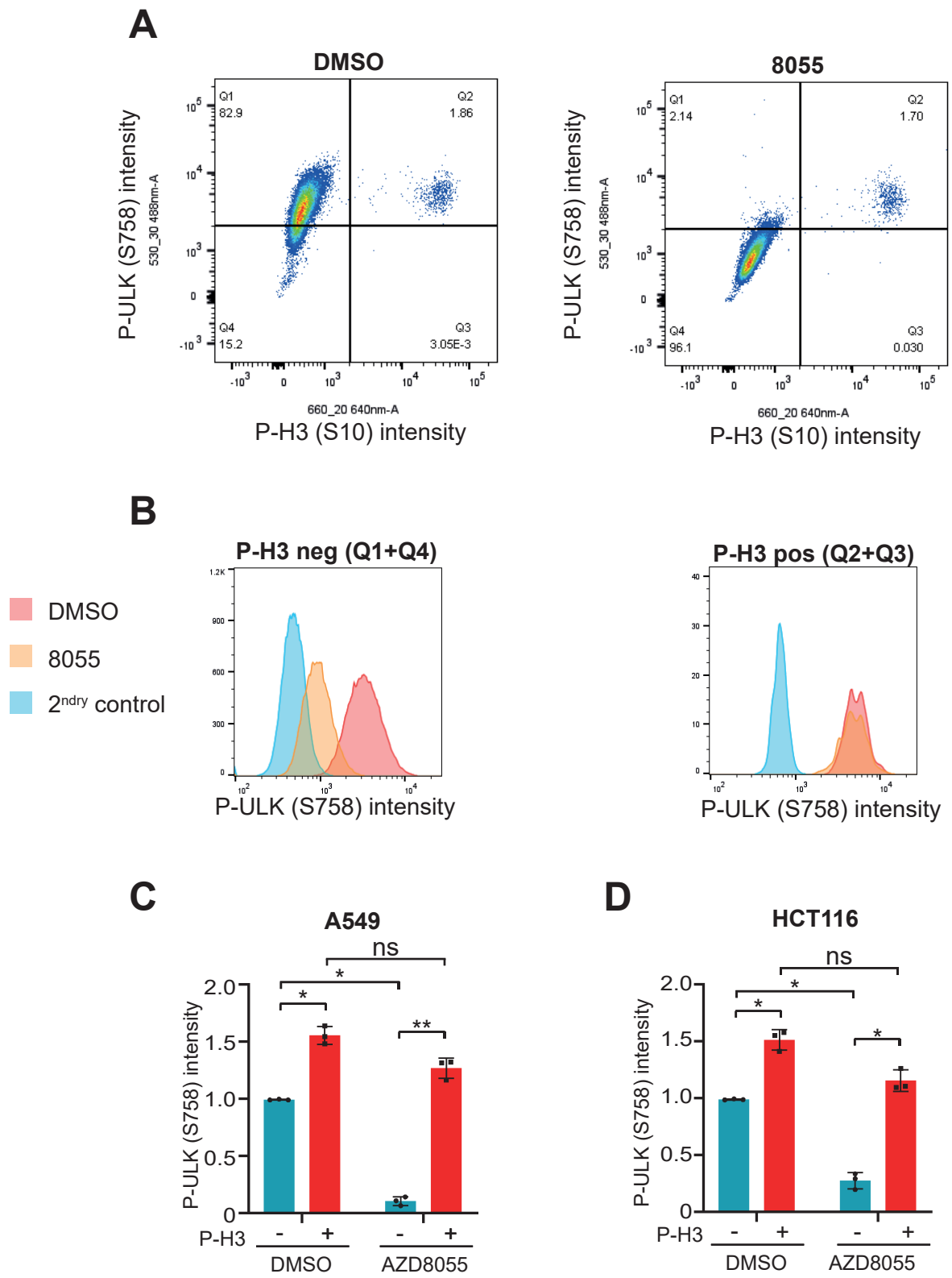

Figure 5.19: Phosphorylation of ULK1 at S758 occurs in an mTOR-independent manner in asynchronous mitotic cells.
A549 cells were treated with either DMSO or AZD8055 (1 μM) two hours prior to fixation. Cells were then stained for P-H3 (S10) or P-ULK1 (S758) prior to analysis by flow-cytometry. **(A)** Example contour plots with gating strategy is shown for A549 cells from both treatment arms. **(B)** Histogram plots of P-ULK (S758) intensity for interphase (Q1 + Q4) and mitotic (Q3 + Q4) populations from (A) are shown. **(C)** Mean P-ULK1 (S758) intensity for different P-H3 (S10) sub-populations (A) is shown for A549 cells. **(D)** Mean P-ULK1 (S758) intensity for different P-H3 (S10) sub-populations is shown for HCT116 cells. Gating strategy was performed as per (A). Mean +/- SD across three independent experiments. P-values calculated using Two-way Anova (Tukey) * $p<0.05$; ** $p<0.01$.

capable of detecting endogenous phosphorylation at this site are not currently feasible. This shared similarity also meant that phosphorylation of overexpressed TFEB at S142 could be detected with the P-MITF (S73) antibody (L. Li *et al.*, 2018). Please note this experiment was performed prior to the development of a specific P-TFEB (S142) antibody, which was used for the experiment shown in Figure 3.5; however, both antibodies were trialled on lysates from the experiment shown in Figure 3.5 and showed similar results. In addition, a recent antibody for S122, an mTORC1 site known to promote TFEB cytosolic localisation (Vega-Rubin-de-Celis *et al.*, 2017), has been developed but requires immunoprecipitation of the protein. In agreement with previous findings, treatment of asynchronous cells with AZD8055 promoted dephosphorylation at both sites (Figure 5.20). Pre-treatment with paclitaxel prevented dephosphorylation at both sites, again indicating that mitotic phosphorylation of known mTORC1 sites in TFEB was independent of mTORC1.

Nutrient responsive phosphorylation of ATG13 also impairs ULK1 kinase activity (Puente, Hendrickson and Jiang, 2016). mTORC1 directly phosphorylates ATG13 at S259 (mouse 258). In addition, there is AMPK-dependent phosphorylation at S224 and both of these phosphorylation events lead to repression of the ULK1 kinase complex. Commercially available antibodies for these sites do not currently exist. Therefore, we decided to interrogate phosphorylation of ATG13 by liquid chromatography tandem mass spectrometry (LC-MS/MS). Consistent with published findings, AZD8055 treatment of asynchronous cells promoted dephosphorylation of ATG13 at S259 but had no effect on S224 (Table 5.1). Pre-treatment of cells with paclitaxel to arrest them in prometaphase promoted phosphorylation at both of these sites. Furthermore, it largely reversed dephosphorylation promoted by AZD8055. It is worth noting that HEK293 cells do not arrest well in mitosis (Figure 5.5.C) and this was likely responsible for the discrepancy between paclitaxel-treated lysates in the presence and absence of AZD8055.

	Treatment (fold change to DMSO control)					
	Paclitaxel		AZD8055		Paclitaxel + AZD8055	
Phosphopeptide Phosphorylation site and relevant interphase kinase	Rep1	Rep2	Rep1	Rep2	Rep1	Rep2
TPPIMGIIIDHFVDRPYPSS**S**PMHPCNYR S224 (known AMPK site)	3.55	2.07	0.94	0.96	3.86	3.00
TAGEDTGVIYPSVEDSQEVCTTSFST**S**P PSQLSSSR S259 (known mTOR site)	1.75	1.90	0.15	0.19	0.81	1.05

Table 5.1: ATG13 is phosphorylated at known repressive sites during mitosis

HEK293 GFP-ATG13 cells were treated with paclitaxel (50 nM, 16 hrs) and/or AZD8055 (1 μM, 2 hrs). GFP-ATG13 was then immunoprecipitated, protease digested, and analysed by LC-MS/MS as outlined in the methods. Data for two phosphopeptides are shown: during interphase S224 is known to be phosphorylated in an AMPK-dependent manner and S259 by mTOR directly. Fold-change compared to DMSO control is presented for two independent replicate experiments.

The preceding results were consistent with mitotic phosphorylation of ARs being catalysed by CDK1 rather than mTORC1. To test if phosphorylation at all of these sites was a direct result of CDK1 was challenging, because adding a CDK1 inhibitor results in cells rapidly exiting mitosis (Vassilev *et al.*, 2006). Whilst we attempted to identify time points when CDK1 inhibition resulted in substrate dephosphorylation during mitosis, we found that dephosphorylation of P-H3 (S10) closely correlated with dephosphorylation of the validated CDK1 substrate P-4E-BP1 (T37/46) and P-ULK (S758) (data not shown). Therefore, whilst CDK1 inhibitor experiments are essential for determining whether paclitaxel-induced phosphorylation events are a result of mitotic arrest and CDK1 activity, they do not directly implicate CDK1. To further interrogate this, we assessed whether CCNB1-CDK1 immunoprecipitated from mitotically-arrested cells could phosphorylate bacterially expressed recombinant GST-tagged peptides, containing regions of ARs usually phosphorylated by mTORC1. AR proteins are intrinsically highly disordered and as such make their purification from bacterial lysates challenging, especially when ATG13, ATG14 and ULK1 are expressed alone rather than in their normal multi-protein complexes (Michael Wilson, personal communication). Hence, we decided to utilise fragments of ARs fused to GST protein to enable purification. Immunoprecipitated CCNB1-CDK1 could phosphorylate all of these GST-tagged constructs *in vitro*, as assessed by ^{32}P incorporation (Figure 5.21.A). Importantly, this was strongly inhibited by the presence of independent CDK1 inhibitors RO-3306 (300 nM) and NU6102 (500 nM). Previous *in vitro* profiling of these inhibitors had demonstrated that only CDK1 (and CDK2 for NU6102) exhibited an IC_{50} below the dose used out of a panel of kinases tested (T. G. Davies *et al.*, 2002; Vassilev *et al.*, 2006). To verify that CDK1 was phosphorylating the mTORC1 target sites, we analysed the *in vitro* reactions of ATG13, ATG14 and ULK1 by LC-MS/MS mass spectrometry which confirmed CCNB1-CDK1-specific phosphorylation of ATG13 (S224, S259), ULK1 (S758) and ATG14 (S383, S440). In addition, CCNB1-CDK1 specific phosphorylation of ULK1 T764 and S781, and ATG14 S392 and S462 was detected in the mass spectrometry analysis of *in vitro* reaction fragments (Table 5.2). For TFEB, immunoprecipitated Cyclin B1-CDK1 could phosphorylate both S122 and S142 as assessed by western blot with the

A

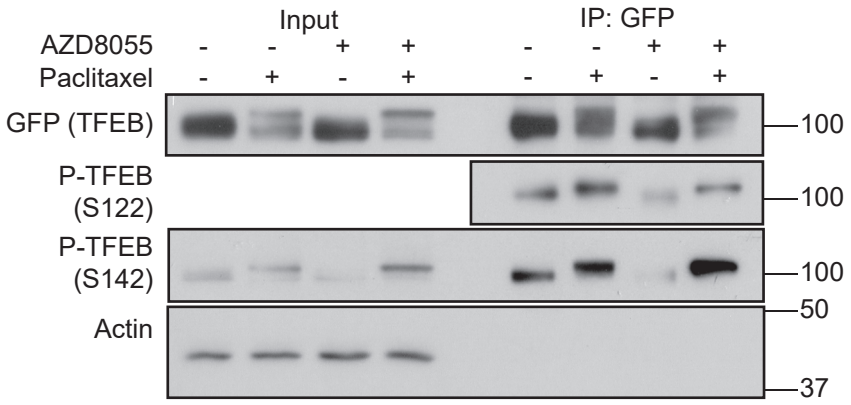

Figure 5.20: TFEB is phosphorylated at S122 and S142 in an mTORC1-independent manner during mitosis.
(A) HeLa cells stably expressing WT-TFEB-GFP were treated with either paclitaxel (50 nM; 16hrs) and/or AZD8055 (1 μM; 2 hrs). Input lysates and immunoprecipitated GFP are shown. Western blots are from a single experiment representative of three independent experiments. Molecular weight markers (kDa) are indicated to the right of each blot.

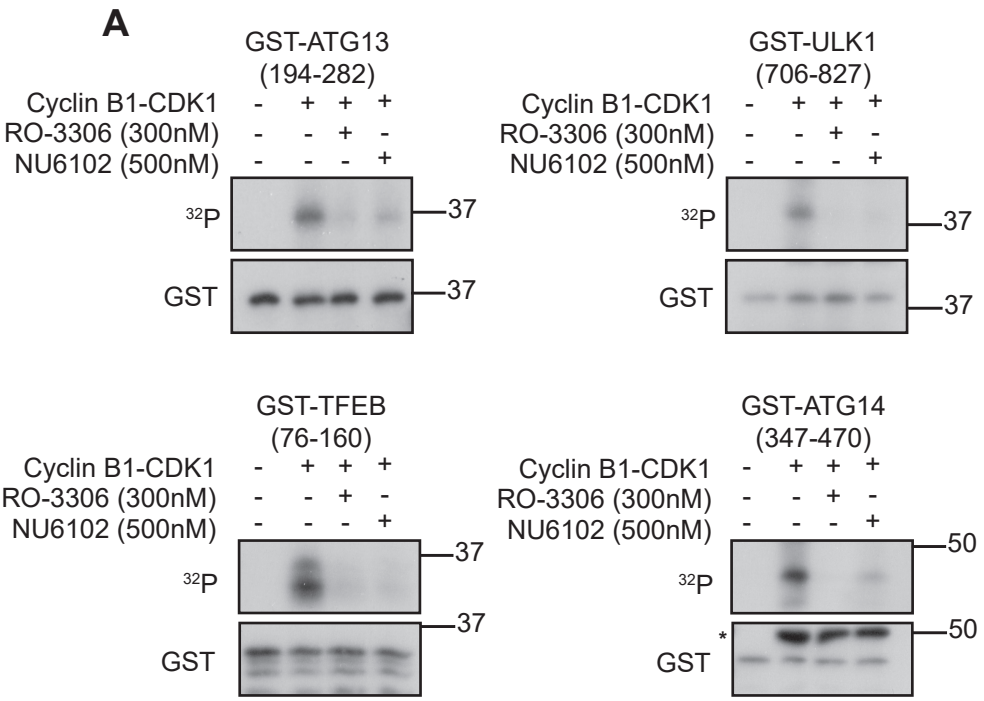

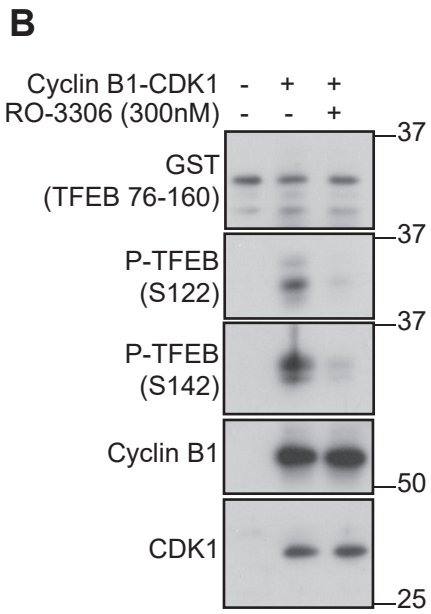

Figure 5.21: Immunoprecipitated CCNB1-CDK1 can phosphorylate ARs *in vitro* at known repressive sites usually phosphorylated by mTORC1.

(A) HAP1 cells were treated with paclitaxel (50 nM; t=16 hrs) prior to lysis and subsequent immunoprecipitation of cyclin B1 (or bead-only control – first lane). The immunoprecipitated CDK1 was then incubated with RO-3306 (300 nM) or NU6102 (500 nM) where indicated. Indicated GST-tagged protein fragments were then added to reaction mixtures and incubated for 15 minutes at 30°C. * indicates detection of heavy-chain antibody from immunoprecipitation. **(B)** Kinase assay performed as in (A) but without the addition of ^{32}P-ATP. Western blots and radiographs are from a single experiment representative of three independent experiments. Molecular weight markers (kDa) are indicated to the right of each blot.

relevant phospho-specific antibodies, and this phosphorylation was again inhibited by the CDK1 inhibitor RO-3306 (Figure 5.21.B). These results, combined with our data acquired from cells, strongly suggests that CDK1 directly phosphorylates ATG13, ULK1, ATG14 and TFEB at known repressive sites which are usually phosphorylated by mTORC1 during interphase.

Phosphopeptide	Site
ATG13 (194-283)	
TPPIMGIIIDHFVDRPYPSS**S**PMHPCNYR	S224
TAGEDTGVIYPSVEDSQEVCTTSFST**S**PPSQLSSSR	S259 (known mTOR site)
ULK1 (706-827)	
AGGTSSPSPVVFTVG**S**PPSGSTPPQGPR	S758 (known mTOR site)
AGGTSSPSPVVFTVGSPPSGS**T**PPQGPR	T764
MFSAGPTG**S**ASSSAR	S781
ATG14 (348-470)	
NLMYLV**S**PSSEHLGR	S383 (known mTOR site)
SGPFEVR	S392
VSDEETDLGTDWENLP**S**PR	S440 (known mTOR site)
FCDIPSQSVEVSQSQSTQA**S**PPIASSSA	S462

Table 5.2: Sites in ATG13, ULK1 and ATG14 phosphorylated by CCNB1-CDK1 *in vitro*

HAP1 cells were treated with paclitaxel (50 nM; t=16 hrs) prior to lysis and subsequent immunoprecipitation of CCNB1 (or bead-only control). The immunoprecipitated CDK1 was then incubated with indicated GST-tagged protein fragments for 15 minutes at 30°C. GST-tagged fragments were then trypsin digested and analysed by mass spectrometry as outlined in the methods. Sites phosphorylated by CCNB1-CDK1 in both of two independent experiments are identified in Red underline.

5.2.8 Functional consequences of CDK1-dependent phosphorylation of ARs

CCNB1-CDK1 activity starts to increase approximately 27 minutes prior to nuclear envelope breakdown in HeLa cells (Gavet and Pines, 2010b). Since S142 has been implicated in the nuclear export of TFEB (L. Li *et al.*, 2018; Napolitano *et al.*, 2018) and we had observed that CCNB1-CDK1 directly phosphorylated this site, we wanted to see whether TFEB was exported from the nucleus in the presence of an mTOR inhibitor just prior to nuclear envelope breakdown. To test this, we generated a stable cell line from the previously characterised HeLa WT-TFEB-GFP cell line expressing the H2B-mCherry protein. We then performed live-cell imaging in the presence of the mTOR inhibitor

AZD8055. As expected, all cells in interphase showed a strong nuclear localisation of TFEB (Figure 5.22). Approximately 10-20 minutes prior to nuclear envelope breakdown, a rapid and pronounced export of TFEB was observed consistent with CDK1 phosphorylation promoting TFEB's nuclear export in an mTORC1-independent manner.

ULK1-catalysed phosphorylation of different substrates has been reported to be important to the initiating events in autophagosome biogenesis. Phosphorylation of ATG14 on S29 by ULK1 stimulates VPS34 activity, PI(3)P synthesis and autophagy initiation (Park *et al.*, 2016). We therefore wanted to evaluate phosphorylation of this site during mitosis as a functional readout of ULK1 activity. We performed fluorescent western blotting with HAP1 cells, selected for their near complete synchronisation (ratio of δ 4E-BP1 to total; number rounded cells upon paclitaxel treatment) (Figure 5.23). As expected, P-S6K (T389) was drastically reduced upon treatment with paclitaxel (80%), though the residual phosphorylation was AZD8055 responsive suggesting a degree of mTORC1 activity persists in mitotic cells. Whilst AZD8055 reduced P-ULK1 (S758) phosphorylation by approximately 90% in asynchronous cells, the phosphorylation was only reduced by approximately 20% in cells pre-treated with paclitaxel to induce mitotic arrest, and this was not significant (One-way Anova (Tukey correction)). AZD8055 treatment of asynchronous cells promoted ATG14 phosphorylation at S29 approximately three-fold, indicating ULK1 activation. This was completely blocked by pre-treatment with paclitaxel to arrest cell in mitosis. These results were also observed in HCT116 cells (Figure 5.24). Thus, a critical signalling pathway responsible for autophagy initiation (dephosphorylation of ULK1 leading to its phosphorylation of ATG14) was absent in early mitosis. This further supports the hypothesis that the ULK1 complex was inhibited and autophagy repressed.

5.3 Discussion

5.3.1 Phosphorylation of ARs during mitosis is independent of mTORC1

Our observations during the work associated with Chapter 4 showed that whilst autophagy initiation was repressed during mitosis, this occurred in an mTORC1-independent manner. Indeed, mTORC1 was likely to be repressed during mitosis, given it fails to localise to lysosomes. Supporting this hypothesis, P-S6K (T389) was found to be reduced during mitosis (Figure 5.23 and 5.24), supporting previous observations (Shah, Ghosh and Hunter, 2003; Ruf *et al.*, 2017). mTORC1 is the master regulator of autophagy via its repressive phosphorylation of ATG13, ULK1, ATG14 and TFEB. We consistently found that treatment of asynchronous cells with the mTOR inhibitor AZD8055 resulted in appreciable hypophosphorylation of ATG13, ULK1 and TFEB. Despite our observations that mTORC1 was inactive during mitosis, ARs were consistently hyperphosphorylated

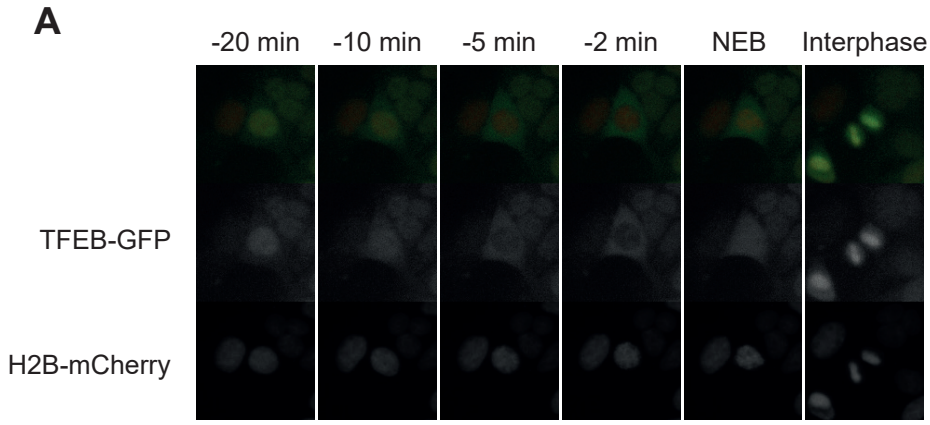

Figure 5.22: TFEB is localised to the cytosol just prior to NEB, even in the presence of AZD8055.
(A) Asynchronous HeLa TFEB-GFP H2B-mCherry were treated with AZD8055 (1 μM) for one hour prior to transfer to a live-cell imaging incubator. Images are a montage from a single experiment representative of three independent experiments.

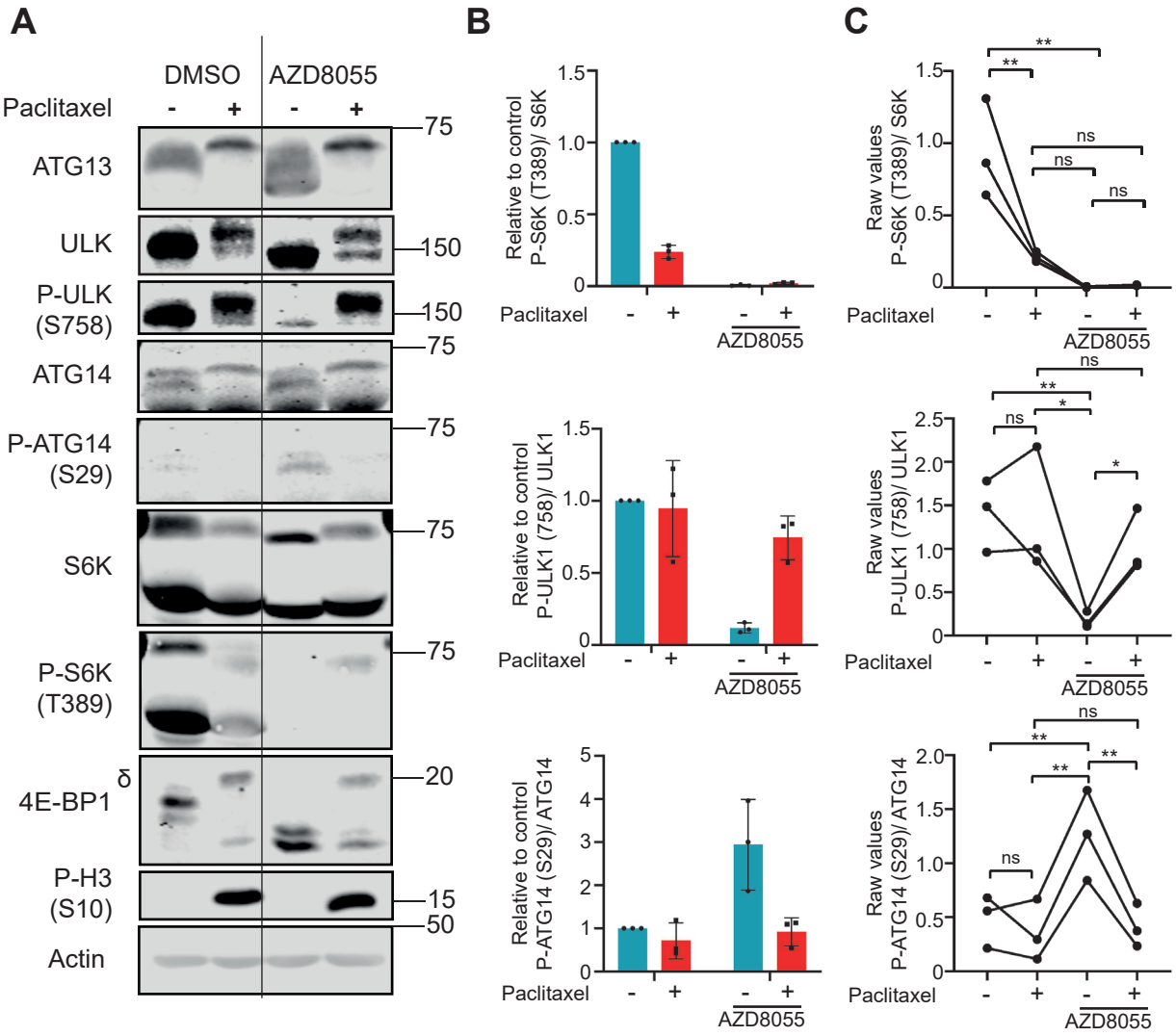

Figure 5.23: Phosphorylation of ATG14 at S29, an ULK1 target site and critical autophagy initiation event, is repressed during mitosis.
(A) HAP1 cells were treated with paclitaxel (50 nM; t=16 hrs) and/or AZD8055 (1 μM; t=2hrs). Western blots are taken from a single experiment representative of three independent experiments. Molecular weight markers (kDa) are indicated to the right of each blot. Quantification from fluorescent western blotting is provided as both relative **(B)** and raw **(C)** values. P-values calculated from raw values using One-way Anova (Tukey). Mean +/- SD across three independent experiments * $p<0.05$; ** $p<0.01$.

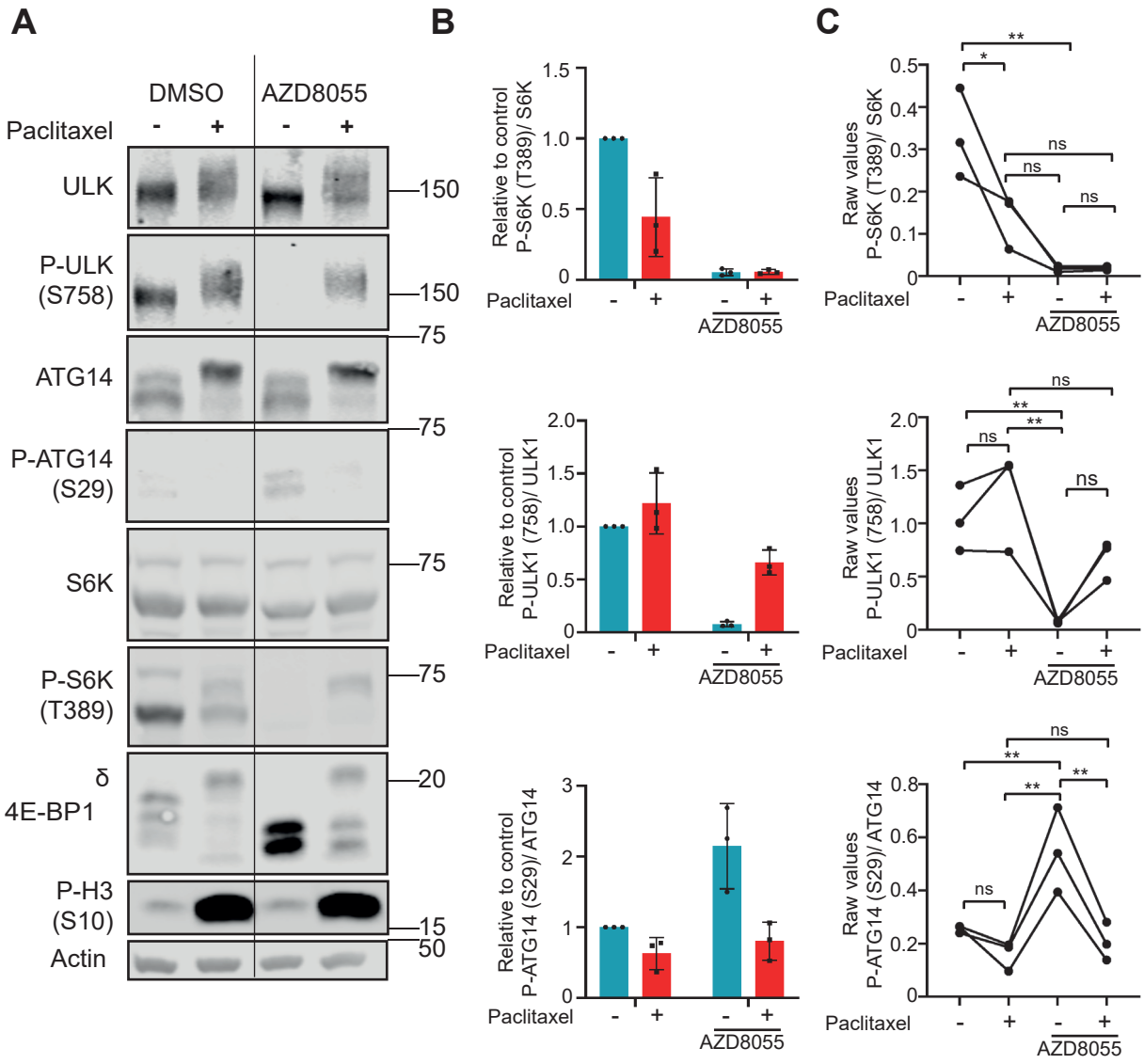

Figure 5.24: Phosphorylation of ATG14 at S29 is also repressed in HCT116 cells during mitosis.

(A) HCT116 cells were treated with paclitaxel (50 nM; t=16 hrs) and/or AZD8055 (1 μM; t=2hrs). Western blots are taken from a single experiment representative of three independent experiments. Molecular weight markers (kDa) are indicated to the right of each blot. Quantification from fluorescent western blotting is provided as both relative **(B)** and raw **(C)** values. P-values calculated from raw values using One-way Anova (Tukey). Mean +/- SD across three independent experiments * $p<0.05$; ** $p<0.01$.

during mitosis. This included at known repressive sites usually phosphorylated by mTORC1: ATG13 S259, ULK1 S758, and TFEB S122 and S142. Furthermore, inhibition of mTOR in cells that were arrested in mitosis failed to reverse the mitotic hyperphosphorylation of ARs. The methods to inhibit mTOR included treatment with three catalytic mTOR inhibitors (AZD8055, Torin1 and PP242), a PI3K class I inhibitor ZSTK474, and HBSS starvation. In addition, mitotic phosphorylation of ARs was observed in SW620:8055R cells. Furthermore, genetic mutation of TFEB such that it cannot be phosphorylated by mTORC1 failed to prevent its mitotic phosphorylation. We further validated that mTORC1-independent phosphorylation of autophagy regulators occurred during mitosis in the absence of microtubule inhibitors. This evidence together strongly suggests that the mitotic phosphorylation of these autophagy regulators occurs in a manner independent of mTOR. Therefore, another kinase must be responsible for the phosphorylation of ARs at known repressive sites during mitosis.

5.3.2 CCNB1-CDK1 is the most likely candidate kinase to catalyse phosphorylation of ARs during mitosis.

It has previously been suggested that 4E-BP1 is a direct substrate of CCNB1-CDK1, with phosphorylation at sites which are usually phosphorylated by mTORC1. Given that mitotic phosphorylation of ARs was occurring in an mTORC1-independent manner, we hypothesised that a global mTORC1-to-CDK1 switch may be occurring during mitosis. There are several lines of evidence which support CDK1 being the direct kinase responsible for phosphorylation of ARs during mitosis at phosphosites usually phosphorylated by mTORC1. The minimum consensus motif of CCNB1-CDK1 is a proline-directed threonine/serine (pS-P or pT-P), and all of these sites fit such a consensus motif. CDK1 inhibitors reverse the mitotic phosphorylation of ARs in a dose-responsive manner, where dephosphorylation of ARs closely correlated with loss of hyperphosphorylated 4E-BP1, a well validated CDK1 substrate. Furthermore, three different CDK1 inhibitors resulted in dephosphorylation of ARs. Temporally, ARs were phosphorylated within 10 minutes of release from CDK1 inhibition, increasing to maximal phosphorylation at 30 minutes and 1 hour which correlates with the hyperphosphorylated form of 4E-BP1. The temporal dynamics of TFEB cytosolic shuttling closely correlate with previous findings of CCNB1-CDK1 activity in cells, that suggest CDK1 activity increases over the period of 20 minutes prior to NEB. With regards to localisation, CCNB1-CDK1 is established to be active in both the nucleus and cytosol (Gavet and Pines, 2010a), thus providing a mechanism for TFEB phosphorylation in the nucleus as well as ULK1 complex phosphorylation in the cytoplasm. Finally, CCNB1-CDK1 was capable of phosphorylating ARs *in vitro* at these proposed sites.

Thus, the hypothesis that CCNB1-CDK1 is responsible for the hyperphosphorylation of ARs during mitosis is entirely consistent with all of our findings.

5.3.3 Known functional consequences of phosphorylation at repressive sites occurs during mitosis

mTORC1 is known to repress autophagy through its phosphorylation of ARs. Whilst PI(3)P synthesis is known to be reduced during mitosis as a result of VPS34 inhibition (Furuya *et al.*, 2010), no readouts of ULK1 activity during mitosis have been explored. ULK1 is activated upon mTORC1 inhibition, and phosphorylates ATG14 at S29 to stimulate VPS34 activity and autophagy (Park *et al.*, 2016; Wold *et al.*, 2016). We therefore used P-ATG14 (S29) as a readout of ULK1 activity. Whilst mTOR inhibition had the expected effect of activating ULK1 in asynchronous cells this was blocked in mitotic cells, suggesting the ULK1 complex was inactive during mitosis. Thus, we show that autophagy initiation is not just impaired at the level of VPS34 but also ULK1 during mitosis. That CCNB1-CDK1 directly phosphorylates ULK1 S758 *in vitro* and this site persists in mitosis, strongly suggests that CDK1 imparts the same repressive control on ULK1 during mitosis as mTORC1 does in interphase.

TFEB is known to be localised to the cytosol in response to mTORC1 phosphorylation of S122, S142 and S211. Mutation of S142 to alanine is alone sufficient to drive TFEB to the nucleus (Settembre *et al.*, 2011). Since we had observed that CCNB1-CDK1 phosphorylates TFEB on S122 and S142, we hypothesised that TFEB nuclear expulsion would be visible just prior to mitosis when CDK1 activity begins to increase, despite the presence of mTOR inhibitors. As predicted, TFEB was rapidly exported over a course of 20 minutes prior to nuclear envelope breakdown. It could be argued that the functional impact of such repression during a normal mitosis is minimal, since TFEB is only in the cytosol for approximately 10-15 minutes of interphase, before chromosome condensation and transcriptional inactivation occurs anyway. There are several reasons why CCNB1-CDK1 may phosphorylate TFEB causing its expulsion from the nucleus to the cytosol. The first is that it is simply a by-product of a global mTORC1-to-CDK1 switch with no functional relevance. However, P-S6K (T389), which is not proline-directed, does not undergo such a switch, therefore suggesting there is a biological separation of certain mTORC1 target sites that do or do not undergo a switch in regulation. The second, is the phosphorylation is in preparation for the next interphase, since transcription factors which are immediately required post-mitosis remain associated with chromatin during mitosis in a “book keeping” mechanism (Teves *et al.*, 2016). A third possibility is that CCNB1-CDK1 terminates any role TFEB plays in a DNA-damage response mediating a G2 arrest.

Topoisomerase inhibitors such as etoposide promote TFEB dephosphorylation and activation (Jeong *et al.*, 2018), and our preliminary data agreed with this and also suggested this was by a mechanism independent of mTORC1 due to sustained P-S6K (T389) and P-ULK (S758) (Figure 5.25). CCNB1-CDK1 is known to terminate components of the DDR (Zhang *et al.*, 2011), thus TFEB could just be inactivated alongside other components of the DDR.

5.3.4 Comparison of our study with other studies of mitotic regulation of autophagy

The results described here suggest a complete switch in regulation of macroautophagy from mTORC1 to CDK1 during mitosis. This was most likely achieved by the direct phosphorylation of ARs by CDK1 on known mTORC1 target sites. These are known to be repressive in nature and the expected effects were observed in mitotic cells, such as the nuclear export of TFEB and absence of the ULK1 target P-ATG14 (S29). These events, in addition to the previous publications on VPS34 inactivity and WIPI2 degradation, mean that autophagy is globally repressed, even during times of stress during mitosis. The scale of the observed repression is likely to hamper efforts to re-initiate autophagy during mitosis. Such efforts are already complicated during interphase, and the original papers which identified mTORC1 phosphorylation of ATG13 (S259) (Puente, Hendrickson and Jiang, 2016) and ULK1 (S758) could only demonstrate their phenotypic effects during starvation, when autophagy was active. Since we have yet to demonstrate a way of initiating autophagy during mitosis, we believe attempting to rescue mitotic autophagy by site-directed mutagenesis of single sites on autophagy regulators is likely futile and runs the risk of coming to a conclusion that sites are not important, when they are more likely merely redundant. Indeed, if the hypothesis is that autophagy is repressed in order to prevent catastrophic damage during mitosis, then such redundancy would be beneficial, enabling autophagy repression even with mutations at one or more sites. Finally, the site-directed mutagenesis of multiple sites could have unpredictable effects on overall protein function during interphase and so must be treated with caution and well-validated to ensure effects observed are a strictly mitotic phenomenon. Such concerns are obvious for a protein like RAPTOR, where multiple sites have been identified to be phosphorylated by more than one kinase, with differential outputs dependent upon the combination of phosphorylation events. Thus site-directed mutagenesis of putative CDK1-sites has not been a focus of this work.

There has been the recent submission of a pre-print which also shows CCNB1-CDK1 phosphorylates both ATG13 and ULK1 (Z. Li *et al.*, 2019). It is important to note that whilst Li and colleagues' pre-print data showing CDK1 interaction with the ULK1 complex

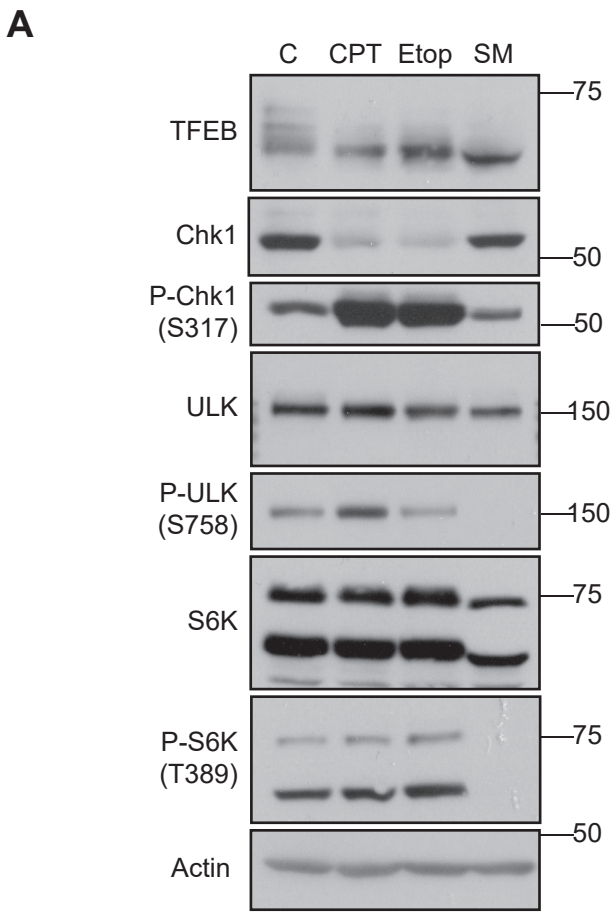

Figure 5.25: TFEB is hypophosphorylated upon treatment with DNA-damage inducing agents camptothecin and etoposide.
(A) HEK293 cells were treated as indicated: DMSO (C); camptothecin (CPT; 1.25 μM; t=16hrs); etoposide (E; 20 μM; t=16 hrs); HBSS + 1% BSA (SM; t=2 hrs). Western blots are from a single experiment. Molecular weight markers (kDa) are indicated to the right of each blot.

complements our data, their conclusions differ from ours in several regards. Firstly, whilst they identified many sites that CDK1 potentially phosphorylated, these did not include the mTORC1 target sites. The sites Li and colleagues identified included 11 sites for ULK1: T282, T401, S403, S405, S411, S413, S479, T502, S543, S622, T635, T653 and 4 sites for ATG13: S44, S224, T332, T342. Importantly, they used a combination of mass spectrometry, phosphosite prediction and site directed mutagenesis to generate this list (though it is not entirely clear within the preprint which of these sites came from phosphosite analysis and which from mass spectrometry). Our results from mass spectrometry analysis of GFP-ATG13 also found paclitaxel-induced increases in phosphorylation of S44 and T342; however, this was a very low-proportion of the total protein and therefore we have not presented this data without further validation. Li generated a 3A mutant of ATG13 (S44A, T332A, T342A) which arguably showed little reversal of the mitotic band shift compared to the WT protein, whereas further addition of S224A, a site we also identified, noticeably reduced the band shift. We attempted to generate stable cell lines with ATG13 and ULK1 mutated at the known mTORC1 target sites; however, these failed to express the protein despite selection. This would therefore need to be attempted again. It is not surprising Li and colleagues did not identify the mTORC1 target sites during mitosis, since they did not employ mTOR inhibitors during their mass spectrometry analysis. Therefore, it is very unlikely they would observe a significant difference from control cells. Indeed, P-ULK (758; Western blot) and P-ATG13 (S259; Mass spectrometry) stoichiometry was only very modestly raised in mitotic cells compared to interphase cells, and mTOR inhibition was required to observe the switch in regulation. Furthermore, Li and colleagues still observed phosphorylation, albeit drastically reduced, of ULK1 and ATG13 by CDK1 in cells and *in vitro*, even after mutating all of their proposed sites. Thus, our data is entirely compatible and complements with the findings of Li and colleagues with regard to ATG13 and ULK1 phosphorylation during mitosis.

A critical difference between ours and Li's study is the proposed effect these phosphorylation events have on autophagy. Li, in line with their group's previous study, suggests that these phosphorylation events stimulate, not repress, autophagy. To assess this, they performed a mitotic shake-off of nocodazole treated cells expressing either the WT or mutant protein (in an ATG13 KO, ULK1 KO background) and then treated these with chloroquine and assessed LC3 lipidation. The arguments against this approach have been addressed several times within this text but briefly they should not be utilised due to the difficulties associated with LC3B interpretation during mitosis and the use of chloroquine promoting non-canonical autophagy. Thus, this experiment would require repeating utilising an omegasome marker such as WIPI2. Overall, our findings, including a failure to induce

P-ATG14 (S29) upon AZD8055 treatment during mitosis, directly challenge the hypothesis that ULK1 and ATG13 hyperphosphorylation stimulates autophagy.

5.3.5 Further validation experiments

Whilst potential future directions are developed in the thesis discussion section, directly linked experiments are outlined here. It would greatly support the hypothesis that CCNB1-CDK1 directly phosphorylates these autophagy regulators if they could be co-immunoprecipitated. Whilst this was attempted with overexpressed GFP-CDK1 and some encouraging data acquired, the degree of co-immunoprecipitation with endogenous autophagy regulators was only moderately enriched compared to controls and, due to potential ambiguity, the data was not shown here. It is worth stressing that kinase-substrate interactions are notoriously transient and co-immunoprecipitation is not always deemed viable. Li and colleagues did show co-immunoprecipitation of CDK1 and overexpressed ULK1 in both asynchronous and mitotically enriched lysates (Z. Li *et al.*, 2019). It is difficult to reconcile why there would be an interaction between these two proteins during interphase, suggesting this maybe an artefact of overexpression. Regardless, this is supportive of our hypothesis that CDK1 directly phosphorylates the ULK1 complex. Other potential methodologies which could be considered to validate an interaction between these proteins is GST-tagged protein pulldowns (either of the kinase or the substrate) or BIOID (Roux *et al.*, 2012).

We observed that whilst mTORC1 failed to recruit to lysosomes during mitosis, TFEB was still recruited to lysosomes in response to AZD8055 treatment. This further supports the hypothesis that alterations in mTORC1 localisation during mitosis are not a result of changes in Rag GTPase activity. To further validate this, the active Rag heteroduplex could be transfected into HeLa TFEB-GFP cells, since this appears to be sufficient to stimulate a prominent lysosomal localisation without the presence of mTOR inhibitors (Martina and Puertollano, 2013).

Whilst we have demonstrated that TFE3 also undergoes mTORC1-independent phosphorylation during mitosis, we have not established if TFE3 can be phosphorylated by CDK1 *in vitro*. This is highly probable, and likely at the same site as TFEB S142 (TFE3 S246). Therefore, since MITF S73 is highly conserved, it seems likely this is also a CDK1 site. Importantly, MITF-M, the isoform present in melanocytes, lacks the N-terminal region required for lysosomal localisation and thus is constitutively nuclear and not phosphorylated by mTORC1 (Roczniak-Ferguson *et al.*, 2012). Therefore, observing whether MITF-M is phosphorylated during mitosis would further support the hypothesis that phosphorylation of the potential CDK1-site (S73) site is independent of mTORC1.

Genetic ablation of a kinase of interest followed by re-expression of either a wild-type, constitutively active or kinase-dead/ dominant-negative is a standard approach to validating kinase-substrate interactions in cells. This is currently not feasible in studies of CDK1 and is not currently employed. There are several reasons for this. CDK1 is an essential gene and its ablation in mouse embryos results in failure to progress beyond the first few cell divisions, whilst conditional knockout of CDK1 in MEFs drives the cells into senescence (Diril *et al.*, 2012). Likewise, expression of a dominant-negative CDK1 causes a G2 arrest and prevents entry into mitosis (van den Heuvel and Harlow, 1993). Due to the failure of cells lacking CDK1 to make it through mitosis, any permanent genetic ablation such as CRISPR or shRNA are guaranteed to be unsuccessful. Whilst it has been suggested that Auxin-inducible degrons (AID) may circumnavigate this problem, there are several disadvantages when compared to inhibitors. Inhibitors will provide a rapid and consistent inhibition of CDK1 across all cells. By comparison, AID will likely lead to a more variable inhibition of CDK1. AID requires the disruption of the gene locus and, in yeast, the degron tag of cdc28 (yeast homolog of CDK1) impaired its interactions with its Cks1 regulatory domain (Papagiannakis *et al.*, 2017), thus demonstrating that this process can have unintended consequences on cell biology. Overall, even if it was feasible, CDK1 depletion would result in mitotic exit, providing no further clarity than a panel of three CDK1 inhibitors.

PP2A-B55α is an established phosphatase of ULK1 at S637 (Wong *et al.*, 2015). PP2A-B55 is also an important family of phosphatases which oppose CDK1 activity, and thus help regulate the mitotic phosphoproteome, as well as timing of mitotic events (explained in detail within thesis introduction). Given this shared phosphatase, identifying mitotic phosphatases for ARs would be an intriguing line of further experimentation.

ULK1 protein levels were consistently found to be reduced upon prolonged mitotic arrest. This could represent ULK1 being targeted for degradation during mitosis or could simply reflect turnover of the protein in a background of lower global translation during mitotic arrest. Distinguishing between these possibilities would mean assessing properties of ULK1 in HCT116 cells during both interphase and mitosis, such as its half-life (assessed by use of emetine to inhibit translation) and whether paclitaxel-induced reductions in ULK1 can be reversed by MG132 (proteasome inhibitor). Should ULK1 be degraded during mitosis, this may be a result of ULK1 hyperphosphorylation at other sites by CDK1 (Z. Li *et al.*, 2019).

Finally, it is clear from both our work, and an examination of the literature that no system of genetic mTORC1 inactivation exists where cell proliferation is unaffected. Whilst

this is unsurprising given mTORC1's role as an essential gene, the fact that SW620:8055R cells proliferate in the presence of AZD8055 without mTORC1 signalling, challenges the notion that a chronic model of mTORC1 inactivation is not possible. Potential methodologies to circumnavigate cell cycle arrest whilst obtaining stable mTORC1 inhibition are discussed in the main thesis discussion. It is worth noting here that even if it were possible to establish mTORC1 knockout cell lines, this would not prevent the development of compensatory mechanisms. Indeed, we observed that SW620:8055R cells exhibited reduced TFEB and ULK1 protein levels. The mechanism causing this reduction in protein requires further investigation. Regardless, the establishment of such a model would aid investigation of both mTORC1 signalling and autophagy research.

6 Discussion

6.1 Is mTORC1 always the master regulator of autophagy?

Autophagy is well described as a nutrient-sensitive catabolic pathway which is primarily regulated by mTOR. Initial studies, prompted by the idea that autophagy regulation was sensitive to both amino acids and insulin, identified that both S6 phosphorylation and autophagy were regulated by the same signalling pathway in rat hepatocytes (Blommaart *et al.*, 1995). Both S6 dephosphorylation and proteolysis, which could be inhibited by 3-methyladenine (an established inhibitor of autophagy), was stimulated by rapamycin (Blommaart *et al.*, 1995). Since then, mTORC1 has been established as directly repressing autophagy via its phosphorylation of ATG13, ULK1, ATG14 and TFEB. In addition, mTOR is frequently described as a master regulator of cellular metabolism, stimulating anabolic processes whilst repressing catabolic ones. David Sabatini recently described how it has sometimes been ridiculed as a kinase capable of “doing everything” (Sabatini, 2017). It is this plethora of functional outputs that has stimulated the search for mTORC1-independent regulation of macroautophagy, with the aim of designing therapeutics with more selective targeting of autophagy. Our lab has extensive experience in studying CMGC kinases, which led us to investigating the potential role of ERK1/2 and CCNB1-CDK1 in the regulation of autophagy. This was prompted by previous studies which had implicated ERK1/2 in the regulation of TFEB and CCNB1-CDK1 in the regulation of VPS34. The results have been discussed in detail within the respective chapters. Briefly, we found little evidence to suggest that ERK1/2 was a key regulatory kinase of TFEB, and mTORC1 appeared to be dominant in this regard. However, mTORC1 was not the dominant regulatory kinase of autophagy during mitosis. Indeed, mTORC1 is inactive during mitosis, likely as a result of CDK1-dependent phosphorylation of RAPTOR. Yet paradoxically macroautophagy is suppressed during mitosis and this occurs even in the presence of mTOR inhibitors or starvation conditions. Instead, we find that CDK1 appears to take over the direct phosphorylation and regulation of ARs, thereby sustaining autophagy repression even in the absence of mTORC1 activity.

Many questions arise from these findings, most of which can be addressed by further experimental work. Others will prove very challenging. It has long been hypothesised that autophagy may be repressed during nuclear envelope breakdown to ensure protection of the genome whilst condensed chromatin is contiguous with the cytosol. Supporting this hypothesis, autophagy repression appears to temporally correlate with nuclear envelope breakdown and CDK1 would appear to be the master regulator of both nuclear envelope breakdown and autophagy in mitosis. The true test of the physiological reasons for

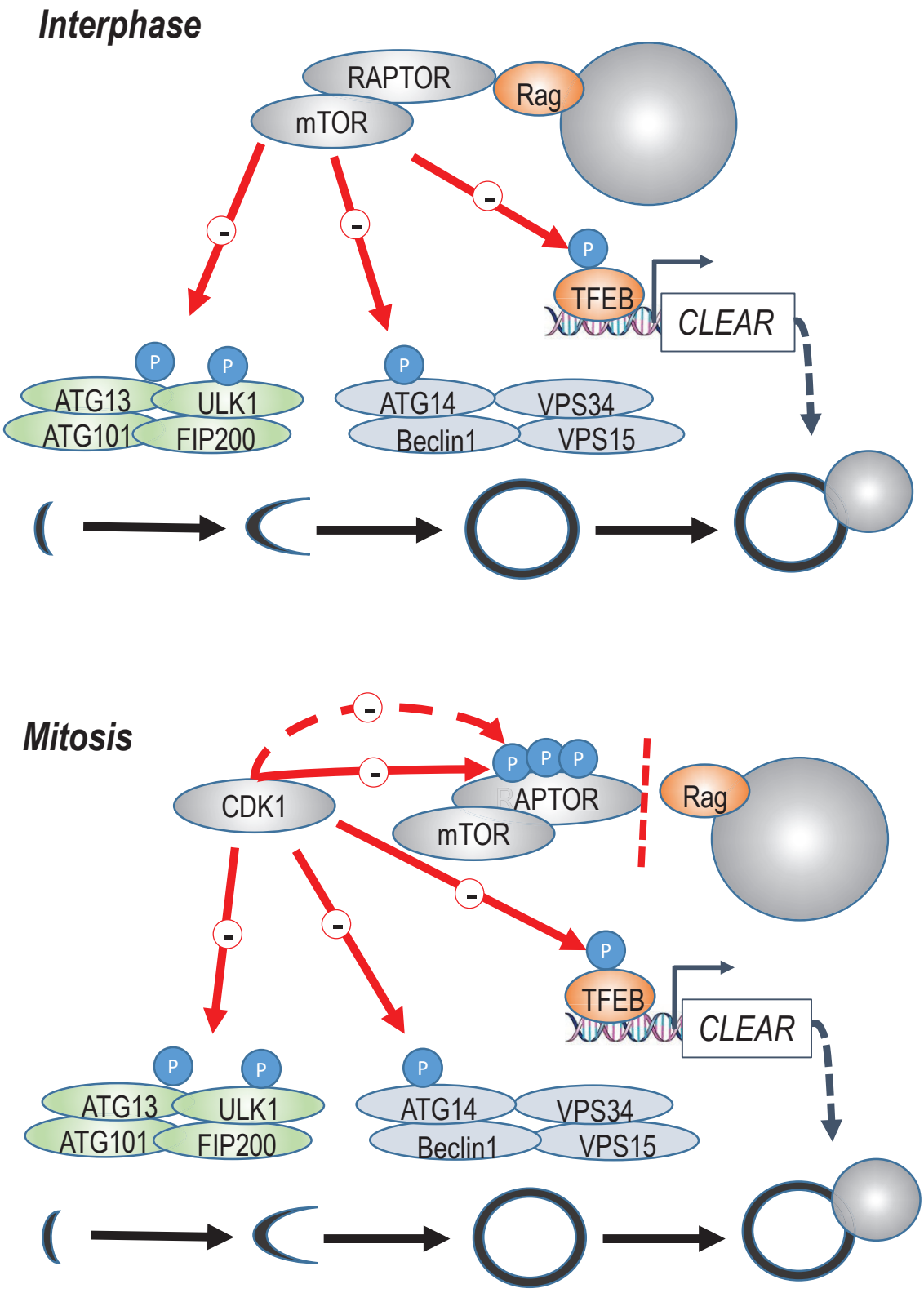

Figure 6.1: Graphical summary of key findings.
During interphase, mTORC1 is localised to the lysosome in a nutrient-dependent manner. This enables its activation, and subsequent phosphorylation of key autophagy regulators ATG13, ULK1, ATG14 and TFEB. However, during mitosis, CDK1-dependent phosphorylation of RAPTOR prevents mTORC1 localisation to the lysosome, thereby preventing its activation. Instead, the repressive phosphorylation of ARs is most likely catalysed by CCNB1-CDK1.

autophagy repression during mitosis will require its reactivation. This is challenging given the numerous points that autophagy is repressed at. The only evidence which suggests that autophagy can be initiated during mitosis, is from electron microscopy evidence of autophagosomal engulfment of mitotic chromosomes (Sit *et al.*, 1996). Whilst the conditions used to induce this were far from physiological, it does suggest it is feasible to initiate autophagy during mitosis. It could be hypothesised that whilst cells may have reserve capacity to sustain themselves through nutrient starvation for the short period of mitosis, how it would adapt to large-scale damage of organelles such as mitochondria or lysosomes is less clear. Likewise, *Salmonella enterica*, a well-established target of selective-autophagy, has been suggested to have a preference for the invasion of mitotic cells (Santos *et al.*, 2013). Thus, the investigation of selective autophagy inducers during mitosis would be an interesting field of study and could potentially open new therapeutic avenues if phenotypic differences are found with interphase cells.

During revisions of the submitted publication associated with the mitosis work, a reviewer suggested exploring cancer lines with mutations in the nutrient sensing pathways such that mTORC1 is constitutively active. As an example, cell lines with mutations in components of GATOR1 have constitutively active mTORC1 and recruitment to lysosomes (Bar-Peled *et al.*, 2013). Thus, it would be useful to explore mTORC1 localisation within HCC1500, SW780, Li7, MRKNU1 or HA7-RCC cell lines during mitosis which would form further genetic validation that alterations to RAPTOR are responsible for mTORC1 localisation during mitosis.

There are also broad concepts which we have not explored which may have a role in our results. Whilst mTORC1 localisation to the lysosome is widely accepted as a critical activation mechanism, less is known about how it is activated by Rheb which has been observed predominantly at the Golgi (see Introduction). It is important to consider that the Golgi undergoes significant alterations during mitosis (reviewed: Colanzi and Sütterlin, 2013). Rather than possessing the interphase morphology of interconnected pericentriolar ribbons, during mitosis the Golgi undergoes fragmentation and forms tubular and vesicular structures (Misteli and Warren, 1995). Likewise, known Golgi functions, such as protein transport, are halted during mitosis (reviewed: Yeong, 2013). Therefore, given that recent evidence suggests that Rheb activation of mTORC1 is dependent upon intricate connections between the lysosome and Golgi (Hao *et al.*, 2017), it is likely that this also plays a role in mTORC1 inactivation. Furthermore, the PI3K/AKT/TSC signalling axis is not even active during mitosis (Ramírez-Valle *et al.*, 2010), suggesting Rheb would be inactive during mitosis. Like the Golgi, the endoplasmic reticulum undergoes morphological changes during mitosis, such that it appears as extended cisternae, with little tubular

morphology (Lu, Ladinsky and Kirchhausen, 2009). Since autophagosomes form around pre-existing VMP1 (Koyama-Honda *et al.*, 2013) and VPS34 (Axe *et al.*, 2008) puncta, imaging of these proteins will provide further information on whether appropriate autophagosome initiation sites exist during mitosis.

There are also a few conceptual points it is worth stressing when considering our findings. We have placed a strong emphasis on studying mTORC1-regulated autophagy during a normal mitosis. We have not looked at periods of mitotic arrest beyond 16 hours when considering the phosphorylation of autophagy regulators and have attempted to validate all our results with experiments not utilising microtubule inhibitors. We can therefore not exclude the possibility of either autophagy reactivation or AR hypophosphorylation during prolonged mitotic-arrest. Furthermore, we cannot rule out selective autophagy occurring during a normal mitosis. Such mechanisms may involve the direct sequestration of cargo and the ULK1 complex by selective receptors. Indeed, we have observed endogenous p62 puncta in mitotic cells (data not shown; Emma Duncan, personal communications). Clearly given the findings of selective autophagy of Cyclin A during prometaphase, this warrants further investigation (Loukil *et al.*, 2014). Furthermore, whilst we postulate that starvation-induced bulk autophagy is repressed to protect exposed nuclear contents, specifically the genome, this need not conflict with previous data which shows selective autophagy of Lamin (Dou *et al.*, 2015) or micronuclei (Rello-Varona *et al.*, 2012).

6.1.1 Future direction: validating autophagy repression during mitosis *in vivo*

In this study of autophagy during mitosis, we have only validated our findings in cell culture. If validation of our findings *in vivo* could be achieved and repression of autophagy during mitosis reversed, it would enable the observation of phenotypic effects including potential disease/ therapeutic implications. It may be possible to observe *in vivo* mitotic repression of autophagy via a number of potential methodologies. Transgenic mice expressing GFP-LC3 can enable cryosections to be obtained and observed by fluorescence microscopy (Mizushima *et al.*, 2004). Whilst this study focused on terminally differentiated tissues, such as skeletal muscle and the glomerulus, focusing on areas of tissue which are usually well stained for proliferative markers (i.e. KI67) such as intestinal crypts may enable observation of mitosis. Since mouse studies typically employ starvation periods of 24 to 48 hours, it may be that similar complications as in tissue culture arise, such as cell cycle arrest. The most rapid way to induce autophagy *in vivo* appears to be artery ligation (with the exception of exercise which affects terminally differentiated structures like the heart and skeletal muscle) (Moulis and Vindis, 2017). Therefore, ligation of the superior mesenteric

artery (SMA) supplying the small intestine may enable rapid ischaemia of tissues such that cells may still be in mitosis at the time of fixation. These proposals are laden with caveats, not least because SMA occlusion leads to inconsistent ischaemic injuries (Gonzalez, Moeser and Blikslager, 2015). Therefore, these studies offer minimal advantages over tissue culture, with a high number of complications.

An alternative strategy may be the use of Caenorhabditis elegans. Like other metazoans, *C.elegans* undergoes an open mitosis; however, there are a number of key differences in both mitosis and autophagy between *C. elegans* and mammals which would affect interpretation of such studies. Mammalian nuclear envelope breakdown occurs in prophase and continues till late anaphase/telophase. By contrast, *C. elegans* nuclear envelope breakdown only occurs during midlate anaphase and reforms during telophase (reviewed Tzur and Gruenbaum, 2013). However, much of the regulatory system of the cell cycle is conserved between *C. elegans* and mammalian cells (Boxem, 2006).

The significant advantage of *C. elegans* over murine models is the ability to perform live-cell imaging. Several publications have successfully monitored autophagy in living C. elegans by imaging GFP:LGG-1, the *C. elegans* ortholog of LC3B (reviewed: Palmisano and Meléndez, 2016). This model is likely to suffer from the same complications we originally attributed to interpreting LC3 in mammalian culture. Whilst an EGP-1-GFP (ATG13 ortholog) *C. elegans* model does exist, whether it forms puncta in response to starvation was not tested (Tian *et al.*, 2009).

6.1.2 Future direction: Assessing autophagy-independent functions of the ULK1 complex.

During the course of Li's pre-print study of CDK1 hyperphosphorylation of the ULK1 complex, they proposed that it may be responsible for autophagy-independent functions (Z. Li *et al.*, 2019). They observed that mutations at CDK1 sites on ATG13 and ULK1 attenuated chemosensitivity to taxol, whilst knockout of ATG13 and ULK1 reduced the mitotic index of nocodazole-treated cells (Z. Li *et al.*, 2019). Recent published evidence suggests that the ULK1 complex phosphorylates MAD1L1 at S546 to mediate MAD1L1 recruitment to the kinetochore, facilitating an appropriate spindle assembly checkpoint, and that knockout of ULK1 mediates aneuploidy (Yuan *et al.*, 2019). Curiously, Yuan identified that this was independent of autophagy as they observed similar results in ATG3/7 knockout lines. Clearly further work is required to validate these findings; however, an interesting hypothesis arising from these two pieces of work is that CDK1 phosphorylates ULK1 at sites other than those that mediate autophagy repression, to direct the timing of

mitotic exit via the SAC. Whilst we observed decreased phosphorylation of ATG14 at S29 during mitosis, this does not exclude the possibility that ULK1 is active against other components.

6.1.3 Future direction: status of selective-autophagy and non-canonical autophagy during mitosis

Our study focuses on macroautophagy and the known mTORC1 repressive sites of autophagy regulation. There are numerous types of selective autophagy which have been suggested to utilise the same initiating complexes such as ULK1 yet appear to have active global mTORC1 signalling. It is not yet understood how this occurs and various models have been proposed such as localised mTORC1 inactivation, increases in phosphatase activity or ULK1 complex trans-autophosphorylation. Therefore, it would be interesting to see whether selective autophagy can be maintained during mitosis. Indeed, of the publications that suggest autophagy is active during mitosis, two of these refer to a high proportion of autophagosomes containing mitochondria (Liu *et al.*, 2009; Doménech *et al.*, 2015). The cargo receptor optineurin is phosphorylated by PLK1 at S177, disrupting its interaction with Rab8 and regulating PLK1 temporal and spatial dynamics (Kachaner *et al.*, 2012); however, selective autophagy of *Salmonella enterica*, a known function of optineurin which involves S177 phosphorylation by TBK1 (Wild *et al.*, 2011), was not assessed. Therefore, there is preliminary evidence that suggests selective autophagy could be maintained in mitosis and future experiments could involve the induction of mitophagy in HEK293 cells, or other Parkin-expressing cell lines, by utilising mitochondrial uncouplers such as oligomycin and antimycin A.

One of the main points for our argument against the continued use of LC3 as a readout of autophagy during mitosis was its ability to be lipidated in response to a range of stimuli that elicit non-canonical autophagy. Whilst entosis (cell-in-cell engulfment) has been shown to be driven by mitosis, this is a complex setting to conclude as to whether non-canonical autophagy can persist during mitosis since the interphase cell is the “host” cell and therefore will not be under an autophagy repression. Since the ULK1 complex (Florey *et al.*, 2011) and ATG14-associated VPS34 complex (Martinez *et al.*, 2015) are not required for non-canonical autophagy, none of the phosphorylation events described in this thesis would act to repress this process. Since the UVRAG-VPS34 complex has been implicated in non-canonical autophagy (Martinez *et al.*, 2015), and VPS34 phosphorylation by CDK1 has been shown to cause its dissociation with Beclin-1 (Furuya *et al.*, 2010) this could impair non-canonical autophagy during mitosis. Clearly more work will be required to clarify this. A number of model systems have been generated which would enable its study, such as

HCT116 cells expressing either an ATG16 mutant deficient in canonical (FIP200-binding domain deletion mutant) or non-canonical autophagy (WD40 domain deletion mutant) (Fletcher *et al.*, 2018). This would enable verification that any changes in LC3 during mitosis as a result of a treatment such as monensin, which induces both pathways, could be attributed to only one pathway within the same system.

6.1.4 Future direction: CDK5 and autophagy

In this thesis, we have described how a switch to CDK1-dependent regulation of key autophagy regulators occurs during mitosis. Given that these phosphorylation events all occur at proline-directed serine sites and that CCNB1-CDK1 can phosphorylate all of these substrates *in vitro*, it is most likely that this is a result of direct phosphorylation. CDK5 exhibits a high homology (61%) with CDK1, and was originally named neuronal Cdc2-like kinase (Hellmich *et al.*, 1992). Like CDK1, CDK5 has already been demonstrated to phosphorylate a number of shared substrates, including S6K at S411 (Lai *et al.*, 2015). CDK5 has been implicated in a number of neurodegenerative pathologies, not least because of its pathological activity when interacting with p25, such as phosphorylation of Tau (Tsai *et al.*, 1999). Given that repression of autophagy has been implicated in a number of neurodegenerative diseases (Menzies *et al.*, 2017), it would be prudent to investigate the potential links between CDK5 and autophagy more thoroughly. Furthermore, given CDK5 is active during interphase, this would be a far more sensible background in which to study the effects of site-directed mutants if it was deemed CDK5 did phosphorylate ARs. Such an approach was taken with CDK-mediated phosphorylation of VPS34 (Furuya *et al.*, 2010).

6.1.5 Future direction: Developing a stable model of mTORC1 inactivation

A weakness of our study into the status of autophagy during mitosis is a lack of genetic inactivation of mTORC1 to further validate that mTORC1 is not the main regulatory kinase of the mitotic phosphorylation events. This is because inhibition of mTORC1 leads to a pronounced G1 cell cycle arrest, most likely as a result of inhibited cap-dependent translation of cyclin D proteins (Cope *et al.*, 2014). Several groups have attempted CRISPR-Cas9 of mTORC1 components, only for it to have failed to produce any clones. Whilst we investigated the use of inducible Raptor knockout MEFs (Cybulski, Zinzalla and Hall, 2012), unsurprisingly these also lead to a pronounced cell cycle arrest (data not shown). Without any RAPTOR antibodies available for immunofluorescence, we cannot confidently be sure whether those few cells that continued to progress into mitosis are knockout or wild-type. The successful development of SW620 clones resistant to AZD8055 suggests that it is feasible for cells to acquire adaptive mechanisms enabling continued proliferation whilst possessing no active mTORC1 signalling. Thus, developing clones with CRISPR to

RAPTOR should be useful and would provide a useful genetic tool to studying mTORC1-independent regulation of autophagy. The difficulty with such a strategy is that the selection pressure against knockout clones will be large, such that a very large number of clones would have to be screened to successfully grow out a resistant population. There are two potential strategies which would be currently feasible to attempt doing. The first is to perform RAPTOR CRISPR in CO115 cells, as these cells have an intrinsic resistance to mTOR inhibition, despite possessing active mTORC1 signalling which is inhibited by AZD8055 (Cope *et al.*, 2014). The second is to perform the CRISPR on HAP1 RAPTOR-GFP cells, since you could culture the cells as a bulk population for a set amount of time post-transfection and then gate for cells no longer expressing GFP. Of these two proposals, we favour CRISPR in CO115 cells, since HAP1 RAPTOR-GFP cells have been previously shown to have altered, albeit active, mTORC1 signalling dynamics in response to amino acid stimulus (Manifava *et al.*, 2016). The development of RAPTOR-null cell lines would likely enable a more suitable background to test different RAPTOR mutants, with the eventual aim of re-establishing mTORC1 signalling during mitosis, to observe phenotypic effects.

It has previously been established that acquired resistance to mTOR/PI3K inhibitors can be established via upregulation of eIF4E (Ilic *et al.*, 2011; Cope *et al.*, 2014). It could therefore be anticipated that a way to avoid cell cycle arrest upon mTOR inhibition is to first exogenously express eIF4E, and then perform CRISPR of RAPTOR. It was found that ectopic expression of eIF4E only resulted in an approximately two-fold increase in total eIF4E protein levels (Ilic *et al.*, 2011) and our research group has similarly struggled to generate cells stably expressing significant amounts of eIF4E (Rebecca Gilley, Personal communication). Overexpression of MYC in immortalized human mammary epithelial cells was found to confer resistance to the dual PI3K-mTOR inhibitor BEZ235 (Ilic *et al.*, 2011). Therefore, overexpression of MYC or identifying high-expressing MYC lines may enable increased efficiency at deriving RAPTOR knockout clones.

6.1.6 Future direction: Links between mitosis and nutrient deprivation

During this work we have provided strong evidence that CCNB1-CDK1 operates to isolate autophagy regulation during acute nutrient deprivation (2 hours). It has been previously shown that the number of cells in mitosis dramatically reduces after 5 hours of leucine deprivation post-release from double-thymidine block (Smith and Proud, 2008). Complementing this, phosphorylation of eEF2K at S359, a CDK1 target site, was reduced during nutrient starvation. Therefore, this suggests that there is a mechanism by which nutrient deprivation promotes a G2/M arrest. Such a mechanism may be beneficial given

that mitosis would theoretically require enough energy to complete. Furthermore, prolonged autophagy during G2 may drastically impair a cell's ability to appropriately divide organelles between two daughter cells.

6.1.7 Future direction: Identifying CCNB1-CDK1 interaction with ARs

It has recently been demonstrated in fission yeast that mitotic cyclin, in complex with Cdk1, interacts with substrates which possess an LXF motif which acts as a docking domain (Örd *et al.*, 2019). Such a docking mechanism has not yet been identified in mammalian substrates of CCNB1-CDK1 (Örd *et al.*, 2019). Identifying how CCNB1-CDK1 interacts with ARs could present experimental opportunities, such as the ability to mutate the site with potential autophagy reactivation in mitotic cells whilst not impairing interphase mTORC1-regulated autophagy regulation.

6.1.8 Future direction: Why is S6 phosphorylation during mitosis rapamycin sensitive?

It is important to note that whilst the conclusions by several independent groups on both autophagy and mTORC1 status are opposing one another, a majority do not identify differences in experimental output as a reason. Our findings here are generally compatible with the findings of the Schneider group, who concluded that mTORC1 is still active during mitosis (Ramírez-Valle *et al.*, 2010). Curiously, they found that S6K and 4E-BP1 mitotic phosphorylation was not responsive to rapamycin, despite the interphase phosphorylation of both substrates being responsive, which would support that CDK1 directly phosphorylates these substrates. However, they did observe that phospho-S6 T240/T244, which was highly elevated in mitosis, was responsive to rapamycin and PP242 treatment (Ramírez-Valle *et al.*, 2010). Likewise, it has been shown that mitotic cells released from RO-3306 mediated G2/M arrest, have elevated p-S6 S240/S244 that is rapamycin responsive (Z. Li *et al.*, 2018). Conversely, the same study found that mitotic phosphorylation of p-S6 was not reversed by starvation, or elevated by insulin (Z. Li *et al.*, 2018). Overall, it is hard to reconcile how S6 is still rapamycin and PP242 responsive since S6K phosphorylation is no longer responsive to rapamycin in both these studies. Curiously, Li and colleagues found that mitotic p-S6 was blocked by the "p70S6K inhibitor" BI-D1870; however, BI-D1870 shows a strong selectivity for RSK over S6K with IC50s of 10-30nM and over 10μM respectively (Sapkota *et al.*, 2007). Therefore, further investigation into RSK activity during mitosis may enable resolution of these confounding findings. Furthermore, the experiment should be repeated comparing both RSK-selective inhibitors such as BI-D1870 with S6K-selective inhibitors such as LY2584702. It is also worth noting that not all

studies agree that phospho-S6 remains under the control of mTOR during mitosis. The dual PI3K-mTOR inhibitor BEZ235 appeared to have no effect on phospho-S6 in mitotic cells, despite significant reductions in phopho-H3 (S10) negative cells (Ryan *et al.*, 2019).

6.1.9 Future directions: A global mTORC1-to-CDK1 switch during mitosis?

Thus far every proline-directed site investigated that mTORC1 usually phosphorylates, undergoes a switch to CDK1 regulation during mitosis. This includes sites on S6K (Shah, Ghosh and Hunter, 2003), 4E-BP1 (Shuda *et al.*, 2015), ATG13, ULK1, ATG14 and TFEB. Proline directed sites on many other proteins, such as LARP1 (S774) and Grb10 (T155 and S476) are also known to be direct substrates of mTORC1 (Hsu *et al.*, 2011). Therefore, it will be important to evaluate the phosphorylation of these other proteins during mitosis and whether they are also insensitive of mTOR inhibition. Likewise, it would be useful to assess phosphorylation of substrates which are not proline-directed, to see whether they follow the trend of P-S6K (T389) of being decreased during mitosis. Examples could include TFEB S211 (Martina *et al.*, 2012; Roczniak-Ferguson *et al.*, 2012) and UVRAG (S550 and S571) (Munson *et al.*, 2015).

6.1.10 Clinical implications of an mTORC1-to-CDK1 switch during mitosis

There is ongoing debate as to the extent cancers are sensitive to autophagy inhibition. Theories regarding autophagy dependence in cancer tend to be based on the idea that rapid cell division will be accompanied by high levels of protein synthesis, therefore requiring autophagy to maintain nutrient demand. Microtubule inhibitors have been a mainstay of chemotherapy in the clinic, and it is a widely held view that the main therapeutic mechanism of action is through the ability to cause mitotic arrest. One curious possibility is whether the variable effectiveness of microtubule inhibitors is at least partially linked to a cancer cell lines dependence on autophagy? Furthermore, it has been suggested that resistance to microtubule therapies is established from cells undergoing eventual mitotic progression. Therefore, there is merit in improving the effectiveness of microtubule therapies in killing cells whilst they are arrested in mitosis. Cancer cells are generally considered to be more sensitive to microtubule inhibition and are more likely to arrest in mitosis compared to untransformed cells, and this is likely to be at least partially responsible for their relative therapeutic window. We postulate that mitotic autophagy is likely to be catastrophic for the cell, thus there may be therapeutic potential if autophagy can be stimulated during mitotic arrest. Since ATG13 puncta and P-H3 (S10) can both be visualised through immunofluorescence, it should be possible to perform high-content microscopy screens using small molecule inhibitors to determine whether additional factors are required for mitotic repression of autophagy other than CCNB1-CDK1.

6.2 Concluding statement

We set out to investigate, via a hypothesis-driven approach, mTORC1-independent regulation of autophagy. Initially, this focused on the proposed ERK2 phosphorylation of S142, and the functional role that ERK2 played in TFEB regulation. Whilst multiple groups have been able to demonstrate that ERK2 can phosphorylate TFEB at S142 *in vitro* and that phosphorylation at this site leads to cytoplasmic retention/ nuclear export of TFEB, we find little evidence to support this in cells. Further experiments using EGF stimulation should be performed to assess what little role ERK1/2 may have in TFEB regulation. Clearly further work clarifying the nuclear export mechanisms of TFEB are also required.

Presented within this thesis are numerous datasets that support the hypothesis that during mitosis, an mTORC1 to CCNB1-CDK1 switch occurs that maintains repression of autophagy. Such a hypothesis is understandably controversial given mTORC1's longstanding status as an absolute master regulator of cellular metabolism. By using markers of the omegasome, we provide strong evidence that starvation-induced autophagy is repressed within mitotic cells and that there is a switch away from mTORC1-mediated regulation. Our preliminary data suggests that RAPTOR phosphorylation, mediated by CCNB1-CDK1, inhibits mTORC1 localisation to lysosomes. This inhibits mTORC1, as evidenced by decreased P-S6K (T389) in paclitaxel-treated lysates. Therefore, it is likely that another proline-directed serine/threonine kinase is responsible for the phosphorylation and repression of ATG13, ULK1, ATG14 and TFEB during mitosis. CCNB1-CDK1 represents the most likely candidate kinase and is capable of phosphorylating fragments of these autophagy regulators at sites known to be targeted by mTORC1. Thus, we present data which suggests a global mTORC1-to-CDK1 switch during mitosis. Further experiments will be required to further investigate the details and potential nuances of this proposed switch in regulation, and some examples of possible experiments is provided in the conclusion.

7 References

Aberle, H. *et al.* (1997) 'β-catenin is a target for the ubiquitin–proteasome pathway', *The EMBO Journal*, 16(13), pp. 3797–3804. doi: 10.1093/emboj/16.13.3797.

Abu-Remaileh, M. *et al.* (2017) 'Lysosomal metabolomics reveals V-ATPase- and mTOR-dependent regulation of amino acid efflux from lysosomes.', *Science (New York, N.Y.)*. NIH Public Access, 358(6364), pp. 807–813. doi: 10.1126/science.aan6298.

Acosta-Jaquez, H. A. *et al.* (2009) 'Site-specific mTOR phosphorylation promotes mTORC1-mediated signaling and cell growth.', *Molecular and cellular biology*. American Society for Microbiology Journals, 29(15), pp. 4308–24. doi: 10.1128/MCB.01665-08.

Alers, S. *et al.* (2011) 'Atg13 and FIP200 act independently of Ulk1 and Ulk2 in autophagy induction', *Autophagy*. Taylor & Francis, 7(12), pp. 1424–1433. doi: 10.4161/auto.7.12.18027.

Alessi, D. R. *et al.* (1994) 'Identification of the sites in MAP kinase kinase-1 phosphorylated by p74raf-1.', *The EMBO journal*, 13(7), pp. 1610–9.

Alessi, D. R. *et al.* (1996) 'Mechanism of activation of protein kinase B by insulin and IGF-1.', *The EMBO journal*, 15(23), pp. 6541–51.

Alessi, D. R. *et al.* (1997) 'Characterization of a 3-phosphoinositide-dependent protein kinase which phosphorylates and activates protein kinase Balpha.', *Current biology : CB*, 7(4), pp. 261–9.

Alsaadi, R. M. *et al.* (2019) 'ULK1-mediated phosphorylation of ATG16L1 promotes xenophagy, but destabilizes the ATG16L1 Crohn's mutant', *EMBO reports*, 20(7), p. e46885. doi: 10.15252/embr.201846885.

Alvarez, B. *et al.* (2001) 'Forkhead transcription factors contribute to execution of the mitotic programme in mammals', *Nature*. Nature Publishing Group, 413(6857), pp. 744–747. doi: 10.1038/35099574.

Amato, S. F. *et al.* (1998) 'Transient stimulation of the c-Jun-NH2-terminal kinase/activator protein 1 pathway and inhibition of extracellular signal-regulated kinase are early effects in paclitaxel-mediated apoptosis in human B lymphoblasts.', *Cancer research*, 58(2), pp. 241–7.

Amit, S. *et al.* (2002) 'Axin-mediated CKI phosphorylation of beta -catenin at Ser 45: a molecular switch for the Wnt pathway', *Genes & Development*, 16(9), pp. 1066–1076. doi: 10.1101/gad.230302.

Andonegui-Elguera, M. A. *et al.* (2016) 'BUB1 and SURVIVIN proteins are not degraded after a prolonged mitosis and accumulate in the nuclei of HCT116 cells', *Cell Death Discovery*. Nature Publishing Group, 2(1), p. 16079. doi: 10.1038/cddiscovery.2016.79.

Argani, P. (2015) 'MiT family translocation renal cell carcinoma', *Seminars in Diagnostic Pathology*, 32(2), pp. 103–113. doi: 10.1053/j.semdp.2015.02.003.

Argani, P. *et al.* (2016) 'TFEB-amplified Renal Cell Carcinomas', *The American Journal of Surgical Pathology*, 40(11), pp. 1484–1495. doi: 10.1097/PAS.0000000000000720.

Ashkenazy, H. *et al.* (2016) 'ConSurf 2016: an improved methodology to estimate and visualize evolutionary conservation in macromolecules.', *Nucleic acids research*. Oxford University Press, 44(W1), pp. W344-50. doi: 10.1093/nar/gkw408.

Astrinidis, A. *et al.* (2003) 'Cell cycle-regulated phosphorylation of hamartin, the product of the tuberous sclerosis complex 1 gene, by cyclin-dependent kinase 1/cyclin B.', *The Journal of biological chemistry*. American Society for Biochemistry and Molecular Biology, 278(51), pp. 51372–9. doi: 10.1074/jbc.M303956200.

Atkin, J. *et al.* (2014) 'Torin1-mediated TOR kinase inhibition reduces Wee1 levels and advances mitotic commitment in fission yeast and HeLa cells.', *Journal of cell science*. Company of Biologists, 127(Pt 6), pp. 1346–56. doi: 10.1242/jcs.146373.

Audet-Walsh, É. *et al.* (2017) 'Nuclear mTOR acts as a transcriptional integrator of the androgen signaling pathway in prostate cancer', *Genes & Development*, 31(12), pp. 1228–1242. doi: 10.1101/gad.299958.117.

Axe, E. L. *et al.* (2008) 'Autophagosome formation from membrane compartments enriched in phosphatidylinositol 3-phosphate and dynamically connected to the endoplasmic reticulum', *The Journal of Cell Biology*, 182(4), pp. 685–701. doi: 10.1083/jcb.200803137.

Aylett, C. H. S. *et al.* (2016) 'Architecture of human mTOR complex 1', *Science*, 351(6268), pp. 48–52. doi: 10.1126/science.aaa3870.

Azoulay-Alfaguter, I. *et al.* (2015) 'Combined regulation of mTORC1 and lysosomal acidification by GSK-3 suppresses autophagy and contributes to cancer cell growth', *Oncogene*. Nature Publishing Group, 34(35), pp. 4613–4623. doi: 10.1038/onc.2014.390.

Bach, M. *et al.* (2011) 'The serine/threonine kinase ULK1 is a target of multiple phosphorylation events.', *The Biochemical journal*, 440(2), pp. 283–91. doi: 10.1042/BJ20101894.

Bachmann, R. A. *et al.* (2006) 'A nuclear transport signal in mammalian target of rapamycin is critical for its cytoplasmic signaling to S6 kinase 1.', *The Journal of biological chemistry*. American Society for Biochemistry and Molecular Biology, 281(11), pp. 7357–63. doi: 10.1074/jbc.M512218200.

Balachandran, R. S. and Kipreos, E. T. (2017) 'Addressing a weakness of anticancer therapy with mitosis inhibitors: Mitotic slippage', *Molecular and Cellular Oncology*. Taylor and Francis Ltd., 4(2). doi: 10.1080/23723556.2016.1277293.

Ballou, L. M. and Lin, R. Z. (2008) 'Rapamycin and mTOR kinase inhibitors.', *Journal of chemical biology*. Springer, 1(1–4), pp. 27–36. doi: 10.1007/s12154-008-0003-5.

Bao, J. *et al.* (2016) 'Deacetylation of TFEB promotes fibrillar Aβ degradation by upregulating lysosomal biogenesis in microglia.', *Protein & cell*. Springer, 7(6), pp. 417–33. doi: 10.1007/s13238-016-0269-2.

Bar-Peled, L. *et al.* (2012) 'Ragulator is a GEF for the rag GTPases that signal amino acid levels to mTORC1.', *Cell*. NIH Public Access, 150(6), pp. 1196–208. doi: 10.1016/j.cell.2012.07.032.

Bar-Peled, L. *et al.* (2013) 'A Tumor suppressor complex with GAP activity for the Rag GTPases that signal amino acid sufficiency to mTORC1.', *Science (New York, N.Y.)*. NIH Public Access, 340(6136), pp. 1100–6. doi: 10.1126/science.1232044.

Bautista, S. J. *et al.* (2018) 'mTOR complex 1 controls the nuclear localization and function of glycogen synthase kinase 3β', *Journal of Biological Chemistry*, 293(38), pp. 14723–14739. doi: 10.1074/jbc.RA118.002800.

Belaid, A. *et al.* (2013) 'Autophagy Plays a Critical Role in the Degradation of Active RHOA, the Control of Cell Cytokinesis, and Genomic Stability', *Cancer Research*, 73(14), pp. 4311–4322. doi: 10.1158/0008-5472.CAN-12-4142.

Bento, C. F. *et al.* (2016) 'Mammalian Autophagy: How Does It Work?', *Annual Review of Biochemistry*, 85(1), pp. 685–713. doi: 10.1146/annurev-biochem-060815-014556.

Bergeland, T. *et al.* (2001) 'Mitotic partitioning of endosomes and lysosomes', *Current Biology*. Cell Press, 11(9), pp. 644–651. doi: 10.1016/S0960-9822(01)00177-4.

Bernardi, R. *et al.* (2006) 'PML inhibits HIF-1α translation and neoangiogenesis through repression of mTOR', *Nature*. Nature Publishing Group, 442(7104), pp. 779–785. doi: 10.1038/nature05029.

Berthet, C. *et al.* (2003) 'Cdk2 knockout mice are viable.', *Current biology : CB*, 13(20), pp. 1775–85.

Beugnet, A., Wang, X. and Proud, C. G. (2003) 'Target of Rapamycin (TOR)-signaling and RAIP Motifs Play Distinct Roles in the Mammalian TOR-dependent Phosphorylation of Initiation Factor 4E-binding Protein 1', *Journal of Biological Chemistry*, 278(42), pp. 40717–40722. doi: 10.1074/jbc.M308573200.

Bilanges, B., Posor, Y. and Vanhaesebroeck, B. (2019) 'PI3K isoforms in cell signalling and vesicle trafficking', *Nature Reviews Molecular Cell Biology*. Nature Publishing Group, p. 1. doi: 10.1038/s41580-019-0129-z.

Bjursell, G. and Reichard, P. (1973) 'Effects of thymidine on deoxyribonucleoside triphosphate pools and deoxyribonucleic acid synthesis in Chinese hamster ovary cells.', *The Journal of biological chemistry*, 248(11), pp. 3904–9.

Blommaart, E. F. C. *et al.* (1995) 'Phosphorylation of Ribosomal Protein S6 Is Inhibitory for Autophagy in Isolated Rat Hepatocytes', *Journal of Biological Chemistry*, 270(5), pp. 2320–2326. doi: 10.1074/jbc.270.5.2320.

Boughan, P. K. *et al.* (2006) 'Nucleotide-binding Oligomerization Domain-1 and Epidermal Growth Factor Receptor: CRITICAL REGULATORS OF beta-DEFENSINS DURING HELICOBACTER PYLORI INFECTION', *Journal of Biological Chemistry*, 281(17), pp. 11637–11648. doi: 10.1074/jbc.M510275200.

Boxem, M. (2006) 'Cyclin-dependent kinases in C. elegans.', *Cell division*. BioMed Central, 1, p. 6. doi: 10.1186/1747-1028-1-6.

Brandeis, M. *et al.* (1998) ‘Cyclin B2-null mice develop normally and are fertile whereas cyclin B1-null mice die in utero.’, *Proceedings of the National Academy of Sciences of the United States of America*. National Academy of Sciences, 95(8), pp. 4344–9. doi: 10.1073/pnas.95.8.4344.

Brito, D. A. and Rieder, C. L. (2006) ‘Mitotic Checkpoint Slippage in Humans Occurs via Cyclin B Destruction in the Presence of an Active Checkpoint’, *Current Biology*. Cell Press, 16(12), pp. 1194–1200. doi: 10.1016/J.CUB.2006.04.043.

Brunn, G. J. *et al.* (1997) ‘The Mammalian Target of Rapamycin Phosphorylates Sites Having a (Ser/Thr)-Pro Motif and Is Activated by Antibodies to a Region near Its COOH Terminus’, *Journal of Biological Chemistry*, 272(51), pp. 32547–32550. doi: 10.1074/jbc.272.51.32547.

Cai, W. *et al.* (2016) ‘The GATOR2 Component Wdr24 Regulates TORC1 Activity and Lysosome Function’, *PLOS Genetics*. Edited by H. Kramer, 12(5), p. e1006036. doi: 10.1371/journal.pgen.1006036.

Capparelli, C. *et al.* (2012) ‘CDK inhibitors (p16/p19/p21) induce senescence and autophagy in cancer-associated fibroblasts, "fueling" tumor growth via paracrine interactions, without an increase in neo-angiogenesis.’, *Cell cycle (Georgetown, Tex.)*. Taylor & Francis, 11(19), pp. 3599–610. doi: 10.4161/cc.21884.

Carreira, S. *et al.* (2005) ‘Mitf cooperates with Rb1 and activates p21Cip1 expression to regulate cell cycle progression’, *Nature*. Nature Publishing Group, 433(7027), pp. 764–769. doi: 10.1038/nature03269.

Carriere, A. *et al.* (2011) ‘ERK1/2 Phosphorylate Raptor to Promote Ras-dependent Activation of mTOR Complex 1 (mTORC1)’, *Journal of Biological Chemistry*, 286(1), pp. 567–577. doi: 10.1074/jbc.M110.159046.

Carrière, A. *et al.* (2008) ‘Oncogenic MAPK Signaling Stimulates mTORC1 Activity by Promoting RSK-Mediated Raptor Phosphorylation’, *Current Biology*. Cell Press, 18(17), pp. 1269–1277.

Carroll, B. *et al.* (2016) ‘Control of TSC2-Rheb signaling axis by arginine regulates mTORC1 activity’, *eLife*, 5. doi: 10.7554/eLife.11058.

Casimiro, M. C. *et al.* (2017) ‘Cyclin D1 Restrains Oncogene-Induced Autophagy by Regulating the AMPK-LKB1 Signaling Axis.’, *Cancer research*. NIH Public Access, 77(13), pp. 3391–3405. doi: 10.1158/0008-5472.CAN-16-0425.

Castel, P. *et al.* (2016) ‘PDK1-SGK1 Signaling Sustains AKT-Independent mTORC1 Activation and Confers Resistance to PI3Kα Inhibition’, *Cancer Cell*, 30(2), pp. 229–242. doi: 10.1016/j.ccell.2016.06.004.

Catalano, M. *et al.* (2015) ‘Autophagy induction impairs migration and invasion by reversing EMT in glioblastoma cells’, *Molecular Oncology*, 9(8), pp. 1612–1625. doi: 10.1016/j.molonc.2015.04.016.

Caunt, C. J. *et al.* (2015) ‘MEK1 and MEK2 inhibitors and cancer therapy: the long and winding road’, *Nature Reviews Cancer*. Nature Research, 15(10), pp. 577–592. doi: 10.1038/nrc4000.

Chadebech, P. *et al.* (2000) ‘Up-regulation of cdc2 protein during paclitaxel-induced apoptosis’, *International Journal of Cancer*. John Wiley & Sons, Inc., 87(6), pp. 779–786. doi: 10.1002/1097-0215(20000915)87:6<779::AID-IJC3>3.0.CO;2-4.

Chalhoub, N. and Baker, S. J. (2009) ‘PTEN and the PI3-kinase pathway in cancer.’, *Annual review of pathology*. NIH Public Access, 4, pp. 127–50. doi: 10.1146/annurev.pathol.4.110807.092311.

Chang, D. C., Xu, N. and Luo, K. Q. (2003) ‘Degradation of Cyclin B Is Required for the Onset of Anaphase in Mammalian Cells’, *Journal of Biological Chemistry*, 278(39), pp. 37865–37873. doi: 10.1074/jbc.M306376200.

Chantranupong, L. *et al.* (2014) ‘The Sestrins Interact with GATOR2 to Negatively Regulate the Amino-Acid-Sensing Pathway Upstream of mTORC1’, *Cell Reports*, 9(1), pp. 1–8. doi: 10.1016/j.celrep.2014.09.014.

Chantranupong, L. *et al.* (2016) ‘The CASTOR Proteins Are Arginine Sensors for the mTORC1 Pathway’, *Cell*, 165(1), pp. 153–164. doi: 10.1016/j.cell.2016.02.035.

Chauhan, Santosh *et al.* (2013) ‘ZKSCAN3 is a master transcriptional repressor of autophagy’, *Molecular Cell*, 50(1), pp. 16–28. doi: 10.1016/j.molcel.2013.01.024.

Chen, C.-H. *et al.* (2011) ‘ER stress inhibits mTORC2 and Akt signaling through GSK-3β-mediated phosphorylation of rictor.’, *Science signaling*. American Association for the Advancement of Science, 4(161), p. ra10. doi: 10.1126/scisignal.2001731.

Chen, R. H., Sarnecki, C. and Blenis, J. (1992) 'Nuclear localization and regulation of erk- and rsk-encoded protein kinases.', *Molecular and cellular biology*, 12(3), pp. 915–27. doi: 10.1128/mcb.12.3.915.

Cheong, H. *et al.* (2011) 'Ammonia-induced autophagy is independent of ULK1/ULK2 kinases', *Proceedings of the National Academy of Sciences*, 108(27), pp. 11121–11126. doi: 10.1073/pnas.1107969108.

Chiang, G. G. and Abraham, R. T. (2005) 'Phosphorylation of Mammalian Target of Rapamycin (mTOR) at Ser-2448 Is Mediated by p70S6 Kinase', *Journal of Biological Chemistry*, 280(27), pp. 25485–25490. doi: 10.1074/jbc.M501707200.

Chresta, C. M. *et al.* (2010) 'AZD8055 Is a Potent, Selective, and Orally Bioavailable ATP-Competitive Mammalian Target of Rapamycin Kinase Inhibitor with In vitro and In vivo Antitumor Activity', *Cancer Research*, 70(1), pp. 288–298. doi: 10.1158/0008-5472.CAN-09-1751.

Colanzi, A. and Sütterlin, C. (2013) 'Signaling at the Golgi during mitosis.', *Methods in cell biology*. NIH Public Access, 118, pp. 383–400. doi: 10.1016/B978-0-12-417164-0.00023-9.

Comes, F. *et al.* (2007) 'A novel cell type-specific role of p38α in the control of autophagy and cell death in colorectal cancer cells', *Cell Death and Differentiation*. Nature Publishing Group, 14(4), pp. 693–702. doi: 10.1038/sj.cdd.4402076.

Cope, C. L. *et al.* (2014) 'Adaptation to mTOR kinase inhibitors by amplification of eIF4E to maintain cap-dependent translation', *Journal of Cell Science*, 127(4).

Copp, J., Manning, G. and Hunter, T. (2009) 'TORC-specific phosphorylation of mammalian target of rapamycin (mTOR): phospho-Ser2481 is a marker for intact mTOR signaling complex 2.', *Cancer research*. NIH Public Access, 69(5), pp. 1821–7. doi: 10.1158/0008-5472.CAN-08-3014.

Cormier, K. W. and Woodgett, J. R. (2017) 'Recent advances in understanding the cellular roles of GSK-3.', *F1000Research*. Faculty of 1000 Ltd, 6. doi: 10.12688/f1000research.10557.1.

Cornelis, S. *et al.* (2000) 'Identification and characterization of a novel cell cycle-regulated internal ribosome entry site.', *Molecular cell*. Elsevier, 5(4), pp. 597–605. doi: 10.1016/S1097-2765(00)80239-7.

Cortes, C. J. *et al.* (2014) 'Polyglutamine-expanded androgen receptor interferes with TFEB to elicit autophagy defects in SBMA', *Nature Neuroscience*, 17(9), pp. 1180–1189. doi: 10.1038/nn.3787.

Cross, D. A. E. *et al.* (1995) 'Inhibition of glycogen synthase kinase-3 by insulin mediated by protein kinase B', *Nature*. Nature Publishing Group, 378(6559), pp. 785–789. doi: 10.1038/378785a0.

Cundell, M. J. *et al.* (2016) 'A PP2A-B55 recognition signal controls substrate dephosphorylation kinetics during mitotic exit.', *The Journal of cell biology*. Rockefeller University Press, 214(5), pp. 539–54. doi: 10.1083/jcb.201606033.

Cybulski, N., Zinzalla, V. and Hall, M. N. (2012) 'Inducible raptor and rictor Knockout Mouse Embryonic Fibroblasts', in *Methods in molecular biology (Clifton, N.J.)*, pp. 267–278. doi: 10.1007/978-1-61779-430-8_16.

Daigle, N. *et al.* (2001) 'Nuclear pore complexes form immobile networks and have a very low turnover in live mammalian cells.', *The Journal of cell biology*. The Rockefeller University Press, 154(1), pp. 71–84. doi: 10.1083/jcb.200101089.

Dalby, K. N. *et al.* (1998) 'Identification of regulatory phosphorylation sites in mitogen-activated protein kinase (MAPK)-activated protein kinase-1a/p90rsk that are inducible by MAPK.', *The Journal of biological chemistry*. American Society for Biochemistry and Molecular Biology, 273(3), pp. 1496–505. doi: 10.1074/JBC.273.3.1496.

Dan, H. C. *et al.* (2014) 'Akt-dependent Activation of mTORC1 Complex Involves Phosphorylation of mTOR (Mammalian Target of Rapamycin) by IκB Kinase α (IKKα)', *Journal of Biological Chemistry*, 289(36), pp. 25227–25240. doi: 10.1074/jbc.M114.554881.

Davies, H. *et al.* (2002) 'Mutations of the BRAF gene in human cancer', *Nature*, 417(6892), pp. 949–954. doi: 10.1038/nature00766.

Davies, T. G. *et al.* (2002) 'Structure-based design of a potent purine-based cyclin-dependent kinase inhibitor', *Nature Structural Biology*. Nature Publishing Group, 9(10), pp. 745–749. doi: 10.1038/nsb842.

Dephoure, N. *et al.* (2008) 'A quantitative atlas of mitotic phosphorylation', *Proceedings of the*

National Academy of Sciences, 105(31), pp. 10762–10767. doi: 10.1073/pnas.0805139105.

Dhillon, A. S. *et al.* (2007) 'MAP kinase signalling pathways in cancer', *Oncogene*. Nature Publishing Group, 26(22), pp. 3279–3290. doi: 10.1038/sj.onc.1210421.

Dibble, C. C., Asara, J. M. and Manning, B. D. (2009) 'Characterization of Rictor phosphorylation sites reveals direct regulation of mTOR complex 2 by S6K1.', *Molecular and cellular biology*. American Society for Microbiology Journals, 29(21), pp. 5657–70. doi: 10.1128/MCB.00735-09.

Ding, V. W., Chen, R. H. and McCormick, F. (2000) 'Differential regulation of glycogen synthase kinase 3beta by insulin and Wnt signaling.', *The Journal of biological chemistry*. American Society for Biochemistry and Molecular Biology, 275(42), pp. 32475–81. doi: 10.1074/jbc.M005342200.

Dionne, L. K. *et al.* (2017) 'FYCO1 regulates accumulation of post-mitotic midbodies by mediating LC3-dependent midbody degradation', *Journal of Cell Science*, 130(23), pp. 4051–4062. doi: 10.1242/jcs.208983.

Diril, M. K. *et al.* (2012) 'Cyclin-dependent kinase 1 (Cdk1) is essential for cell division and suppression of DNA re-replication but not for liver regeneration', *Proceedings of the National Academy of Sciences*, 109(10), pp. 3826–3831. doi: 10.1073/pnas.1115201109.

Dohadwala, M. *et al.* (1994) 'Phosphorylation and inactivation of protein phosphatase 1 by cyclin-dependent kinases.', *Proceedings of the National Academy of Sciences*, 91(14), pp. 6408–6412. doi: 10.1073/pnas.91.14.6408.

Dokladda, K. *et al.* (2005) 'PD98059 and U0126 activate AMP-activated protein kinase by increasing the cellular AMP:ATP ratio and not via inhibition of the MAP kinase pathway', *FEBS Letters*, 579(1), pp. 236–240. doi: 10.1016/j.febslet.2004.11.084.

Doménech, E. *et al.* (2015) 'AMPK and PFKFB3 mediate glycolysis and survival in response to mitophagy during mitotic arrest', *Nature Cell Biology*, 17(10), pp. 1304–1316. doi: 10.1038/ncb3231.

Dooley, H. C. *et al.* (2014) 'WIPI2 links LC3 conjugation with PI3P, autophagosome formation, and pathogen clearance by recruiting Atg12-5-16L1.', *Molecular cell*. Elsevier, 55(2), pp. 238–52. doi: 10.1016/j.molcel.2014.05.021.

Dou, Z. *et al.* (2015) 'Autophagy mediates degradation of nuclear lamina.', *Nature*. NIH Public Access, 527(7576), pp. 105–9. doi: 10.1038/nature15548.

Dowdle, W. E. *et al.* (2014) 'Selective VPS34 inhibitor blocks autophagy and uncovers a role for NCOA4 in ferritin degradation and iron homeostasis in vivo.', *Nature cell biology*, 16(11), pp. 1069–79. doi: 10.1038/ncb3053.

Dudley, L. J. *et al.* (2019) ' Intrinsic lipid binding activity of ATG 16L1 supports efficient membrane anchoring and autophagy ', *The EMBO Journal*. EMBO, 38(9). doi: 10.15252/embj.2018100554.

Dultz, E. *et al.* (2008) 'Systematic kinetic analysis of mitotic dis- and reassembly of the nuclear pore in living cells', *The Journal of Cell Biology*, 180(5), pp. 857–865. doi: 10.1083/jcb.200707026.

Dunlop, E. A. *et al.* (2011) 'ULK1 inhibits mTORC1 signaling, promotes multisite Raptor phosphorylation and hinders substrate binding', *Autophagy*, 7(7), pp. 737–747. doi: 10.4161/auto.7.7.15491.

Ebner, M. *et al.* (2017) 'Localization of mTORC2 activity inside cells.', *The Journal of cell biology*. Rockefeller University Press, 216(2), pp. 343–353. doi: 10.1083/jcb.201610060.

Egan, D. F. *et al.* (2015) 'Small Molecule Inhibition of the Autophagy Kinase ULK1 and Identification of ULK1 Substrates', *Molecular Cell*, 59(2), pp. 285–297. doi: 10.1016/j.molcel.2015.05.031.

Eskelinen, E.-L. *et al.* (2002) 'Inhibition of autophagy in mitotic animal cells.', *Traffic (Copenhagen, Denmark)*, 3(12), pp. 878–93.

Evans, C. *et al.* (2013) 'MEK Inhibitor U0126 Reverses Protection of Axons from Wallerian Degeneration Independently of MEK–ERK Signaling', *PLoS ONE*. Edited by K. Arai, 8(10), p. e76505. doi: 10.1371/journal.pone.0076505.

Fawal, M.-A., Brandt, M. and Djouder, N. (2015) 'MCRS1 Binds and Couples Rheb to Amino Acid-Dependent mTORC1 Activation', *Developmental Cell*, 33(1), pp. 67–81. doi: 10.1016/j.devcel.2015.02.010.

Fazeli, G. *et al.* (2016) 'C. elegans midbodies are released, phagocytosed and undergo LC3-dependent degradation independent of macroautophagy.', *Journal of cell science*. Company of Biologists, 129(20), pp. 3721–3731. doi: 10.1242/jcs.190223.

Feldman, M. E. *et al.* (2009) 'Active-Site Inhibitors of mTOR Target Rapamycin-Resistant Outputs of mTORC1 and mTORC2', *PLoS Biology*. Edited by T. Hunter, 7(2), p. e1000038. doi: 10.1371/journal.pbio.1000038.

Feng, Y. *et al.* (2013) 'The machinery of macroautophagy', *Cell Research, Published online: 24 December 2013;* | *doi:10.1038/cr.2013.168*. Nature Publishing Group, 24(1), p. 24. doi: 10.1038/cr.2013.168.

Ferron, M. *et al.* (2013) 'A RANKL-PKCβ-TFEB signaling cascade is necessary for lysosomal biogenesis in osteoclasts.', *Genes & development*. Cold Spring Harbor Laboratory Press, 27(8), pp. 955–69. doi: 10.1101/gad.213827.113.

Findlay, G. M. *et al.* (2007) 'A MAP4 kinase related to Ste20 is a nutrient-sensitive regulator of mTOR signalling.', *The Biochemical journal*. Portland Press Ltd, 403(1), pp. 13–20. doi: 10.1042/BJ20061881.

Fingar, D. C. *et al.* (2004) 'mTOR controls cell cycle progression through its cell growth effectors S6K1 and 4E-BP1/eukaryotic translation initiation factor 4E.', *Molecular and cellular biology*. American Society for Microbiology (ASM), 24(1), pp. 200–16. doi: 10.1128/mcb.24.1.200-216.2004.

Fingar, D. C. and Blenis, J. (2004) 'Target of rapamycin (TOR): an integrator of nutrient and growth factor signals and coordinator of cell growth and cell cycle progression', *Oncogene*. Nature Publishing Group, 23(18), pp. 3151–3171. doi: 10.1038/sj.onc.1207542.

Fletcher, K. *et al.* (2018) 'The WD40 domain of ATG16L1 is required for its non-canonical role in lipidation of LC3 at single membranes.', *The EMBO journal*. European Molecular Biology Organization, 37(4). doi: 10.15252/embj.201797840.

Florey, O. *et al.* (2011) 'Autophagy machinery mediates macroendocytic processing and entotic cell death by targeting single membranes.', *Nature cell biology*. NIH Public Access, 13(11), pp. 1335–43. doi: 10.1038/ncb2363.

Foster, K. G. *et al.* (2010) 'Regulation of mTOR Complex 1 (mTORC1) by Raptor Ser ^{863} and Multisite Phosphorylation', *Journal of Biological Chemistry*, 285(1), pp. 80–94. doi: 10.1074/jbc.M109.029637.

Franco, J. *et al.* (2016) 'Metabolic Reprogramming of Pancreatic Cancer Mediated by CDK4/6 Inhibition Elicits Unique Vulnerabilities.', *Cell reports*. NIH Public Access, 14(5), pp. 979–90. doi: 10.1016/j.celrep.2015.12.094.

Freeman, M. R. *et al.* (2011) 'A metabolic perturbation by U0126 identifies a role for glutamine in resveratrol-induced cell death.', *Cancer biology & therapy*. Taylor & Francis, 12(11), pp. 966–77. doi: 10.4161/cbt.12.11.18136.

Fujita, N. *et al.* (2008) 'The Atg16L complex specifies the site of LC3 lipidation for membrane biogenesis in autophagy.', *Molecular biology of the cell*. American Society for Cell Biology, 19(5), pp. 2092–100. doi: 10.1091/mbc.E07-12-1257.

Furuya, T. *et al.* (2010) 'Negative regulation of Vps34 by Cdk mediated phosphorylation.', *Molecular cell*. NIH Public Access, 38(4), pp. 500–11. doi: 10.1016/j.molcel.2010.05.009.

Gammoh, N. *et al.* (2013) 'Interaction between FIP200 and ATG16L1 distinguishes ULK1 complex-dependent and -independent autophagy.', *Nature structural & molecular biology*. NIH Public Access, 20(2), pp. 144–9. doi: 10.1038/nsmb.2475.

Ganley, I. G. *et al.* (2009) 'ULK1.ATG13.FIP200 complex mediates mTOR signaling and is essential for autophagy.', *The Journal of biological chemistry*. American Society for Biochemistry and Molecular Biology, 284(18), pp. 12297–305. doi: 10.1074/jbc.M900573200.

Ganley, I. G. (2013) '6 Autophagosome maturation and lysosomal fusion', *Essays Biochem*, 55, pp. 65–78. doi: 10.1042/BSE0550065.

Gao, N. *et al.* (2003) 'Role of PI3K/AKT/mTOR signaling in the cell cycle progression of human prostate cancer', *Biochemical and Biophysical Research Communications*, 310(4), pp. 1124–1132. doi: 10.1016/j.bbrc.2003.09.132.

Gao, X. *et al.* (2002) 'Tsc tumour suppressor proteins antagonize amino-acid–TOR signalling', *Nature Cell Biology*, 4(9), pp. 699–704. doi: 10.1038/ncb847.

Garami, A. *et al.* (2003) 'Insulin activation of Rheb, a mediator of mTOR/S6K/4E-BP signaling, is inhibited by TSC1 and 2.', *Molecular cell*, 11(6), pp. 1457–66.

García-Martínez, J. M. and Alessi, D. R. (2008) 'mTOR complex 2 (mTORC2) controls hydrophobic

motif phosphorylation and activation of serum- and glucocorticoid-induced protein kinase 1 (SGK1)', *Biochemical Journal*, 416(3), pp. 375–385. doi: 10.1042/BJ20081668.

Garner, A. P. *et al.* (2002) 'ΔMEKK3:ER* activation induces a p38α/β2-dependent cell cycle arrest at the G2 checkpoint', *Oncogene*. Nature Publishing Group, 21(53), pp. 8089–8104. doi: 10.1038/sj.onc.1206000.

Gaullier, J.-M. *et al.* (1998) 'FYVE fingers bind PtdIns(3)P', *Nature*, 394(6692), pp. 432–433. doi: 10.1038/28767.

Gautier, J. *et al.* (1991) 'cdc25 is a specific tyrosine phosphatase that directly activates p34cdc2.', *Cell*, 67(1), pp. 197–211.

Gavet, O. and Pines, J. (2010a) 'Activation of cyclin B1-Cdk1 synchronizes events in the nucleus and the cytoplasm at mitosis.', *The Journal of cell biology*. Rockefeller University Press, 189(2), pp. 247–59. doi: 10.1083/jcb.200909144.

Gavet, O. and Pines, J. (2010b) 'Progressive activation of CyclinB1-Cdk1 coordinates entry to mitosis', *Developmental cell*. Europe PMC Funders, 18(4), p. 533. doi: 10.1016/J.DEVCEL.2010.02.013.

Gelbert, L. M. *et al.* (2014) 'Preclinical characterization of the CDK4/6 inhibitor LY2835219: in-vivo cell cycle-dependent/independent anti-tumor activities alone/in combination with gemcitabine.', *Investigational new drugs*. Springer, 32(5), pp. 825–37. doi: 10.1007/s10637-014-0120-7.

Giangrande, P. H. *et al.* (2003) 'Identification of E-box factor TFE3 as a functional partner for the E2F3 transcription factor.', *Molecular and cellular biology*. American Society for Microbiology (ASM), 23(11), pp. 3707–20. doi: 10.1128/mcb.23.11.3707-3720.2003.

Giatromanolaki, A. *et al.* (2015) 'Increased expression of transcription factor EB (TFEB) is associated with autophagy, migratory phenotype and poor prognosis in non-small cell lung cancer', *Lung Cancer*, 90(1), pp. 98–105. doi: 10.1016/j.lungcan.2015.07.008.

Gilley, R. *et al.* (2012) 'CDK1, not ERK1/2 or ERK5, is required for mitotic phosphorylation of BIMEL', *Cellular Signalling*, 24(1), pp. 170–180. doi: 10.1016/j.cellsig.2011.08.018.

Gingras, A.-C. *et al.* (1999) 'Regulation of 4E-BP1 phosphorylation: a novel two-step mechanism', *Genes & Development*, 13(11), pp. 1422–1437. doi: 10.1101/gad.13.11.1422.

Gingras, A. C. *et al.* (1996) 'Activation of the translational suppressor 4E-BP1 following infection with encephalomyocarditis virus and poliovirus.', *Proceedings of the National Academy of Sciences*, 93(11), pp. 5578–5583. doi: 10.1073/pnas.93.11.5578.

Gkotinakou, I.-M. *et al.* (2019) 'ERK1/2 phosphorylates HIF-2α and regulates its activity by controlling its CRM1-dependent nuclear shuttling', *Journal of Cell Science*, 132(7), p. jcs225698. doi: 10.1242/jcs.225698.

Gonzalez, L. M., Moeser, A. J. and Blikslager, A. T. (2015) 'Animal models of ischemia-reperfusion-induced intestinal injury: progress and promise for translational research.', *American journal of physiology. Gastrointestinal and liver physiology*. American Physiological Society, 308(2), pp. G63-75. doi: 10.1152/ajpgi.00112.2013.

Goorden, S. M. I. *et al.* (2011) 'Rheb is essential for murine development.', *Molecular and cellular biology*. American Society for Microbiology (ASM), 31(8), pp. 1672–8. doi: 10.1128/MCB.00985-10.

Gould, K. L. and Nurse, P. (1989) 'Tyrosine phosphorylation of the fission yeast cdc2+ protein kinase regulates entry into mitosis', *Nature*, 342(6245), pp. 39–45. doi: 10.1038/342039a0.

Grallert, A. *et al.* (2015) 'A PP1–PP2A phosphatase relay controls mitotic progression', *Nature*, 517(7532), pp. 94–98. doi: 10.1038/nature14019.

Greenberg, V. L. and Zimmer, S. G. (2005) 'Paclitaxel induces the phosphorylation of the eukaryotic translation initiation factor 4E-binding protein 1 through a Cdk1-dependent mechanism', *Oncogene*. Nature Publishing Group, 24(30), pp. 4851–4860. doi: 10.1038/sj.onc.1208624.

Grunwald, D. S. *et al.* (2019) 'GABARAPs and LC3s have opposite roles in regulating ULK1 for autophagy induction', *Autophagy*. Taylor and Francis Inc. doi: 10.1080/15548627.2019.1632620.

Güttinger, S., Laurell, E. and Kutay, U. (2009) 'Orchestrating nuclear envelope disassembly and reassembly during mitosis', *Nature Reviews Molecular Cell Biology*. Nature Publishing Group, 10(3), pp. 178–191. doi: 10.1038/nrm2641.

Gwinn, D. M. *et al.* (2008) 'AMPK phosphorylation of raptor mediates a metabolic checkpoint.', *Molecular cell*, 30(2), pp. 214–26. doi: 10.1016/j.molcel.2008.03.003.

Gwinn, D. M., Asara, J. M. and Shaw, R. J. (2010) 'Raptor is Phosphorylated by cdc2 during

Mitosis', *PLoS ONE*. Edited by M. Kaeberlein, 5(2), p. e9197. doi: 10.1371/journal.pone.0009197.

Halilovic, E. *et al.* (2010) 'PIK3CA Mutation Uncouples Tumor Growth and Cyclin D1 Regulation from MEK/ERK and Mutant KRAS Signaling', *Cancer Research*, 70(17), pp. 6804–6814. doi: 10.1158/0008-5472.CAN-10-0409.

Hálová, L. *et al.* (2013) 'Phosphorylation of the TOR ATP binding domain by AGC kinase constitutes a novel mode of TOR inhibition.', *The Journal of cell biology*. Rockefeller University Press, 203(4), pp. 595–604. doi: 10.1083/jcb.201305103.

Han, J. M. *et al.* (2012) 'Leucyl-tRNA Synthetase Is an Intracellular Leucine Sensor for the mTORC1-Signaling Pathway', *Cell*, 149(2), pp. 410–424. doi: 10.1016/j.cell.2012.02.044.

Hao, F. *et al.* (2017) 'Rheb localized on the Golgi membrane activates lysosome-localized mTORC1 at the Golgi-lysosome contact site', *Journal of Cell Science*, 131(3), p. jcs.208017. doi: 10.1242/jcs.208017.

Haq, R. *et al.* (2013) 'BCL2A1 is a lineage-specific antiapoptotic melanoma oncogene that confers resistance to BRAF inhibition', *Proceedings of the National Academy of Sciences*, 110(11), pp. 4321–4326. doi: 10.1073/pnas.1205575110.

Hara, T. *et al.* (2008) 'FIP200, a ULK-interacting protein, is required for autophagosome formation in mammalian cells.', *The Journal of cell biology*, 181(3), pp. 497–510. doi: 10.1083/jcb.200712064.

Hawley, S. A. *et al.* (2003) 'Complexes between the LKB1 tumor suppressor, STRAD alpha/beta and MO25 alpha/beta are upstream kinases in the AMP-activated protein kinase cascade.', *Journal of Biology*, 2(4), p. 28. doi: 10.1186/1475-4924-2-28.

Haystead, T. A. J. *et al.* (1992) 'Ordered phosphorylation of p42 ^{mapk} by MAP kinase kinase', *FEBS Letters*, 306(1), pp. 17–22. doi: 10.1016/0014-5793(92)80828-5.

He, H. *et al.* (2003) 'Post-translational modifications of three members of the human MAP1LC3 family and detection of a novel type of modification for MAP1LC3B', *Journal of Biological Chemistry*, 278(31), pp. 29278–29287. doi: 10.1074/jbc.M303800200.

Heald, R. and McKeon, F. (1990) 'Mutations of phosphorylation sites in lamin A that prevent nuclear lamina disassembly in mitosis.', *Cell*, 61(4), pp. 579–89.

Heesom, K. J. *et al.* (2001) 'Cell cycle-dependent phosphorylation of the translational repressor eIF-4E binding protein-1 (4E-BP1).', *Current biology : CB*, 11(17), pp. 1374–9.

Hellmich, M. R. *et al.* (1992) 'Neuronal cdc2-like kinase: a cdc2-related protein kinase with predominantly neuronal expression.', *Proceedings of the National Academy of Sciences*, 89(22), pp. 10867–10871. doi: 10.1073/pnas.89.22.10867.

Hemesath, T. J. *et al.* (1994) 'microphthalmia, a critical factor in melanocyte development, defines a discrete transcription factor family.', *Genes & development*, 8(22), pp. 2770–80.

Hemesath, T. J. *et al.* (1998) 'MAP kinase links the transcription factor Microphthalmia to c-Kit signalling in melanocytes', *Nature*, 391(6664), pp. 298–301. doi: 10.1038/34681.

Hendzel, M. J. *et al.* (1997) 'Mitosis-specific phosphorylation of histone H3 initiates primarily within pericentromeric heterochromatin during G2 and spreads in an ordered fashion coincident with mitotic chromosome condensation.', *Chromosoma*, 106(6), pp. 348–60.

van den Heuvel, S. and Harlow, E. (1993) 'Distinct roles for cyclin-dependent kinases in cell cycle control.', *Science (New York, N.Y.)*, 262(5142), pp. 2050–4.

Holz, M. K. *et al.* (2005) 'mTOR and S6K1 Mediate Assembly of the Translation Preinitiation Complex through Dynamic Protein Interchange and Ordered Phosphorylation Events', *Cell*, 123(4), pp. 569–580. doi: 10.1016/j.cell.2005.10.024.

Holz, M. K. and Blenis, J. (2005) 'Identification of S6 Kinase 1 as a Novel Mammalian Target of Rapamycin (mTOR)-phosphorylating Kinase', *Journal of Biological Chemistry*, 280(28), pp. 26089–26093. doi: 10.1074/jbc.M504045200.

Hong, F. *et al.* (2008) 'mTOR-Raptor Binds and Activates SGK1 to Regulate p27 Phosphorylation', *Molecular Cell*, 30(6), pp. 701–711. doi: 10.1016/j.molcel.2008.04.027.

Hong, S.-P. *et al.* (2003) 'Activation of yeast Snf1 and mammalian AMP-activated protein kinase by upstream kinases', *Proceedings of the National Academy of Sciences*, 100(15), pp. 8839–8843. doi: 10.1073/pnas.1533136100.

Horikawa, I. *et al.* (2014) 'Autophagic degradation of the inhibitory p53 isoform Δ133p53α as a regulatory mechanism for p53-mediated senescence', *Nature Communications*, 5(1), p. 4706. doi:

10.1038/ncomms5706.

Horman, S. *et al.* (2006) 'Insulin antagonizes ischemia-induced Thr172 phosphorylation of AMP-activated protein kinase alpha-subunits in heart via hierarchical phosphorylation of Ser485/491.', *The Journal of biological chemistry*. American Society for Biochemistry and Molecular Biology, 281(9), pp. 5335–40. doi: 10.1074/jbc.M506850200.

Hosokawa, N., Sasaki, T., *et al.* (2009) 'Atg101, a novel mammalian autophagy protein interacting with Atg13.', *Autophagy*, 5(7), pp. 973–9. doi: 10.4161/auto.5.7.9296.

Hosokawa, N., Hara, T., *et al.* (2009) 'Nutrient-dependent mTORC1 association with the ULK1-Atg13-FIP200 complex required for autophagy.', *Molecular biology of the cell*, 20(7), pp. 1981–91. doi: 10.1091/mbc.E08-12-1248.

Hsu, C. L. *et al.* (2018) 'MAP4K3 mediates amino acid-dependent regulation of autophagy via phosphorylation of TFEB', *Nature Communications*. Nature Publishing Group, 9(1), p. 942. doi: 10.1038/s41467-018-03340-7.

Hsu, P. P. *et al.* (2011) 'The mTOR-regulated phosphoproteome reveals a mechanism of mTORC1-mediated inhibition of growth factor signaling.', *Science (New York, N.Y.)*. NIH Public Access, 332(6035), pp. 1317–22. doi: 10.1126/science.1199498.

Huang, J. and Manning, B. D. (2008) 'The TSC1-TSC2 complex: a molecular switchboard controlling cell growth.', *The Biochemical journal*. NIH Public Access, 412(2), pp. 179–90. doi: 10.1042/BJ20080281.

Ilic, N. *et al.* (2011) 'PI3K-targeted therapy can be evaded by gene amplification along the MYC-eukaryotic translation initiation factor 4E (eIF4E) axis.', *Proceedings of the National Academy of Sciences of the United States of America*. National Academy of Sciences, 108(37), pp. E699-708. doi: 10.1073/pnas.1108237108.

Impey, S. *et al.* (1998) 'Cross Talk between ERK and PKA Is Required for Ca2+ Stimulation of CREB-Dependent Transcription and ERK Nuclear Translocation', *Neuron*, 21(4), pp. 869–883. doi: 10.1016/S0896-6273(00)80602-9.

Inoki, K. *et al.* (2002) 'TSC2 is phosphorylated and inhibited by Akt and suppresses mTOR signalling.', *Nature cell biology*, 4(9), pp. 648–57. doi: 10.1038/ncb839.

Inoki, K. *et al.* (2003) 'Rheb GTPase is a direct target of TSC2 GAP activity and regulates mTOR signaling.', *Genes & development*, 17(15), pp. 1829–34. doi: 10.1101/gad.1110003.

Inoki, K. *et al.* (2006) 'TSC2 Integrates Wnt and Energy Signals via a Coordinated Phosphorylation by AMPK and GSK3 to Regulate Cell Growth', *Cell*, 126(5), pp. 955–968. doi: 10.1016/j.cell.2006.06.055.

Inoki, K., Zhu, T. and Guan, K.-L. (2003) 'TSC2 mediates cellular energy response to control cell growth and survival.', *Cell*, 115(5), pp. 577–90. doi: 10.1016/S0092-8674(03)00929-2.

Itakura, E. *et al.* (2008) 'Beclin 1 Forms Two Distinct Phosphatidylinositol 3-Kinase Complexes with Mammalian Atg14 and UVRAG', *Molecular Biology of the Cell*. Edited by S. Subramani, 19(12), pp. 5360–5372. doi: 10.1091/mbc.e08-01-0080.

Itakura, E., Kishi-Itakura, C. and Mizushima, N. (2012) 'The Hairpin-type Tail-Anchored SNARE Syntaxin 17 Targets to Autophagosomes for Fusion with Endosomes/Lysosomes', *Cell*, 151(6), pp. 1256–1269. doi: 10.1016/j.cell.2012.11.001.

Itakura, E. and Mizushima, N. (2010) 'Characterization of autophagosome formation site by a hierarchical analysis of mammalian Atg proteins.', *Autophagy*, 6(6), pp. 764–76.

Jaber, N. *et al.* (2012) 'Class III PI3K Vps34 plays an essential role in autophagy and in heart and liver function.', *Proceedings of the National Academy of Sciences of the United States of America*. National Academy of Sciences, 109(6), pp. 2003–8. doi: 10.1073/pnas.1112848109.

Jacobs, J. P., Jones, C. M. and Baille, J. P. (1970) 'Characteristics of a human diploid cell designated MRC-5.', *Nature*, 227(5254), pp. 168–70.

Jacquin, E. *et al.* (2017) 'Pharmacological modulators of autophagy activate a parallel noncanonical pathway driving unconventional LC3 lipidation', *Autophagy*, 13(5), pp. 854–867. doi: 10.1080/15548627.2017.1287653.

Jakhar, R. *et al.* (2018) 'Autophagy Governs Protumorigenic Effects of Mitotic Slippage–induced Senescence', *Molecular Cancer Research*, 16(11), pp. 1625–1640. doi: 10.1158/1541-7786.MCR-18-0024.

Jean, S. and Kiger, A. A. (2014) 'Classes of phosphoinositide 3-kinases at a glance.', *Journal of*

cell science. Company of Biologists, 127(Pt 5), pp. 923–8. doi: 10.1242/jcs.093773.

Jeong, E. *et al.* (2018) 'The transcription factors TFE3 and TFEB amplify p53 dependent transcriptional programs in response to DNA damage', *eLife*, 7. doi: 10.7554/eLife.40856.

Jiang, P. *et al.* (2014) 'The HOPS complex mediates autophagosome-lysosome fusion through interaction with syntaxin 17.', *Molecular biology of the cell*. American Society for Cell Biology, 25(8), pp. 1327–37. doi: 10.1091/mbc.E13-08-0447.

Johansen, T. and Lamark, T. (2019) 'Selective Autophagy: ATG8 Family Proteins, LIR Motifs and Cargo Receptors', *Journal of Molecular Biology*. Academic Press. doi: 10.1016/J.JMB.2019.07.016.

Johnson, G. L. and Lapadat, R. (2002) 'Mitogen-activated protein kinase pathways mediated by ERK, JNK, and p38 protein kinases.', *Science (New York, N.Y.)*. American Association for the Advancement of Science, 298(5600), pp. 1911–2. doi: 10.1126/science.1072682.

Jung, C. H. *et al.* (2009) 'ULK-Atg13-FIP200 complexes mediate mTOR signaling to the autophagy machinery.', *Molecular biology of the cell*. American Society for Cell Biology, 20(7), pp. 1992–2003. doi: 10.1091/mbc.E08-12-1249.

Jung, C. H. *et al.* (2011) 'ULK1 inhibits the kinase activity of mTORC1 and cell proliferation', *Autophagy*, 7(10), pp. 1212–1221. doi: 10.4161/auto.7.10.16660.

Kachaner, D. *et al.* (2012) 'Plk1-Dependent Phosphorylation of Optineurin Provides a Negative Feedback Mechanism for Mitotic Progression', *Molecular Cell*, 45(4), pp. 553–566. doi: 10.1016/j.molcel.2011.12.030.

Kamada, Y. *et al.* (2000) 'Tor-Mediated Induction of Autophagy via an Apg1 Protein Kinase Complex', *The Journal of Cell Biology*, 150(6).

Kamber, R. A., Shoemaker, C. J. and Denic, V. (2015) 'Receptor-Bound Targets of Selective Autophagy Use a Scaffold Protein to Activate the Atg1 Kinase', *Molecular Cell*. Cell Press, 59(3), pp. 372–381. doi: 10.1016/J.MOLCEL.2015.06.009.

Kang, H. T. *et al.* (2011) 'Autophagy Impairment Induces Premature Senescence in Primary Human Fibroblasts', *PLoS ONE*. Edited by A. T. Y. Lau, 6(8), p. e23367. doi: 10.1371/journal.pone.0023367.

Kang, S. A. *et al.* (2013) 'mTORC1 phosphorylation sites encode their sensitivity to starvation and rapamycin.', *Science (New York, N.Y.)*. NIH Public Access, 341(6144), p. 1236566. doi: 10.1126/science.1236566.

Karanasios, E. *et al.* (2013) 'Dynamic association of the ULK1 complex with omegasomes during autophagy induction', *Journal of Cell Science*, 126(22), pp. 5224–5238. doi: 10.1242/jcs.132415.

Kauffman, E. C. *et al.* (2014) 'Molecular genetics and cellular features of TFE3 and TFEB fusion kidney cancers', *Nature Reviews. Urology*, 11(8), pp. 465–475. doi: 10.1038/nrurol.2014.162.

Kazyken, D. *et al.* (2014) 'The nuclear import of ribosomal proteins is regulated by mTOR', *Oncotarget*. Impact Journals, 5(20), pp. 9577–9593. doi: 10.18632/oncotarget.2473.

Kim, D.-H. *et al.* (2003) 'GβL, a Positive Regulator of the Rapamycin-Sensitive Pathway Required for the Nutrient-Sensitive Interaction between Raptor and mTOR', *Molecular Cell*, 11(4), pp. 895–904. doi: 10.1016/S1097-2765(03)00114-X.

Kim, D. H. *et al.* (2002) 'mTOR interacts with raptor to form a nutrient-sensitive complex that signals to the cell growth machinery', *Cell*, 110(2), pp. 163–175. doi: 10.1016/S0092-8674(02)00808-5.

Kim, E. *et al.* (2008) 'Regulation of TORC1 by Rag GTPases in nutrient response.', *Nature cell biology*. NIH Public Access, 10(8), pp. 935–45. doi: 10.1038/ncb1753.

Kim, J.-H. *et al.* (2014) 'Raf/MEK/ERK can regulate cellular levels of LC3B and SQSTM1/p62 at expression levels', *Experimental Cell Research*, 327(2), pp. 340–352. doi: 10.1016/j.yexcr.2014.08.001.

Kim, J. *et al.* (2011) 'AMPK and mTOR regulate autophagy through direct phosphorylation of Ulk1', *Nature Cell Biology*, 13(2), pp. 132–141. doi: 10.1038/ncb2152.

Kim, J. *et al.* (2013) 'Differential regulation of distinct Vps34 complexes by AMPK in nutrient stress and autophagy.', *Cell*. NIH Public Access, 152(1–2), pp. 290–303. doi: 10.1016/j.cell.2012.12.016.

Kim, Y.-M. *et al.* (2015) 'mTORC1 Phosphorylates UVRAG to Negatively Regulate Autophagosome and Endosome Maturation', *Molecular Cell*, 57(2), pp. 207–218. doi: 10.1016/j.molcel.2014.11.013.

Kimura, S., Noda, T. and Yoshimori, T. (no date) 'Dissection of the autophagosome maturation process by a novel reporter protein, tandem fluorescent-tagged LC3.', *Autophagy*, 3(5), pp. 452–60.

Klein, K. *et al.* (2016) 'Role of TFEB-driven autophagy regulation in pancreatic cancer treatment', *International Journal of Oncology*, 49(1), pp. 164–72. doi: 10.3892/ijo.2016.3505.

Klionsky, D. J. *et al.* (2008) 'Does bafilomycin A1 block the fusion of autophagosomes with lysosomes?', *Autophagy*, 4(7), pp. 849–50. doi: 10.4161/auto.6845.

Klionsky, D. J. *et al.* (2016) 'Guidelines for the use and interpretation of assays for monitoring autophagy (3rd edition)', *Autophagy*, 12(1), pp. 1–222. doi: 10.1080/15548627.2015.1100356.

Knudsen, E. S. *et al.* (2017) 'Biological specificity of CDK4/6 inhibitors: dose response relationship, <i>in vivo</i> signaling, and composite response signature', *Oncotarget*. doi: 10.18632/oncotarget.18435.

Kolch, W. (2000) 'Meaningful relationships: the regulation of the Ras/Raf/MEK/ERK pathway by protein interactions.', *The Biochemical journal*, 351 Pt 2, pp. 289–305.

Koo, J. *et al.* (2015) 'Rictor Undergoes Glycogen Synthase Kinase 3 (GSK3)-dependent, FBXW7-mediated Ubiquitination and Proteasomal Degradation.', *The Journal of biological chemistry*. American Society for Biochemistry and Molecular Biology, 290(22), pp. 14120–9. doi: 10.1074/jbc.M114.633057.

Koren, I., Reem, E. and Kimchi, A. (2010) 'DAP1, a Novel Substrate of mTOR, Negatively Regulates Autophagy', *Current Biology*, 20(12), pp. 1093–1098. doi: 10.1016/j.cub.2010.04.041.

Korolchuk, V. I. *et al.* (2011) 'Lysosomal positioning coordinates cellular nutrient responses', *Nature Cell Biology*, 13(4), pp. 453–460. doi: 10.1038/ncb2204.

Kotani, T. *et al.* (2018) 'The Atg2-Atg18 complex tethers pre-autophagosomal membranes to the endoplasmic reticulum for autophagosome formation', *Proceedings of the National Academy of Sciences of the United States of America*. National Academy of Sciences, 115(41), pp. 10363–10368. doi: 10.1073/pnas.1806727115.

Koyama-Honda, I. *et al.* (2013) 'Temporal analysis of recruitment of mammalian ATG proteins to the autophagosome formation site', *Autophagy*, 9(10), pp. 1491–1499. doi: 10.4161/auto.25529.

Kraft, C. *et al.* (2012) 'Binding of the Atg1/ULK1 kinase to the ubiquitin-like protein Atg8 regulates autophagy.', *The EMBO journal*. European Molecular Biology Organization, 31(18), pp. 3691–703. doi: 10.1038/emboj.2012.225.

Krieg, J., Hofsteenge, J. and Thomas, G. (1988) 'Identification of the 40 S ribosomal protein S6 phosphorylation sites induced by cycloheximide.', *The Journal of biological chemistry*, 263(23), pp. 11473–7.

Kristensen, A. R. *et al.* (2008) 'Ordered Organelle Degradation during Starvation-induced Autophagy', *Molecular & Cellular Proteomics*, 7(12), pp. 2419–2428. doi: 10.1074/mcp.M800184-MCP200.

Ku, B. M. *et al.* (2016) 'The CDK4/6 inhibitor LY2835219 has potent activity in combination with mTOR inhibitor in head and neck squamous cell carcinoma', *Oncotarget*. Impact Journals, 7(12), pp. 14803–14813. doi: 10.18632/oncotarget.7543.

Kuma, A. (2002) 'Formation of the 350-kDa Apg12-Apg5middle dotApg16 Multimeric Complex, Mediated by Apg16 Oligomerization, Is Essential for Autophagy in Yeast', *Journal of Biological Chemistry*, 277(21), pp. 18619–18625. doi: 10.1074/jbc.M111889200.

Kuma, A., Matsui, M. and Mizushima, N. (no date) 'LC3, an autophagosome marker, can be incorporated into protein aggregates independent of autophagy: caution in the interpretation of LC3 localization.', *Autophagy*, 3(4), pp. 323–8.

Kuo, T.-C. *et al.* (2011) 'Midbody accumulation through evasion of autophagy contributes to cellular reprogramming and tumorigenicity', *Nature Cell Biology*, 13(10), pp. 1214–1223. doi: 10.1038/ncb2332.

Kwak, D. *et al.* (2012) 'Osmotic Stress Regulates Mammalian Target of Rapamycin (mTOR) Complex 1 via c-Jun N-terminal Kinase (JNK)-mediated Raptor Protein Phosphorylation', *Journal of Biological Chemistry*, 287(22), pp. 18398–18407. doi: 10.1074/jbc.M111.326538.

Kwon, Y. *et al.* (2017) 'Autophagy Is Pro-Senescence When Seen in Close-Up, but Anti-Senescence in Long-Shot.', *Molecules and cells*. Korean Society for Molecular and Cellular Biology, 40(9), pp. 607–612. doi: 10.14348/molcells.2017.0151.

de la Cruz-Morcillo, M. A. *et al.* (2012) 'P38MAPK is a major determinant of the balance between apoptosis and autophagy triggered by 5-fluorouracil: implication in resistance', *Oncogene*. Nature Publishing Group, 31(9), pp. 1073–1085. doi: 10.1038/onc.2011.321.

Lai, K.-O. *et al.* (2015) 'Cyclin-dependent Kinase 5 (Cdk5)-dependent Phosphorylation of p70 Ribosomal S6 Kinase 1 (S6K) Is Required for Dendritic Spine Morphogenesis', *Journal of Biological Chemistry*, 290(23), pp. 14637–14646. doi: 10.1074/jbc.M114.627117.

Lamb, C. A., Yoshimori, T. and Tooze, S. A. (2013) 'The autophagosome: Origins unknown, biogenesis complex', *Nature Reviews Molecular Cell Biology*, pp. 759–774. doi: 10.1038/nrm3696.

Lara-Gonzalez, P., Westhorpe, F. G. and Taylor, S. S. (2012) 'The Spindle Assembly Checkpoint', *Current Biology*. Cell Press, 22(22), pp. R966–R980. doi: 10.1016/J.CUB.2012.10.006.

Larochelle, S. *et al.* (2007) 'Requirements for Cdk7 in the assembly of Cdk1/cyclin B and activation of Cdk2 revealed by chemical genetics in human cells.', *Molecular cell*. NIH Public Access, 25(6), pp. 839–50. doi: 10.1016/j.molcel.2007.02.003.

Le, X.-F. *et al.* (2003) 'Paclitaxel induces inactivation of p70 S6 kinase and phosphorylation of Thr421 and Ser424 via multiple signaling pathways in mitosis1', *Oncogene*. Nature Publishing Group, 22(4), pp. 484–497. doi: 10.1038/sj.onc.1206175.

Lee, D.-F. *et al.* (2007) 'IKKβ Suppression of TSC1 Links Inflammation and Tumor Angiogenesis via the mTOR Pathway', *Cell*, 130(3), pp. 440–455. doi: 10.1016/j.cell.2007.05.058.

Lee, K. M., Choi, K. H. and Ouellette, M. M. (2004) 'Use of exogenous hTERT to immortalize primary human cells.', *Cytotechnology*. Springer, 45(1–2), pp. 33–8. doi: 10.1007/10.1007/s10616-004-5123-3.

Levy, C., Khaled, M. and Fisher, D. E. (2006) 'MITF: master regulator of melanocyte development and melanoma oncogene', *Trends in Molecular Medicine*, 12(9), pp. 406–414. doi: 10.1016/j.molmed.2006.07.008.

Levy, J. M. M., Towers, C. G. and Thorburn, A. (2017) 'Targeting autophagy in cancer', *Nature Reviews Cancer*, 17(9), pp. 528–542. doi: 10.1038/nrc.2017.53.

Li, L. *et al.* (2018) 'A TFEB nuclear export signal integrates amino acid supply and glucose availability', *Nature Communications*, 9(1), p. 2685. doi: 10.1038/s41467-018-04849-7.

Li, S. *et al.* (2019) 'Transcriptional regulation of autophagy-lysosomal function in BRAF-driven melanoma progression and chemoresistance', *Nature Communications*. Nature Publishing Group, 10(1), p. 1693. doi: 10.1038/s41467-019-09634-8.

Li, T. *et al.* (2004) 'Failure to proliferate and mitotic arrest of CDK11(p110/p58)-null mutant mice at the blastocyst stage of embryonic cell development.', *Molecular and cellular biology*, 24(8), pp. 3188–97. doi: 10.1128/mcb.24.8.3188-3197.2004.

Li, Y. *et al.* (2016) 'Protein kinase C controls lysosome biogenesis independently of mTORC1', *Nature Cell Biology*, 18(10), pp. 1065–1077. doi: 10.1038/ncb3407.

Li, Y., Dowbenko, D. and Lasky, L. A. (2002) 'AKT/PKB phosphorylation of p21Cip/WAF1 enhances protein stability of p21Cip/WAF1 and promotes cell survival.', *The Journal of biological chemistry*. American Society for Biochemistry and Molecular Biology, 277(13), pp. 11352–61. doi: 10.1074/jbc.M109062200.

Li, Z. *et al.* (2016) 'Autophagic flux is highly active in early mitosis and differentially regulated throughout the cell cycle', *Oncotarget*, 7(26), pp. 39705–39718. doi: 10.18632/oncotarget.9451.

Li, Z. *et al.* (2018) 'Plk1-Mediated Phosphorylation of TSC1 Enhances the Efficacy of Rapamycin', *Cancer Research*, 78(11), pp. 2864–2875. doi: 10.1158/0008-5472.CAN-17-3046.

Li, Z. *et al.* (2019) 'CDK1 phosphorylates ULK1-ATG13 complex to regulate mitotic autophagy and Taxol chemosensitivity', *bioRxiv*. Cold Spring Harbor Laboratory, p. 634733. doi: 10.1101/634733.

Liang, C. *et al.* (2008) 'Beclin1-binding UVRAG targets the class C Vps complex to coordinate autophagosome maturation and endocytic trafficking', *Nature Cell Biology*. Nature Publishing Group, 10(7), pp. 776–787. doi: 10.1038/ncb1740.

Liang, J. *et al.* (2007) 'The energy sensing LKB1–AMPK pathway regulates p27kip1 phosphorylation mediating the decision to enter autophagy or apoptosis', *Nature Cell Biology*. Nature Publishing Group, 9(2), pp. 218–224. doi: 10.1038/ncb1537.

Liang, X. H. *et al.* (1999) 'Induction of autophagy and inhibition of tumorigenesis by beclin 1', *Nature*, 402(6762), pp. 672–676. doi: 10.1038/45257.

Lin, M. G. and Hurley, J. H. (2016) 'Structure and function of the ULK1 complex in autophagy.',

Current opinion in cell biology. NIH Public Access, 39, pp. 61–8. doi: 10.1016/j.ceb.2016.02.010.

Linares, J. F. *et al.* (2011) 'Phosphorylation of p62 by cdk1 Controls the Timely Transit of Cells through Mitosis and Tumor Cell Proliferation', *Molecular and Cellular Biology*, 31(1), pp. 105–117. doi: 10.1128/MCB.00620-10.

Little, A. S. *et al.* (2011) 'Amplification of the Driving Oncogene, KRAS or BRAF, Underpins Acquired Resistance to MEK1/2 Inhibitors in Colorectal Cancer Cells', *Science Signaling*, 4(166), pp. ra17–ra17. doi: 10.1126/scisignal.2001752.

Liu, C.-C. *et al.* (2016) 'Cul3-KLHL20 Ubiquitin Ligase Governs the Turnover of ULK1 and VPS34 Complexes to Control Autophagy Termination', *Molecular Cell*, 61(1), pp. 84–97. doi: 10.1016/j.molcel.2015.11.001.

Liu, C. *et al.* (2002) 'Control of beta-catenin phosphorylation/degradation by a dual-kinase mechanism.', *Cell*, 108(6), pp. 837–47. doi: 10.1016/s0092-8674(02)00685-2.

Liu, E. Y. *et al.* (2015) 'Loss of autophagy causes a synthetic lethal deficiency in DNA repair', *Proceedings of the National Academy of Sciences*, 112(3), pp. 773–778. doi: 10.1073/pnas.1409563112.

Liu, F. *et al.* (2010) 'MiTF links Erk1/2 kinase and p21CIP1/WAF1 activation after UVC radiation in normal human melanocytes and melanoma cells', *Molecular Cancer*, 9(1), p. 214. doi: 10.1186/1476-4598-9-214.

Liu, H. *et al.* (2013) 'Down-Regulation of Autophagy-Related Protein 5 (ATG5) Contributes to the Pathogenesis of Early-Stage Cutaneous Melanoma', *Science Translational Medicine*, 5(202), pp. 202ra123-202ra123. doi: 10.1126/scitranslmed.3005864.

Liu, L. *et al.* (2009) 'Robust autophagy/mitophagy persists during mitosis', *Cell Cycle*, 8(10), pp. 1616–1620. doi: 10.4161/cc.8.10.8577.

Liu, M. *et al.* (2006) 'Inhibition of the mitotic kinesin Eg5 up-regulates Hsp70 through the phosphatidylinositol 3-kinase/Akt pathway in multiple myeloma cells.', *The Journal of biological chemistry*. American Society for Biochemistry and Molecular Biology, 281(26), pp. 18090–7. doi: 10.1074/jbc.M601324200.

Liu, P. *et al.* (2014) 'Cell-cycle-regulated activation of Akt kinase by phosphorylation at its carboxyl terminus', *Nature*, 508(7497), pp. 541–545. doi: 10.1038/nature13079.

Llanos, S. *et al.* (2019) 'Lysosomal trapping of palbociclib and its functional implications', *Oncogene*. Nature Publishing Group, 38(20), pp. 3886–3902. doi: 10.1038/s41388-019-0695-8.

Long, X. *et al.* (2005) 'Rheb Binds and Regulates the mTOR Kinase', *Current Biology*, 15(8), pp. 702–713. doi: 10.1016/j.cub.2005.02.053.

Lonsdale, J. *et al.* (2013) 'The Genotype-Tissue Expression (GTEx) project', *Nature Genetics*, 45(6), pp. 580–585. doi: 10.1038/ng.2653.

Lopez-Bonet, E. *et al.* (2010) 'Serine 2481-autophosphorylation of mammalian target of rapamycin (mTOR) couples with chromosome condensation and segregation during mitosis: confocal microscopy characterization and immunohistochemical validation of PP-mTOR(Ser2481) as a novel high-contrast mitosis marker in breast cancer core biopsies.', *International journal of oncology*, 36(1), pp. 107–15.

Losier, T. T. *et al.* (2019) 'AMPK Promotes Xenophagy through Priming of Autophagic Kinases upon Detection of Bacterial Outer Membrane Vesicles', *Cell Reports*, 26(8), pp. 2150-2165.e5. doi: 10.1016/j.celrep.2019.01.062.

Loukil, A. *et al.* (2014) 'High-resolution live-cell imaging reveals novel cyclin A2 degradation foci involving autophagy', *Journal of Cell Science*, 127(10), pp. 2145–2150. doi: 10.1242/jcs.139188.

Lu, G. *et al.* (2019) 'Suppression of autophagy during mitosis via CUL4-RING ubiquitin ligases-mediated WIPI2 polyubiquitination and proteasomal degradation', *Autophagy*, pp. 1–18. doi: 10.1080/15548627.2019.1596484.

Lu, L., Ladinsky, M. S. and Kirchhausen, T. (2009) 'Cisternal organization of the endoplasmic reticulum during mitosis.', *Molecular biology of the cell*. American Society for Cell Biology, 20(15), pp. 3471–80. doi: 10.1091/mbc.E09-04-0327.

Lu, S.-Y., Li, M. and Lin, Y.-L. (2010) 'Mitf induction by RANKL is critical for osteoclastogenesis.', *Molecular biology of the cell*. American Society for Cell Biology, 21(10), pp. 1763–71. doi: 10.1091/mbc.E09-07-0584.

Lundgren, K. *et al.* (1991) 'mik1 and wee1 cooperate in the inhibitory tyrosine phosphorylation of

cdc2.', *Cell*, 64(6), pp. 1111–22.

Ma, L. *et al.* (2005) 'Phosphorylation and Functional Inactivation of TSC2 by Erk', *Cell*, 121(2), pp. 179–193. doi: 10.1016/j.cell.2005.02.031.

Mackeh, R. *et al.* (2013) 'Autophagy and microtubules - new story, old players.', *Journal of cell science*. The Company of Biologists Ltd, 126(Pt 5), pp. 1071–80. doi: 10.1242/jcs.115626.

Maday, S. and Holzbaur, E. L. F. (2014) 'Autophagosome Biogenesis in Primary Neurons Follows an Ordered and Spatially Regulated Pathway', *Developmental Cell*. Cell Press, 30(1), pp. 71–85. doi: 10.1016/J.DEVCEL.2014.06.001.

Maehama, T. and Dixon, J. E. (1998) 'The tumor suppressor, PTEN/MMAC1, dephosphorylates the lipid second messenger, phosphatidylinositol 3,4,5-trisphosphate.', *The Journal of biological chemistry*. American Society for Biochemistry and Molecular Biology, 273(22), pp. 13375–8. doi: 10.1074/jbc.273.22.13375.

Malumbres, M. *et al.* (2004) 'Mammalian Cells Cycle without the D-Type Cyclin-Dependent Kinases Cdk4 and Cdk6', *Cell*, 118(4), pp. 493–504. doi: 10.1016/j.cell.2004.08.002.

Manifava, M. *et al.* (2016) 'Dynamics of mTORC1 activation in response to amino acids', *eLife*, 5. doi: 10.7554/eLife.19960.

Marchand, B. *et al.* (2015) 'Glycogen synthase kinase-3 (GSK3) inhibition induces prosurvival autophagic signals in human pancreatic cancer cells', *The Journal of Biological Chemistry*, 290(9), pp. 5592–5605. doi: 10.1074/jbc.M114.616714.

Mari, M., Tooze, S. A. and Reggiori, F. (2011) 'The puzzling origin of the autophagosomal membrane.', *F1000 biology reports*. Faculty of 1000 Ltd, 3, p. 25. doi: 10.3410/B3-25.

Marin Zapata, P. A. *et al.* (2016) 'Time course decomposition of cell heterogeneity in TFEB signaling states reveals homeostatic mechanisms restricting the magnitude and duration of TFEB responses to mTOR activity modulation', *BMC Cancer*, 16(1), p. 355. doi: 10.1186/s12885-016-2388-9.

Martina, J. A. *et al.* (2012) 'MTORC1 functions as a transcriptional regulator of autophagy by preventing nuclear transport of TFEB', *Autophagy*, 8(6), pp. 903–914. doi: 10.4161/auto.19653.

Martina, J. A. *et al.* (2014) 'The Nutrient-Responsive Transcription Factor TFE3, Promotes Autophagy, Lysosomal Biogenesis, and Clearance of Cellular Debris', *Science signaling*, 7(309), p. ra9. doi: 10.1126/scisignal.2004754.

Martina, J. A. J. *et al.* (2016) 'TFEB and TFE3 are novel components of the integrated stress response', *The EMBO journal*. EMBO Press, 35(5), pp. 479–495. doi: 10.15252/embj.201593428.

Martina, J. A. and Puertollano, R. (2013) 'Rag GTPases mediate amino acid-dependent recruitment of TFEB and MITF to lysosomes', *The Journal of Cell Biology*, 200(4), pp. 475–491. doi: 10.1083/jcb.201209135.

Martinez-Lopez, N. *et al.* (2013) 'Autophagy proteins regulate ERK phosphorylation', *Nature Communications*, 4, p. 2799. doi: 10.1038/ncomms3799.

Martinez, J. *et al.* (2015) 'Molecular characterization of LC3-associated phagocytosis reveals distinct roles for Rubicon, NOX2 and autophagy proteins.', *Nature cell biology*. NIH Public Access, 17(7), pp. 893–906. doi: 10.1038/ncb3192.

Maruyama, T. and Noda, N. N. (2018) 'Autophagy-regulating protease Atg4: Structure, function, regulation and inhibition', *Journal of Antibiotics*. Nature Publishing Group, pp. 72–78. doi: 10.1038/ja.2017.104.

Mathiassen, S. G., De Zio, D. and Cecconi, F. (2017) 'Autophagy and the Cell Cycle: A Complex Landscape.', *Frontiers in oncology*. Frontiers Media SA, 7, p. 51. doi: 10.3389/fonc.2017.00051.

Matsui, A. *et al.* (2013) 'The Role of Autophagy in Genome Stability through Suppression of Abnormal Mitosis under Starvation', *PLoS Genetics*. Edited by G. P. Copenhaver. Public Library of Science, 9(1), p. e1003245. doi: 10.1371/journal.pgen.1003245.

McAlpine, F. *et al.* (2013) 'Regulation of nutrient-sensitive autophagy by uncoordinated 51-like kinases 1 and 2', *Autophagy*, 9(3), pp. 361–373. doi: 10.4161/auto.23066.

McGill, G. G. *et al.* (2002) 'Bcl2 regulation by the melanocyte master regulator Mitf modulates lineage survival and melanoma cell viability.', *Cell*. Elsevier, 109(6), pp. 707–18. doi: 10.1016/S0092-8674(02)00762-6.

Medina, D. L. *et al.* (2015) 'Lysosomal calcium signalling regulates autophagy through calcineurin and TFEB.', *Nature cell biology*. NIH Public Access, 17(3), pp. 288–99. doi: 10.1038/ncb3114.

Mehsen, H. *et al.* (2018) 'PP2A-B55 promotes nuclear envelope reformation after mitosis in Drosophila.', *The Journal of cell biology*. Rockefeller University Press, 217(12), pp. 4106–4123. doi: 10.1083/jcb.201804018.

Meijer, L. *et al.* (1997) 'Biochemical and Cellular Effects of Roscovitine, a Potent and Selective Inhibitor of the Cyclin-Dependent Kinases cdc2, cdk2 and cdk5', *European Journal of Biochemistry*. Blackwell Science Ltd, 243(1–2), pp. 527–536. doi: 10.1111/j.1432-1033.1997.t01-2-00527.x.

Mejlvang, J. *et al.* (2018) 'Starvation induces rapid degradation of selective autophagy receptors by endosomal microautophagy.', *The Journal of cell biology*. Rockefeller University Press, 217(10), pp. 3640–3655. doi: 10.1083/jcb.201711002.

Menon, S. *et al.* (2014) 'Spatial Control of the TSC Complex Integrates Insulin and Nutrient Regulation of mTORC1 at the Lysosome', *Cell*, 156(4), pp. 771–785. doi: 10.1016/j.cell.2013.11.049.

Menzies, F. M. *et al.* (2017) 'Autophagy and Neurodegeneration: Pathogenic Mechanisms and Therapeutic Opportunities', *Neuron*, 93(5), pp. 1015–1034. doi: 10.1016/j.neuron.2017.01.022.

Metlagel, Z. *et al.* (2013) 'Structural basis of ATG3 recognition by the autophagic ubiquitin-like protein ATG12.', *Proceedings of the National Academy of Sciences of the United States of America*. National Academy of Sciences, 110(47), pp. 18844–9. doi: 10.1073/pnas.1314755110.

Miao, B. *et al.* (2010) 'Small molecule inhibition of phosphatidylinositol-3,4,5-triphosphate (PIP3) binding to pleckstrin homology domains.', *Proceedings of the National Academy of Sciences of the United States of America*. National Academy of Sciences, 107(46), pp. 20126–31. doi: 10.1073/pnas.1004522107.

Mimoto, R. *et al.* (2017) 'Diminished DYRK2 sensitizes hormone receptor-positive breast cancer to everolimus by the escape from degrading mTOR', *Cancer Letters*, 384, pp. 27–38. doi: 10.1016/j.canlet.2016.10.015.

Misteli, T. and Warren, G. (1995) 'Mitotic disassembly of the Golgi apparatus in vivo.', *Journal of cell science*, 108 (Pt 7), pp. 2715–27.

Mizushima, N. *et al.* (2004) 'In Vivo Analysis of Autophagy in Response to Nutrient Starvation Using Transgenic Mice Expressing a Fluorescent Autophagosome Marker', *Molecular Biology of the Cell*, 15(3), pp. 1101–1111. doi: 10.1091/mbc.e03-09-0704.

Mizushima, N., Yoshimori, T. and Levine, B. (2010) 'Methods in mammalian autophagy research.', *Cell*. NIH Public Access, 140(3), pp. 313–26. doi: 10.1016/j.cell.2010.01.028.

Molina, D. M., Grewal, S. and Bardwell, L. (2005) 'Characterization of an ERK-binding domain in microphthalmia-associated transcription factor and differential inhibition of ERK2-mediated substrate phosphorylation.', *Journal of Biological Chemistry*, 280(51), pp. 42051–42060. doi: 10.1074/jbc.M510590200.

Mothe-Satney, I. *et al.* (2000) 'Mammalian Target of Rapamycin-dependent Phosphorylation of PHAS-I in Four (S/T)P Sites Detected by Phospho-specific Antibodies', *Journal of Biological Chemistry*, 275(43), pp. 33836–33843. doi: 10.1074/jbc.M006005200.

Moulis, M. and Vindis, C. (2017) 'Methods for Measuring Autophagy in Mice.', *Cells*. Multidisciplinary Digital Publishing Institute (MDPI), 6(2). doi: 10.3390/cells6020014.

Munson, M. J. *et al.* (2015) 'mTOR activates the VPS34-UVRAG complex to regulate autolysosomal tubulation and cell survival.', *The EMBO journal*. European Molecular Biology Organization, 34(17), pp. 2272–90. doi: 10.15252/embj.201590992.

Murakami, M. *et al.* (2004) 'mTOR is essential for growth and proliferation in early mouse embryos and embryonic stem cells.', *Molecular and cellular biology*. American Society for Microbiology (ASM), 24(15), pp. 6710–8. doi: 10.1128/MCB.24.15.6710-6718.2004.

Murano, T. *et al.* (2017) 'Transcription factor TFEB cell-autonomously modulates susceptibility to intestinal epithelial cell injury in vivo', *Scientific Reports*. Nature Publishing Group, 7(1), p. 13938. doi: 10.1038/s41598-017-14370-4.

Murphy, M. *et al.* (1997) 'Delayed early embryonic lethality following disruption of the murine cyclin A2 gene', *Nature Genetics*, 15(1), pp. 83–86. doi: 10.1038/ng0197-83.

Musgrove, E. A. *et al.* (2011) 'Cyclin D as a therapeutic target in cancer', *Nature Reviews Cancer*. Nature Publishing Group, 11(8), pp. 558–572. doi: 10.1038/nrc3090.

Najafov, A. *et al.* (2011) 'Characterization of GSK2334470, a novel and highly specific inhibitor of

PDK1.', *The Biochemical journal*. Portland Press Limited, 433(2), pp. 357–69. doi: 10.1042/BJ20101732.

Nakamura, S. and Yoshimori, T. (2018) 'Autophagy and Longevity.', *Molecules and cells*, 41(1), pp. 65–72. doi: 10.14348/molcells.2018.2333.

Nam, H. and Benezra, R. (2009) 'High Levels of Id1 Expression Define B1 Type Adult Neural Stem Cells', *Cell Stem Cell*, 5(5), pp. 515–526. doi: 10.1016/j.stem.2009.08.017.

Nam, H. Y. *et al.* (2013) 'Radioresistant cancer cells can be conditioned to enter senescence by mTOR inhibition.', *Cancer research*. American Association for Cancer Research, 73(14), pp. 4267–77. doi: 10.1158/0008-5472.CAN-12-3516.

Nandi, N. *et al.* (2017) 'Stress-induced Cdk5 activity enhances cytoprotective basal autophagy in Drosophila melanogaster by phosphorylating acinus at serine437.', *eLife*. eLife Sciences Publications, Ltd, 6. doi: 10.7554/eLife.30760.

Napolitano, G. *et al.* (2018) 'mTOR-dependent phosphorylation controls TFEB nuclear export', *Nature Communications*, 9(1), p. 3312. doi: 10.1038/s41467-018-05862-6.

Narita, M. *et al.* (2011) 'Spatial Coupling of mTOR and Autophagy Augments Secretory Phenotypes', *Science*, 332(6032), pp. 966–970. doi: 10.1126/science.1205407.

Nasa, I. and Kettenbach, A. N. (2018) 'Coordination of Protein Kinase and Phosphoprotein Phosphatase Activities in Mitosis', *Frontiers in Cell and Developmental Biology*. Frontiers, 6, p. 30. doi: 10.3389/fcell.2018.00030.

Nazio, F. *et al.* (2013) 'mTOR inhibits autophagy by controlling ULK1 ubiquitylation, self-association and function through AMBRA1 and TRAF6', *Nature Cell Biology*, 15(4), pp. 406–416. doi: 10.1038/ncb2708.

Ngeow, K. C. *et al.* (2018) 'BRAF/MAPK and GSK3 signaling converges to control MITF nuclear export', *Proceedings of the National Academy of Sciences*, 115(37), pp. E8668–E8677. doi: 10.1073/pnas.1810498115.

Nishimura, T. *et al.* (2013) 'FIP200 regulates targeting of Atg16L1 to the isolation membrane', *EMBO reports*, 14(3), pp. 284–291. doi: 10.1038/embor.2013.6.

Nishimura, T. *et al.* (2017) 'Autophagosome formation is initiated at phosphatidylinositol synthase-enriched ER subdomains.', *The EMBO journal*. European Molecular Biology Organization, 36(12), pp. 1719–1735. doi: 10.15252/embj.201695189.

Noda, T. and Ohsumi, Y. (1998) 'Tor, a phosphatidylinositol kinase homologue, controls autophagy in yeast.', *The Journal of biological chemistry*, 273(7), pp. 3963–6.

Nojima, H. *et al.* (2003) 'The Mammalian Target of Rapamycin (mTOR) Partner, Raptor, Binds the mTOR Substrates p70 S6 Kinase and 4E-BP1 through Their TOR Signaling (TOS) Motif', *Journal of Biological Chemistry*, 278(18), pp. 15461–15464. doi: 10.1074/jbc.C200665200.

Oakhill, J. S. *et al.* (2010) 'β-Subunit myristoylation is the gatekeeper for initiating metabolic stress sensing by AMP-activated protein kinase (AMPK).', *Proceedings of the National Academy of Sciences of the United States of America*. National Academy of Sciences, 107(45), pp. 19237–41. doi: 10.1073/pnas.1009705107.

Oakhill, J. S. *et al.* (2011) 'AMPK Is a Direct Adenylate Charge-Regulated Protein Kinase', *Science*, 332(6036), pp. 1433–1435. doi: 10.1126/science.1200094.

Ohashi, Y., Tremel, S. and Williams, R. L. (2019) 'VPS34 complexes from a structural perspective', *Journal of Lipid Research*, 60(2), pp. 229–241. doi: 10.1194/jlr.R089490.

Ohsaki, Y. *et al.* (2010) 'Lysosomal accumulation of mTOR is enhanced by rapamycin', *Histochemistry and Cell Biology*, 134(6), pp. 537–544. doi: 10.1007/s00418-010-0759-x.

Olsen, J. V. *et al.* (2010) 'Quantitative Phosphoproteomics Reveals Widespread Full Phosphorylation Site Occupancy During Mitosis', *Science Signaling*, 3(104), pp. ra3–ra3. doi: 10.1126/scisignal.2000475.

Ong, Q. *et al.* (2015) 'U0126 protects cells against oxidative stress independent of its function as a MEK inhibitor.', *ACS chemical neuroscience*. American Chemical Society, 6(1), pp. 130–7. doi: 10.1021/cn500288n.

Örd, M. *et al.* (2019) 'Cyclin-Specific Docking Mechanisms Reveal the Complexity of M-CDK Function in the Cell Cycle', *Molecular Cell*. doi: 10.1016/j.molcel.2019.04.026.

Oshiro, N. *et al.* (2007) 'The Proline-rich Akt Substrate of 40 kDa (PRAS40) Is a Physiological Substrate of Mammalian Target of Rapamycin Complex 1', *Journal of Biological Chemistry*,

282(28), pp. 20329–20339. doi: 10.1074/jbc.M702636200.

Oshiro, N., Rapley, J. and Avruch, J. (2014) 'Amino Acids Activate Mammalian Target of Rapamycin (mTOR) Complex 1 without Changing Rag GTPase Guanyl Nucleotide Charging', *Journal of Biological Chemistry*, 289(5), pp. 2658–2674. doi: 10.1074/jbc.M113.528505.

Pacold, M. E. *et al.* (2000) 'Crystal structure and functional analysis of Ras binding to its effector phosphoinositide 3-kinase gamma.', *Cell*, 103(6), pp. 931–43. doi: 10.1016/s0092-8674(00)00196-3.

Palmieri, M. *et al.* (2011) 'Characterization of the CLEAR network reveals an integrated control of cellular clearance pathways', *Human Molecular Genetics*. BioMed Central, 20(19), pp. 3852–3866. doi: 10.1093/hmg/ddr306.

Palmieri, Michela *et al.* (2011) 'Characterization of the CLEAR network reveals an integrated control of cellular clearance pathways', *Human Molecular Genetics*, 20(19), pp. 3852–3866. doi: 10.1093/hmg/ddr306.

Palmieri, M. *et al.* (2017) 'mTORC1-independent TFEB activation via Akt inhibition promotes cellular clearance in neurodegenerative storage diseases', *Nature Communications*. Nature Publishing Group, 8(1), p. 14338. doi: 10.1038/ncomms14338.

Palmisano, N. J. and Meléndez, A. (2016) 'Detection of Autophagy in Caenorhabditis elegans Using GFP::LGG-1 as an Autophagy Marker.', *Cold Spring Harbor protocols*. NIH Public Access, 2016(1), p. pdb.prot086496. doi: 10.1101/pdb.prot086496.

Papagiannakis, A. *et al.* (2017) 'Quantitative characterization of the auxin-inducible degron: a guide for dynamic protein depletion in single yeast cells.', *Scientific reports*. Nature Publishing Group, 7(1), p. 4704. doi: 10.1038/s41598-017-04791-6.

Papst, P. J. *et al.* (1998) 'Cdc2-Cyclin B Phosphorylates p70 S6 Kinase on Ser411at Mitosis', *Journal of Biological Chemistry*. American Society for Biochemistry and Molecular Biology, 273(24), pp. 15077–15084. doi: 10.1074/jbc.273.24.15077.

Park, J.-M. *et al.* (2016) 'The ULK1 complex mediates MTORC1 signaling to the autophagy initiation machinery via binding and phosphorylating ATG14.', *Autophagy*. Taylor & Francis, 12(3), pp. 547–64. doi: 10.1080/15548627.2016.1140293.

Parr, C. *et al.* (2012) 'Glycogen synthase kinase 3 inhibition promotes lysosomal biogenesis and autophagic degradation of the amyloid-β precursor protein.', *Molecular and cellular biology*. American Society for Microbiology (ASM), 32(21), pp. 4410–8. doi: 10.1128/MCB.00930-12.

Peña-Llopis, S. *et al.* (2011) 'Regulation of TFEB and V-ATPases by mTORC1', *The EMBO journal*, 30(16), pp. 3242–3258. doi: 10.1038/emboj.2011.257.

Pende, M. *et al.* (2004) 'S6K1(-/-)/S6K2(-/-) mice exhibit perinatal lethality and rapamycin-sensitive 5'-terminal oligopyrimidine mRNA translation and reveal a mitogen-activated protein kinase-dependent S6 kinase pathway.', *Molecular and cellular biology*, 24(8), pp. 3112–24. doi: 10.1128/mcb.24.8.3112-3124.2004.

Perera, R. M. *et al.* (2015) 'Transcriptional control of autophagy-lysosome function drives pancreatic cancer metabolism', *Nature*, 524(7565), pp. 361–365. doi: 10.1038/nature14587.

Petersen, J. and Nurse, P. (2007) 'TOR signalling regulates mitotic commitment through the stress MAP kinase pathway and the Polo and Cdc2 kinases', *Nature Cell Biology*, 9(11), pp. 1263–1272. doi: 10.1038/ncb1646.

Peterson, R. T. *et al.* (2000) 'FKBP12-Rapamycin-associated Protein (FRAP) Autophosphorylates at Serine 2481 under Translationally Repressive Conditions', *Journal of Biological Chemistry*, 275(10), pp. 7416–7423. doi: 10.1074/jbc.275.10.7416.

Peterson, T. R. *et al.* (2009) 'DEPTOR Is an mTOR Inhibitor Frequently Overexpressed in Multiple Myeloma Cells and Required for Their Survival', *Cell*, 137(5), pp. 873–886. doi: 10.1016/j.cell.2009.03.046.

Petit, C. S., Roczniak-Ferguson, A. and Ferguson, S. M. (2013) 'Recruitment of folliculin to lysosomes supports the amino acid–dependent activation of Rag GTPases', *The Journal of Cell Biology*, 202(7), pp. 1107–1122. doi: 10.1083/jcb.201307084.

Pi, H. *et al.* (2019) 'AKT inhibition-mediated dephosphorylation of TFE3 promotes overactive autophagy independent of MTORC1 in cadmium-exposed bone mesenchymal stem cells', *Autophagy*, 15(4), pp. 565–582. doi: 10.1080/15548627.2018.1531198.

Pines, J. and Hunter, T. (1989) 'Isolation of a human cyclin cDNA: evidence for cyclin mRNA and

protein regulation in the cell cycle and for interaction with p34cdc2.', *Cell*, 58(5), pp. 833–46.

Platani, M. *et al.* (2015) 'Mio depletion links mTOR regulation to Aurora A and Plk1 activation at mitotic centrosomes', *The Journal of Cell Biology*, 210(1), pp. 45–62. doi: 10.1083/jcb.201410001.

Pohl, C. and Jentsch, S. (2009) 'Midbody ring disposal by autophagy is a post-abscission event of cytokinesis', *Nature Cell Biology*, 11(1), pp. 65–70. doi: 10.1038/ncb1813.

Polson, H. E. J. *et al.* (2010) 'Mammalian Atg18 (WIPI2) localizes to omegasome-anchored phagophores and positively regulates LC3 lipidation', *Autophagy*, 6(4), pp. 506–522. doi: 10.4161/auto.6.4.11863.

Powis, K. and De Virgilio, C. (2016) 'Conserved regulators of Rag GTPases orchestrate amino acid-dependent TORC1 signaling', *Cell Discovery*, 2(1), p. 15049. doi: 10.1038/celldisc.2015.49.

Puente, C., Hendrickson, R. C. and Jiang, X. (2016) 'Nutrient-regulated Phosphorylation of ATG13 Inhibits Starvation-induced Autophagy', *Journal of Biological Chemistry*, 291(11), pp. 6026–6035. doi: 10.1074/jbc.M115.689646.

Pylayeva-Gupta, Y., Grabocka, E. and Bar-Sagi, D. (2011) 'RAS oncogenes: weaving a tumorigenic web', *Nature Reviews Cancer*. Nature Publishing Group, 11(11), pp. 761–774. doi: 10.1038/nrc3106.

Ramírez-Valle, F. *et al.* (2010) 'Mitotic raptor promotes mTORC1 activity, G(2)/M cell cycle progression, and internal ribosome entry site-mediated mRNA translation.', *Molecular and cellular biology*. American Society for Microbiology (ASM), 30(13), pp. 3151–64. doi: 10.1128/MCB.00322-09.

Rane, S. G. *et al.* (1999) 'Loss of Cdk4 expression causes insulin-deficient diabetes and Cdk4 activation results in β-islet cell hyperplasia', *Nature Genetics*, 22(1), pp. 44–52. doi: 10.1038/8751.

Ravenhill, B. J. *et al.* (2019) 'The Cargo Receptor NDP52 Initiates Selective Autophagy by Recruiting the ULK Complex to Cytosol-Invading Bacteria', *Molecular Cell*, 74(2), pp. 320-329.e6. doi: 10.1016/j.molcel.2019.01.041.

REDPATH, N. T. *et al.* (1993) 'Regulation of elongation factor-2 by multisite phosphorylation', *European Journal of Biochemistry*. John Wiley & Sons, Ltd (10.1111), 213(2), pp. 689–699. doi: 10.1111/j.1432-1033.1993.tb17809.x.

Rello-Varona, S. *et al.* (2012) 'Autophagic removal of micronuclei', *Cell Cycle*, 11(1), pp. 170–176. doi: 10.4161/cc.11.1.18564.

Renner, A. G. *et al.* (2010) 'A functional link between Polo-like kinase 1 and the mammalian Target-Of-Rapamycin pathway?', *Cell Cycle*, 9(9), pp. 1690–1696. doi: 10.4161/cc.9.9.11295.

Ridley, S. H. *et al.* (2001) 'FENS-1 and DFCP1 are FYVE domain-containing proteins with distinct functions in the endosomal and Golgi compartments.', *Journal of cell science*, 114(Pt 22), pp. 3991–4000.

Ripple, M. O., Kim, N. and Springett, R. (2013) 'Acute Mitochondrial Inhibition by Mitogen-activated Protein Kinase/Extracellular Signal-regulated Kinase Kinase (MEK) 1/2 Inhibitors Regulates Proliferation', *Journal of Biological Chemistry*, 288(5), pp. 2933–2940. doi: 10.1074/jbc.M112.430082.

Roczniak-Ferguson, A. *et al.* (2012) 'The transcription factor TFEB links mTORC1 signaling to transcriptional control of lysosome homeostasis', *Science Signaling*, 5(228), p. ra42. doi: 10.1126/scisignal.2002790.

Rodriguez-Viciana, P. *et al.* (1994) 'Phosphatidylinositol-3-OH kinase direct target of Ras', *Nature*, 370(6490), pp. 527–532. doi: 10.1038/370527a0.

Ronan, B. *et al.* (2014) 'A highly potent and selective Vps34 inhibitor alters vesicle trafficking and autophagy', *Nature Chemical Biology*, 10(12), pp. 1013–1019. doi: 10.1038/nchembio.1681.

Ropolo, A. *et al.* (2007) 'The Pancreatitis-induced Vacuole Membrane Protein 1 Triggers Autophagy in Mammalian Cells', *Journal of Biological Chemistry*, 282(51), pp. 37124–37133. doi: 10.1074/jbc.M706956200.

Rosenwald, I. B. *et al.* (1993) 'Elevated levels of cyclin D1 protein in response to increased expression of eukaryotic initiation factor 4E.', *Molecular and cellular biology*, 13(12), pp. 7358–63.

Roskoski, R. (2012) 'ERK1/2 MAP kinases: Structure, function, and regulation', *Pharmacological Research*, 66(2), pp. 105–143. doi: 10.1016/j.phrs.2012.04.005.

Roux, K. J. *et al.* (2012) 'A promiscuous biotin ligase fusion protein identifies proximal and interacting proteins in mammalian cells', *The Journal of Cell Biology*, 196(6), pp. 801–810. doi:

10.1083/jcb.201112098.

Roux, P. P. *et al.* (2004) 'Tumor-promoting phorbol esters and activated Ras inactivate the tuberous sclerosis tumor suppressor complex via p90 ribosomal S6 kinase', *Proceedings of the National Academy of Sciences*, 101(37), pp. 13489–13494. doi: 10.1073/pnas.0405659101.

Roux, P. P. *et al.* (2007) 'RAS/ERK Signaling Promotes Site-specific Ribosomal Protein S6 Phosphorylation via RSK and Stimulates Cap-dependent Translation', *Journal of Biological Chemistry*, 282(19), pp. 14056–14064. doi: 10.1074/jbc.M700906200.

Ruf, S. *et al.* (2017) 'PLK1 (polo like kinase 1) inhibits MTOR complex 1 and promotes autophagy', *Autophagy*, 13(3), pp. 486–505. doi: 10.1080/15548627.2016.1263781.

Rushworth, L. K. *et al.* (2006) 'Regulation and role of Raf-1/B-Raf heterodimerization.', *Molecular and cellular biology*. American Society for Microbiology (ASM), 26(6), pp. 2262–72. doi: 10.1128/MCB.26.6.2262-2272.2006.

Russell, R. C. *et al.* (2013) 'ULK1 induces autophagy by phosphorylating Beclin-1 and activating VPS34 lipid kinase.', *Nature cell biology*, 15(7), pp. 741–50. doi: 10.1038/ncb2757.

Ryan, W. K. *et al.* (2019) 'Activation of S6 signaling is associated with cell survival and multinucleation in hyperplastic skin after epidermal loss of AURORA-A Kinase', *Cell Death & Differentiation*. Nature Publishing Group, 26(3), pp. 548–564. doi: 10.1038/s41418-018-0167-7.

Sabatini, D. M. (2017) 'Twenty-five years of mTOR: Uncovering the link from nutrients to growth.', *Proceedings of the National Academy of Sciences of the United States of America*. National Academy of Sciences, 114(45), pp. 11818–11825. doi: 10.1073/pnas.1716173114.

Saitoh, M. *et al.* (2002) 'Regulation of an Activated S6 Kinase 1 Variant Reveals a Novel Mammalian Target of Rapamycin Phosphorylation Site', *Journal of Biological Chemistry*, 277(22), pp. 20104–20112. doi: 10.1074/jbc.M201745200.

Sakoh-Nakatogawa, M. *et al.* (2013) 'Atg12–Atg5 conjugate enhances E2 activity of Atg3 by rearranging its catalytic site', *Nature Structural & Molecular Biology*, 20(4), pp. 433–439. doi: 10.1038/nsmb.2527.

Sale, M. J. *et al.* (2019) 'MEK1/2 inhibitor withdrawal reverses acquired resistance driven by BRAFV600E amplification whereas KRASG13D amplification promotes EMT-chemoresistance', *Nature Communications*. Nature Publishing Group, 10(1), p. 2030. doi: 10.1038/s41467-019-09438-w.

Sancak, Y. *et al.* (2008) 'The Rag GTPases Bind Raptor and Mediate Amino Acid Signaling to mTORC1', *Science*, 320(5882), pp. 1496–1501. doi: 10.1126/science.1157535.

Sancak, Y. *et al.* (2010) 'Ragulator-Rag Complex Targets mTORC1 to the Lysosomal Surface and Is Necessary for Its Activation by Amino Acids', *Cell*, 141(2), pp. 290–303. doi: 10.1016/j.cell.2010.02.024.

Santamaría, D. *et al.* (2007) 'Cdk1 is sufficient to drive the mammalian cell cycle', *Nature*, 448(7155), pp. 811–815. doi: 10.1038/nature06046.

Santos, A. J. M. *et al.* (2013) 'Preferential invasion of mitotic cells by Salmonella reveals that cell surface cholesterol is maximal during metaphase', *Journal of Cell Science*, 126(14), pp. 2990–2996. doi: 10.1242/jcs.115253.

Sapkota, G. P. *et al.* (2007) 'BI-D1870 is a specific inhibitor of the p90 RSK (ribosomal S6 kinase) isoforms in vitro and in vivo.', *The Biochemical journal*. Portland Press Ltd, 401(1), pp. 29–38. doi: 10.1042/BJ20061088.

Sarbassov, D. D. *et al.* (2005) 'Phosphorylation and Regulation of Akt/PKB by the Rictor-mTOR Complex', *Science*, 307(5712), pp. 1098–1101. doi: 10.1126/science.1106148.

Sardiello, M. *et al.* (2009) 'A Gene Network Regulating Lysosomal Biogenesis and Function', *Science*. doi: 10.1126/science.1174447.

Sathe, A. *et al.* (2018) 'Parallel PI3K, AKT and mTOR inhibition is required to control feedback loops that limit tumor therapy', *PLOS ONE*. Edited by A. Ahmad. Public Library of Science, 13(1), p. e0190854. doi: 10.1371/journal.pone.0190854.

Sato, T. *et al.* (2009) 'Specific Activation of mTORC1 by Rheb G-protein *in Vitro* Involves Enhanced Recruitment of Its Substrate Protein', *Journal of Biological Chemistry*, 284(19), pp. 12783–12791. doi: 10.1074/jbc.M809207200.

Saucedo, L. J. *et al.* (2003) 'Erratum: Rheb promotes cell growth as a component of the insulin/TOR signalling network', *Nature Cell Biology*. Nature Publishing Group, 5(6), pp. 566–571.

doi: 10.1038/ncb996.

Saxton, R. A. and Sabatini, D. M. (2017) ‘mTOR Signaling in Growth, Metabolism, and Disease.’, *Cell*, 168(6), pp. 960–976. doi: 10.1016/j.cell.2017.02.004.

Schalm, S. S. and Blenis, J. (2002) ‘Identification of a conserved motif required for mTOR signaling.’, *Current biology : CB*, 12(8), pp. 632–9.

Scheffzek, K. *et al.* (1997) ‘The Ras-RasGAP Complex: Structural Basis for GTPase Activation and Its Loss in Oncogenic Ras Mutants’, *Science*, 277(5324), pp. 333–338. doi: 10.1126/science.277.5324.333.

Scheper, G. C. *et al.* (2002) ‘Phosphorylation of eukaryotic initiation factor 4E markedly reduces its affinity for capped mRNA.’, *The Journal of biological chemistry*. American Society for Biochemistry and Molecular Biology, 277(5), pp. 3303–9. doi: 10.1074/jbc.M103607200.

Schlicker, A. *et al.* (2012) ‘Subtypes of primary colorectal tumors correlate with response to targeted treatment in colorectal cell lines’, *BMC Medical Genomics*, 5(1), p. 66. doi: 10.1186/1755-8794-5-66.

Sekulić, A. *et al.* (2000) ‘A direct linkage between the phosphoinositide 3-kinase-AKT signaling pathway and the mammalian target of rapamycin in mitogen-stimulated and transformed cells.’, *Cancer research*, 60(13), pp. 3504–13.

Seok, S. *et al.* (2014) ‘Transcriptional regulation of autophagy by an FXR-CREB axis’, *Nature*, 516(7529), pp. 108–111. doi: 10.1038/nature13949.

Serrano, M. *et al.* (1997) ‘Oncogenic ras provokes premature cell senescence associated with accumulation of p53 and p16INK4a.’, *Cell*, 88(5), pp. 593–602.

Settembre, C. *et al.* (2011) ‘TFEB links autophagy to lysosomal biogenesis’, *Science (New York, N.Y.)*, 332(6036), pp. 1429–1433. doi: 10.1126/science.1204592.

Settembre, C. *et al.* (2012) ‘A lysosome-to-nucleus signalling mechanism senses and regulates the lysosome via mTOR and TFEB’, *The EMBO journal*, 31(5), pp. 1095–1108. doi: 10.1038/emboj.2012.32.

Settembre, C. *et al.* (2013) ‘TFEB controls cellular lipid metabolism through a starvation-induced autoregulatory loop’, *Nature Cell Biology*, 15(6), pp. 647–658. doi: 10.1038/ncb2718.

Sha, Y. *et al.* (2017) ‘STUB1 regulates TFEB-induced autophagy–lysosome pathway’, *The EMBO Journal*, 36(17), pp. 2544–2552. doi: 10.15252/embj.201796699.

Shah, O. J., Ghosh, S. and Hunter, T. (2003) ‘Mitotic Regulation of Ribosomal S6 Kinase 1 Involves Ser/Thr, Pro Phosphorylation of Consensus and Non-consensus Sites by Cdc2’, *Journal of Biological Chemistry*, 278(18), pp. 16433–16442. doi: 10.1074/jbc.M300435200.

Shang, L. *et al.* (2011) ‘Nutrient starvation elicits an acute autophagic response mediated by Ulk1 dephosphorylation and its subsequent dissociation from AMPK’, *Proceedings of the National Academy of Sciences*, 108(12), pp. 4788–4793. doi: 10.1073/pnas.1100844108.

Shuda, M. *et al.* (2015) ‘CDK1 substitutes for mTOR kinase to activate mitotic cap-dependent protein translation.’, *Proceedings of the National Academy of Sciences of the United States of America*. National Academy of Sciences, 112(19), pp. 5875–82. doi: 10.1073/pnas.1505787112.

Sit, K. H. *et al.* (1996) ‘Sequestration of mitotic (M-phase) chromosomes in autophagosomes: Mitotic programmed cell death in human Chang liver cells induced by an OH* burst from vanadyl(4)’, *The Anatomical Record*, 245(1), pp. 1–8. doi: 10.1002/(SICI)1097-0185(199605)245:1<1::AID-AR1>3.0.CO;2-2.

van Slegtenhorst, M. *et al.* (1998) ‘Interaction between hamartin and tuberin, the TSC1 and TSC2 gene products’, *Human Molecular Genetics*, 7(6), pp. 1053–1057. doi: 10.1093/hmg/7.6.1053.

Sloss, O. *et al.* (2016) ‘Mcl-1 dynamics influence mitotic slippage and death in mitosis.’, *Oncotarget*. Impact Journals, LLC, 7(5), pp. 5176–92. doi: 10.18632/oncotarget.6894.

Smith, E. M. *et al.* (2005) ‘The Tuberous Sclerosis Protein TSC2 Is Not Required for the Regulation of the Mammalian Target of Rapamycin by Amino Acids and Certain Cellular Stresses’, *Journal of Biological Chemistry*, 280(19), pp. 18717–18727. doi: 10.1074/jbc.M414499200.

Smith, E. M. and Proud, C. G. (2008) ‘cdc2–cyclin B regulates eEF2 kinase activity in a cell cycle- and amino acid-dependent manner’, *The EMBO Journal*, 27(7), pp. 1005–1016. doi: 10.1038/emboj.2008.39.

Soliman, G. A. *et al.* (2010) ‘mTOR Ser-2481 autophosphorylation monitors mTORC-specific catalytic activity and clarifies rapamycin mechanism of action.’, *The Journal of biological chemistry*.

American Society for Biochemistry and Molecular Biology, 285(11), pp. 7866–79. doi: 10.1074/jbc.M109.096222.

Son, S. M. *et al.* (2019) 'Leucine Signals to mTORC1 via Its Metabolite Acetyl-Coenzyme A.', *Cell metabolism*. Elsevier, 29(1), pp. 192-201.e7. doi: 10.1016/j.cmet.2018.08.013.

Sonenberg, N. and Hinnebusch, A. G. (2009) 'Regulation of Translation Initiation in Eukaryotes: Mechanisms and Biological Targets', *Cell*. Cell Press, 136(4), pp. 731–745. doi: 10.1016/J.CELL.2009.01.042.

Sorokina, I. V. *et al.* (2017) 'Involvement of autophagy in the outcome of mitotic catastrophe', *Scientific Reports*. Nature Publishing Group, 7(1), p. 14571. doi: 10.1038/s41598-017-14901-z.

Steen, R. L. *et al.* (2000) 'Recruitment of Protein Phosphatase 1 to the Nuclear Envelope by a-Kinase Anchoring Protein Akap149 Is a Prerequisite for Nuclear Lamina Assembly', 150(6). doi: 10.1083/jcb.150.6.1251.

Steingrímsson, E. *et al.* (1998) 'The bHLH-Zip transcription factor Tfeb is essential for placental vascularization.', *Development (Cambridge, England)*, 125(23), pp. 4607–16.

Steingrímsson, E., Copeland, N. G. and Jenkins, N. A. (2004) 'Melanocytes and the *Microphthalmia* Transcription Factor Network', *Annual Review of Genetics*, 38(1), pp. 365–411. doi: 10.1146/annurev.genet.38.072902.092717.

Stratford, A. L. *et al.* (2008) 'Y-box binding protein-1 serine 102 is a downstream target of p90 ribosomal S6 kinase in basal-like breast cancer cells', *Breast Cancer Research*, 10(6), p. R99. doi: 10.1186/bcr2202.

Stretton, C. *et al.* (2015) 'GSK3-mediated raptor phosphorylation supports amino-acid-dependent mTORC1-directed signalling', *Biochemical Journal*, 470(2), pp. 207–221. doi: 10.1042/BJ20150404.

Strub, T. *et al.* (2011) 'Essential role of microphthalmia transcription factor for DNA replication, mitosis and genomic stability in melanoma', *Oncogene*, 30(20), pp. 2319–2332. doi: 10.1038/onc.2010.612.

Sueda, T. *et al.* (2016) 'BRAF V600E inhibition stimulates AMP-activated protein kinase-mediated autophagy in colorectal cancer cells.', *Scientific reports*. Nature Publishing Group, 6, p. 18949. doi: 10.1038/srep18949.

Sun, Q. *et al.* (2011) 'The RUN domain of rubicon is important for hVps34 binding, lipid kinase inhibition, and autophagy suppression.', *The Journal of biological chemistry*. American Society for Biochemistry and Molecular Biology, 286(1), pp. 185–91. doi: 10.1074/jbc.M110.126425.

Tai, H. *et al.* (2017) 'Autophagy impairment with lysosomal and mitochondrial dysfunction is an important characteristic of oxidative stress-induced senescence', *Autophagy*, 13(1), pp. 99–113. doi: 10.1080/15548627.2016.1247143.

Takahashi, Y. *et al.* (2007) 'Bif-1 interacts with Beclin 1 through UVRAG and regulates autophagy and tumorigenesis', *Nature Cell Biology*, 9(10), pp. 1142–1151. doi: 10.1038/ncb1634.

Takamura, A. *et al.* (2011) 'Autophagy-deficient mice develop multiple liver tumors', *Genes & Development*, 25(8), pp. 795–800. doi: 10.1101/gad.2016211.

Tan, H. W. S., Sim, A. Y. L. and Long, Y. C. (2017) 'Glutamine metabolism regulates autophagy-dependent mTORC1 reactivation during amino acid starvation', *Nature Communications*. Nature Publishing Group, 8(1), p. 338. doi: 10.1038/s41467-017-00369-y.

Tang, Z., Coleman, T. R. and Dunphy, W. G. (1993) 'Two distinct mechanisms for negative regulation of the Wee1 protein kinase.', *The EMBO journal*, 12(9), pp. 3427–36.

Tee, A. R. *et al.* (2003) 'Tuberous sclerosis complex gene products, Tuberin and Hamartin, control mTOR signaling by acting as a GTPase-activating protein complex toward Rheb.', *Current biology : CB*, 13(15), pp. 1259–68.

Teves, S. S. *et al.* (2016) 'A dynamic mode of mitotic bookmarking by transcription factors', *eLife*, 5. doi: 10.7554/eLife.22280.

Thoreen, C. C. *et al.* (2009) 'An ATP-competitive mammalian target of rapamycin inhibitor reveals rapamycin-resistant functions of mTORC1.', *The Journal of biological chemistry*. American Society for Biochemistry and Molecular Biology, 284(12), pp. 8023–32. doi: 10.1074/jbc.M900301200.

Thoreen, C. C. and Sabatini, D. M. (2009) 'Rapamycin inhibits mTORC1, but not completely', *Autophagy*, 5(5), pp. 725–726.

Tian, E. *et al.* (2009) '*epg-1* functions in autophagy-regulated processes and may encode a highly

divergent Atg13 homolog in *C. elegans*', *Autophagy*, 5(5), pp. 608–615. doi: 10.4161/auto.5.5.8624.

Todd, D. E. *et al.* (2004) 'ERK1/2 and p38 cooperate to induce a p21CIP1-dependent G1 cell cycle arrest.', *Oncogene*, 23(19), pp. 3284–95. doi: 10.1038/sj.onc.1207467.

Torggler, R. *et al.* (2016) 'Two Independent Pathways within Selective Autophagy Converge to Activate Atg1 Kinase at the Vacuole', *Molecular Cell*. Cell Press, 64(2), pp. 221–235. doi: 10.1016/J.MOLCEL.2016.09.008.

Tsai, L.-H. *et al.* (1999) 'Conversion of p35 to p25 deregulates Cdk5 activity and promotes neurodegeneration', *Nature*. Nature Publishing Group, 402(6762), pp. 615–622. doi: 10.1038/45159.

Tsun, Z.-Y. *et al.* (2013) 'The Folliculin Tumor Suppressor Is a GAP for the RagC/D GTPases That Signal Amino Acid Levels to mTORC1', *Molecular Cell*, 52(4), pp. 495–505. doi: 10.1016/j.molcel.2013.09.016.

Turco, E. *et al.* (2019) 'FIP200 Claw Domain Binding to p62 Promotes Autophagosome Formation at Ubiquitin Condensates', *Molecular Cell*, 74(2), pp. 330-346.e11. doi: 10.1016/j.molcel.2019.01.035.

Turco, E., Fracchiolla, D. and Martens, S. (2019) 'Recruitment and Activation of the ULK1/Atg1 Kinase Complex in Selective Autophagy', *Journal of Molecular Biology*. Academic Press. doi: 10.1016/J.JMB.2019.07.027.

Tzur, Y. B. and Gruenbaum, Y. (2013) 'Nuclear Envelope Breakdown and Reassembly in C. elegans: Evolutionary Aspects of Lamina Structure and Function'. Landes Bioscience.

Urbanelli, L. *et al.* (2014) 'Oncogenic H-Ras up-regulates acid β-hexosaminidase by a mechanism dependent on the autophagy regulator TFEB', *PloS One*, 9(2), p. e89485. doi: 10.1371/journal.pone.0089485.

Valverde, D. P. *et al.* (2019) 'ATG2 transports lipids to promote autophagosome biogenesis', *The Journal of cell biology*. NLM (Medline), 218(6), pp. 1787–1798. doi: 10.1083/jcb.201811139.

Vanhaesebroeck, B. *et al.* (2010) 'The emerging mechanisms of isoform-specific PI3K signalling', *Nature Reviews Molecular Cell Biology*. Nature Publishing Group, 11(5), pp. 329–341. doi: 10.1038/nrm2882.

Vargas, J. N. S. *et al.* (2019) 'Spatiotemporal Control of ULK1 Activation by NDP52 and TBK1 during Selective Autophagy', *Molecular Cell*, 74(2), pp. 347-362.e6. doi: 10.1016/j.molcel.2019.02.010.

Vassilev, L. T. *et al.* (2006) 'Selective small-molecule inhibitor reveals critical mitotic functions of human CDK1.', *Proceedings of the National Academy of Sciences of the United States of America*. National Academy of Sciences, 103(28), pp. 10660–5. doi: 10.1073/pnas.0600447103.

Vazquez-Martin, A. *et al.* (2009) 'The serine 2481-autophosphorylated form of mammalian Target Of Rapamycin (mTOR) is localized to midzone and midbody in dividing cancer cells', *Biochemical and Biophysical Research Communications*, 380(3), pp. 638–643. doi: 10.1016/j.bbrc.2009.01.153.

Vazquez-Martin, A. *et al.* (2011) 'Raptor, a positive regulatory subunit of mTOR complex 1, is a novel phosphoprotein of the rDNA transcription machinery in nucleoli and chromosomal nucleolus organizer regions (NORs)', *Cell Cycle*, 10(18), pp. 3140–3152. doi: 10.4161/cc.10.18.17376.

Vega-Rubin-de-Celis, S. *et al.* (2017) 'Multistep regulation of TFEB by MTORC1', *Autophagy*. Taylor & Francis, pp. 00–00. doi: 10.1080/15548627.2016.1271514.

Velásquez, C. *et al.* (2016) 'Mitotic protein kinase CDK1 phosphorylation of mRNA translation regulator 4E-BP1 Ser83 may contribute to cell transformation', *Proceedings of the National Academy of Sciences*, 113(30), pp. 8466–8471. doi: 10.1073/pnas.1607768113.

Veldhoen, R. A. *et al.* (2013) 'The chemotherapeutic agent paclitaxel inhibits autophagy through two distinct mechanisms that regulate apoptosis', *Oncogene*. Nature Publishing Group, 32(6), pp. 736–746. doi: 10.1038/onc.2012.92.

Voong, L. N. *et al.* (2008) 'Mitogen-activated protein kinase ERK1/2 regulates the class II transactivator.', *The Journal of biological chemistry*. American Society for Biochemistry and Molecular Biology, 283(14), pp. 9031–9. doi: 10.1074/jbc.M706487200.

Wan, W. *et al.* (2018) 'mTORC1-Regulated and HUWE1-Mediated WIPI2 Degradation Controls Autophagy Flux', *Molecular Cell*, 72(2), pp. 303-315.e6. doi: 10.1016/j.molcel.2018.09.017.

Wang, A. *et al.* (2017) 'Activity-independent targeting of mTOR to lysosomes in primary

osteoclasts.', *Scientific reports*. Nature Publishing Group, 7(1), p. 3005. doi: 10.1038/s41598-017-03494-2.

Wang, L. *et al.* (2007) 'PRAS40 Regulates mTORC1 Kinase Activity by Functioning as a Direct Inhibitor of Substrate Binding', *Journal of Biological Chemistry*, 282(27), pp. 20036–20044. doi: 10.1074/jbc.M702376200.

Wang, R. and Brattain, M. G. (2007) 'The maximal size of protein to diffuse through the nuclear pore is larger than 60kDa.', *FEBS letters*. NIH Public Access, 581(17), pp. 3164–70. doi: 10.1016/j.febslet.2007.05.082.

Wang, S. *et al.* (2015) 'Lysosomal amino acid transporter SLC38A9 signals arginine sufficiency to mTORC1', *Science*, 347(6218), pp. 188–194. doi: 10.1126/science.1257132.

Wang, T. H. *et al.* (1998) 'Microtubule-interfering agents activate c-Jun N-terminal kinase/stress-activated protein kinase through both Ras and apoptosis signal-regulating kinase pathways.', *The Journal of biological chemistry*. American Society for Biochemistry and Molecular Biology, 273(9), pp. 4928–36. doi: 10.1074/jbc.273.9.4928.

Wang, X. *et al.* (2001) 'Regulation of elongation factor 2 kinase by p90(RSK1) and p70 S6 kinase.', *The EMBO journal*. European Molecular Biology Organization, 20(16), pp. 4370–9. doi: 10.1093/emboj/20.16.4370.

Wang, X. *et al.* (2003) 'The C terminus of initiation factor 4E-binding protein 1 contains multiple regulatory features that influence its function and phosphorylation.', *Molecular and cellular biology*. American Society for Microbiology (ASM), 23(5), pp. 1546–57. doi: 10.1128/MCB.23.5.1546-1557.2003.

Wang, X. and Proud, C. G. (2011) 'mTORC1 signaling: what we still don't know', *Journal of Molecular Cell Biology*. Narnia, 3(4), pp. 206–220. doi: 10.1093/jmcb/mjq038.

Waskiewicz, A. J. *et al.* (1997) 'Mitogen-activated protein kinases activate the serine/threonine kinases Mnk1 and Mnk2', *The EMBO Journal*, 16(8), pp. 1909–1920. doi: 10.1093/emboj/16.8.1909.

Watanabe, N. *et al.* (2005) 'Cyclin-dependent kinase (CDK) phosphorylation destabilizes somatic Wee1 via multiple pathways', *Proceedings of the National Academy of Sciences*, 102(33), pp. 11663–11668. doi: 10.1073/pnas.0500410102.

Wauson, E. M. *et al.* (2013) 'Off-target effects of MEK inhibitors.', *Biochemistry*. NIH Public Access, 52(31), pp. 5164–6. doi: 10.1021/bi4007644.

Weber, C. K. *et al.* (2001) 'Active Ras induces heterodimerization of cRaf and BRaf.', *Cancer research*, 61(9), pp. 3595–8.

Webster, J. and Oxley, D. (2009) 'Protein Identification by Peptide Mass Fingerprinting using MALDI-TOF Mass Spectrometry', in. Humana Press, Totowa, NJ, pp. 1117–1129. doi: 10.1007/978-1-59745-198-7_120.

Wei, Y. *et al.* (2008) 'JNK1-Mediated Phosphorylation of Bcl-2 Regulates Starvation-Induced Autophagy', *Molecular Cell*, 30(6), pp. 678–688. doi: 10.1016/j.molcel.2008.06.001.

Weilbaecher, K. N. *et al.* (2001) 'Linkage of M-CSF Signaling to Mitf, TFE3, and the Osteoclast Defect in Mitfmi/mi Mice', *Molecular Cell*, 8(4), pp. 749–758. doi: 10.1016/S1097-2765(01)00360-4.

Wellbrock, C., Karasarides, M. and Marais, R. (2004) 'The RAF proteins take centre stage', *Nature Reviews Molecular Cell Biology*. Nature Publishing Group, 5(11), pp. 875–885. doi: 10.1038/nrm1498.

Wild, P. *et al.* (2011) 'Phosphorylation of the Autophagy Receptor Optineurin Restricts Salmonella Growth', *Science*, 333(6039), pp. 228–233. doi: 10.1126/science.1205405.

Wilkinson, S. *et al.* (2011) 'The cyclin-dependent kinase PITSLRE/CDK11 is required for successful autophagy.', *Autophagy*. Taylor & Francis, 7(11), pp. 1295–301. doi: 10.4161/auto.7.11.16646.

Wold, M. S. *et al.* (2016) 'ULK1-mediated phosphorylation of ATG14 promotes autophagy and is impaired in Huntington's disease models', *Molecular Neurodegeneration*. BioMed Central, 11(1), p. 76. doi: 10.1186/s13024-016-0141-0.

Wolfson, R. L. *et al.* (2016) 'Sestrin2 is a leucine sensor for the mTORC1 pathway', *Science*, 351(6268), pp. 43–48. doi: 10.1126/science.aab2674.

Wong, A. S. L. *et al.* (2011) 'Cdk5-mediated phosphorylation of endophilin B1 is required for induced autophagy in models of Parkinson's disease', *Nature Cell Biology*, 13(5), pp. 568–579. doi:

10.1038/ncb2217.

Wong, P.-M. *et al.* (2015) 'Regulation of autophagy by coordinated action of mTORC1 and protein phosphatase 2A', *Nature Communications*. Nature Publishing Group, 6(1), p. 8048. doi: 10.1038/ncomms9048.

Wu, D. *et al.* (2012) 'Intestinal Cell Kinase (ICK) Promotes Activation of mTOR Complex 1 (mTORC1) through Phosphorylation of Raptor Thr-908', *Journal of Biological Chemistry*, 287(15), pp. 12510–12519. doi: 10.1074/jbc.M111.302117.

Wu, M. *et al.* (2000) 'c-Kit triggers dual phosphorylations, which couple activation and degradation of the essential melanocyte factor Mi', *Genes & Development*, 14(3), pp. 301–312.

Wu, X.-N. *et al.* (2011) 'Phosphorylation of Raptor by p38β Participates in Arsenite-induced Mammalian Target of Rapamycin Complex 1 (mTORC1) Activation', *Journal of Biological Chemistry*, 286(36), pp. 31501–31511. doi: 10.1074/jbc.M111.233122.

Wyant, G. A. *et al.* (2017) 'mTORC1 Activator SLC38A9 Is Required to Efflux Essential Amino Acids from Lysosomes and Use Protein as a Nutrient', *Cell*. Cell Press, 171(3), pp. 642-654.e12. doi: 10.1016/J.CELL.2017.09.046.

Xie, J., Wang, X. and Proud, C. G. (2016) 'mTOR inhibitors in cancer therapy.', *F1000Research*. Faculty of 1000 Ltd, 5. doi: 10.12688/f1000research.9207.1.

Yang, H. *et al.* (2017) 'Mechanisms of mTORC1 activation by RHEB and inhibition by PRAS40.', *Nature*. NIH Public Access, 552(7685), pp. 368–373. doi: 10.1038/nature25023.

Yeong, F. M. (2013) 'Multi-step down-regulation of the secretory pathway in mitosis: A fresh perspective on protein trafficking', *Bioessays*. Wiley-Blackwell, 35(5), p. 462. doi: 10.1002/BIES.201200144.

Yip, C. K. *et al.* (2010) 'Structure of the Human mTOR Complex I and Its Implications for Rapamycin Inhibition', *Molecular Cell*, 38(5), pp. 768–774. doi: 10.1016/j.molcel.2010.05.017.

Ylä-Anttila, P. *et al.* (2009) '3D tomography reveals connections between the phagophore and endoplasmic reticulum.', *Autophagy*, 5(8), pp. 1180–5.

Yonekawa, T. *et al.* (2015) 'RIP1 negatively regulates basal autophagic flux through TFEB to control sensitivity to apoptosis', *EMBO reports*, 16(6), pp. 700–708. doi: 10.15252/embr.201439496.

Yoshii, S. R. and Mizushima, N. (2017) 'Monitoring and Measuring Autophagy', *International Journal of Molecular Sciences*, 18(9), p. 1865. doi: 10.3390/ijms18091865.

Young, A. R. J. *et al.* (2009) 'Autophagy mediates the mitotic senescence transition.', *Genes & development*. Cold Spring Harbor Laboratory Press, 23(7), pp. 798–803. doi: 10.1101/gad.519709.

Yuan, F. *et al.* (2019) 'ULK1 phosphorylates Mad1 to regulate spindle assembly checkpoint', *Nucleic Acids Research*. doi: 10.1093/nar/gkz602.

Yuan, H.-X., Russell, R. C. and Guan, K.-L. (2013) 'Regulation of PIK3C3/VPS34 complexes by MTOR in nutrient stress-induced autophagy.', *Autophagy*, 9(12), pp. 1983–95.

Yun, C. W. and Lee, S. H. (2018) 'The Roles of Autophagy in Cancer.', *International journal of molecular sciences*. Multidisciplinary Digital Publishing Institute (MDPI), 19(11). doi: 10.3390/ijms19113466.

Zhang, J. *et al.* (2018) 'Importance of TFEB acetylation in control of its transcriptional activity and lysosomal function in response to histone deacetylase inhibitors', *Autophagy*, pp. 1–17. doi: 10.1080/15548627.2018.1447290.

Zhang, W. *et al.* (2011) 'DNA Damage Response Is Suppressed by the High Cyclin-dependent Kinase 1 Activity in Mitotic Mammalian Cells', *Journal of Biological Chemistry*, 286(41), pp. 35899–35905. doi: 10.1074/jbc.M111.267690.

Zhang, X. *et al.* (2002) 'Predominant Nuclear Localization of Mammalian Target of Rapamycin in Normal and Malignant Cells in Culture', *Journal of Biological Chemistry*, 277(31), pp. 28127–28134. doi: 10.1074/jbc.M202625200.

Zhang, Y. *et al.* (2003) 'Rheb is a direct target of the tuberous sclerosis tumour suppressor proteins.', *Nature cell biology*, 5(6), pp. 578–81. doi: 10.1038/ncb999.

Zhou, J. *et al.* (2013) 'Activation of lysosomal function in the course of autophagy via mTORC1 suppression and autophagosome-lysosome fusion', *Cell Research*, 23(4), pp. 508–523. doi: 10.1038/cr.2013.11.

Zoncu, R. *et al.* (2011) ‘mTORC1 Senses Lysosomal Amino Acids Through an Inside-Out Mechanism That Requires the Vacuolar H+-ATPase’, *Science*, 334(6056), pp. 678–683. doi: 10.1126/science.1207056.

7.1 Links to databases

Consurf:

Used for analysis of gene conservation through evolution

Link: http://consurf.tau.ac.il/credits.php

Reference: Ashkenazy H. *et al.* (2016) ConSurf 2016: an improved methodology to estimate and visualize evolutionary conservation in macromolecules, *Nucl. Acids Res.,* doi: 10.1093/nar/gkw408

Cancer Cell Line Encyclopaedia (CCLE)

Used to acquire TFEB mRNA values for gastrointestinal cell lines

Link: https://portals.broadinstitute.org/ccle

Reference: Barretina J. *et al.* (2012) The Cancer Cell Line Encyclopedia enables predictive modeling of anticancer drug sensitivity, *Nature,* doi: 10.1038/nature11003

Cansar 4.0

Used to acquire copy number variation data for TFEB

Link:
https://cansar.icr.ac.uk/cansar/#main_tab_holder:tab_search_main_protein:tab_search_1

Reference: Halling-Brown M. et al. (2011) canSAR: an integrated cancer public translational research and drug discovery resource, *Nucl. Acids Res*., doi: 10.1093/nar/gkr881